

CONTRACTOR REPORT

SAND96-1062
Unlimited Release
UC-1350

Sodium/Sulfur Battery Engineering for Stationary Energy Storage

Final Report

Albert Koenig, James Rasmussen
Silent Power, Inc.
163 West 1700 South
Salt Lake City, UT 84115

Prepared by
Sandia National Laboratories
Albuquerque, New Mexico 87185 and Livermore, California 94550
for the United States Department of Energy
under Contract DE-AC04-94AL85000

Approved for public release; distribution is unlimited.

Printed April 1996

Issued by Sandia National Laboratories, operated for the United States Department of Energy by Sandia Corporation.

NOTICE: This report was prepared as an account of work sponsored by an agency of the United States Government. Neither the United States Government nor any agency thereof, nor any of their employees, nor any of their contractors, subcontractors, or their employees, makes any warranty, express or implied, or assumes any legal liability or responsibility for the accuracy, completeness, or usefulness of any information, apparatus, product, or process disclosed, or represents that its use would not infringe privately owned rights. Reference herein to any specific commercial product, process, or service by trade name, trademark, manufacturer, or otherwise, does not necessarily constitute or imply its endorsement, recommendation, or favoring by the United States Government, any agency thereof or any of their contractors or subcontractors. The views and opinions expressed herein do not necessarily state or reflect those of the United States Government, any agency thereof or any of their contractors.

Printed in the United States of America. This report has been reproduced directly from the best available copy.

Available to DOE and DOE contractors from
Office of Scientific and Technical Information
PO Box 62
Oak Ridge, TN 37831

Prices available from (615) 576-8401, FTS 626-8401

Available to the public from
National Technical Information Service
US Department of Commerce
5285 Port Royal RD
Springfield, VA 22161

NTIS price codes
Printed copy: A08
Microfiche copy: A01

SAND96-1062
Unlimited Release
Printed April 1996

Distribution
Category UC-1350

Sodium/Sulfur Battery Engineering for Stationary Energy Storage Final Report

Albert Koenig
James Rasmussen
Silent Power, Inc.
163 West 1700 South
Salt Lake City, UT 84115

Abstract

The use of modular systems to distribute power using batteries to store off-peak energy and a state-of-the-art power inverter is envisioned to offer important national benefits. A 4-year, cost-shared contract was performed by Silent Power, Inc., to design and develop a modular, 300-kVA/300-kWh system for utility and customer applications. Called Nas-P_{AC}, this system uses advanced sodium/sulfur batteries and requires only about 20% of the space of a lead-acid-based system with a smaller energy content. Ten, 300-VDC, 40-kWh sodium/sulfur battery packs are accommodated behind a power conversion system (PCS) envelope with integrated digital control. The resulting design facilitates transportation, site selection, and deployment because the system is quiet and non-polluting, and can be located in proximity to the load. This report contains a detailed description of the design and supporting hardware development performed under this contract.

TABLE OF CONTENTS

List of Figures	iii
List of Tables	vi
Acronyms and Abbreviations	vii
Abstract	ix
Executive Summary	x
I. Introduction and Program Plan	1-1
II. The Silent Power Sodium Sulfur Battery	2-1
III. Utility Energy Storage (UES) Applications	3-1
3.1 Modular Integrated System Approach	3-1
3.2 Opportunities Assessment	3-4
3.3 Utility-Industry Outreach	3-9
3.4 BESS Product Viability	3-12
IV. Battery Energy Storage System (BESS) Design and Price Development	4-1
4.1 Development of a 300 kVA/300 kWh NaS-P _{AC} Modular System Design ..	4-1
4.1.1 NaS-P _{AC} System Design Considerations	4-1
4.1.2 Design Specifications	4-3
4.1.3 System Control and Connection Schemes	4-6
4.1.4 NaS-P _{AC} System Benefits	4-13
4.2 NaS-P _{AC} BESS Price Analysis	4-15
4.3 Other NaS-P _{AC} System Designs	4-18
4.4 A Future Custom UES Battery Design	4-26
V. Component Development	5-1
5.1 Cell Design and Component Development	5-1
5.1.1 Preliminary Cell Design	5-1
5.1.1.1 Preliminary Freeze/Thaw Durability Assessment	5-5
5.1.1.2 Preliminary Sodium Electrode Seal Trials	5-7
5.1.1.3 Preliminary Cell Trials	5-8
5.1.2 Seal Development	5-9
5.1.2.1 Sodium Seal Development	5-9
5.1.2.1.1 Liquid Metal Embrittlement	5-9
5.1.2.1.2 Seal Modification Trials	5-10
5.1.2.2 Sulfur Electrode Seal Development	5-15
5.1.3 Current Collector Coatings	5-15
5.1.3.1 Half Cell Testing	5-15
5.1.3.2 Full Cell Testing	5-16
5.1.3.2.1 Molybdenum Coated Current Collectors	5-16
5.1.3.2.2 TiN Coated Current Collectors	5-18
5.1.3.2.3 Nichrome Coated Current Collectors	5-21
5.1.4 Safety Feature Development	5-21

5.1.5	Sodium Filling Process	5-25
5.1.6	Prototype Cell Design	5-27
5.2	Prototype Cell Design Verification and Testing	5-31
5.2.1	Prototype Cell Fabrication	5-31
5.2.2	Cell Testing	5-34
5.2.2.1	Safety Testing	5-34
5.2.2.2	Freeze/Thaw	5-36
5.2.2.3	Cell Performance and Repeatability	5-40
5.3	Battery Component Development	5-42
5.3.1	Thermal Management	5-42
5.3.1.1	Molten Salt Thermal Energy Storage	5-42
5.3.1.1.1	Molten Salt Thermal Energy Storage Capsule Development	5-42
5.3.1.2	Thermosyphon Cooling System	5-47
5.3.2	Cell-to-Cell Bonding Material Evaluation	5-51
5.3.3	Cell String Fuse Development	5-54
5.3.4	Battery Management System Design	5-57
VI.	13 kWh Deliverable Module Development and Test	6-1
6.1	Deliverable Module Design	6-1
6.2	Module Fabrication	6-3
6.2.1	Half Bank Assembly	6-3
6.2.2	Module Assembly	6-4
6.3	Module Testing	6-11
6.4	Post Test Analysis	6-12
VII.	Hardware Development Summary and Recommendations for Future Work	7-1
7.1	Cell Development	7-1
7.2	Deliverable Module	7-3

References

Acknowledgments

APPENDIX A

APPENDIX B

List of Figures

Figure 2-1.	The New High Power 20Wh Sodium Sulfur Cell from Silent Power . . .	2-1
Figure 2-2.	Performance of SP Batteries Relative to the USABC Mid-term Requirements	2-2
Figure 2-3.	300 VDC, 40 kWh, Sodium Sulfur Battery from Silent Power	2-2
Figure 3-1.	Distributed Utility Battery Energy Storage Opportunity	3-3
Figure 3-2.	Combined Application II: Distribution Facility Deferral and Voltage Regulation	3-8
Figure 3-3.	Combined Application III: Customer Reliability and Customer Demand Peak Shaving	3-8
Figure 3-4.	Utility Applications Response	3-12
Figure 3-5.	300 kVA NaS-P _{AC} System Net Present Value Analysis	3-16
Figure 3-6.	NaS-P _{AC} Cash Flow Sensitivity to Battery Replacement Period . . .	3-17
Figure 3-7.	Possible Scenario for Leasing BESS Equipment	3-17
Figure 3-8.	Impact of BESS Size on Payback Using Real Time Pricing	3-18
Figure 4-1.	300 kVA - 1 hour, 480 VAC, NaS-P _{AC} System	4-1
Figure 4-2.	NaS-P _{AC} System with Replaceable Sodium Sulfur Batteries	4-2
Figure 4-3a.	Battery Support Structure, Right Half	4-4
Figure 4-3b.	Battery Support Structure, Left Half	4-4
Figure 4-4.	Battery Sustained Discharge Capability at 300 kVA	4-5
Figure 4-5.	Battery Performance Degradation Scenario with Time	4-5
Figure 4-6.	Battery Cooling Via an Oil-Air Heat Exchanger	4-7
Figure 4-7.	Blower Mount and Air Ducting Design for Multi-Battery Cooling	4-8
Figure 4-8.	Air Vent Design for Multi-Battery Chimney	4-9
Figure 4-9.	Battery PCS Integrated System Control Scheme	4-11
Figure 4-10a.	BESS Connection for Parallel Operation with Utility	4-12
Figure 4-10b.	BESS Series Connection for Power Quality/Reliability	4-12
Figure 4-11.	Transportation and Substation Deployment of Modular NaS-P _{AC} Units	4-14
Figure 4-12.	Power Inverter Cost-Size Relationship	4-16
Figure 4-13.	NaS-P _{AC} System Price Projection with Market Development	4-18
Figure 4-14.	NaS-P _{AC} System Near Term Price: Power and Energy Composition	4-19
Figure 4-15.	NaS-P _{AC} System Future Price Composition	4-20
Figure 4-16.	30 kVA - 2 hour NaS-P _{AC} System Design for Commercial Applications	4-22
Figure 4-17.	30 kVA System Mockup for Thermal Testing	4-23
Figure 4-18.	3.5 kVA - 2 Hour NaS-P _{AC} System Design for Residential Applications	4-24
Figure 4-19.	24 VDC Custom Battery Design for Residential BESS	4-25
Figure 4-20.	75 kWh Custom UES Battery Pack Design, Cut-Away Side View . .	4-27
Figure 4-21.	75 kWh Custom UES Battery Pack Design, Cut-Away Top View . . .	4-28
Figure 4-22.	75 kWh Battery Performance at Constant Power for 2 Hours	4-29

Figure 4-23.	Cell Matrix Temperature Rise During 2 hour Sustained Discharge	4-29
Figure 5-1.	SPL's Technology Demonstration Cell Design	5-2
Figure 5-2.	Resistance of TD Cell 5601	5-3
Figure 5-3.	Preliminary Central Sulfur Cell Design	5-4
Figure 5-4.	PB and XPB Cell Designs	5-5
Figure 5-5.	Seal Strength Test Fixture	5-11
Figure 5-6.	Tapered Seal Configuration	5-13
Figure 5-7.	Planar Seal Configuration	5-14
Figure 5-8.	Half Cell Corrosion Test Set-Up	5-16
Figure 5-9.	Cell Voltages for Cycles 7, 38, 75, 87, and 107 for Cell 107	5-17
Figure 5-10.	Typical Resistance of a Cell with a Molybdenum Coated Current Collector	5-19
Figure 5-11.	Effect of Changing Cycling Conditions on Molybdenum Cell Capacity	5-19
Figure 5-12.	Resistance for Cell with an Ion Plated TiN Current Collector	5-20
Figure 5-13.	DoD and f_1 for Cell with an Ion Plated TiN Current Collector	5-20
Figure 5-14.	Cell Voltages for Cycles 12, 31, and 84 for Cell 019	5-22
Figure 5-15.	Typical f_1 and DoD for a Cell with a Nichrome Coated Current Collector	5-23
Figure 5-16.	Typical Resistance for a Cell with a Nichrome Coated Current Collector	5-23
Figure 5-17.	Resistance of Longest Lived Cell	5-24
Figure 5-18.	DoD and f_1 for Longest Lived Cell	5-24
Figure 5-19.	Sodium Filling Schematic	5-26
Figure 5-20.	Prototype Central Sulfur Cell Design	5-27
Figure 5-21.	Typical Ceramic Fracture in a Failed TCB Sodium Electrode Seal	5-33
Figure 5-22.	Probability of Peak Temperature during Failure Exceeding Specified Temperature	5-35
Figure 5-23.	Prototype Cell Resistance during Freeze/Thaw Cycling	5-37
Figure 5-24.	Prototype Cell Capacity and f_1 during Freeze/Thaw Cycling	5-37
Figure 5-25.	Resistance for Cell 168 during Freeze/Thaw Cycling	5-39
Figure 5-26.	Eleven Cell Average Resistance during Break-in	5-40
Figure 5-27.	Eleven Cell Average f_1 during Break-in	5-41
Figure 5-28.	30 Cell Test Module Showing Relative Positions of PB Cell Strings and TES Capsules	5-44
Figure 5-29.	Temperature Response of the 30 Cell TES Experiment for the 240 W Discharge Test Condition	5-44
Figure 5-30.	Temperature Response of the 30 Cell TES Experiment for the 300 W Discharge Test Condition	5-45
Figure 5-31.	Temperature Response for the 30 Cell TES Experiment for the 400 W Discharge Test Condition	5-45
Figure 5-32.	Actual Temperature Rise in 30 Cell TES Experiment Compared to Calculated Temperature Rise without TES Capsules	5-46
Figure 5-33.	Thermosyphon Experimental Apparatus	5-48
Figure 5-34.	Typical Thermosyphon Response for the FC-71 Fluid	5-49

Figure 5-35.	Heat Removed as a Function of Boiler Power for the FC-71 Fluid	5-50
Figure 5-36.	Typical Thermosyphon Response for the FC-5312 Fluid	5-50
Figure 5-37.	Heat Removed as a Function of Boiler Power for the FC-5312 Fluid	5-51
Figure 5-38.	Typical Thermosyphon Response for the FC-5312 Fluid at an Elevated Head	5-51
Figure 5-39.	Heat Removed as a Function of Boiler Power; FC-5312; 0.45 m Head	5-52
Figure 5-40.	Thermosyphon Response at High Power Input Level for the FC-5312	5-53
Figure 5-41.	Fuse Current/Resistance Relationship	5-56
Figure 5-42.	Battery Energy Storage System Block Diagram	5-58
Figure 5-43.	Battery Management System Block Diagram	5-59
Figure 6-1.	Cut-Away View of the "Core" of the Deliverable 13 kWh Sodium Sulfur Module	6-1
Figure 6-2.	Interior of the Deliverable 13 kWh Sodium Sulfur Module Prior to Bank Installation	6-4
Figure 6-3.	An 8V, 400 Ah Bank Comprising the 13 kWh Sodium Sulfur Module	6-6
Figure 6-4.	The Welding of Adjacent Bank Plates	6-6
Figure 6-5.	Completed Bank Assembly	6-7
Figure 6-6.	The Top View of the Module with Split Heaters and Control Thermocouples In-Place	6-8
Figure 6-7.	Wiring Board Installed on Top of the Module	6-8
Figure 6-8.	Battery Management System (BMS) During Assembly	6-9
Figure 6-9.	Completed 13 kWh Module with Assembly Team	6-9
Figure 6-10.	Cycle 124 Discharge and Hold, Bank 1 Open Circuit Voltage Monitor	6-13
Figure 6-11.	Cycle 124, Bank 2 Open Circuit Voltage Monitor	6-13
Figure 6-12.	Cycle 124, Bank 3 Open Circuit Voltage Monitor	6-14
Figure 6-13.	Cycle 124, Bank 4 Open Circuit Voltage Monitor	6-14
Figure 6-14.	PTA of the Deliverable 13 kWh Module Showing a Layer of Rust on the Inside Surface of the Enclosure	6-16
Figure 6-15.	PTA of the Deliverable 13 kWh Module Showing the Clean Appearance of the Top of the Banks	6-16
Figure 6-16.	Deliverable 13 kWh Module: Distribution of Failed Cells in Bank 1 ..	6-18
Figure 6-17.	Deliverable 13 kWh Module: Distribution of Failed Cells in Bank 2 ..	6-19
Figure 6-18.	Deliverable 13 kWh Module: Distribution of Failed Cells in Bank 3 ..	6-20
Figure 6-19.	Deliverable 13 kWh Module: Distribution of Failed Cells in Bank 4 ..	6-21

List of Tables

Table 3-1.	Summary of Utility Energy Storage Applications Requirements	3-6
Table 3-2.	300 kVA/300 kWh NaS-P _{AC} System Investment Cash Flow Analysis	3-15
Table 4-1.	Power Conversion System (PCS) Specification	4-10
Table 4-2.	The Case for Advanced Batteries: A Comparison of BESS	4-13
Table 4-3.	Summary of NaS-P _{AC} System Benefits	4-15
Table 4-4.	NaS-P _{AC} System Price Breakdown	4-17
Table 5-1.	Preliminary Cell Design Specifications	5-6
Table 5-2.	Preliminary Central Sulfur Cell Performance Projections	5-6
Table 5-3.	TCB Seal Strength	5-10
Table 5-4.	Sodium Seal Freeze/Thaw Durability	5-12
Table 5-5.	Preliminary Safety Test Summary	5-25
Table 5-6.	Cell Design Specification Comparison	5-28
Table 5-7.	Seal Design Comparison	5-29
Table 5-8.	Prototype Central Sulfur Cell Performance Projections	5-30
Table 5-9.	Fabrication Failure Distribution	5-31
Table 5-10.	Freeze/Thaw Test Status	5-38
Table 6-1.	Bank Voltages of Deliverable Module During Initial Heat-Up	6-10
Table 6-2.	Available Module Capacity Toward the EoL for the Deliverable 13 kWh Module	6-15
Table 6-3.	Failed Cell Distribution in the Deliverable 13 kWh Module	6-22

Acronyms and Abbreviations

A/D	analog to digital
BESS	battery energy storage system
BMS	battery management system
BoD	beginning-of-discharge
BoL	beginning-of-life
CAES	compressed air energy storage
c/S	central Sulfur
CPQ/R	customer power quality/reliability
DG	distributed generation
DSP	digital signal processor
DOE	Department of Energy
DSM	demand side management
EMF	electromotive force
EoL	end-of-life
EPRI	Electric Power Research Institute
EV	electric vehicle
f_1	fraction of theoretical capacity which is not recoverable on recharge
IGBT	integrated gate bipolar transistor
IPP	independent power producer
IRR	internal rate of return
LME	liquid metal embrittlement
MUX	multiplexer
NaS- P_{AC}	Sodium Sulfur AC Power System
NPV	net present value
PCS	power conversion system; power conditioning system
PREPA	Puerto Rico Electric Power Authority
PUC	Public Utility Commission
PWM	pulse width modulation
PB	a10AH sodium sulfur cell developed for low power EV application
PS	peak shaving
PTA	post test analysis
SES	stationary energy storage; used interchanably with UES
SMES	superconductive magnetic energy storage
SNL	Sandia National Laboratories
SoA	state-of-the-art
SP	Silent Power

SPI	Silent Power Inc
SPL	Silent Power Ltd
SR	spinning reserve
TCB	thermoccompression bond
TD	technology demonstration
T&D	transmission and distribution
TES	thermal energy storage
THD	total harmonic distortion
UBG	Utility Battery Group
UES	utility energy storage
UPQ/R	utility power quality/reliability
UPS	uninterruptible power supply
USABC	United States Advanced Battery Consortium
VARs	volt-amp reactive
XPB	a 28 AH sodium sulfur cell; an extended version of the PB cell

ABSTRACT

The development and the eventual commercial introduction of a modular, outdoor package for distributed power using batteries to store off-peak energy and a state-of-the-art power inverter is envisioned to offer national benefits. This Program supported the design and development of a modular 300 kVA/300 kWh system for utility and customer applications. Called NaS-P_{AC}, it is a system which is 20% of the size of a comparable lead acid based system. Ten, 300 VDC, 40 kWh, sodium sulfur battery packs from Silent Power, Ltd. are accommodated behind a power conversion system (PCS) envelope with integrated digital control. The resulting design facilitates transportation, site selection and deployment, as a quiet, non-polluting, source located in proximity to the load.

EXECUTIVE SUMMARY

Introduction

The *Sodium Sulfur Battery Engineering for Stationary Energy Storage* Program was sponsored by the DOE Office of Utility Technologies. Their goal is to reduce the country's reliance on imported oil, to improve generating reliability, and to reduce the cost of electricity while lowering environmentally damaging emissions from fossil fuel generators. This program was performed by Silent Power, Inc. (SPI) under a \$4.1 million, 4½ year contract with Sandia National Laboratories (SNL) that was cost shared by SPI at 22%. The primary objectives of the program as proposed were: 1) to develop a preliminary design of a Utility Energy Storage (UES) battery, 2) to build and deliver a battery module representative of state-of-the-art technology and 3) to progress the development of components comprising the battery to improve life, durability, reliability and safety. To accomplish this, the program was divided into the following four tasks:

1. Utility Applications Assessment
2. UES Cell and Battery Development
3. Assembly and Test of a Prototype Battery
4. Battery Energy Storage System Design and Cost Development

The applications task was originally included to gain a better understanding of the needs of the utilities so that effective design activities could be pursued. However, as the program was carried forward, this work became a keystone around which the program evolved. Silent Power's approach regarding the design requirements and applications changed during the course of the program. Initially, it was thought that the UES battery would be a relatively large system which would be custom built at the site for the specific utility application. However, a small, modular energy storage system that is easily transportable and may not even be owned by a utility was found to be the most attractive for the sodium sulfur Battery Energy Storage System (BESS).

This report summarizes the accomplishments of the program.

Applications

SPI participated in an Opportunities Assessment Forum held by SNL in which utility and customer applications were considered and a relative assessment made of the most promising BESS applications. For the NaS-P_{AC} system – the name chosen for the sodium sulfur BESS – the important characteristics identified were:

- <1MW to 2MW power
- 1 to 2 hours duration
- daily utilization
- small footprint
- transportability

Matching the characteristics of the sodium sulfur BESS with the requirements for the candidate applications, the NaS-P_{AC} system offers advantages for renewable generation, as a means to defer upgrades to distribution substations, and as a reduction to transient and customer peak demand. All combined, the benefits identified for NaS-P_{AC} systems amounted to \$14 billion over the next 15 years.

Rather than have the customer accept the risk of peak clipping, it might be more acceptable to allow the utility to dispatch the power to meet its system peak. The on-site storage, then, can provide power quality/reliability as a net benefit to the customer. This is one way of insuring lower cost premium services, a goal that utilities today are trying to meet in order to remain competitive.

The 300 kVA Modular Design

Prior to the program start in 1991, large utility battery projects, such as the 10 MW/40 MWh SCE facility in Chino, CA, and the 5 MW/10 MWh BEWAG facility in Berlin, Germany, stood as working BESS showpieces. These BESS's were designed for utility load leveling, frequency control and spinning reserve. The magnitude of the large battery projects required the coordination of battery, power converter and control electronics manufacturers, as well as the design and site engineering firm that managed the project. Moreover, the risk associated with integrating such capital intensive projects could be an impediment to the successful introduction of BESS.

To circumvent these issues, SPI proposes that modular (300 kVA/300 kWh) units be assembled and transported as "turn-key" systems which utilize state-of-the-art power inverters from the UPS industry and sodium sulfur batteries similar to those being developed for electric vehicles (EV's). The result is a very compact package designed to facilitate transport with a visual appearance and size commensurate to a standard commercial power transformer. The systems are targeted for use with the applications noted above and can simultaneously serve a number of other functions, including insuring power quality and reliability. Unlike the large BESS projects, these modular systems can provide a dispatchable source of distributed power close to the load that allow better load management. By so doing, a utility can operate more efficiently and serve its customers better.

The latest sodium sulfur EV batteries from Silent Power, Ltd. (SPL) still offer excellent energy density but have been redesigned to provide a power density that now exceeds the USABC Mid-Term EV battery goal. The following performance has been measured for a 28 kWh prototype battery developed for a specific EV: 115 Wh/kg, 150 Wh/liter, 240 W/kg and 310 W/liter. Consequently, the sodium sulfur BESS offers application flexibility in that a single design can be developed to provide both high power pulses for power quality/reliability and also sustained power for peak shaving and extended outage protection.

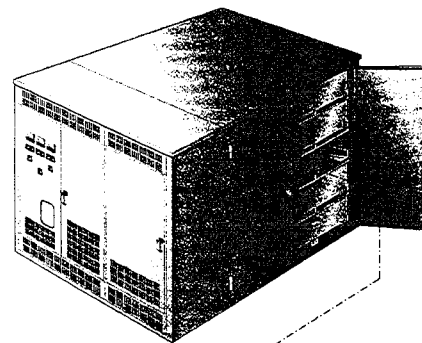
Since the sodium sulfur battery must be kept thermally hot in order for the electrochemical reactions to take place, the system must be well insulated and, in addition, possibly cooled

for high rate discharge applications. This has been highlighted as a disadvantage by opponents of high temperature battery technology due to the associated cost, volume and weight. For the stationary outdoor application, however, this perceived penalty is an advantage because the cooling system is able to efficiently reject heat from the inverter and the battery during sustained power discharge and the insulation system allows the BESS to be ambient temperature insensitive. The compactness of NaS-P_{AC}, then, is due to the nature of the battery, the number of batteries required to insure warranted life, and the efficient cooling design. The end result is a complete system that is five times smaller and three times lighter than a lead acid based system with a comparable energy content. Importantly, sodium sulfur batteries are expected to be warranted for 5 years, independent of the number of cycles, in a sealed maintenance-free package. As a result, SPI believes that these features will enhance customer siting opportunities and acceptance.

The 300 kVA/300 kWh modular system design that was developed during the program is depicted in the adjacent artist's drawing. An entry market product such as this would use a 300 VDC, 40 kWh EV battery design. Ten battery packs, connected two in series by five in parallel, fit conveniently behind the 2.3 m (7½') high by 2.1 m (7') wide face area of an available 300 kVA power conversion system (PCS). The attached structure was designed to support and access the battery packs for eventual on-site replacement.

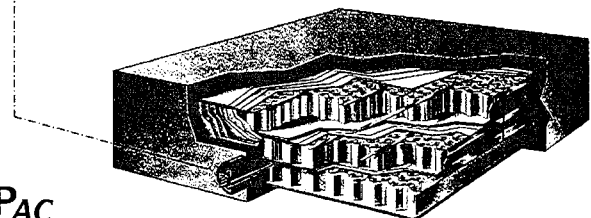
The NaS-P_{AC} system was designed to deliver up to 1 hour of continuous power in a single package. An option exists to add-on a modular block for an additional hour of service that may be required for specific applications. To lower system cost, the battery management system (BMS) function was integrated into the existing power conditioning system (PCS) digital processor control.

NaS-P_{AC} Modular Battery Energy Storage Unit



- 300 kW, 480 VAC, 3 Phase Power Converter
- Multi-battery Options for Pulsed and Continuous 1-2 Hour Operation
- Pad Mounted and Ready to Use
- Dimensions: 7'W x 7.5'H x 8'D
- Weight: 16,000 lbs.

- 40 kWh, 240-320 VDC
- Sodium Sulfur Technology from Silent Power, Ltd.
- Sealed
- No Maintenance
- Self Contained Electrical and Thermal Management



NaS-P_{AC} Replaceable Battery Pack

The projected selling price for the 300 kVA/300 kWh NaS-P_{AC} was developed from quotes furnished by the suppliers of the individual components; these included the battery, the PCS, the support structure, and associated electrical components; additionally, the effort to assemble and qualify the BESS was estimated and costed in detail. A costing study based upon the first stage of commercial production had been performed by SPL for a

40 kWh EV battery; for a production volume of 10,000 batteries per annum, a price of \$245/kWh is projected. As the EV market grows to 100,000 batteries per annum, the price is expected to decline to less than \$150/kWh. The rationale for using EV batteries is that a market of this size would determine production investment decisions. Combining manufacturing volumes of a common EV/BESS battery will benefit the sodium sulfur BESS in that lower battery prices will be available when the NaS-P_{AC} is first commercially introduced and prices will then decline in the subsequent years.

The price of the specified 300 kVA bi-directional inverter was quoted as \$260/kW in limited volume, approaching \$180/kW for larger quantity orders for the fully mature product. The PCS was specified to be self-commutated, using insulated gate bipolar transistor switching and pulse width modulation control with four quadrant operation capability. It also included event storage and remote access for status and maintenance, features that are available on high end UPS equipment today. With this capability, the BESS deployed throughout the country can be accessed, interrogated and even serviced from a single location. The controller includes a user friendly interface which will permit a utility to dispatch the power according to their specific protocol.

The total system selling price for the NaS-P_{AC} is \$189,000, or \$630/kW (also, \$630/kWh). At higher production volumes, it is estimated that this price would be reduced to \$428/kW. At this lower level, the system is competitive with today's low emission diesel and small gas turbine generator sets. The distinct advantages, however, for the sodium sulfur BESS are its instantaneous availability, quiet operation, air quality benefits, and small footprint.

For the customer peak shaving application where the utility demand charges can be as high as \$17/kW, the payback period on the purchase of a NaS-P_{AC} system is 3 years, assuming that the peak is clipped each month. A net present value (NPV) analysis was undertaken, which assumed an after-tax discount rate of 7.0%, battery replacement every 5 years, and a proper accounting for energy losses. The return on this investment (ROI) is 30% with an NPV of \$500,000 over the 30 year life of the investment. The ROI declined below 15% for cases in which the amount of storage had to be increased to 2 hours.

Alternative BESS Designs

In addition to the 300 kVA modular size, SPI developed designs for smaller systems that might be more appropriate for some commercial and residential applications. The smaller size classes include 30 kVA (50 kVA peak) and 3-4 kVA, each with 2 hours of useful storage. The larger unit contains two of the 28 kWh EV batteries and includes a fully integrated PCS with similar features as the 300 kVA design. The 30 kVA system could serve multiple functions by storing off-peak energy and providing peak power, providing outage protection and power quality, or serving as a storage unit for a renewable application. The advantage of the design is again its compactness, being only 1.1m tall with a total volume of 1.24 m³. This 30 kVA BESS is estimated to cost \$31,500.

The smaller 3-4 kVA system is proposed for dispatchable service to a residential heat pump/air conditioner, possibly in a utility demand side management program. The unit

would store off-peak energy to drive a heat pump for 4 hours during the utility load peak. A 24 VDC cylindrical sodium sulfur battery design was developed specifically for this application. Four of these cylindrical batteries are employed in the system design to provide 48 VDC, which is converted to 120 VAC/208 VAC, single phase. This system was conceived as a possible add-on to a 3 ton residential heat pump, permitting utility dispatch as well as providing outage protection for the home. The expected price for this system is \$5000, but, in volume, this price could conceivably be reduced to \$2700.

Battery Component Development

Development of battery components for a sodium sulfur BESS comprised a major portion of the overall program effort. Development of a sodium sulfur cell specific to the BESS application was the primary focus, but effort was also devoted to improving the design of the battery core and the thermal management system.

An activity was undertaken to develop a cell larger and longer lived than what was being developed by Silent Power for the EV application. The design goal for this cell was 60 Wh and a 10 year life. With such a cell, the first cost of the battery and its life cycle cost would be significantly reduced, stimulating rapid market growth following the early introduction period during which the low risk – financial and technical – approach of having utilized the EV product was taken. In order to show technical feasibility of this c/S cell design, freeze/thaw durability, cell safety, and performance reliability had to be demonstrated. These objectives were satisfactorily accomplished, though a number of issues remain to be resolved before the cell is ready for commercial production.

The cell development task began with a preliminary design which was loosely based on an earlier c/S cell design, designated as the TD cell, which had been developed and tested at SPL. A build of 15 of these cells have been the longest lived sodium sulfur cells ever fabricated by Silent Power; they had lifetimes exceeding eight years. The major differences between the preliminary c/S cell design and the TD cell design were the configuration of the electrode seals and the sodium reservoir. Both changes were introduced to reduce the volume and eventual manufacturing cost of the cell. During the course of the program, a number of component design changes were incorporated into and tested in the preliminary design. During this developmental effort, approximately 145 preliminary cells were fabricated and tested. A large part of the developmental effort was devoted to developing a sodium electrode seal which was not susceptible to environment assisted cracking. Several current collector coating materials were evaluated in an effort to find a non-chromium bearing material which would perform at least as well as nichrome. Other developments were enhanced safety features and an improved method for filling cells with sodium. At the end of the cell component development effort, the best component designs and materials were incorporated into the prototype design for fabrication and testing of a number of nearly identical cells.

The total number of prototype cell builds initiated was 125. Of these, 25 failed at various points during the fabrication process, and 55 of the cells placed on test failed as a result of latent fabrication defects. Of the combined fabrication and latent defect failures, 35

were associated with sodium electrode seals and 37 were associated with sulfur compartment final closure welds. Forty-five prototype cells were tested for freeze/thaw durability, safety verification, and beginning-of-life performance.

The freeze/thaw test results of the prototype cells far exceeded the goals set at the beginning of the program. The goal was to expose each of 10 cells to 10 freeze/thaw cycles without any failures occurring. In the group of ten prototype cells tested, all ten survived a minimum of ten thermal cycles without failure. In fact, throughout the program, no cells failed during freeze/thaw cycling as a result of electrolyte fracture. Several cells were also subjected to a number of freeze/thaw cycles in the fully discharged condition without failure. No goal had been set for this test condition, but this testing was added following the initial successes, for it is viewed as being the most severe freeze/thaw condition; prior experience with larger, central sodium cells at Silent Power showed that cells did not survive thermal cycling in the fully discharged state-of-charge.

The results of the safety testing did not fully meet the goal initially established for safety during electrolyte fracture. The goal was that the temperature of the cell remain below 500°C following the intentional fracture of the electrolyte and that no breach occur in a population of ten cells tested. Only one of 15 prototype design cells breached its container, but three of the cells did experience temperature excursions over 500°C following fracture of the electrolyte.

The 20 remaining prototype cells were electrically cycled to evaluate their early life performance. At the close of the program, eleven cells had completed over 200 cycles and their performance was stable. Most of the cells required between 50 and 100 cycles before their resistance and rechargeability stabilized. The resistance of many cells was over 30 mΩ at the beginning of test, but after break-in, the average resistance of the eleven cell sample was 13.2 ±2.3 mΩ compared to the design goal of 12 to 13 mΩ. The rechargeability of the cells was generally good during the first few cycles, with acceptable average unrecoverable capacity values of 8.7 ±2.2% of theoretical.

More work needs to be done to optimize the cell design and fabrication processes in order to improve manufacturing yields, to reduce the number of latent defect failures, and to attain acceptably low manufacturing costs. If at some time in the future the decision is made to commercialize batteries with c/S cells, a number of cell issues need to be resolved. Among the most important of these are: thermocompression bond seals, final sulfur compartment closure welds, cell safety, and cell life.

Battery component development was directed toward design options that promised to be lower in cost or more efficient than the present EV related designs. For the stationary BESS application, the battery size and weight design constraints can be relaxed relative to the EV design. Therefore, specific battery development was undertaken to tailor the design to lower cost features. This included eliminating an evacuated thermal enclosure in favor of using conventional low cost insulation. This also simplified the power feedthrough design and eliminated the cost of bellows and a fully welded assembly. In

place of an active oil cooling, a passive design using a low cost salt eutectic (KCl-LiCl) was located in the free interstitial space between cells and was used to limit cell temperature rise during sustained discharge periods. To improve the heat transfer, cells and salt capsules were bonded together into a matrix using a ceramic (MgO) cement. Tests with cell strings proved the superiority of this cement over more labor intensive isolation approaches. Utilizing the volume available between cells to store the salt extends the battery full power discharge period by approximately ½ hour.

Deliverable Module

All of the above battery component developments were included in a 32 VDC, 13 kWh prototype battery module that was delivered to SNL for testing. Since the development status of the c/S cell was immature, it was decided to utilize EV cells fabricated at the SPL pilot plant for the module build. Cell strings received from SPL were dipped in a MgO slurry, air dried and assembled along with the thermal energy storage capsules into bank halves. Each half bank was made-up of 24, 4-cell strings. The entire half bank was then dipped in the MgO slurry to complete the rigidized matrix. Rather than impose an additional thermal cure, the banks were allowed to air dry before final assembly. The completed module was then assembled from four series connected banks.

The battery and its attending BMS completed a series of break-in tests at Sandia National Laboratories. The initial performance of the battery met expectations for available capacity (460 Ah) and internal resistance (13.1 mΩ). Shortly after break-in, the battery began to rapidly lose capacity, and testing was discontinued after five months and 133 cycles. A post test analysis of the battery showed that the rapid loss of capacity was mainly due to a high number of failed strings comprised of cells from a single manufacturing lot. The rate at which the battery capacity declined was aggravated by the fact that cells from the three manufacturing lots were not uniformly distributed throughout the battery. Had this been done, the life of the battery, defined as the point at which the battery was no longer able to deliver the rated capacity of 400 Ah, would have been somewhat longer.

Conclusions

The program was successful in its efforts to produce a modular sodium sulfur BESS design that is compact, transportable, and cost competitive. Through several outreach activities, a number of utilities, each with specific problems, were attracted to the technology. The NaS-P_{AC} system prices developed in this study appear to be in line with utility investment criteria. What remains is to work with a few select utilities in order to develop a design and control algorithm that addresses their immediate needs.

The larger cell development activity, though not totally successful, did make significant advances in the technology and can be picked-up and re-introduced at a later time when profits from the sale of BESS's are sufficient to allow for product development.

Overall, this program was completed at a cost less than the \$4.1 million contract value, on-time, and the milestones and deliverables having been met.

I. Introduction and Program Plan

In August 1991, Silent Power, Inc. (SPI) was awarded a \$4.1 million cost shared contract by the Department of Energy (DOE), Office of Utility Technologies, to perform application and design studies and to provide engineering development of an advanced (sodium sulfur) battery energy storage system directed toward the utility market. The program, which was directed by Sandia National Laboratory (SNL), Storage Batteries Department, was part of a broader DOE program to develop battery storage systems for utilities and utility customers that offer national benefits in regards to more efficient use of natural resources and improved air quality. This contract was cost shared by SPI at 22%.

The program that SPI undertook was divided into four technical tasks:

- Task 1 - Utility Applications Assessment
- Task 2 - Utility Energy Storage (UES) Cell and Battery Development
- Task 3 - Assembly and Test of a Prototype Battery
- Task 4 - Battery Energy Storage System Design and Cost Development

The tasks were organized so that the output of Task 1 could be utilized to drive the design and development tasks that followed. The Task 1 activity, in coordination with the SNL sponsored Battery Systems Opportunity Assessment sought to determine utility applications in which sodium sulfur batteries, with their high energy density, offer significant advantage. Several applications were selected as a basis for the battery design and development performed in Task 2 and for the full scale system design in Task 4. Task 3 provided a representative battery deliverable that showcased the performance features of a cost effective design that are believed necessary for UES applications.

Tasks 1 and 4, in particular, were highly interactive, resulting in a modular system design, termed NaS-P_{AC}. Consequently, these activities are discussed consecutively in this report. The bulk of the hardware effort (Task 2) developed a larger*, low corrosion cell configuration that is believed necessary to provide the required life and cost in order for this technology to be competitive compared to alternative storage and generation systems. The following sections describe the work that was accomplished on this program.

* As compared to the 10Ah PB cell.

II. The Silent Power Sodium Sulfur Battery

As background to the implementation of this Program, it should be recognized that Silent Power has been developing the sodium sulfur battery over the past 20 years primarily for the electric vehicle market. This experience base has been utilized in order to take advantage of demonstrated battery reliability and safety as well as manufacturing economies that can be realized during the early stages of product introduction. The Program therefore builds upon this extensive design and manufacturing base established for the electric vehicle market.

A well known attribute of the sodium sulfur battery has been its excellent energy density. Batteries built using cells manufactured in a semi-automated pilot plant in the early 1990 time frame had energy densities approaching 100 Wh/kg. This technology was directed toward a delivery van application, and power was therefore not a design driver. As a result of the USABC goals, improved power capability was dictated. Silent Power re-designed the cell, which is shown in Figure 2-1, to achieve a specific power at the battery level of 240 W/kg; this is twice that of the earlier design. There was also an accompanying improvement in the specific energy; it increased to 117 Wh/kg. Figure 2-2 illustrates that the performance of this high power sodium sulfur battery now exceeds the Mid-Term USABC goals.

Batteries employing this improved technology have been built and demonstrated in vehicles. A cutaway of a 40 kWh sodium sulfur battery is depicted in Figure 2-3.



Figure 2-1. The New High Power 20Wh Sodium Sulfur Cell from Silent Power

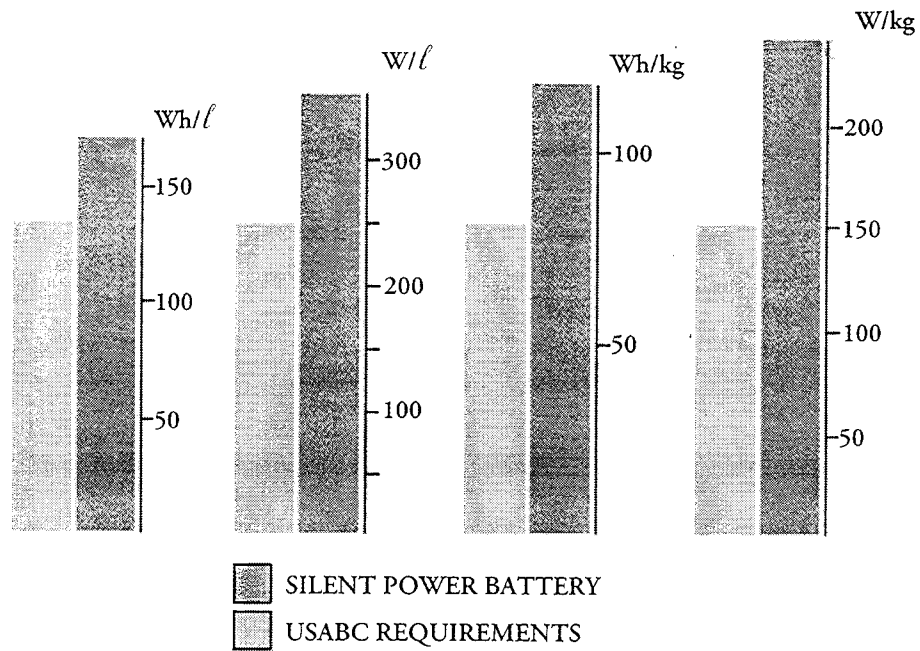


Figure 2-2. Performance of SP Batteries Relative to the USABC Mid-term Requirements

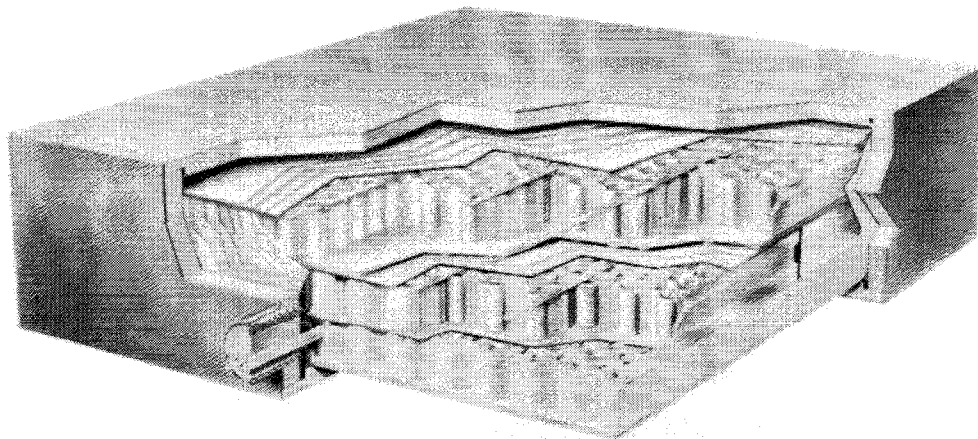


Figure 2-3. 300 VDC, 40 kWh, Sodium Sulfur Battery from Silent Power

The battery is comprised of approximately 2000 "small" cells. Each cell fully contains the liquid sodium and sulfur reactants in a hermetically sealed enclosure. A solid beta alumina ceramic tube is the electrolyte, separating the two reactants. The cell electrochemistry is exceedingly simple, involving sodium ion transport through the ceramic and subsequent reaction with sulfur to form sodium polysulfides. The reaction takes place within a temperature range of 320 °C and 350 °C. Favorable characteristics of this cell are a flat EMF of 2.074 volts for 80% of the discharge and a 100% columbic efficiency.

The cells are arranged in a series/parallel network to obtain the desired battery voltage and capacity. For the 40 kWh battery shown, 14, 4-cell strings form planar banks; 40 of these 8 volts banks are then connected in series. The banks are cast into a "cement" matrix to form a component that will carry the internal loads and is handable for the assembly of the battery. The cast matrix material also provides a redundant safety feature in that it can absorb and "trap" any cell effluents in the event of breaching. Between the two planar layers are cooling plenums. The battery's active cooling system is designed to allow for a 1 hour continuous discharge; this is a USABC requirement. However, it also provides the capability for a quick cool-down of the battery so that it can be recharged immediately following a fast discharge drive or in the event of an anomalous operation.

Being a high temperature battery, an effective thermal insulation is required to maintain the battery at operating temperature. Furthermore, volume is a critical design driver for the EV application, so a "high tech" solution employing a double skinned evacuated enclosure has been developed. This enclosure is evident in Figure 2-3.

The sodium sulfur battery described above is the present state-of-the-art of the technology. Furthermore, it is the basis for the design of the BESS (Task 4) which would be initially introduced into the market place. The prototype battery which would be built and delivered to Sandia utilized the "low" power cell technology that was still being manufactured in Silent Power's pilot plant during the early years of the program.

III. Utility Energy Storage Applications

One of the most dynamic aspects of the Program has been the evolving understanding of the potential uses for Battery Energy Storage Systems by utilities or through utilities to their customers. In its original proposal, Silent Power, Inc. intended to use this task as a means of selecting an appropriate utility application as a basis for battery component development, system design, and, finally, for a future demonstration of its technology. The approach was to develop preliminary battery system designs for three utility applications, to cost these designs, and then to make a decision as to which design to pursue in detail. In actuality, what occurred was somewhat different in that the application's assessment and the design activities were highly interactive and were performed in parallel. This section describes the work which was performed to identify the utility applications and to specify the requirements for the sodium sulfur BESS which provide the most attractive cost benefit.

3.1 Modular Integrated System Approach

SPI recognized early in the implementation of Task 1 that modular, utility class (200 to 500 kVA with 1 to 2 hours of storage), integrated battery-inverter systems offer a very important ingredient missing in most, if not all, of the large 10 to 20 MW demonstration projects that are presently operating. The modular design offers a "turn-key" system, meaning a fully self-contained system that integrates the operation of the battery with the power electronics and controls. The BESS operation would be verified at the manufacturer's facility so that commissioning could be completed shortly after arrival at site. Having one or, at most, two manufacturers involved in the production of a complete system is a definite benefit. The large BESS projects involve separate manufacturers of specialized components with the system integration burden falling on the shoulders of the utility or a designated A&E firm.

For SPI, the modular system approach is consistent with its current battery manufacturing limitations. Previously, SPI had completed battery engineering studies -- *Core Technology Program* [1] and the *EPRI Phase P - Commercialization Planning Program* [2] -- which had considered large 100 MWh battery plant designs. The present Program provided an opportunity to reassess the battery system design in light of the realities of present manufacturing capabilities, while offering the potential for reduced cost by eliminating the need for custom (purpose built) designs.

Modular integrated systems offer convenient transportability in that they can be sized for overland truck transport and/or shipped in a seabox. A utility or large customer site might require many such modular systems to fulfill its needs. In principle, the BESS comprised of several modular units operating in parallel appear to offer better reliability than a system comprised of one or two large power converters, fed by a few battery strings, all of which are critical to the operation of the battery plant. There are economic and technical limitations as to how large of an installation (capacity) which can be satisfactorily addressed by these modular systems. Certainly, they are appropriate for loads requiring

1 to 2 MW, but, at the 10 MW level, modularity is likely to result in a higher overall system cost; however, this penalty may be justifiable in order to achieve higher system reliability.

Distinctions between modular integrated and large BESS are the functions that each would serve and where they might be located. Large systems can be designed to "catch" generator outages so as to prevent voltage and frequency sag; in this way, they would provide the "ride-through" time necessary for the electrical system to compensate without having to shed load. This situation is more apt to occur in stand-alone grids, such as island electrical supply, rather than on the mainland where utilities are interconnected to stiffen the overall system. The large systems are appropriate for transmission stabilization and spinning reserve functions. In these cases, the BESS is likely to be located in close proximity to the transmission line and central to the participating utilities. Important to recognize is that the large systems are centralized under the direct control of the utilities and are strategically located to serve the utility interest.

The modular systems, as are being proposed, are located close to the load – i.e., at a distribution facility, substation or customer site. This is the basic concept of a distributed generation/storage scenario. As depicted in Figure 3-1, BESS could serve industrial and commercial customers with non-polluting, on-site power and, in the future, provide storage for residential solar applications. The value of storage, however, is dependent on its benefits as compared to other competing technologies. A unique feature of battery systems is their instantaneous response; whereas, diesel and gas turbine generator sets require a finite period of time to start-up and to accept load. Although the start times for these devices have been improved, it is unlikely that stable operation can be achieved in seconds. Therefore, battery powered systems will always maintain this advantage.

Discussions with utilities have revealed that, in order to be competitive with diesel generators for substation peaking power, a hurdle price of \$350/kW is required. In some cases, there is an opportunity for 5 hours of load leveling to handle the summer air conditioning load, provided the price of the system is less than \$475/kW. It will be difficult for BESS manufacturers to achieve these cost targets. Unfortunately, the price of a BESS includes a significant capital cost component which is directly attributable to energy or operating duration. For the combustion systems, this is handled as a fuel charge or operating expense. As long as the fuel remains inexpensive, abundant, and imposes no pollution penalty, BESS will remain a niche market. Given a mature market, one can attempt to estimate the maximum amount of storage that will allow a BESS to compete with combustion equipment. In the following equation, the right-hand side contains the costs associated with power, energy and miscellaneous items comprised of housing and

$$\text{Hurdle Price} = \$200/\text{kW} * P + (1.25) \$150/\text{kWh} * P * T + \$50/\text{kWh} * P * T$$

structure and battery related electronics, respectively. The battery portion contains a factor of 1.25 to include the effects of aging – i.e., the manufacturer could oversize the battery capacity initially to allow batteries to degrade by 20% before replacement. Inspection suggests that the \$350/kW hurdle could be met if the system provided less than 1 hour of battery storage. What is acceptable based on relative economics, however, may

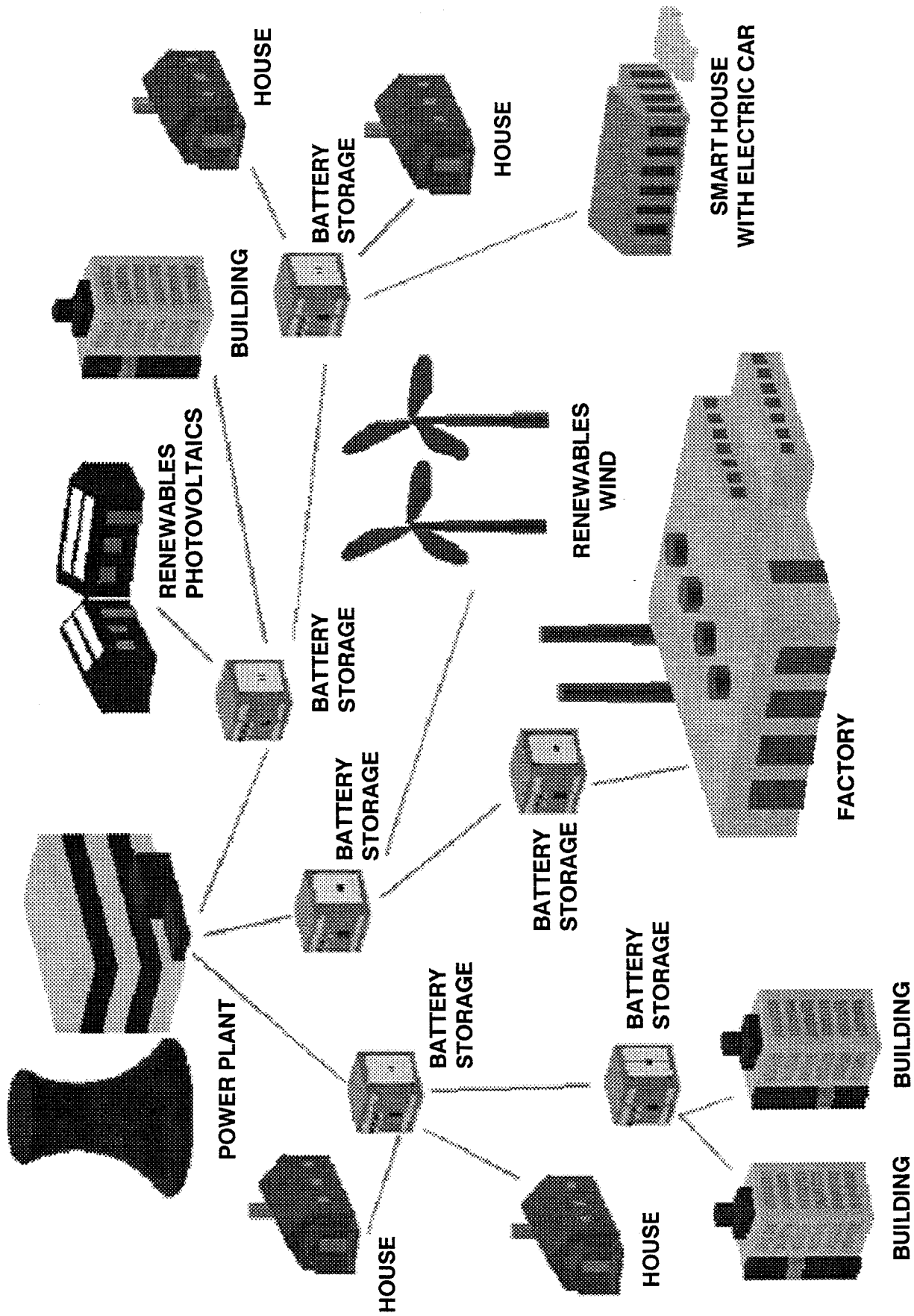


Figure 3-1. Distributed Utility Battery Energy Storage Opportunity

not be relevant to what can be tolerated in the application. If the application required 2 hours at rated power, the cost of the BESS at \$675/kW would not be acceptable unless an instantaneous response time was mandated. If it is important not to be tied to the limits set by installed battery capacity, a hybrid system employing both batteries and a thermal generator may be a viable alternative. The battery capacity would be sized only to allow sufficient time for the generator to stabilize and to accept load; this may be only 15 minutes. The mature cost of such a hybrid system, however, is likely to be \$550/kW and could be higher based on system control complexity. At this price, one could afford an all-battery design with 1.5 hours of storage.

3.2 Opportunities Assessment

In order to characterize the capabilities and opportunities for BESS, DOE through SNL conducted two Opportunity Assessment forums with battery manufacturers, system integrators, utilities, and industrial consultants. The output from these forums was the identification of viable utility-related applications for BESS and a preliminary definition of their benefits and costs.

One of the outputs of the Opportunities Assessment was a set of weekly load profiles representative of mutually compatible applications. The premise was that enhanced benefit would result from addressing several combined applications that could be met with a single BESS design. Increased benefit also implied the potential for increased allowable system cost. It has been SPI's experience, however, that some utilities make purchase assessments based on a single application and that attempts to enhance benefit by combining applications is interpreted to mean that the technology is not cost effective. This view may be a direct result of present day utility structure – one perhaps constrained by compartmentalization. According to one utility, if the customer is the primary beneficiary, then the system cost must be in-line with the customer's investment criteria. This attitude may be changing with the threat of competition among utilities. Utilities are recognizing that they will have to offer lower cost services and increased service options in order to retain their important customers. Perhaps there is a role for BESS in this competitive environment based on mutual benefits in this new era of cooperation between utilities and their customers.

The results of the two Opportunities Assessment forums are summarized in a Sandia report [3]. The discussion that follows draws from this report but highlight, in particular, SPI's input into this report.

A list of applications was compiled along the lines of traditional utility components – viz., generation, transmission and distribution (T&D) and customer service. Specific applications, where BESS might offer benefit, were identified under each category; these include spinning reserve, capacity deferral, area/frequency regulation, load leveling and renewable applications identified under generation. For each specific application, seven parameters were listed as characterizing the needs of the application. These included:

Power
Storage Time
AC Voltage
PCS Type
Annual Utilization
Footprint
Portability

Table 3-1 summarizes the requirements for each application identified according to the input from Opportunity Assessment participants. The first three parameters characterize the size and cost of the BESS to serve the specified application. The converter (commutation) type relates to the complexity and cost of the PCS portion of the system cost; in manufacturing volumes, however, this is not expected to be a significant factor. Utilization (cycles/year) is an important issue for those battery technologies whose life is cycle limited. Time-at-temperature (calendar life) is the more important factor in establishing the life of high temperature batteries and not the number of charge/discharge cycles. However, this parameter (cycles/year) may be useful as a measure of annual value or benefit, since, for applications in which the BESS is dedicated, the expected benefit is proportional to utilization. The final two parameters – footprint and portability – are desirable features; they may offer flexibility in the siting of the BESS which could be an overriding consideration in the decision to go forward with the capital project by the utility. For utilities, portability implies that the system can be transported to a substation site according to the seasonal demand. In principle, both of these features can be related to an installation cost savings.

There are other parameters that could have been included in the list, such as turn-key system and outdoor deployment. The benefit to the utility of having a turn-key installation was discussed earlier in this section. A BESS that can operate effectively independent of ambient conditions will reduce capital costs, for an environmentally controlled building will not have to be provided. It will also eliminate, or substantially reduce, the costs associated with engineering design, permitting, and site work; all of these are major factors in the overall installed system cost.

Advanced battery systems, such as sodium sulfur, offer certain advantages depending on the application. Sodium sulfur batteries provide excellent energy density and high electrical efficiency with good power characteristics. BESS based on these batteries have a definite marketable advantage over lead acid systems for applications which demand 1 to 2 hours of storage. Applications that require ½ hour or less of storage are probably served more favorably by lead acid BESS, flywheel energy storage systems or SMES systems. On the other end of the spectrum, technologies such as pumped hydro and CAES provide long duration storage (5 to 9 hours). Application of these technologies is constrained due to the availability of suitable sites for storage and environmental factors that tend to limit operation. When compared to other storage technologies, the siting flexibility and the instantaneous response of BESS are strong attributes that provide attractive benefits.

Table 3-1. Summary of Utility Energy Storage Application Requirements

Applications	Approx. Power (MW)	Approx. Storage (hr)	AC Voltage (kV _{ac})	Converter Type	Cycles Year	Footprint (Importance)	Portability (Importance)
Generation Applications							
Spinning Reserve	10-100	0.5	12-138	Line	20-50	Medium	Low
Capacity Deferral	10-100	2-4	12-138	Line	5-100	Medium	Medium
Area/Frequency Regulation	10	<1	12-138	Line	250	Low	Low
Renewables Applications	1	1-4	0.48-12	Line	250	Medium	Low
Load Leveling †	100	>4	69-765	Line	250	Medium	Negligible
Transmission & Distribution Applications							
Transmission Line Stability	100	<0.01	69-765	Self	100	Medium	Low
Voltage Regulation	1 (MVAR)	<0.25	12-34.5	Self	250	High	High
Transmission Facility Deferral	10	2-4	12-138	Line	5-20	High	Medium
Distribution Facility Deferral	1	1-3	4-34.5	Line	30	High	High
Customer Service Applications							
Demand Peak Reduction	1	1-2	0.48-12	Line	50-500	High	Low
Transit System Peak Reduction	1	1-2	0.48-2.4	Line	250-500	Medium	Low
Reliability & Power Quality (< 1MW)	0.1	<0.25	0.48	Self	<10	High	Low
Reliability & Power Quality (> 1MW)	1	1-2	0.48-12	Self	<10	High	Low

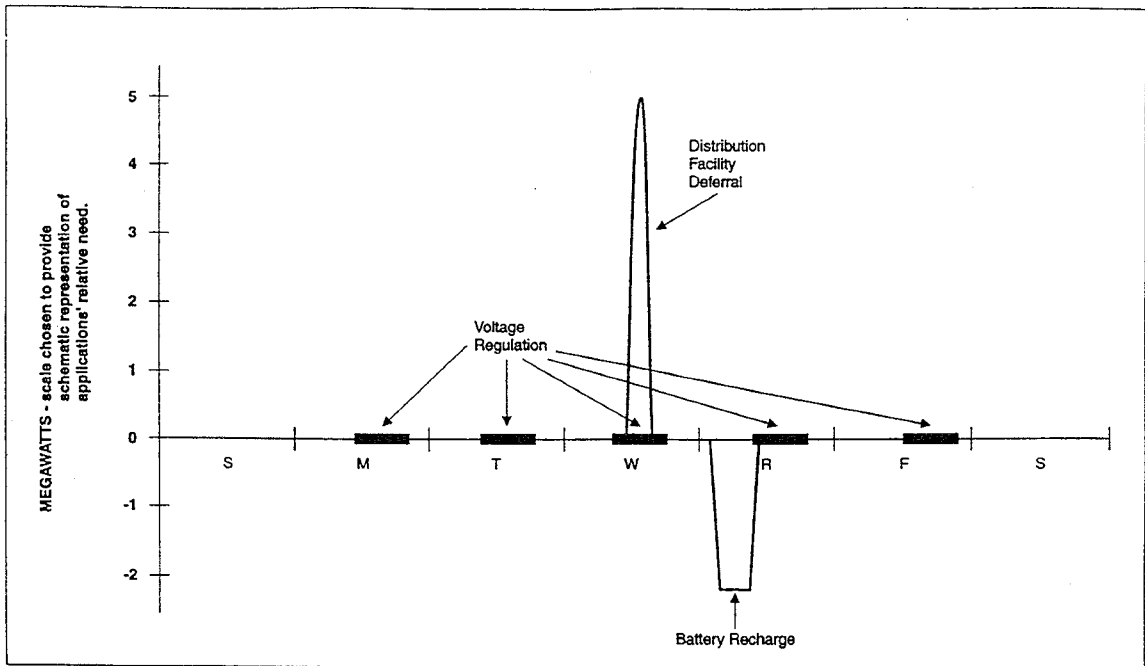
In assessing its position with regard to the applications identified in Table 3-1, sodium sulfur batteries can offer significant size (footprint) and weight savings over a lead acid based BESS. As a result, it makes for a more transportable system in the 500 kVA/ 500 kWh minimum utility power block size. Additionally, since each battery is already burdened with its own thermal enclosure, outdoor operation is facilitated. To reduce the parasitic load associated with maintaining battery temperature, applications which regularly utilize the BESS should be pursued; those applications which have frequent and/or long stand times between use periods will not offer a cost benefit. If the system is used daily, there is essentially no thermal parasitic load; otherwise, for each day of non-use, 7% of the stored energy must be used for maintaining battery temperature. Since the system is connected to the electrical grid, this make-up heat is provided automatically. Offsetting this loss relative to lead acid systems, sodium sulfur batteries do not have any self discharge.

Since sodium sulfur batteries are sealed modular units of a size suitable for EV applications (typically, 40 kWh at 300 VDC), is no on-site maintenance that can be or needs to be done. The current plan is to warrant these batteries for 5 years, independent of cycling history, and to replace them on site at that point in time. Finally, and perhaps most importantly, SPI recognizes a limitation due to its present battery manufacturing capability. Since batteries are being developed by SPL for the post-2000 year EV market, high volume, automated production facilities are not yet in place to serve near term battery needs. As a result, SPI has limited its early BESS designs to small modular turn-key systems requiring a relatively few number of batteries supplied from a pilot plant manufacturing facility.

In summary, applications which meet the following criteria listed appear to be most favorable for sodium sulfur based BESS:

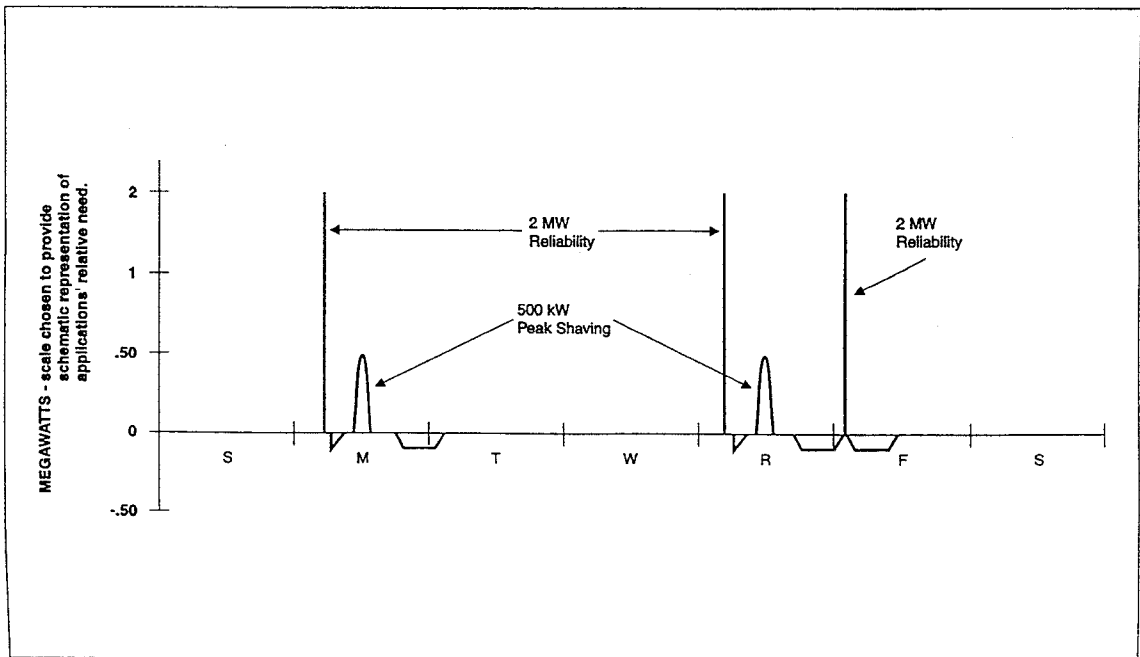
- 2 MW or less
- 1 to 2 hour Duration
- Low Voltage (0.48-12 kV)
- Daily Utilization
- Small Size (Footprint)
- Portability
- Outdoor Operation
- Maintenance-Free Operation

In reviewing the potential applications listed in Table 3-1, a good fit for sodium sulfur is storage for renewables, distribution facility deferral, demand and transit system peak reduction. In order to enhance the overall benefit, several single applications were combined into a group of realistic power profiles characterizing the generation, distribution and customer-side demands. Of these, Group II (Figure 3-2): Distribution Facility Deferral and Voltage Regulation, and Group III (Figure 3-3): Customer Reliability and Peak Shaving, were identified as good candidate applications for sodium sulfur.



Utilities with Voltage Regulation needs in the ones-of-megawatts can add this application to batteries installed for Distribution Facilities Deferral by making small increases in battery and inverter sizes to allow delivery of VARs during maximum discharge of WATTS.

Figure 3-2. Combined Application II: Distribution Facility Deferral and Voltage Regulation



This example illustrates a particular case in which a utility employs a battery system to meet a 500 kW/2 hr Peak Shaving Demand and to ensure power reliability to 2 MW for durations of seconds to 15 minutes. Although a fault is instantaneous, and requires only seconds of ride-through, facilities with safety specifications that require manual reset after a fault may require minutes of storage.

Figure 3-3. Combined Application III: Customer Reliability and Customer Demand Peak Shaving

Using the results of the Gateway Study – *Battery Energy Storage: A Preliminary Assessment of National Benefits* [4], the national market size and benefits were estimated to the year 2010 for each of the applications identified. In addition, a list of competing technologies or measures were identified that could be used to fulfill the need. The T&D benefit, at \$39 billion, offers the largest benefit with deferral of lines and transformers as the single largest entry. While this was not a good candidate application for sodium sulfur, the combined market benefit for applications attractive to sodium sulfur amounted to a total of \$14.3 billion, or 25% of the total cumulative benefit for all applications.

3.3 Utility-Industry Outreach

Over the course of the program, SPI developed and distributed two brochures (the first was released in November 1991 and the second in November 1994). The purpose of these brochures was to assist utility planners, engineering staff and decision makers in understanding, in general, the benefits of battery energy storage and, specifically, the advantages of a “turn-key” sodium sulfur based BESS. The intent was to help potential users envision how such a system might be deployed in their service territory, how it might look, and what it might cost. Since the NaS- P_{AC} system is not a product that is presently available commercially, the representation in the brochure was meant to attract attention, solicit a response, and provide feedback as to the potential size of the UES market. These elements were all part of the UES Applications Study (Task 1). What follows is a chronology and description of the development of each of these brochures within the context of the program.

The earlier brochure is presented in Appendix A. It was based on a 500 kVA/500 kWh modular (stackable) ACUnit, comprised of a 480 VAC power converter (PCS) and sodium sulfur battery packs designed specifically for this UES application. At the time, the PCS was considered to be an “off-the-shelf” item; – i.e., equipment that was available from manufacturers of power inverters and UPS systems. For the two applications examined in the brochure, a simple (low cost) line commutated inverter was adequate, since the electrical grid could provide the commutation. The price of the inverter was quoted at \$200/kW in low production volumes, reducing to \$150/kW in production quantities, depending on the details of the specification.

The 500 kWh battery was comprised of four sealed, series connected, sodium sulfur battery packs, each with the capability of delivering 150 kWh at a nominal 200 VDC. The voltage window of a single pack was specified at 240 to 170 VDC, which is the range from full charge to discharge at a 2 hour rate. The battery pack was made up of 70 Wh cells (discussed in Section V), designed and developed by SPI specifically for the UES application. The rated power response was shown in graphical form to demonstrate operation under conditions of steady load duration ($\frac{1}{2}$ to 5 hours). This duration was limited thermally (maximum temperature) for high rate, short duration discharge and by rated capacity for the long sustained duration.

The brochure concluded with examples of two applications; these being the PREPA 20 MW/4 MWh frequency control/voltage stabilization and spinning reserve application and a transit peak shaving application. The examples demonstrated that a BESS based on the use of modular ACUnits with sodium sulfur batteries have the potential to significantly decrease the system footprint and the cost for these applications.

The later brochure, included in Appendix B, was developed as a realistic pre-commercial BESS, called NaS-P_{AC}, employing sodium sulfur batteries designed by Silent Power, Ltd. (SPL) for electric vehicle use. This brochure featured a 480 VAC, 3 phase, 300 kVA/300 kWh (rated) modular BESS deployed at a commercial site for customer power quality/reliability and peak shaving opportunity. The system also offered utility dispatch capability in a distributed generation/storage scenario. The system was designed around a 300 kVA self-commutated power converter (PCS), the high end of what is commonly available today from UPS and PCS manufacturers. The envelope selected was 2.1 m (7.0') wide by 2.3 m (7.5') high, which is convenient for transportation purposes. The height allowed a stack of 5 battery packs to fit conveniently behind this envelope. To ensure a 5 year operation before battery replacement is required, 10, 40 kWh battery packs were fitted within this envelope. These were connected 2 in series by 5 in parallel to achieve the rated system specifications for the proposed 5 year warranty period.

Under conditions of a sustained 300 kVA load, the NaS-P_{AC} system electrical performance was shown graphically as a function of the number of battery packs employed in the system. With 10 batteries, the system could continuously provide 70 minutes of operation. For applications requiring less duration, however, a system employing 4 batteries could provide up to 6 minutes of 300 kVA power before hitting a thermal limit. It should be noted that these EV batteries were designed to deliver 60 kW of power for acceleration; in fact, the ratio of peak to sustained power for these batteries is typically 8/3. This suggests that the ten battery NaS-P_{AC} system could be designed to deliver nearly 800 kW of pulsed power, provided the PCS and wiring were chosen to meet that requirement.

The brochure included a depiction of truck mounted systems at a utility substation setting. At 8 tons each, two NaS-P_{AC} systems would fit comfortably on a standard flat bed trailer.

The brochure was developed to attract utility interest in BESS as to how it could help solve some of their immediate problems regarding reliability and power quality. More than 250 of these brochures were mailed to utilities with a self-addressed return postcard requesting feedback on how the utility might use the system within their service territory.

The utilities that were targeted for the brochure mailer were screened by their reported cost of electricity purchases. Mr. Brendan Kirby at Oak Ridge National Laboratory performed a search of their 1993 utility database using \$.08/kWh as the minimum transaction cost for electricity purchases. All utilities that paid \$.08/kWh or more for their electricity purchases would be targeted. In addition to several investor owned utilities, a large number of small public power companies, cooperatives, and municipals were identified. Initially, information was sought on power transactions, looking for high peak demand charges. This information, however, was sparsely reported within the database.

One difficulty that surfaced in the process was determining whom to direct the brochure within the utility. In general, the utility departments that seemed most appropriate – engineering, research and development staff, corporate planning, T&D and customer account engineering staff – do not necessarily interface with each other on a regular basis. The hope was that the brochure would circulate around the various departments within a utility and that an interested party would be identified

A second mailing was directed to managers of demand side management (DSM) practices within the utility. Utilities were screened by their DSM expenditures during the year. The premise was that utilities who were spending significant amounts of money in this area were seeking to defer capital investment or to minimize their expenditures in peaking equipment and associated operating expenses. This is an area in which BESS can play a significant role.

The four questions asked on the return mailer were:

- (1) At \$.50/watt for a turn-key system, do you see battery energy storage (BESS) as having a benefit within your utility or in customer side applications?
 Yes No
 For which application?
 Within Utility Customer Side Both
- (2) What is your primary interest (use/perceived benefit) in BESS?
 Dispatchable Distributed Generation Spinning Reserve
 Seamless DSM Program T&D Deferrals
 Utility Power Quality/Reliability Peak Demand Reduction
 Customer Power Quality/Reliability
- (3) Do you see advantages to any of the features associated with the NaS-P_{AC} system design?
 Compact/Portable System Design Yes No
 5 Year No-Maintenance Batteries Yes No
 Outdoor Siting (Insensitive to Ambient) Yes No
- (4) Would your utility be interested in participating in a BESS demonstration program?
 Yes No

A 10% response to the mailer was obtained. Of these, approximately 2/3 were interested in BESS at a capital cost of \$.50/watt. The remainder implied that the cost was too high, or they were not sure. Fifty percent were interested in BESS applied on the utility side; 33% saw the benefit on the customer side, while 17% were interested in both applications. Figure 3-4 summarizes the utility responses to question (2) regarding possible applications for BESS within their user territory. Over 80% valued utility power quality/reliability (UPQ/R); 66% were interested in the customer side application (CPQ/R), leaving 33% seeking either DSM or peak shaving solutions. All of the responding utility representatives saw advantages in the stated NaS-P_{AC} system features, and, while the majority said that

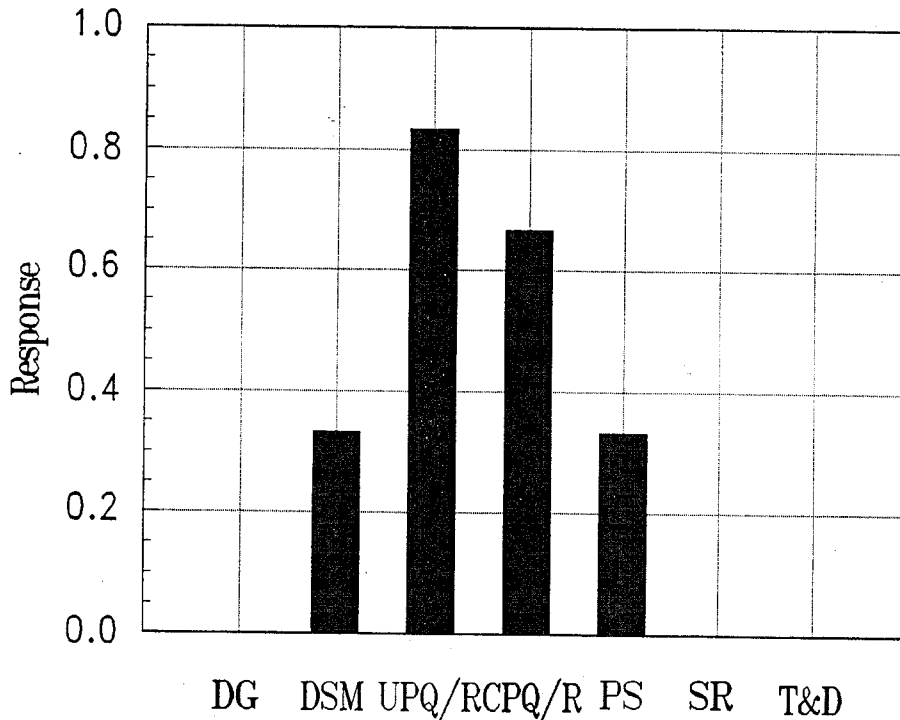


Figure 3-4. Utility Applications Response

they would be interested in participating in a demonstration, there were several that declined.

In addition to developing utility interest via the brochure, SPI gave presentations at utility association meetings, such as the Utility Battery Group (UBG), Pennsylvania Electric Association and numerous east coast investor owned utilities and rural electric cooperatives to discuss potential applications for BESS. Similarly, an industry outreach effort was made either by way of direct telephone inquiries to specific industry, such as plastic extruders and blow molders, or through the American Council for an Energy Efficient Economy. Through these efforts, SPI was able to develop a more realistic picture of the emerging opportunities for BESS. A summary of the challenges and potential benefits for this technology in a new utility environment is given in the following section.

3.4 BESS Product Viability

Utility monthly peak power demand charges typically range from \$10 to \$25/kW across the U.S. For industrial and most commercial customers, this is a significant portion of their bill. In general, power charges occupy 50% to 65% of industrial customer bills, depending on load factor and power factor; for commercial businesses, the range is 35% to 50%. The balance constitutes the energy related portion of the billing. Utilities charge these customers for both their connected power (a fixed charge) and for their monthly power

utilization. This covers the utility's cost for these fixed assets, including a portion of the distribution network, the transmission system and generation investments. Into this protected investment structure enters battery energy storage. In this setting, one would at first think that a utility would have no incentive to support a technology that could potentially reduce its revenues – i.e., customer peak shaving is aimed directly at reducing peak power demand and its associated monthly charges. However, if the customer uses less power, the utility might benefit by possibly being able to defer investment in additional peaking generation equipment due to growth within its territory. There is a limit to this argument, for, if every customer employed a BESS, the utility would have excess peaking generation capability and would be forced to request from the PUC a rate increase to recover these revenue losses. It remains that battery energy storage is perceived by many utilities to be a threat to their status quo.

The changes that are taking place in the utility industry today as a result of deregulation are fostering competition. As a result of open transmission access, the threat is coming from everywhere and not just from local utilities. Lower prices and increased services are the bottom line to increasing the customer base. Utility mergers appear to be the first response to this challenge. Summer peaking utilities are looking to merge with winter peakers in order to improve their combined asset utilization throughout the year. Traditional departments within the utility are being downsized and combined to serve the various business areas more effectively with fewer resources. Utilities are “snapping-up” efficient independent power producers (IPPs) where there is a strategic advantage to do so. At the same time, utilities are attempting to sign their large customers to long term contracts at favorable rates in order to retain them in the face of this competition. Amidst all of these changes, utilities are forced to think about ways of lowering charges and improving services so that they can gain a competitive edge. Into this environment enters the threat of battery energy storage. Can the threat be transformed into a strategy, giving a utility a competitive advantage?

At this stage, utilities appear to be sitting on the side lines, waiting to see who makes the first move and to see what develops from the on-going BESS demonstrations. A few utilities are taking a more active role in this demonstration and pre-commercial phase. The challenge for BESS manufacturers is to develop a well engineered product that will avoid the pitfalls of custom designs in regards to field integration start-up problems and their associated project costs. Here, then, enters the role for the factory integrated modular systems and for systems that can be expanded as needed to serve the changing needs of the application. Most importantly, the modular systems address the immediate need by reducing capital outlay and lowering risk. In the end, these systems may serve to stimulate the market as an expedient way of reducing the BESS cost to a level where they are competitive with other more traditional solutions. Utilities are looking for products that can be “plugged” into their grid to solve particular problems; they are not looking to fund a long term development project.

The viability of BESS is based on both first cost and life cycle cost investment criteria which are measured against the environmentally burdened cost of current combustion generation equipment. Applications that demand instantaneous response to handle critical

loads for power quality and reliability can only be addressed today by UPS systems applied directly to the critical load. Utilities can offer multiple feed service and provide spinning reserve as insurance to stiffen the system against failures. The BESS offers an alternative and perhaps better solution by locating the source close to the point of use. Distributed BESS offers utility dispatch during peak demand, while prioritizing the customer with dedicated power quality/reliability. These dual benefits could help provide the lower cost and improved services that utilities want to provide and customers want to receive.

For the case of a customer monthly demand charge of \$13 to \$17/kW, a BESS that costs \$630/kW for an hour of storage (or, \$630/kWh) requires 3 to 4 years to payback the investment, provided the BESS control is successful in clipping the peak for each month. The resulting benefit depends on the specifics of the application – i.e., the sharpness, number, and predictability of the load peaks. This is why transit applications, such as light rail service, are so appealing; morning and afternoon rush hours define daily power peaks that are easily identifiable. For most industrial customers, the BESS investment consideration comes after internal DSM measures to reduce the peak load are not achieving expected results. The BESS complements this effort by offering a seamless power transfer without having to resort to cutting back power service and affecting production.

In the dual benefits scenario presented above, the price that a utility will pay for peak electricity, unfortunately, is less than what the utility will sell it for. With the advent of widespread distributed BESS, it is worth revisiting the question of whether complete reciprocity of electricity pricing should be mandated, especially in the face of the premium services offered by BESS. In the future, will it be accepted practice to drive the electricity meter backwards?

A cash flow analysis was performed on an initial investment of \$189,000 for a 300 kW/300 kWh BESS with a thirty year equipment life; an after-tax discounted rate of 7.5% was assumed. The results of this cash analysis is shown in Table 3-2. Included in the analysis was battery replacement after 5 years, a 4% escalation rate, and excess energy provided at beginning-of-life to handle the energy inefficiency of the BESS in operation, including that needed to maintain the temperature of the battery. Assuming that customer monthly peaks are successfully clipped by the BESS, the results support a 30% internal rate of return and a net present value (NPV) after 30 years amounting to \$500,000. With a lower after tax discount rate, the investment can be expected to look even more attractive. As the amount of battery (discharge duration) required to satisfy the application increases, the cost of the system can be expected to increase, while the rate of return and NPV declines. This is shown in Figure 3-5. For a system requiring 2 hours of storage, for example, the return is reduced to 13% and the NPV is less than \$200,000 over the 30 year life. Therefore, those applications requiring the least amount of storage should be pursued initially as part of any commercialization plan.

Table 3-2. 300 kVA/300 kWh NaS-P_{AC} System Investment Cash Flow Analysis

	0	1	2	3	4	5	6	7	8	9	10	11	12	13	14	15
Project Year	1994	1995	1996	1997	1998	1999	2000	2001	2002	2003	2004	2005	2006	2007	2008	2009
Total Project Cost	189.0 k\$															
Service Charge	1.6 k\$	1.7	1.8	1.9	1.9	2.0	2.1	2.2	2.3	2.5	2.6	2.7	2.8	3.0	3.1	3.2
Battery Replacement Cost	98.0 k\$						122.1					152.2				
Replacement Labor Cost	6.1 k\$	1.9	2.0	2.0	2.1	2.2	2.3	2.4	2.5	2.6	2.7	2.8	2.9	3.0	3.2	3.3
Project Year		16	17	18	19	20	21	22	23	24	25	26	27	28	29	30
Calendar Year		2010	2011	2012	2013	2014	2015	2016	2017	2018	2019	2020	2021	2022	2023	2024
Service		3.4	3.6	3.7	3.9	4.1	4.3	4.5	4.7	4.9	5.2	5.4	5.7	5.9	6.2	6.5
Battery Replacement		189.7					236.4				294.5					
Energy Deficit Cost		3.4	3.5	3.7	3.8	4.0	4.2	4.3	4.5	4.7	4.9	5.0	5.3	5.5	5.7	5.9
Total Annual Cost		196.5	7.1	7.4	7.7	8.1	244.8	8.8	9.2	9.6	10.0	305.0	10.9	11.4	11.9	12.4
Annual Savings		113.9	118.4	123.2	128.1	133.2	138.6	144.1	149.9	155.9	162.1	168.6	175.3	182.3	189.6	197.2
Net Cash Flow	-189.0	-82.6	111.3	115.8	120.4	125.1	-106.2	135.3	140.7	146.3	152.1	-136.4	164.4	170.9	177.7	184.8
Cumulative N.P.V.	-189.0	303.3	335.8	367.3	397.8	427.3	404.0	431.6	458.2	484.0	508.9	488.1	511.5	534.0	555.8	577.0
Cost for IRR		184.2	185.5	186.5	187.2	187.9	187.5	187.8	188.2	188.4	188.6	188.5	188.6	188.7	188.8	188.9
Net Present Value	577.0 K\$															
Internal Rate of Return	30.4 %		188.9 K\$ Cost for IRR													
Profitability Index	4.1		189.0 K\$ Actual Cost													

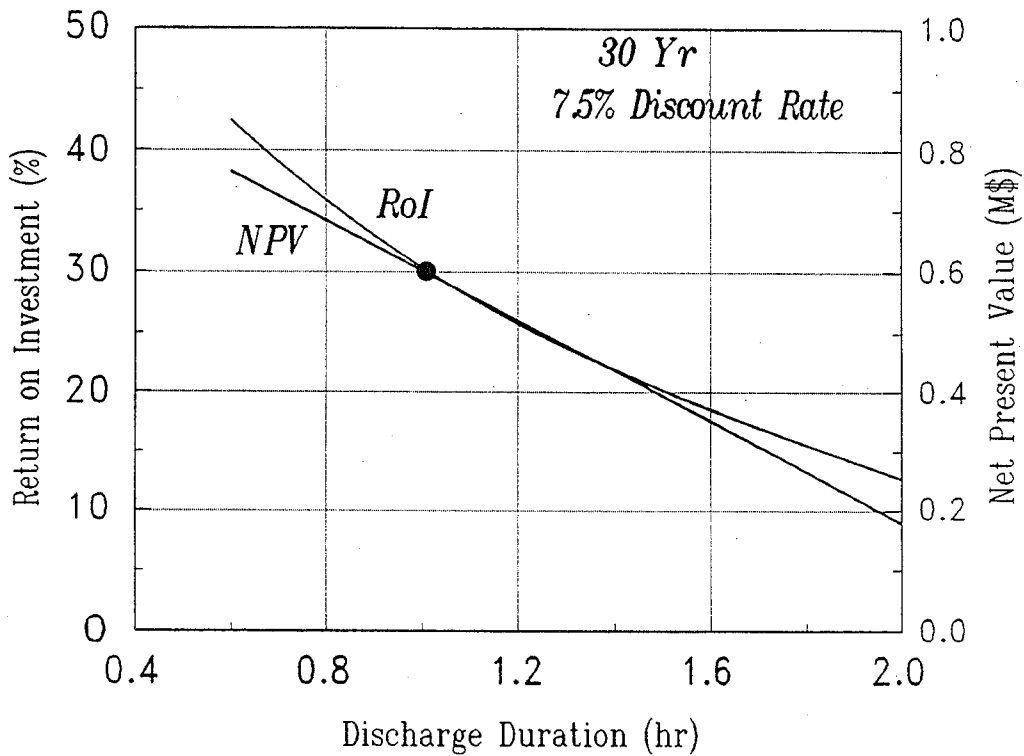


Figure 3-5. 300 kVA NaS-P_{AC} System Net Present Value Analysis

Customer power quality/reliability, on the other hand, has a benefit proportional to the value of the product manufactured. Production losses are likely more significant than utility expenses, and the benefit will vary directly with the number of times per year that the quality of the manufactured product would be compromised by poor power quality or outage periods. As an example, a plastic extruder who stands to lose \$35,000 per event could pay back an investment in a BESS if he were to experience only 5 events over a 5 year period (1 event/year).

If sodium sulfur batteries could be offered in the future which would permit longer periods between replacement, the impact on system life cycle cost could be significant. To investigate this, a cash flow analysis similar to that shown in Table 3-2 was performed; these results are shown in Figure 3-6. It is noteworthy that the rate of return appears to be more sensitive for battery replacement periods less than six years. Beyond this point, the return is fairly insensitive, even though the 30 year NPV continues to increase.

Utilities interested in BESS might lease equipment. In fact, investor owned utilities have unregulated arms and financial shells that might serve as the lease company. Figure 3-7

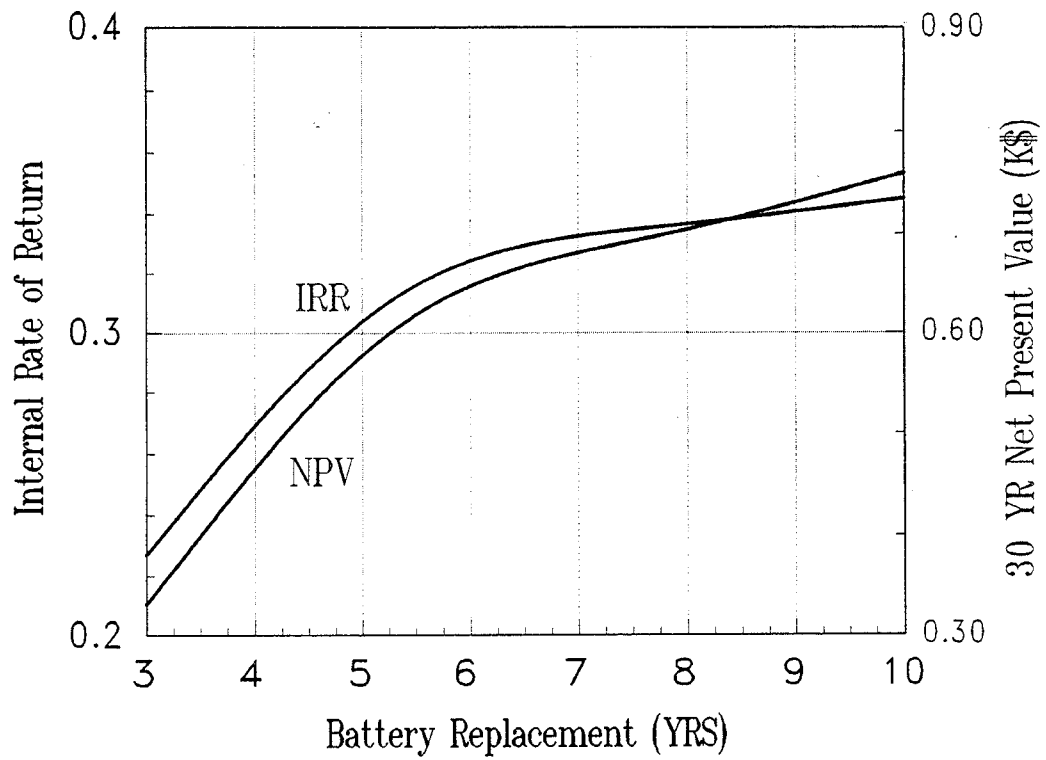


Figure 3-6. NaS-P_{AC} Cash Flow Sensitivity to Battery Replacement Period

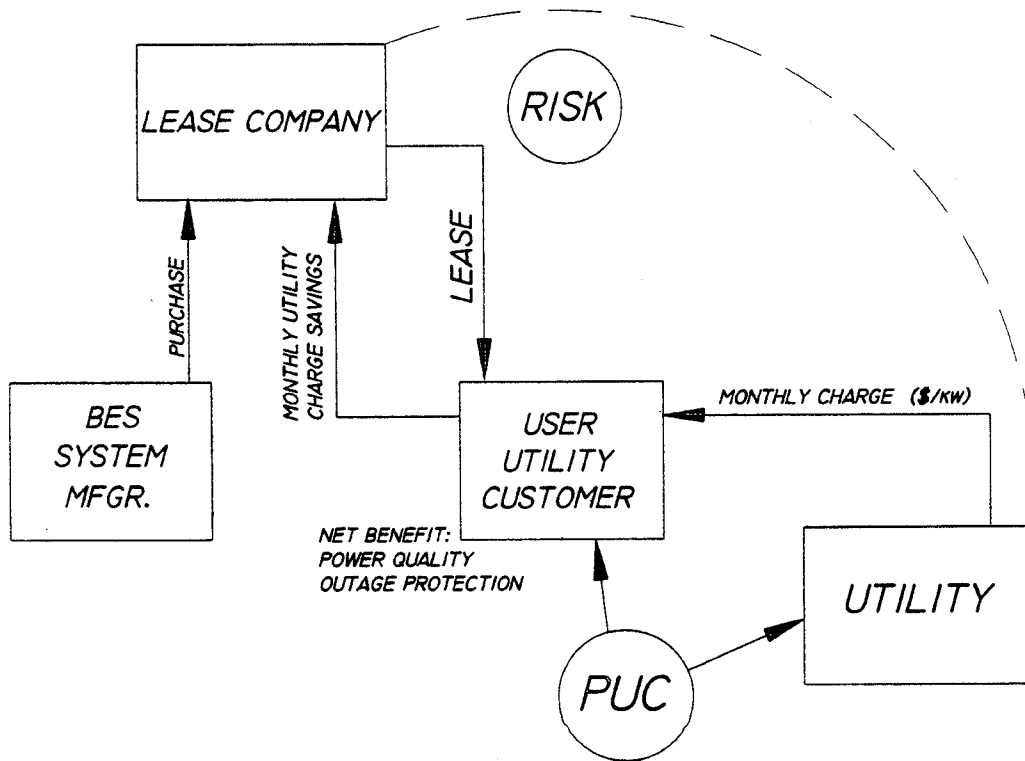


Figure 3-7. Possible Scenario for Leasing BESS Equipment

presents a lease scenario in which the BESS manufacturer sells his product to the lease company, who, in turn, leases it to a utility customer. The customer saves on his monthly utility power charges and pays back the lease. A lower risk alternative is for the utility to dispatch the power to meet his system peak and pay the customer accordingly. The customer receives a net benefit of power quality/reliability protection. To insure this benefit, the PUC sanctions the process by which the customer receives improved service at lower cost.

High end residential developments are also looking toward UPS type of hardware to protect their investments. A BESS might serve at the entrance to such a development where power lines are transitioned from the pole to underground cable. In this way, the entire development is protected against losses, while the capital investment is spread among the number of residential customers served. With the advent of real time pricing comes a significant opportunity for BESS. As suggested in Figure 3-8, with differential energy prices of \$.20/kWh to \$.30/kWh, future BESS systems with 2 to 3 hours of storage begin to look attractive.

In closing this section, a summary of BESS market opportunities, or "How to provide lower cost services." is listed below:

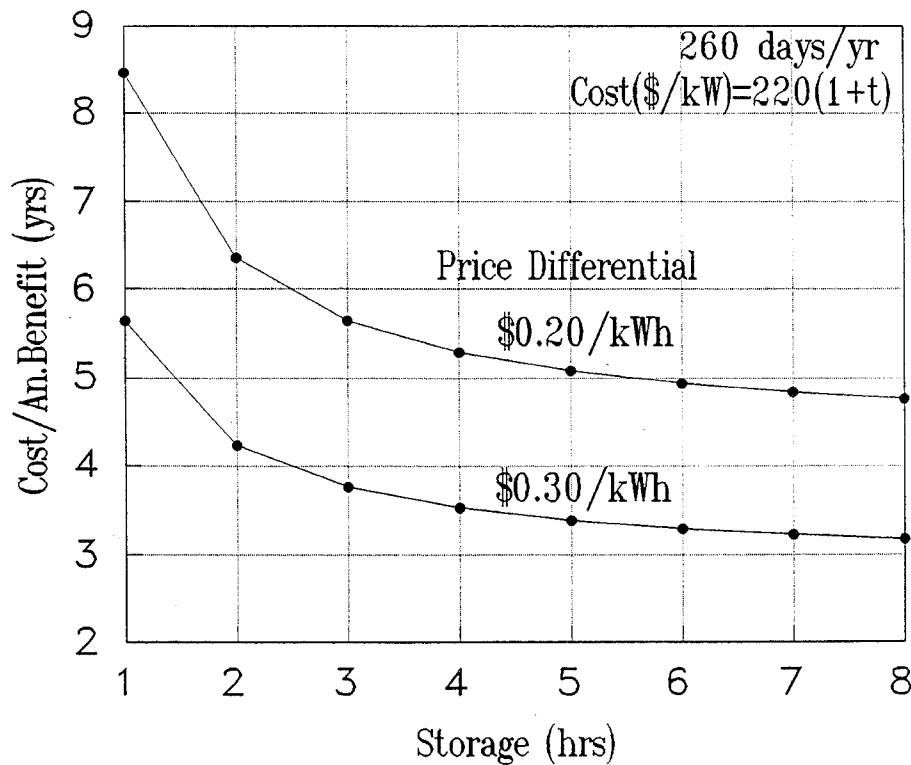


Figure 3-8. Impact of BESS Size on Payback Using Real Time Pricing

Application

Benefit

- | | |
|--|--|
| 1. Small Public Service Utilities,
Municipals, Cooperatives | coincident peak reduction
at tie-points |
| 2. Distributed Dispatchable Power:
- light industry (1 to 5 MW)
- commercial sites (0.1 to 1 MW) | on-site power for outage
protection and utility
dispatch |
| 3. Residential Developments | outage protection |
| 4. Storage for Renewables | improved availability and
value |

IV. Battery Energy Storage System Design and Price Development

The development of the sodium sulfur BESS design and associated selling price was accomplished in parallel with the Task 1 Applications Assessment. The two activities are integrally related and inseparable, although, for programmatic reasons, each is discussed within their appropriate section.

In order to differentiate the sodium sulfur BESS design, the name "NaS-P_{AC}" was coined; it is an acronym for Sodium (Na) Sulfur AC Power System. The development of a preliminary design of the commercial NaS-P_{AC} product is presented in the following sections.

4.1 Development of a 300 kVA/300 kWh NaS-P_{AC} Modular System Design

As discussed in Section 3.1, the development of a modular BESS progressed from the idea of a "turn-key" system that would be a modular building block for larger systems and which would be transported on a flat bed truck. The smaller size offering would also be compatible with a start-up manufacturing business so as to reduce its financial risk.

4.1.1 NaS-P_{AC} System Design Considerations

In the interest of minimizing cost and enhancing utility and utility customer applications, an available 300 kVA power converter (PCS) was selected as the basis for the design. This was the largest standard inverter size that was commercially available for UPS

applications. Figure 4-1 shows the NaS-P_{AC} integrated into a standard PCS weatherized enclosure. The dimensions of this box are 2.3 m (7.5') high by 2.1 m (7') wide by 2.6 m (8.5') deep, which are fully compatible for overland trucking or to fit in a standard seabox.

In order to deliver 300 kVA continuously for one hour so that operation will be maintenance-free over the five year life, ten, 40 kWh Silent Power EV sodium sulfur batteries are required. As shown in Figure 4-2, five of these batteries can be conveniently stacked within this height limitation, and the width can accommodate two battery stacks.

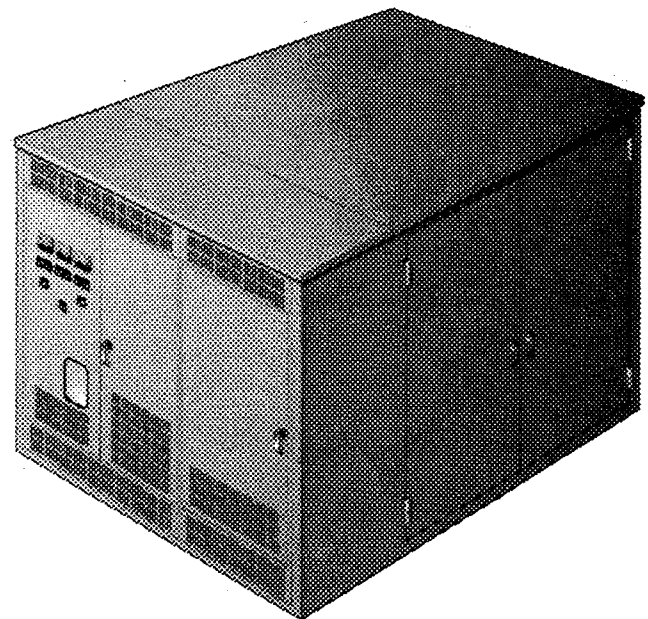
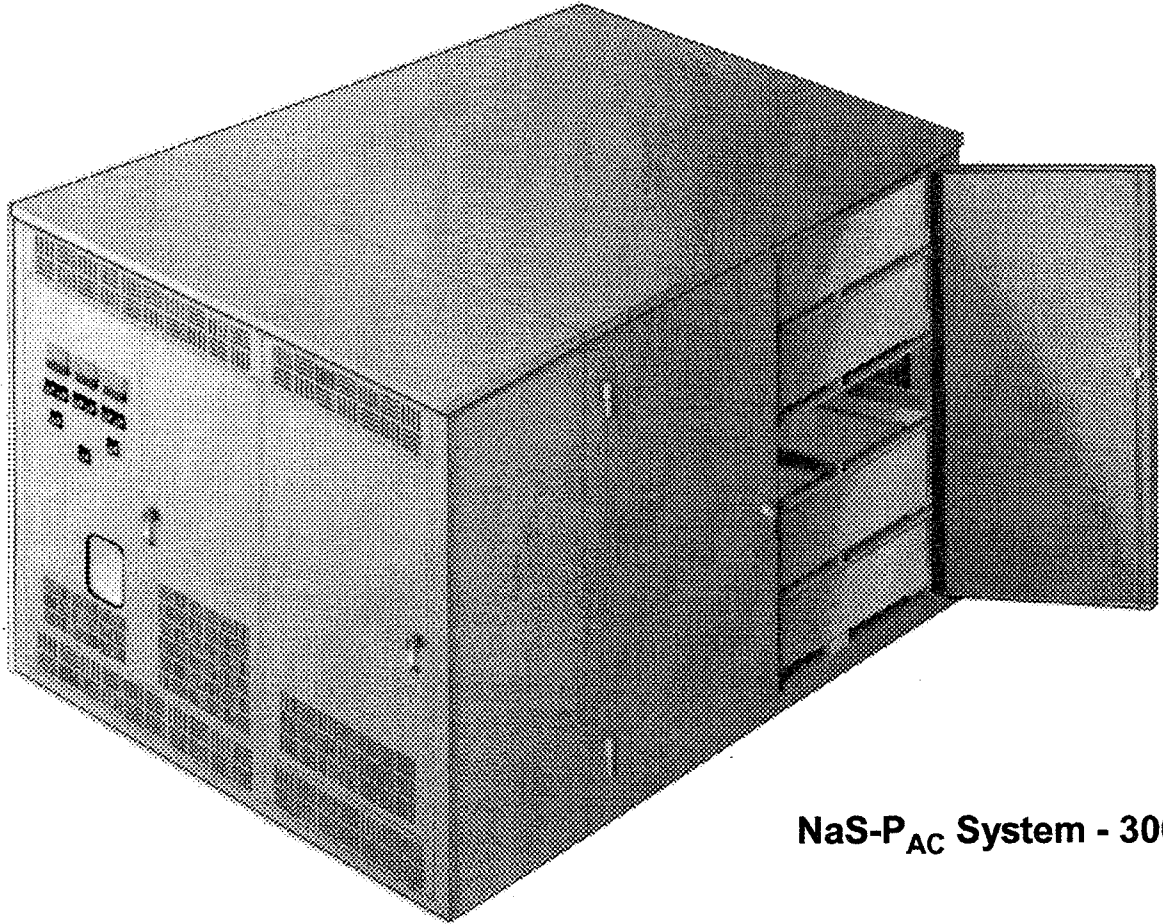
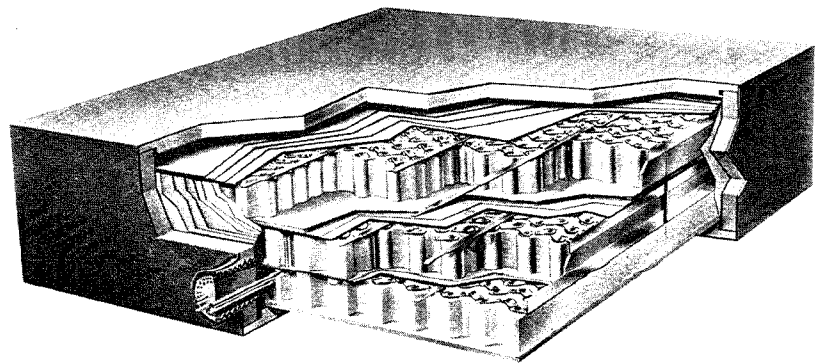


Figure 4-1. 300 kVA - 1 hour, 480 VAC, NaS-P_{AC} System



NaS-P_{AC} System - 300 kW



40 kWh - Replacement Battery

Figure 4-2. NaS-P_{AC} System with Replaceable Sodium Sulfur Batteries

The 40 kWh EV battery designs are flexible in that they can be packaged to deliver DC voltages ranging from 240 to 320 VDC. Connecting the battery packs two in series by five in parallel provides a convenient DC voltage for commercially available 480 VAC inverter. If possible, it is desirable to keep the DC voltage under the 600 V, for, then, the BESS can be classified below the UL limit designation for high voltage.

The support structures housing the batteries are depicted in Figures 4-3a and 4-3b. The outdoor enclosure also contains the temperature controllers (upper block) and isolation switches (middle block) for each battery, as well as a battery management system (BMS) (lower block). An earlier version included a separate BMS to control the battery packs and communicate with the PCS controller. The later version, however, has integrated the function of the BMS into the existing PCS digital processor/controller.

To serve the power quality and reliability needs of utility customers, the NaS- P_{AC} system can be designed to provide up to 800 kW of pulsed power (a 2.67-fold increase over its rated power) with the ten EV batteries. Alternatively, by reducing the number of batteries feeding the 300 kVA inverter, Figure 4-4 shows that the length of time over which the system can be expected to continuously deliver full power will decrease accordingly. With six batteries, for example, full power can be delivered for over 20 minutes before hitting a thermal limit. Since the battery is a significant contributor to system price, there may be applications that benefit from this tradeoff between operation time and price.

The decline in system discharge capability at rated power as cells fail over the battery lifetime is summarized in Figure 4-5 as a function of the number of batteries comprising the system. For this investigation, Weibull parameters ($\alpha=11$ years, $\beta=4.5$) were chosen to statistically represent the rate of cell failure in a battery population. With ten batteries, for example, the system discharge capability at rated power at beginning-of-life is approximately 70 minutes. As cells fail, the capacity of the battery system will gradually decline; after 4.5 years of operation, rated power will be provided for only 50 minutes. This analysis was based upon a conservative estimate for the Weibull parameters – i.e., those which are achievable from cells manufactured in a pilot plant. By the time that volume manufacturing is introduced for commercial production, latent defects in cells should be significantly reduced due to quality assurance methods. It is therefore expected that improvements will be seen in the above Weibull parameters, especially in the shape factor, thereby, extending service life.

4.1.2 Design Specifications

Whether the batteries are high temperature sodium batteries or ambient temperature batteries, the battery subsystem will have to be thermally managed. In an outdoor setting,

* where α is the characteristic life and α is the shape factor of the population.

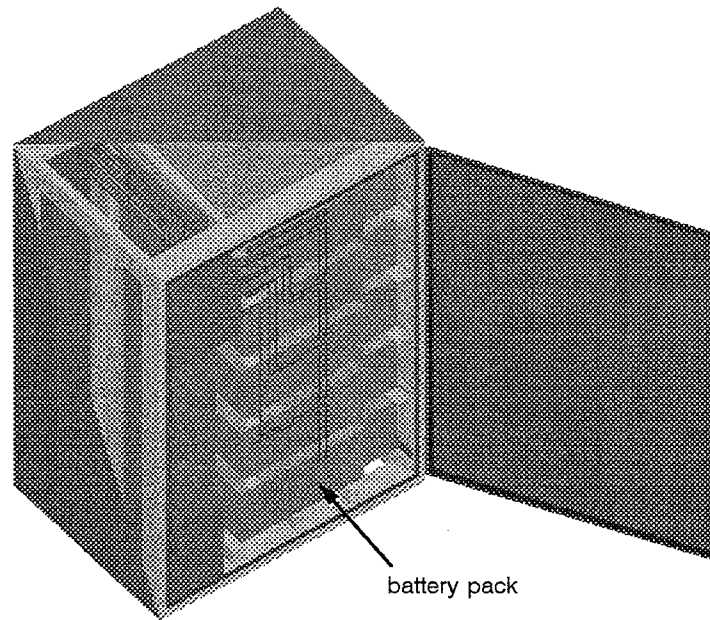


Figure 4-3a. Battery Support Structure, Right Half

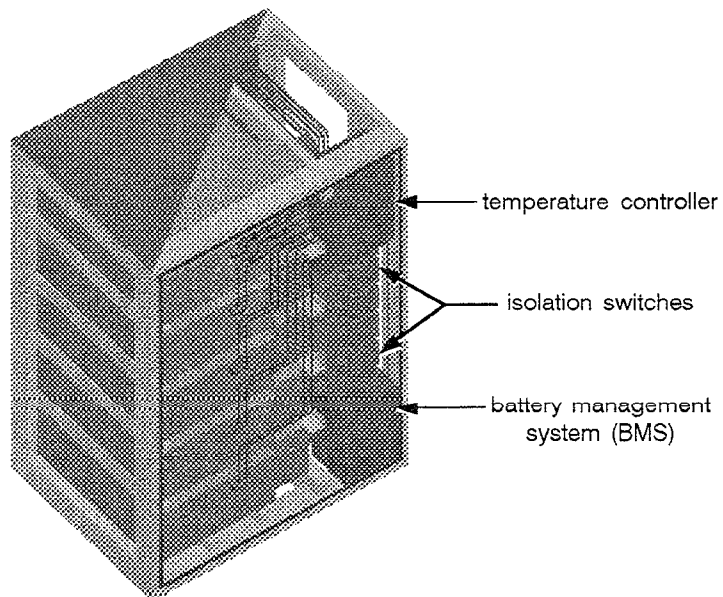


Figure 4-3b. Battery Support Structure, Left Half

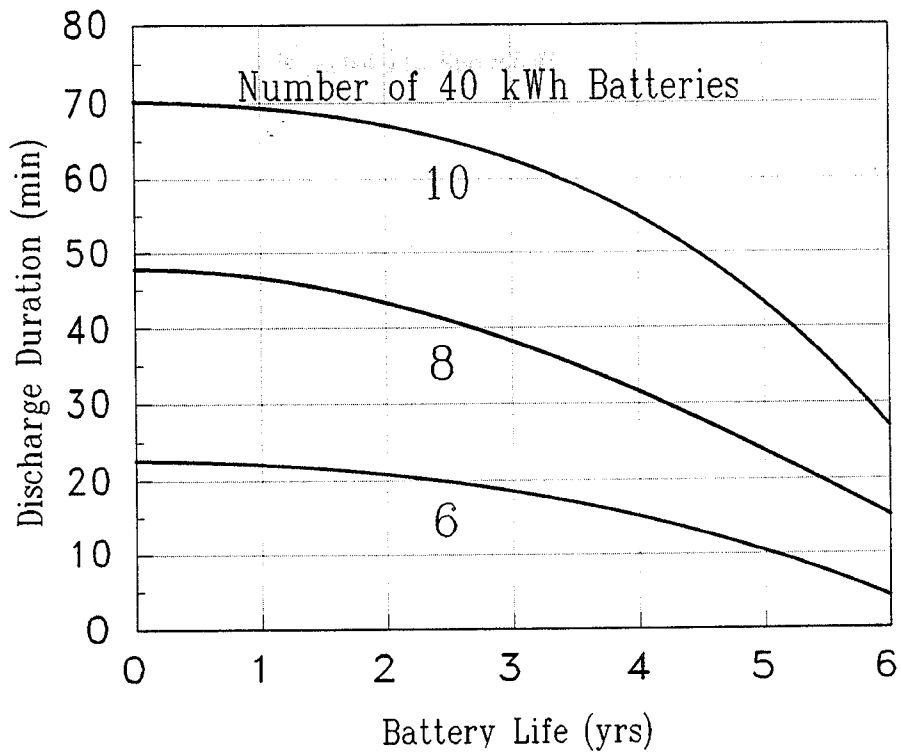


Figure 4-4. Battery Sustained Discharge Capability at 300 kVA

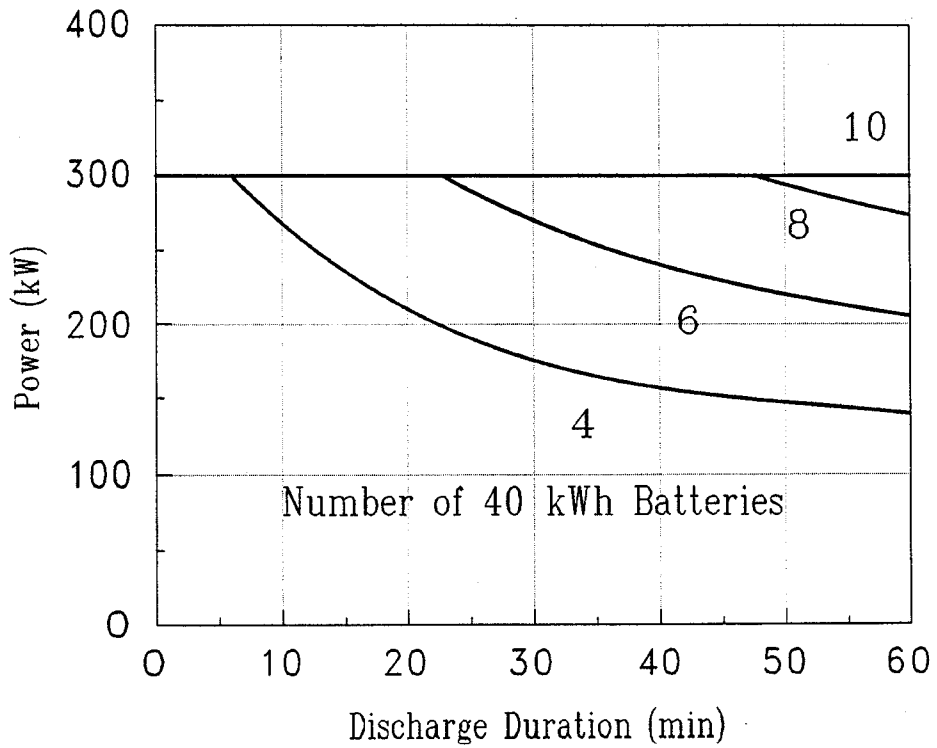


Figure 4-5. Battery Performance Degradation Scenario with Time

the task of thermal management is particularly onerous. For the sodium sulfur battery, the fact that battery packs are already equipped with separate thermal enclosures facilitates outdoor deployment with the cost already accounted for. Moreover, in a stationary application in which batteries are stacked, the heat loss is only 60% of that which an individual battery would experience installed in an EV. The make-up heat required during quiescent periods for the NaS-P_{AC} system design is 1.2 kW. This raises an important consideration regarding preferred applications. In order to avoid a potentially significant parasitic load associated with make-up heat, applications that regularly utilize the sodium sulfur BESS should be selected and not those that intermittently utilize the systems and/or involve long standby periods

The system was designed around the battery sustained power limitation. This necessitated that active cooling be employed as a means of rejecting heat from the internal cell matrix so that rated power operation can be sustained. An oil cooling system is already incorporated into the EV battery and includes a heat exchange plenum internal to the battery and a pump, reservoir and secondary heat exchanger package mounted to the outside of the battery. This cooling system has been designed to transfer up to 4 kW per battery. For the stationary application, only 2.6 kW per battery is required near the end-of-life in order to limit the battery core temperature rise to 30°C for continuous power operation. As part of the NaS-P_{AC} system design, an oil-to-air heat exchanger, indicated in Figure 4-6, is specified for each battery to reject the required heat. The stacked battery pack arrangement permits the heat from each battery to be dissipated into a common chimney and rejected during periods of sustained power discharge. The cooling scheme includes a 1000 CFM blower to reject 13 kW at a 20°C design air temperature rise. The blower, duct work and venting scheme are depicted in Figures 4-7 and 4-8.

The specifications for the 300 kVA PCS are listed in Table 4-1. The PCS produces 480 VAC, 3 phase and is self-commutated using insulated gate bipolar transistor (IGBT) technology with pulse width modulation (PWM). The switching rate is consistent with a 36 pulse simulation of a sine wave with low harmonic distortion (THD<5%), meeting IEEE-519 standards. The control system will allow operation in all four quadrants, permitting the system to act as a current source (line commutated), a voltage source (self-commutated) and/or inject or absorb reactive power (VARs). The regulation modes consist of constant power, voltage, current, VAR or frequency, as well as operation in the load following mode or performing harmonic correction. The PCS will synchronize with the utility for parallel operation and transfer to a user specified regulation mode. The digital control system oversees and controls the operation of the PCS, as well as the batteries, and provides the interface to the user. The system provides a flexible user interface with a remote dispatch and monitoring capability, thereby facilitating service.

4.1.3 System Control and Connection Schemes

Key to the performance benefits of the NaS-P_{AC} system is the battery and its control. This is the reason that SPI has taken on the role of system integrator, rather than the more traditional role of battery supplier. UPS manufacturers and PCS suppliers over the years

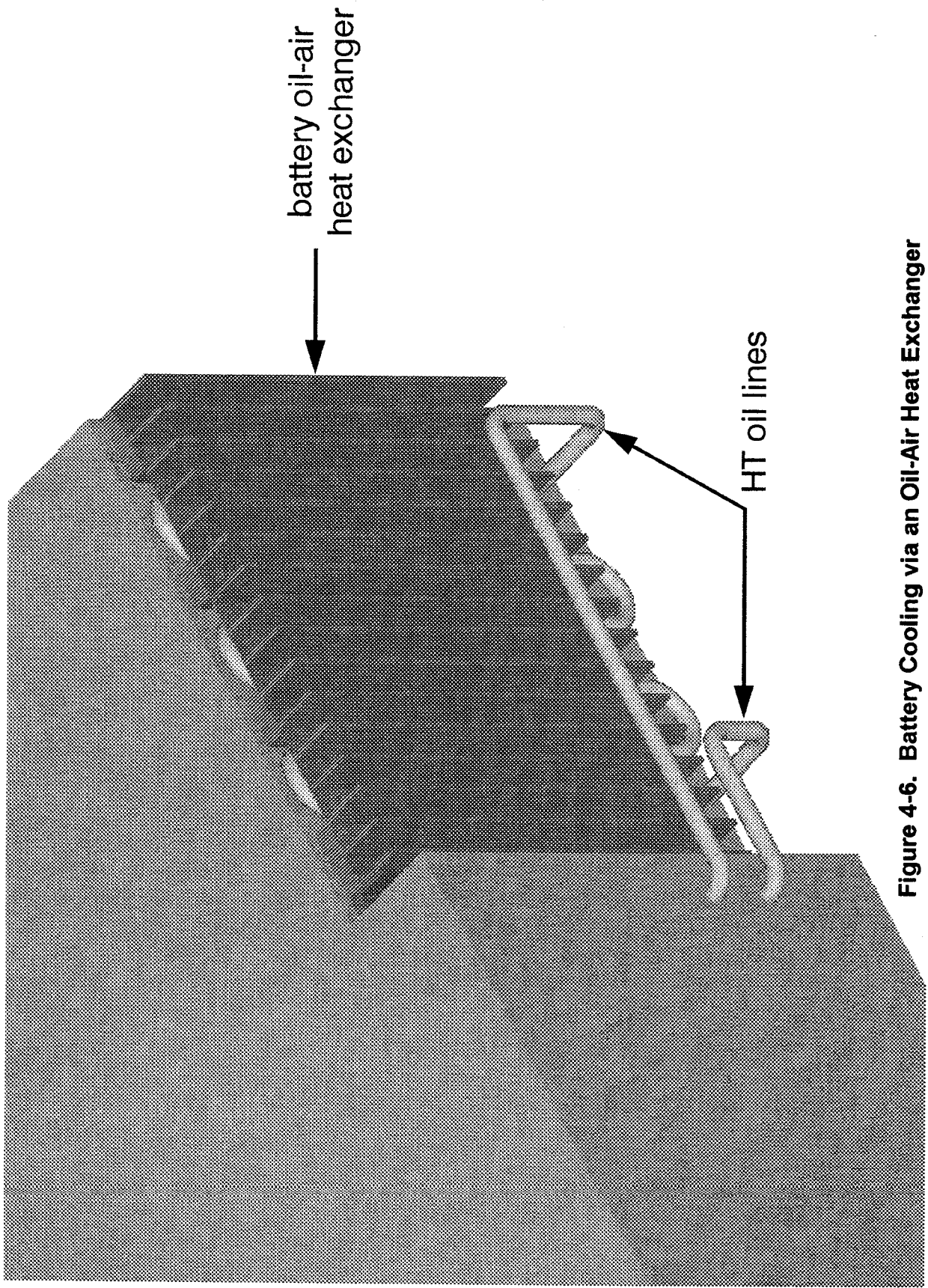


Figure 4-6. Battery Cooling via an Oil-Air Heat Exchanger

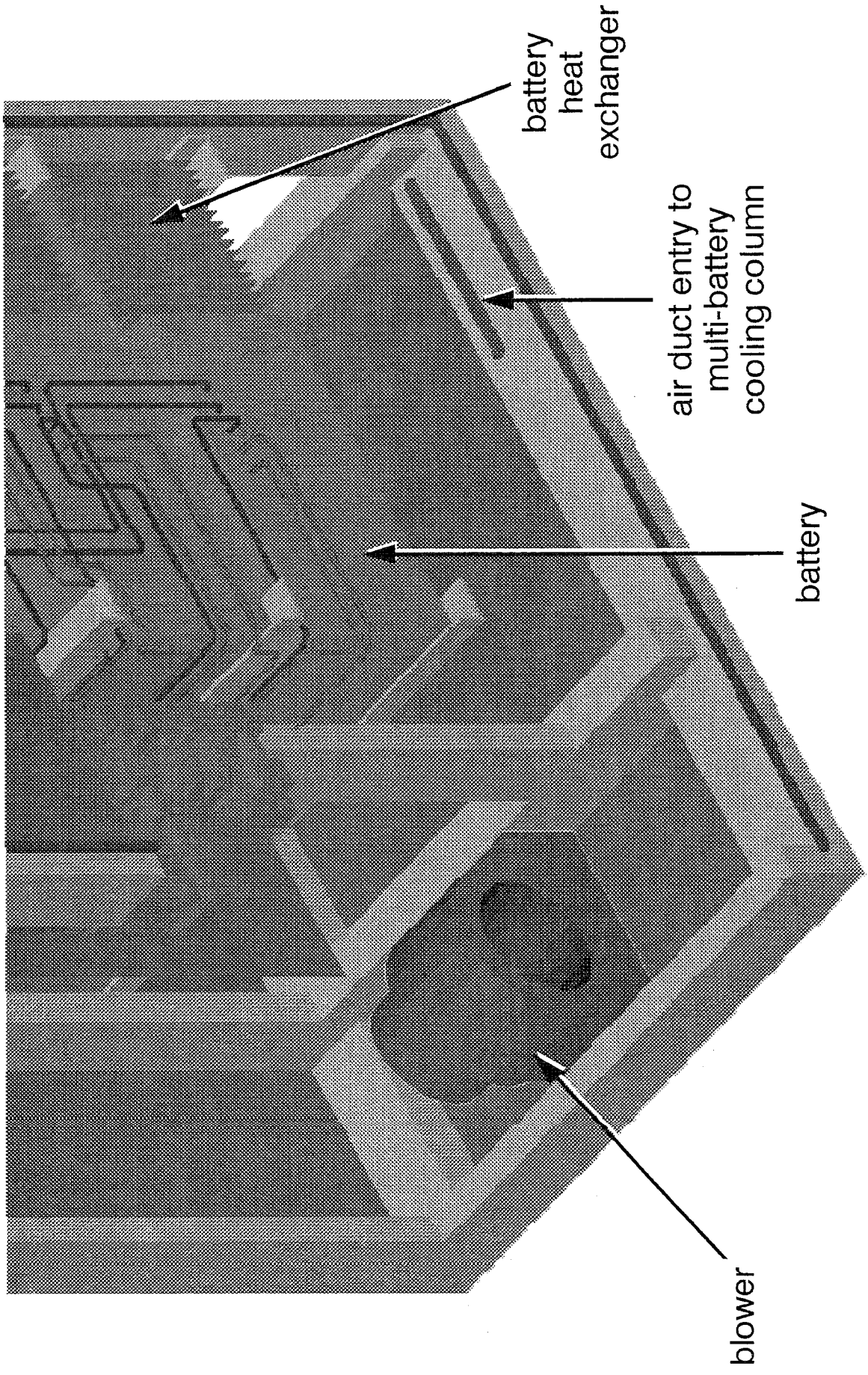


Figure 4-7. Blower Mount and Air Ducting Design for Multi-Battery Cooling

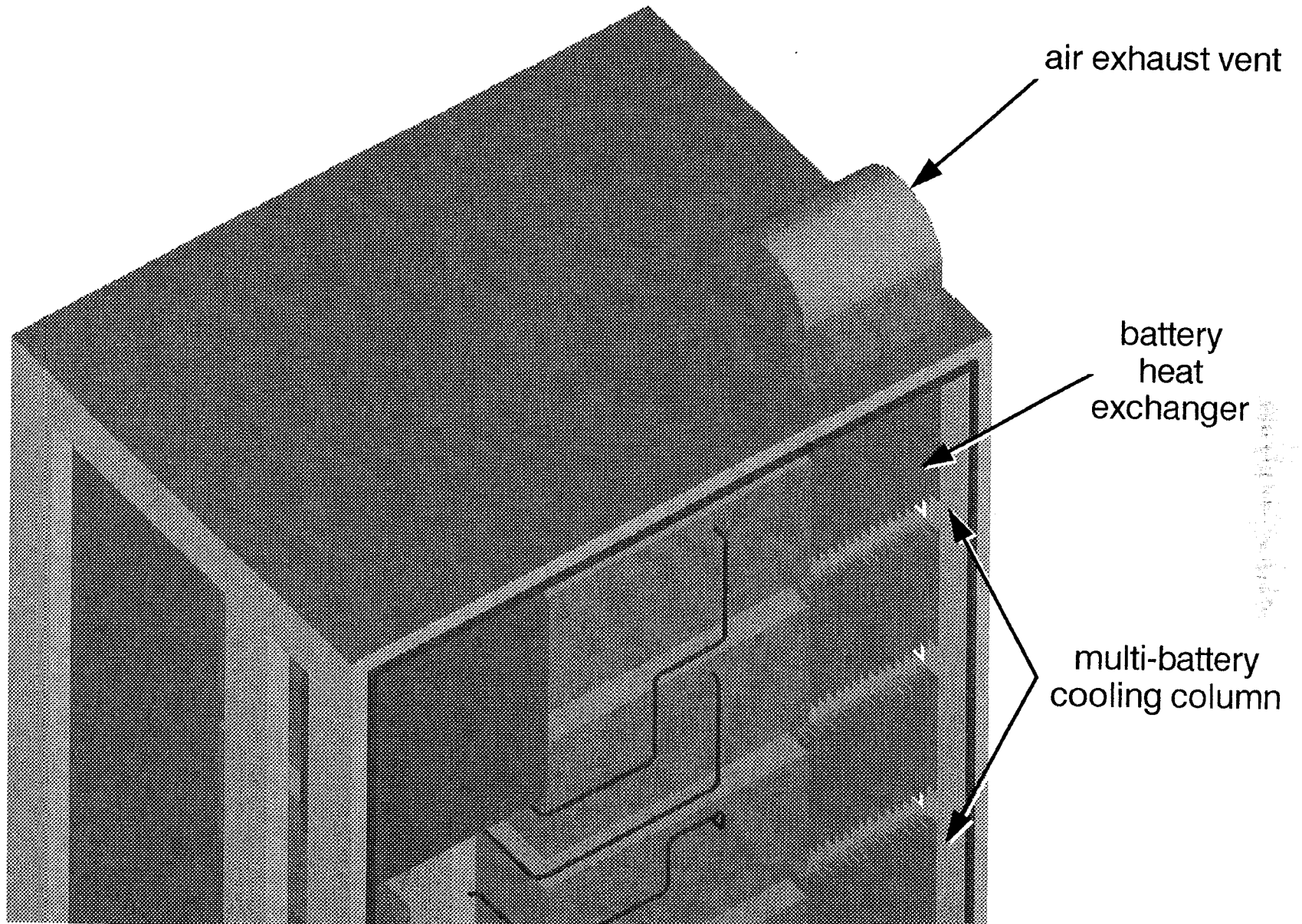


Figure 4-8. Air Vent Design for Multi-Battery Chimney

Table 4-1. PCS Specification

1.	Battery Voltage Range	480 - 650 VDC (EoD - ToC)
2.	Inverter AC Voltage	480 VAC, 3 phase
3.	Inverter Power Rating	300 kVA (500 kVA Peak)
4.	Rectifier Power Rqmt	100 kVA
5.	Topology	Self-Commutated, IGBT
6.	Regulation	4 Quadrant Operation
7.	Efficiency	≥ 95% @ Full Load
8.	Harmonic Distortion	THD <5% (IEEE-519)
9.	Operating Temperature	-5°C to +50°C
10.	AC Protection	6 Circuit Breakers (Under-Voltage/Shunt Trip)
11.	Regulation Modes:	Constant Voltage/Current Constant Power Constant VAR Constant Frequency Load Following Harmonic Correction
12.	Synchronization with Utility for parallel operation and seamless transfer to user specified regulation mode via front panel or monitoring system.	
13.	Digital Control System with capability to incorporate the control of 10 - 40 kWh batteries.	
14.	Flexible user interface (remote dispatch option).	
15.	Remote monitoring of stored events.	

have been successful in developing and manufacturing inverters with field proven hardware and software sophisticated control features. SPI was interested in tapping this resource and utilizing the on-board digital processing capability available as a means to monitor and control each battery pack.

The initial BESS control approach involved a separate BMS serving each battery stack that had to communicate with the PCS controller. By integrating the functions of the BMS into the PCS controller, a significant portion of the battery related cost can be replaced with software development costs that can be amortized over several years against the entire BESS production. Figure 4-9 presents a simplified block diagram of the proposed integrated control. In this scheme, each battery contains an interface board which reads bank voltage and temperature data, converts the analog signals to digital (A/D) and performs multiplexing (MUX) to drive a serial input to the PCS system controller. The main

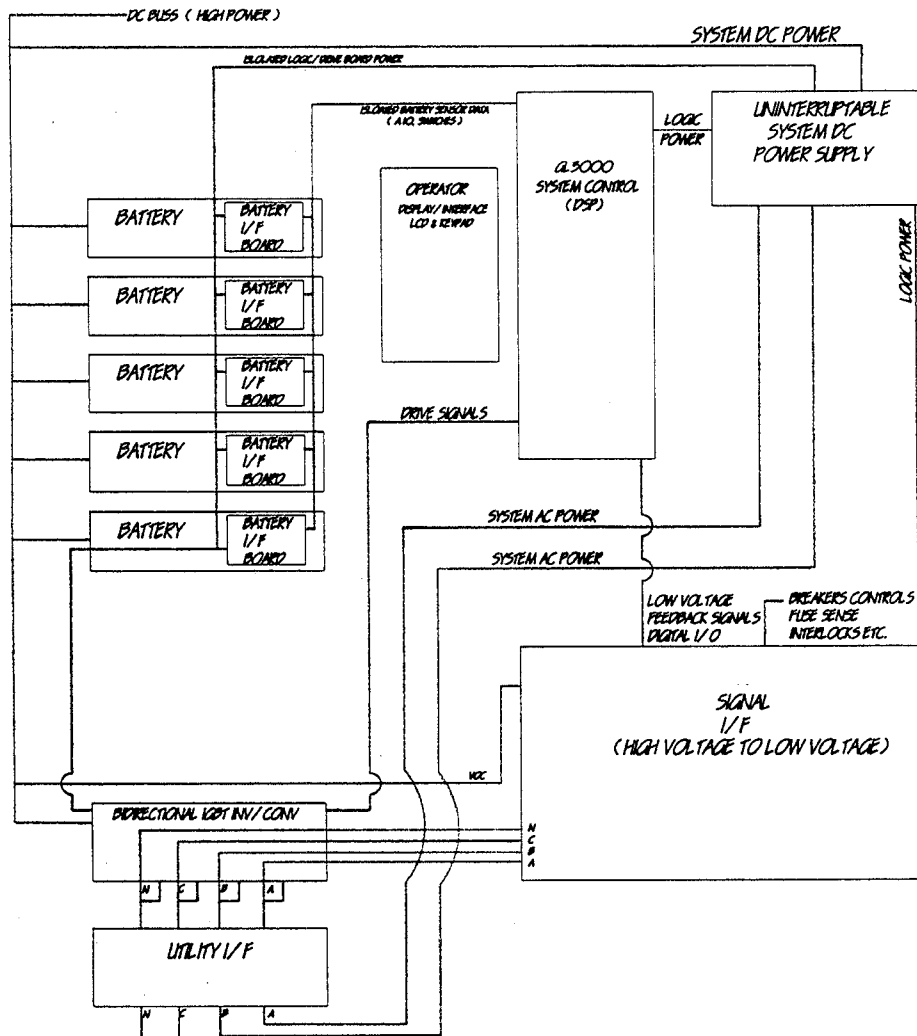
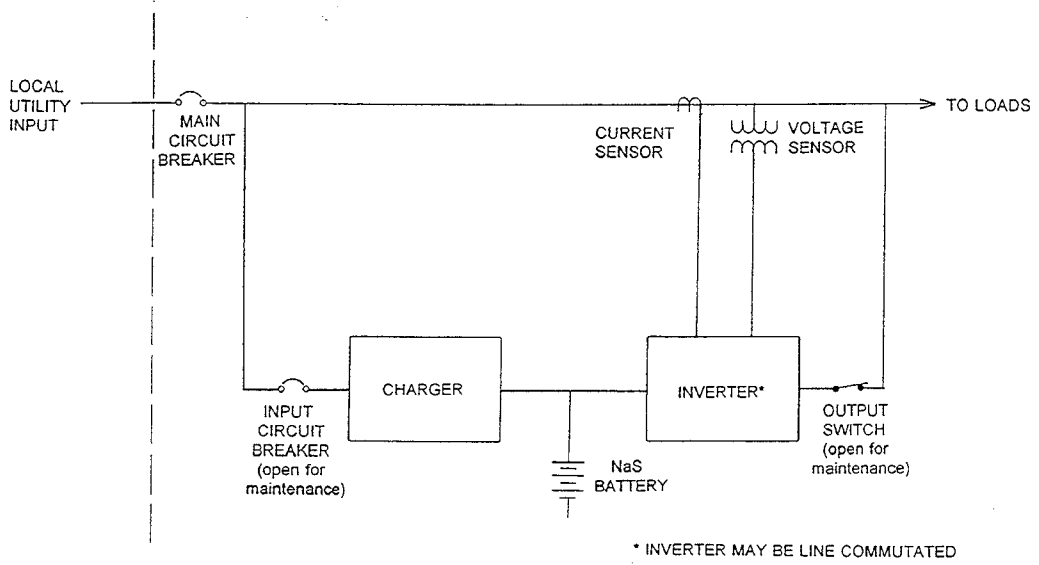


Figure 4-9. Battery PCS Integrated System Control Scheme

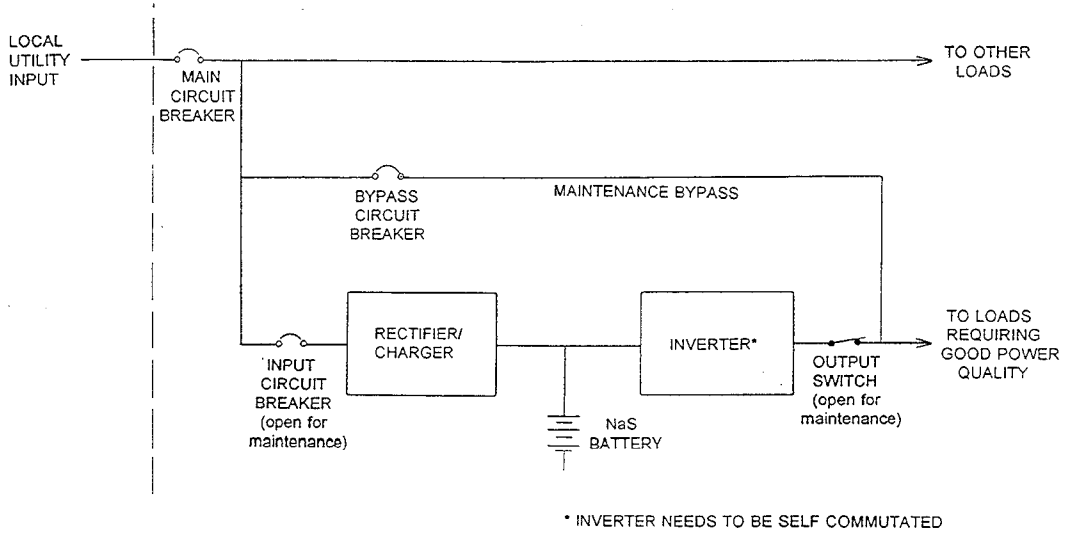
function of the system controller was to control the gating of the transistors in the PCS. The additional workload of the digital signal processor (DSP) in taking on the BMS function was deemed to be acceptable, based on the system clock rate and the rate at which battery control data had to be transferred and processed.

The simplified diagrams presented in Figures 4-10a and 4-10b indicate two methods for connecting the NaS- P_{AC} BESS to serve a load in a peak shaving and a power quality/reliability application, respectively. In the former case, the BESS is available to supply power to meet the peak demand either via a local signal based on real time power utilization, or through a remote dispatch signal from the utility as part of their DSM



BATTERY STORAGE SYSTEM TO PROVIDE PEAK SHAVING

Figure 4-10a. BESS Connection for Parallel Operation with Utility



BATTERY STORAGE SYSTEM TO PROVIDE IMPROVED POWER QUALITY

Figure 4-10b. BESS Series Connection for Power Quality/Reliability

program. To serve the power quality and outage protection needs of utility customers, the latter connection scheme supplies continuous quality power for critical loads, such as computer systems. An alternate method is to use a static switch to detect loss of the utility and to switch in the BESS, all within milliseconds. As opposed to the series connection suggested in Figure 4-10b, the alternate approach has the advantage of operating the BESS in a standby parallel mode, which could extend the maintenance period.

4.1.4 NaS-P_{AC} System Benefits

Relative to a comparable lead acid BESS, the NaS-P_{AC} system design offers substantial size and weight advantages which may be important for acceptance in a particular application. A performance comparison is listed in Table 4-2.

At 8 tons, two NaS-P_{AC} systems can be transported on a standard flat bed truck. Portability is demonstrated in Figure 4-11, in which a 1.2 MW/1.2 MWh BESS is available to handle seasonal load peaks at a utility substation. In this application, the utility may be interested in a BESS as a means of deferring the capital expense associated with a transmission line or substation transformer upgrade. At the end of the peak season, the units could be transported to serve an alternate site.

Table 4-2. The Case for Advanced Batteries: A Comparison of BESS

NaS-P_{AC} System Specifications	Lead Acid BESS Specifications
300 kVA	250 kVA
300 kWh (400 kWh Installed)	167 kWh
7.5'(H) x 7'(W) x 8.5'	11'(H) x 7'(W) x 15'
16000 lb	38000 lb
23.7 W/liter	7.6 W/liter
23.7 /liter (Rated)	5.1 GWh/liter
41.3 W/kg	14.5 W/kg
41.3 Wh/kg (Rated)	9.7 Wh/kg

NaS-P_{AC} System Benefit

Factor of 3 Improvement in Specific Power
Factor of 4 to 5 Improvement in Specific Energy

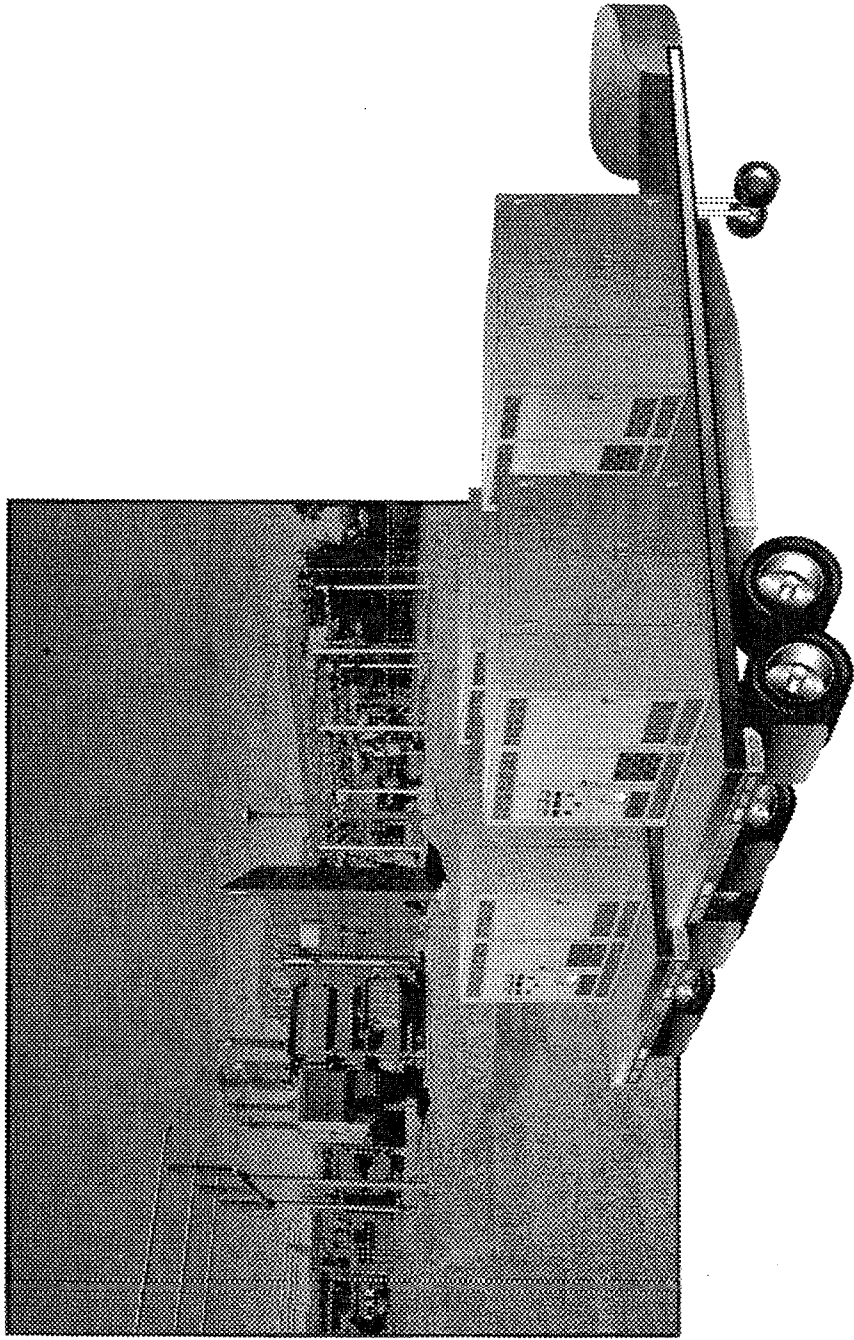


Figure 4-11. Transportation and Substation Deployment of Modular NaS-P_{AC} Units

In summary, the proposed 300 kVA/300 kWh NaS-P_{AC} system design offers several distinct advantages that no other BESS can provide, which, potentially, may stimulate significant utility and customer interest. A list of these assets is given in Table 4-3.

Table 4-3. Summary of NaS-P_{AC} System Benefits

- The most compact BESS available; it is significantly smaller and lighter than competitive battery energy storage systems.
- Designed to facilitate transportation by standard truck or seabox.
- Five year, maintenance-free batteries with integral thermal management.
- Deployable outdoors with battery power and capacity insensitive to ambient conditions.
- High system AC-AC electrical efficiency – 80% (BoL) to 74% (EoL).

4.2 NaS-P_{AC} BESS Price Analysis

The most significant impact on near term NaS-P_{AC} system price was the decision to employ sodium sulfur batteries developed and manufactured for electric vehicle applications. Because of the potentially large volume that this market brings, it was advantageous, as far as near term pricing is concerned, to utilize these batteries for stationary applications. The program took advantage of a detailed costing analysis of the 40 kWh EV battery that had already been performed by Silent Power Ltd in early 1994. The costs were developed for manufacturing equipment, facilities and labor required to produce 10,000 units per annum. The accounting included taxes, insurance, profit and battery reclamation costs. The resulting battery selling price was \$245/kWh, which included the external mounted heat exchanger package but not the BMS; for the EV application, the vehicle manufacturers will integrate the BMS into the vehicle controller. As a result of learning and manufacturing economies of scale, the future price of the battery is estimated to be less than \$150/kWh.

The other major element of the system price is the power conversion system. As mentioned previously, the intent is not to develop a PCS specifically for this application but to utilize a state-of-the-art (SOA) system available for the UPS application. This is a stable market for which competitive pricing exists; moreover, most of the design/development iterations have taken place. The SOA PCS designs that exist include controllers based on the use of digital processing and remote servicing features, including event records

and waveform capture options. Based on quotations received from both PCS and UPS system manufacturers, the PCS cost in \$/kW was compiled as a function of PCS size (rated continuous power). The size range was aggregated into the following classifications: 3-5 kVA, 30-50 kVA and 200-300 kVA. The data, which is presented as a smoothed curve in Figure 4-12, indicate that the lowest cost/kW occurs for the larger systems. The price has a gradual decline between \$300/kW to \$230/kW over the size range of 200 kVA to 500 kVA, while, below 100 kVA, the PCS cost/kW tends to rise sharply. It should be noted that the PCS specification presented in Table 4-1 was tailored to the particular classification and offered as a basis for quotation. A possible explanation for why the smaller systems cost significantly more per kW is that the power related hardware does not scale linearly with size – i.e., some components/subsystems are common to all PCS systems and cannot be scaled down. As a result of this analysis, the 300 kVA PCS system having a cost of \$260/kW was selected; it offers a relatively low cost, mature product for incorporation into the NaS- P_{AC} system.

Other elements comprising the complete system price are listed in Table 4-4; these are presented for both a near term, low production volume BESS and for a fully “learned-out”, large production volume system. The support structure prices were based on quotations received from several vendors for a fully welded assembly design. The temperature controllers, power wiring, isolation switches, current sensor, breakers and fuses were compiled from catalogues of various equipment manufacturers.

Normalized to its rated power or energy, the near term price is expected to be \$630/kW (\$630/kWh) for the 1 hour system design and decreases to \$428/kW (\$428/kWh) as the production volume increases in response to mature combined EV and stationary markets.

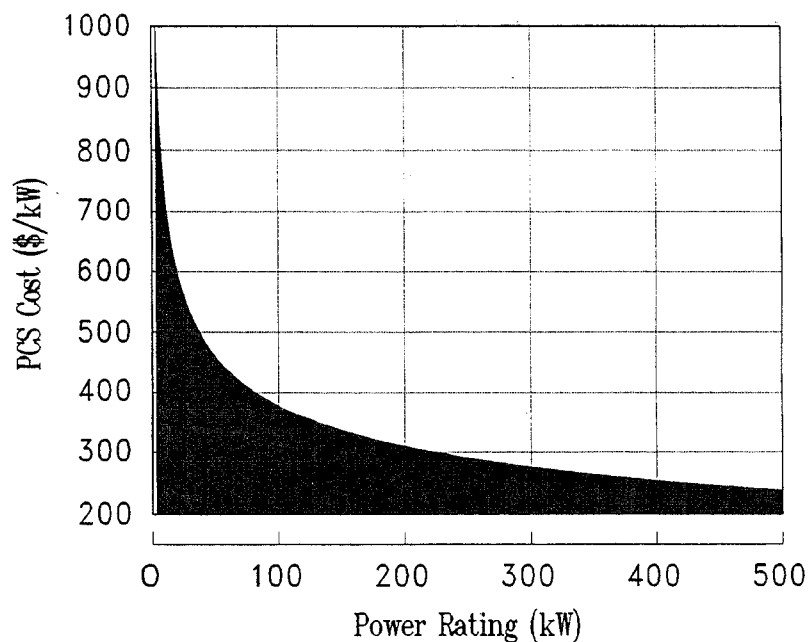


Figure 4-12. Power Inverter Cost - Size Relationship

Table 4-4. NaS-P_{AC} System Price Breakdown

Component/Subsystem	Calculation	Cost/Price
NEAR TERM PRODUCT		
Batteries	\$245/kW x 40kWh x 10	\$ 98,000
PCS	\$259/kW x 300kW	\$ 77,000
Structure and Cabinet		\$ 8,000
Software Development		\$ 2,000
Electrical Hardware		\$ 3,400
Total		\$189,000
Price per Rated kW = \$630/kW		
FULLY LEARNED-OUT, MATURE PRODUCT		
Batteries	\$150/kW x 40kWh x 10	\$ 60,000
PCS	\$183/kW x 300kW	\$ 55,000
Balance of Equipment		\$ 13,400
Total		\$128,400
Price per Rated kW = \$428/kW		

Based upon a learning rate of 85%, Figure 4-13 shows the decline in the selling price of the NaS-P_{AC} following the introduction of commercial manufacture. For this scenario, the assumption was made that the battery production level will be driven principally by the development of an EV market.

A pictorial allocation of major component price contributions to the overall system price is shown in Figure 4-14. Note that all of the battery peripheral costs are lumped into a housing (energy based) contribution. This permits the development of a simplified system price equation with separable power and energy related parts. The "1.33" factor applied to the battery price accounts for the installed energy (400 kWh) versus the rated power which normalizes the price. As a result, the energy portion accounts for 59% of the overall system price. In the future for the fully learned-out product, Figure 4-15 indicates that the overall system price can be expected to decrease to \$428/kW, with a balanced contribution between power and energy related component costs.

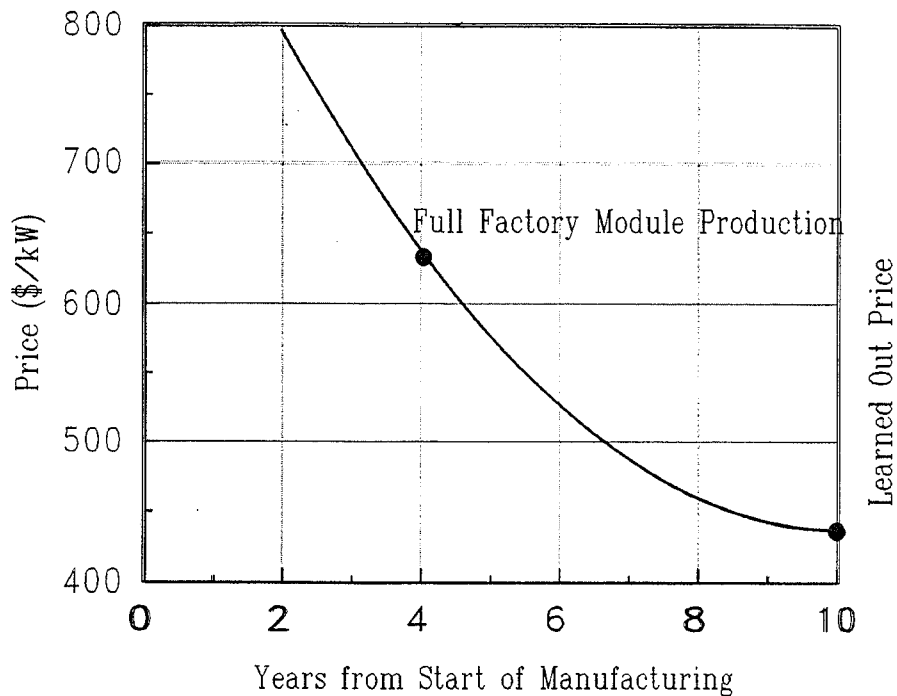


Figure 4-13. NaS-P_{AC} System Price Projection with Market Development

This selling price analysis was the basis for the estimation of payback period and the cash flow analysis (levelized life cycle cost) presented in Section 3.5.

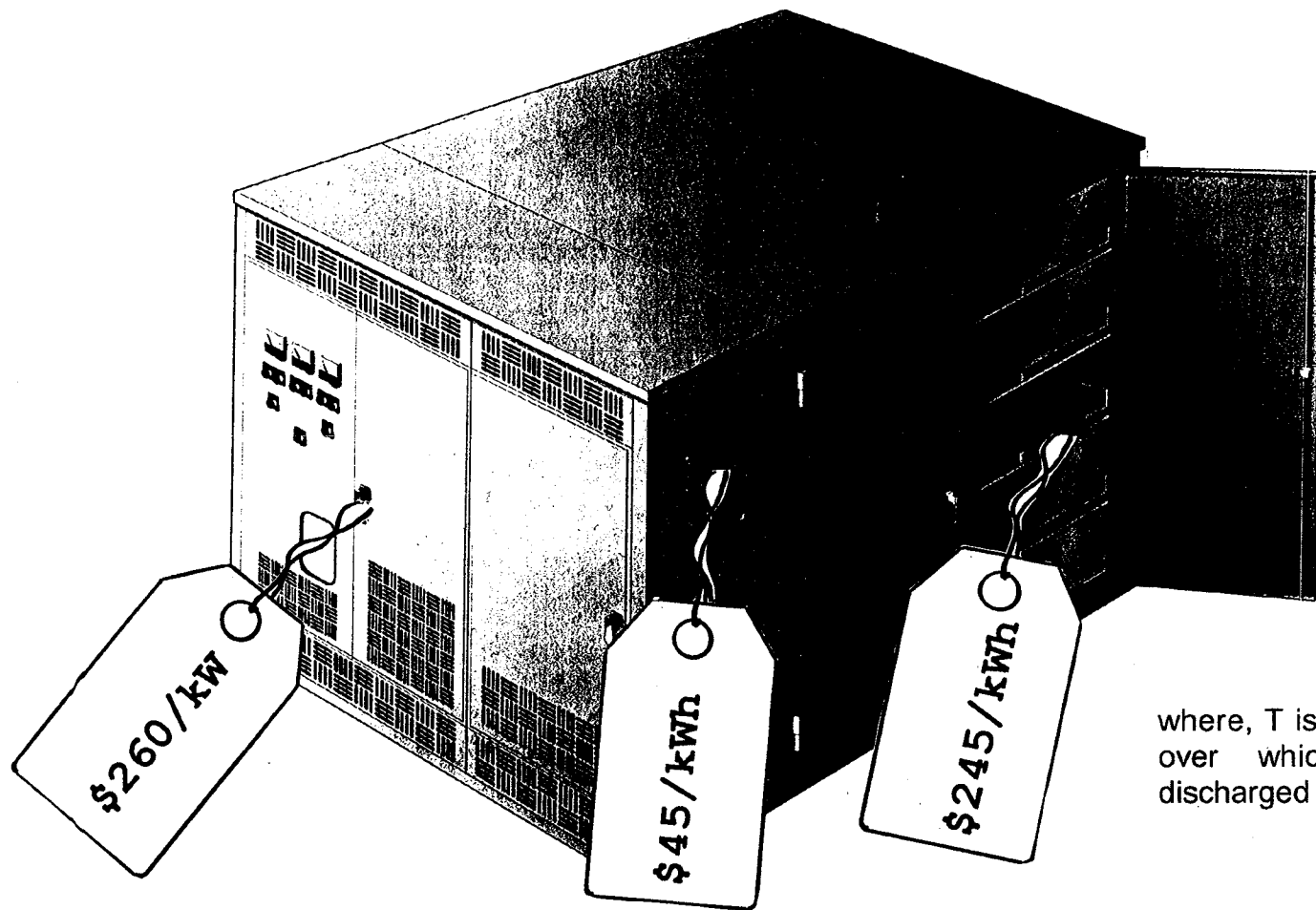
4.3 Other NaS-P_{AC} System Designs

As a follow-on to the 300 kVA/300 kWh NaS-P_{AC} system design, designs for several smaller systems were pursued. One was a 30 kVA (50 kVA peak) BESS that could sustain 2 hours of operation at rated power. The design was conceived to approximate the size of a 5 ton residential heat pump. This system was comprised of two, 28 kWh sodium sulfur EV batteries connected in series to operate over the range 312 VDC to 400 VDC (end of discharge to top of charge). The PCS was specified to utilize this DC input and to provide 480 VAC, 3 phase, to operate, for example, in a peak shaving mode for light industrial or commercial applications. Another potential application would be to provide energy storage capability for distributed renewable energy generation systems – i.e., for wind or photovoltaic systems.

The other design was a 3 to 4 kVA BESS for residential applications. This design was conceived as a possible dispatchable add-on to a commercial 3 ton residential air conditioner, perhaps as part of a utility DSM program. In practice, it could be used to store energy from a residential PV array. Operating at 48 VDC, there were a number of battery design innovations offered as part of this system that are discussed in this section.

Production Volume Assumption:

10 to 20 BESS/year combined with an EV market for 400 MWh of annual battery production



where, T is the duration in hours over which the system is discharged

$$PRICE(\$/kW) = 260 + [1.33 (245) + 45] T = \$630/kW \text{ for } T=1 \text{ hour}$$

Figure 4-14. NaS-P_{AC} System Near Term Price: Power and Energy Composition

Production Volume Assumption:

100 to 500 BESS/year combined with an EV market for 400 MWh of annual battery production

FAVORABLE

$$PRICE(\$ / kW) = 220 + [1.25 (140) + 35] \tau = \$428 / kW \text{ for } \tau = 1 \text{ hour}$$

Figure 4-15. NaS-P_{AC} System Future Price Composition

Before pursuing these designs in detail, it is worth noting the difficulty faced in attempting to make these systems viable from a cost standpoint as the system size decreases. The issue is: Are there individual residential customers who need these services and who can afford to purchase them? If the equipment is located at a distribution point that serves numerous customers, the cost of a larger system would be spread among all of the subscribers over a reasonable recovery period. However, since the system is smaller, the residential owner is paying a higher \$/kW cost, possibly making the purchase no longer economically justifiable.

The 30 kVA, 2 hour NaS- P_{AC} system is presented in Figure 4-16. The envelope dimensions are 1067 mm (H) x 914 mm (W) x 1270 mm (L). The system layout is divided into a PCS compartment (front end) and a battery compartment located in the rear. The system is depicted with the "skins" removed to show the locations of the various PCS and battery components. The major packages within the PCS compartment include the inverter stages and associated gating circuitry, the digital controller and user interface, and an isolation transformer. The two batteries are stacked which facilitates cooling during a 2 hour sustained power discharge. A single blower is located below the battery stack and draws in ambient air from above the PCS compartment; this air flow first cools the inverter stages. This now pre-heated air is drawn into the blower and discharged into the battery chimney which contains the battery oil-to-air heat exchangers. The hot air is finally discharged at the top of the battery compartment. The cooling design was based upon dissipating 1500 watts from the inverter and batteries during discharge. The resultant air temperature rise is 10°C per cooling surface, or 30°C overall from inlet to outlet.

To verify the design, a full scale mock-up of the proposed design, shown in Figure 4-17, was constructed using the actual heat sinks. Heaters were mounted on the back of each heat sink to simulate the actual heat sources. Testing verified that the system pressure drop was consistent for the design volumetric air flow rate of 270 cfm; the power consumption was 330 watts. The 10°C air temperature rise design requirement was achieved for all but the top battery heat exchanger, which operated at a temperature higher than anticipated. It was shown that this was caused by a transition to laminar flow encouraged by the air straightening effect of the previously encountered finned heat sink. A modification was made to the design to insure turbulent conditions. This corrected the cooling deficiency in the upper heat sink so that the design cooling specification was met.

In addition to verifying the design fit-up and cooling scheme, an effort was undertaken to integrate the battery control function into the PCS digital controller. Eventually, the processor will be capable of implementing the battery control algorithm through the development of specific software. This will include the start-up and shutdown sequence associated with the temperature activation or deactivation of the batteries. The output of this effort was limited to the development of a complete electrical design and specification to implement the proposed integration.

An idea evolved from discussions with utility DSM managers that a small BESS might be feasible for residential customers. At first, the design was predicated on the use of distributed off-peak storage to offset utility power demand during peak air conditioner

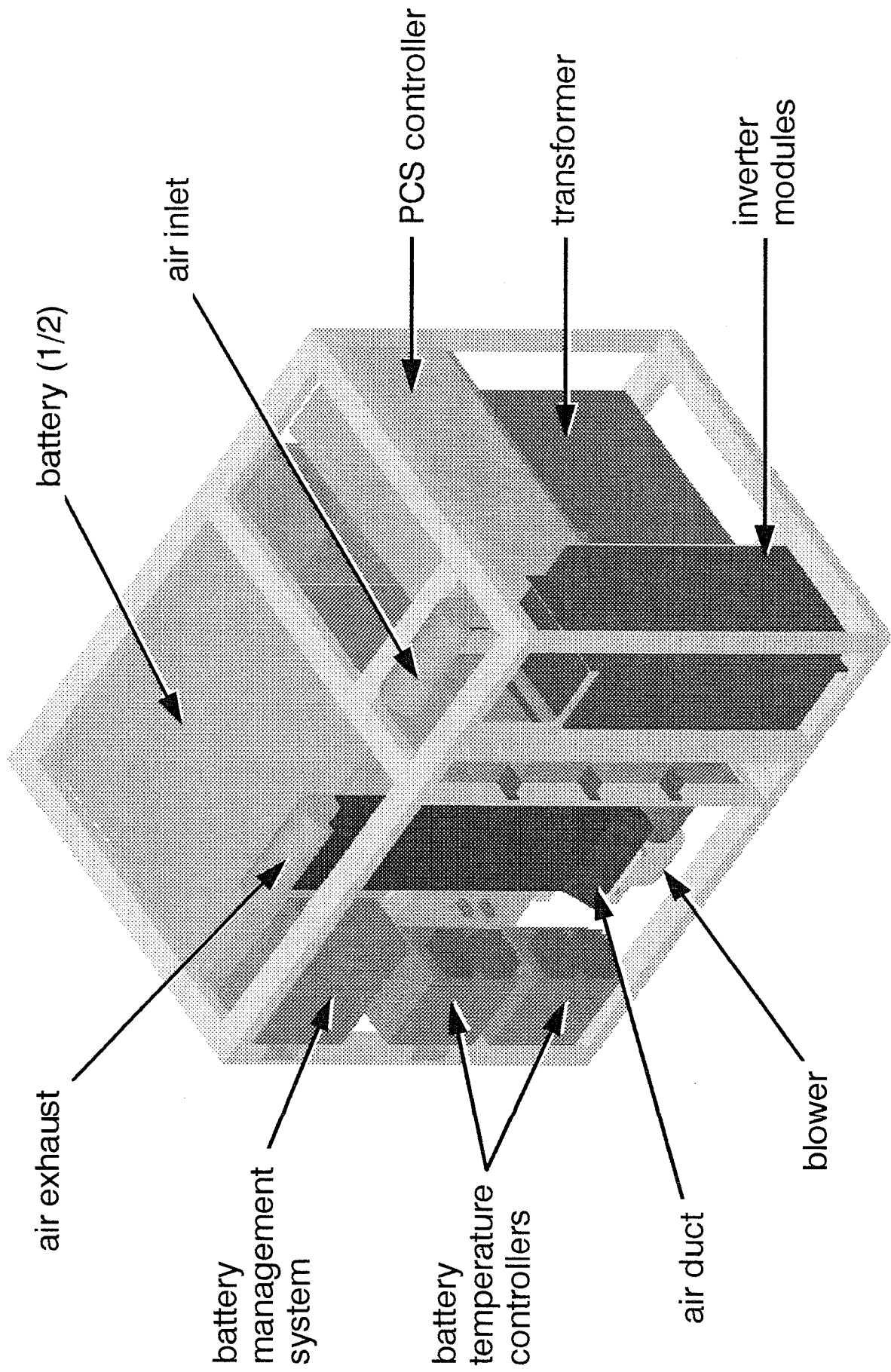


Figure 4-16. 30 kVA - 2 hour NaS-P_{AC} System Design for Commercial Applications

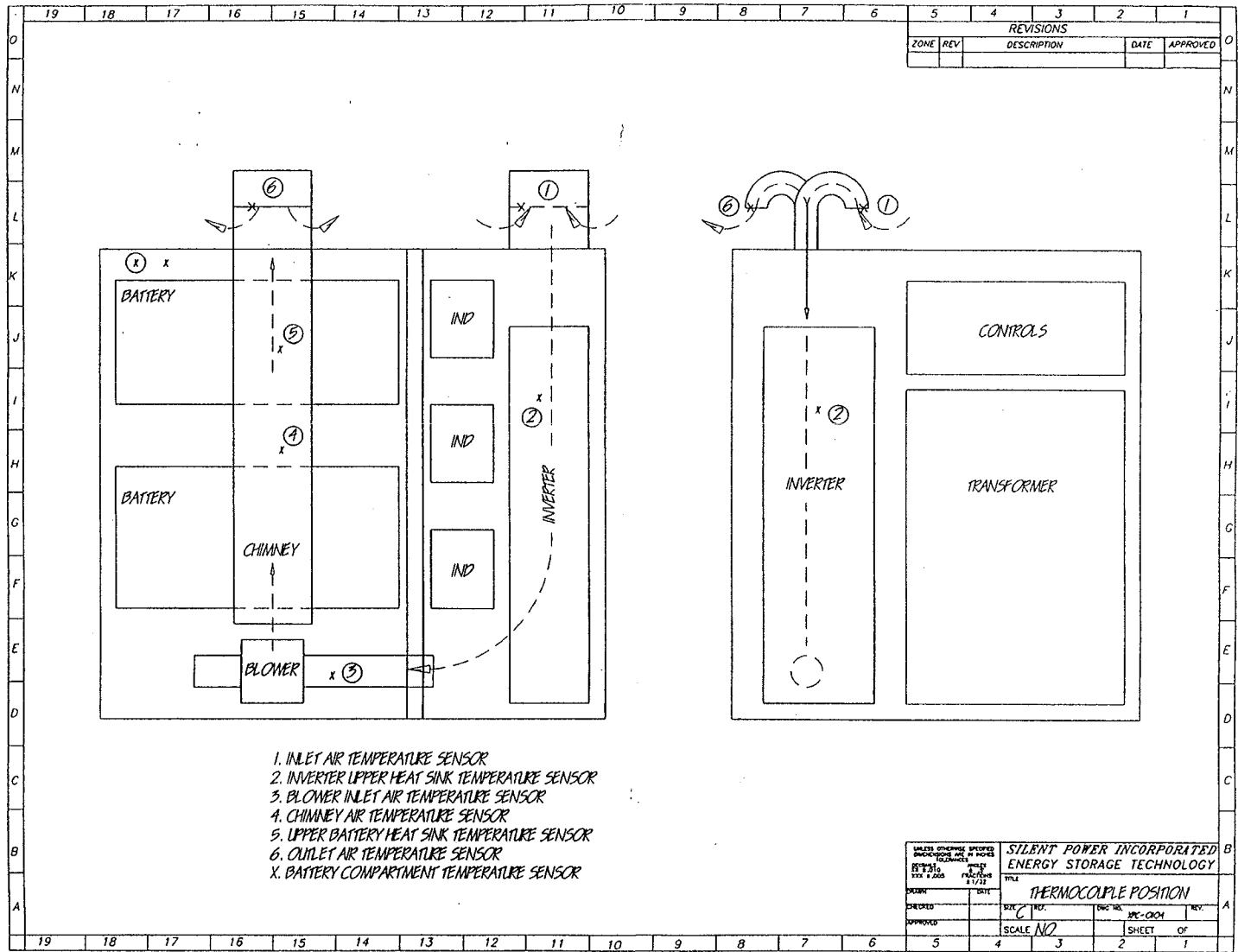


Figure 4-17. 30 kVA System Mock-Up for Thermal Testing

periods. A small 3.5 kVA BESS package, possibly designed as an add-on to a standard 3 ton residential heat pump, would be feasible provided the costs are not significantly greater than the installed cost of the heat pump. Rather than offering curtailment as the only option, the unit could be remotely dispatched by the utility as part of their DSM program. An alternate use would be for the BESS to provide dedicated outage protection and to guarantee power quality. In fact, these services may ultimately be the most important residential customer benefits as computers continue to establish a firm foothold in the household. In practice, the BESS will likely be called upon to accomplish both tasks; and, in this way, utilities can begin to offer lower cost premium services. Assuming that the costs can be made reasonable, the other opportunity is for the ownership to rest with the homeowner or with a third party.

The 3.5 kVA - 2 hour BESS design package is depicted in Figure 4-18. The outside envelope dimensions, 914 mm (H) x 584 mm (W), were chosen to be consistent with a standard 3 ton heat pump and with the size constraints imposed by available PCS hardware and the sodium sulfur battery. The PCS inverter, which is shown mounted at the front in Figure 4-18, uses 48 VDC to provide 120 VAC single phase; however, a distribution box, which is shown located at the bottom of the package, provides for 208 VAC applications. The battery heater controls, isolation switches and interface control boxes are mounted on the facing side.

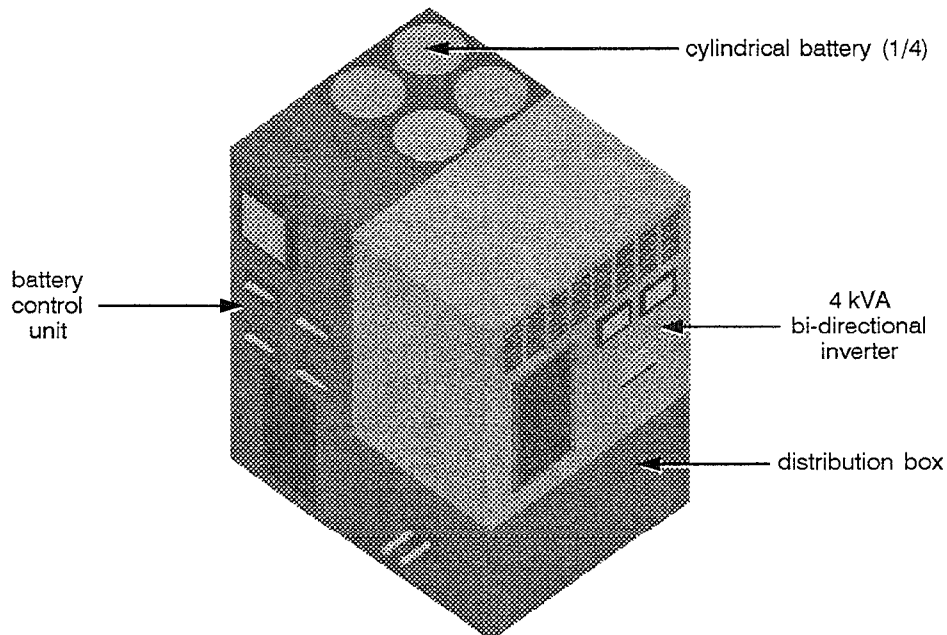


Figure 4-18. 3.5 kVA - 2 Hour NaS-P_{AC} System Design for Residential Applications

The 3.5 kVA - 2 hour BESS design includes four cylindrical battery packs that were designed specifically for this application. The batteries, which are shown housed in the back of the package in Figure 4-18, are connected two in series by two in parallel. Each battery pack is rated to deliver 1.7 kWh at 24 VDC and weighs approximately 27 kg (60 lb), making them convenient to handle. As shown in Figure 4-19, each battery contains four banks of seven, 4-cell series strings. The cylindrical design facilitates the manufacture of the evacuated enclosure, making for a simple, low cost construction utilizing common steel tubes. The power connections and instrumentation exit the thermal environment through a thick molded insulation cap. The advantage that sodium sulfur brings to this application is, once again, size and weight.

Assuming a 50% duty cycle on the air conditioner, the proposed BESS design should be able to supplant utility power during the four hours of peak demand. Alternatively, the unit could provide direct household power during utility outage periods and also could insure the power quality/premium service that will be mandated in the near future. The estimated price of such a system is \$5000 initially with the inverter assuming 60% of the cost. In high production volumes, however, the system price should come down to \$2700 (\$0.77/watt), which is less than the installed price of a conventional 3 ton heat pump. At this price and assuming \$20/kWh peak demand charge, the payback period is less than 3 years.

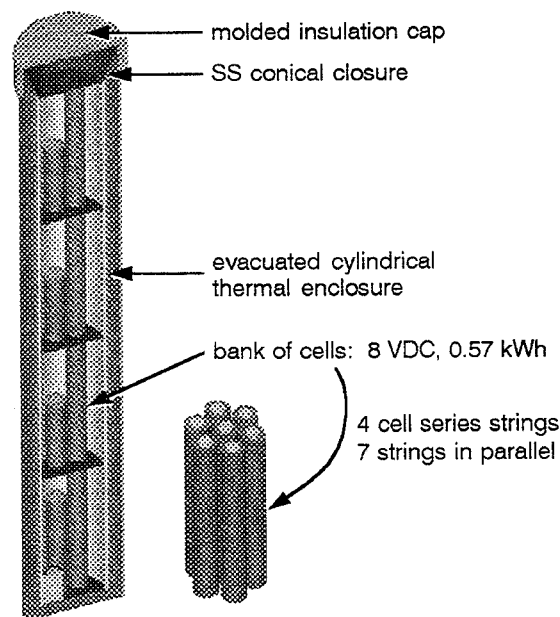


Figure 4-19. 24 VDC Custom Battery Design for Residential BESS

4.4 A Future Custom UES Battery Design

The cell and battery hardware development activities in this program were directed by the need for lower cost and longer lived sodium sulfur batteries to serve the utility and utility customer applications identified in Section III. Toward this end, a preferred battery design was generated based on the use of the 70 Wh central sulfur cell developed in this program. While the details of this cell and battery development effort are described in Sections V and VI of this report, the battery design is presented here as a part of the overall NaS-P_{AC} design activity. Furthermore, this provides a natural lead-in to the hardware development tasks which follow.

The initial BESS design was specified as a 300 kVA/600 kWh system. The battery was comprised of 8 packs, connected 4 in series by 2 in parallel. The working voltage range for this system from end of discharge to the top of charge was 444 VDC to 540 VDC. As shown in Figures 4-20 and 4-21, each battery pack was made-up of 1920 cells arranged in two layers. The two layer design was preferred from the standpoint of temperature uniformity as a result of each cell experiencing the same thermal environment. The five-cell string was the fundamental building block of the battery. This string length was selected to insure that, statistically over the 1500 cycle battery life, no string would have five failed cells.

The battery plan area shows the in-line cell matrix with interstitially located thermal energy storage (TES) capsules embedded. These capsules contained the eutectic salt (LiCl-KCl) described in Section 5.3.1.1. Over the 2 hour rated discharge, the cells, which have an initial temperature of 330°C, will heat-up gradually until the salt begins to melt. At this stage, the cell temperature rise will be arrested as heat is transferred from cell to the salt capsule. The benefit of storing the heat is the elimination of an active cooling system and any maintenance that may be associated with it. The initial design electrically isolated the cells and TES capsules with thin mica sheets; but later, owing to the assembly difficulties presented by such a design, this was changed to an MgO cemented matrix. The properties of the MgO provide the required electrical isolation while insuring good thermal contact. This was verified as part of the battery development activity and put into practice in the assembly of the prototype battery module delivered to Sandia for testing.

The thermal enclosure employed 76 mm (3") of conventional ceramic fiber insulation. The rationale for this design was the emphasis on low cost and no maintenance. The exterior dimensions of the battery pack are 1.56 m (L) x 1.48 m (W) x 0.43 m (H), and the calculated heat loss is 1100 watts. Figures 4-22 and 4-23 summarize the predicted performance of the battery pack as a function of time, under the premise that the cell Weibull statistics, representative of the cell population, can be modeled by a characteristic life (α) of 3500 cycles and a shape factor (β) of 3.3. At the beginning-of-life (BoL) with

* The Weibull characteristics for this cell are lower than that for the cell used in the EV battery

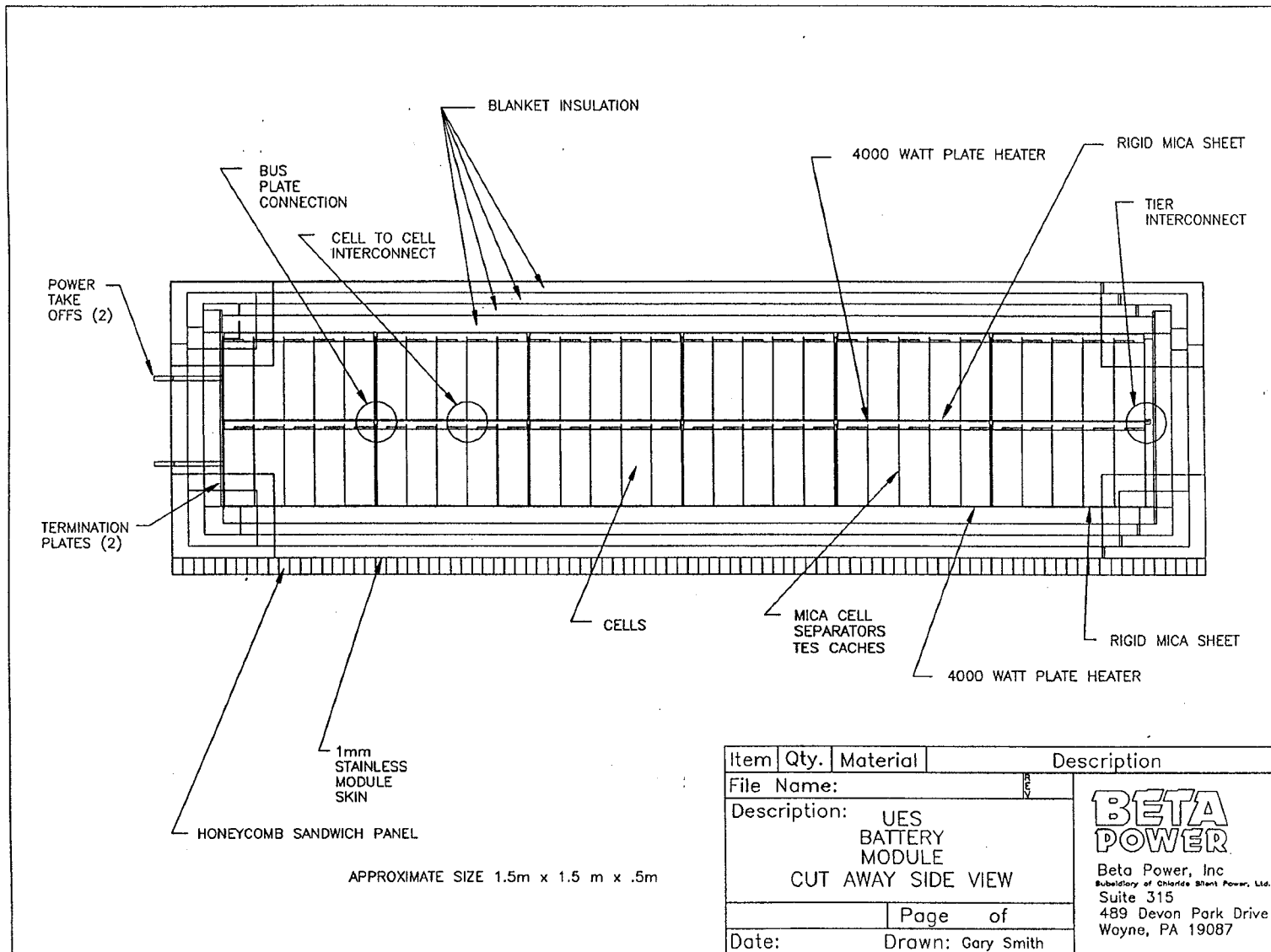


Figure 4-20. 75 kWh Custom UES Battery Pack Design, Cut-Away Side View

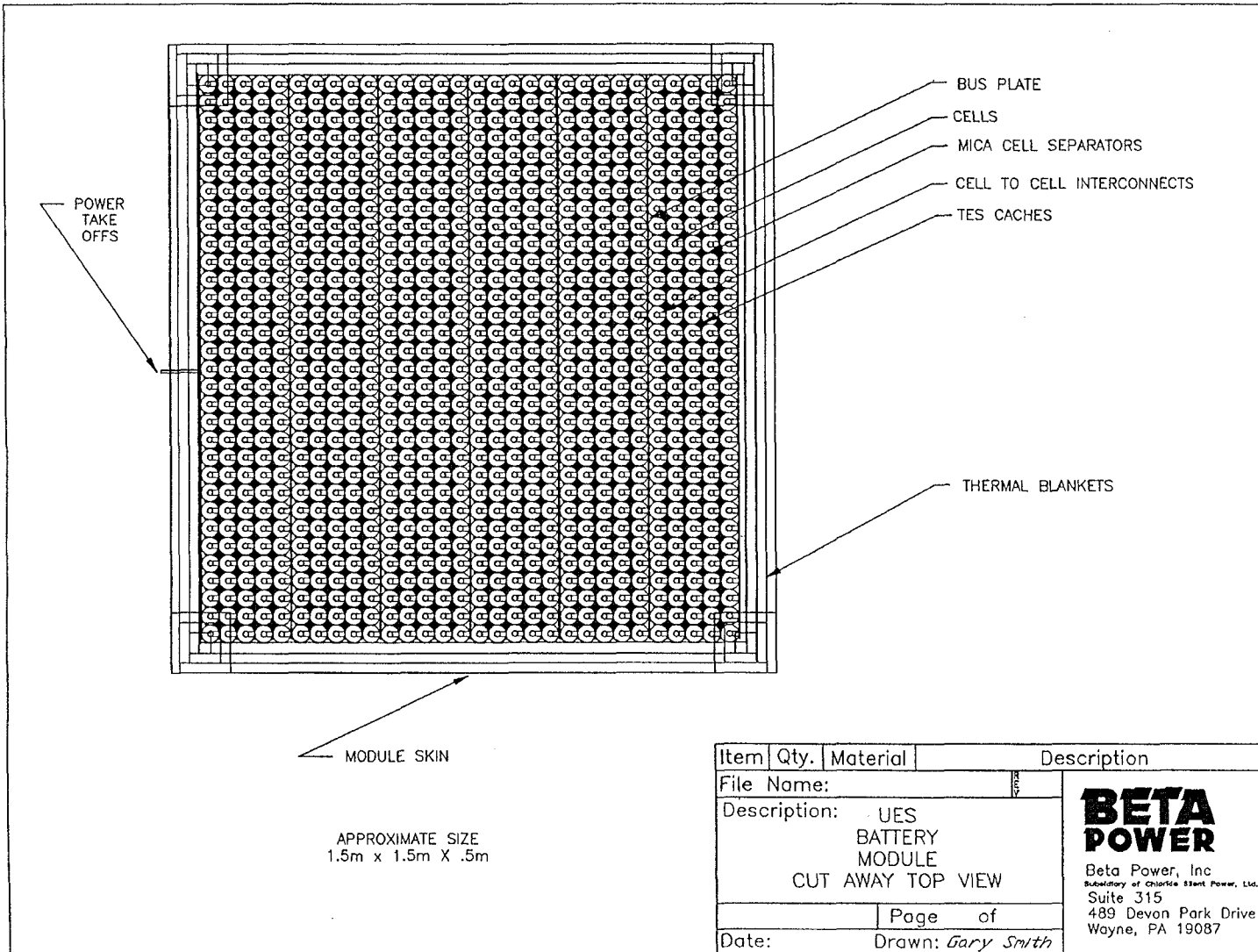


Figure 4-21. 75 kWh Custom UES Battery Pack Design, Cut-Away Top View

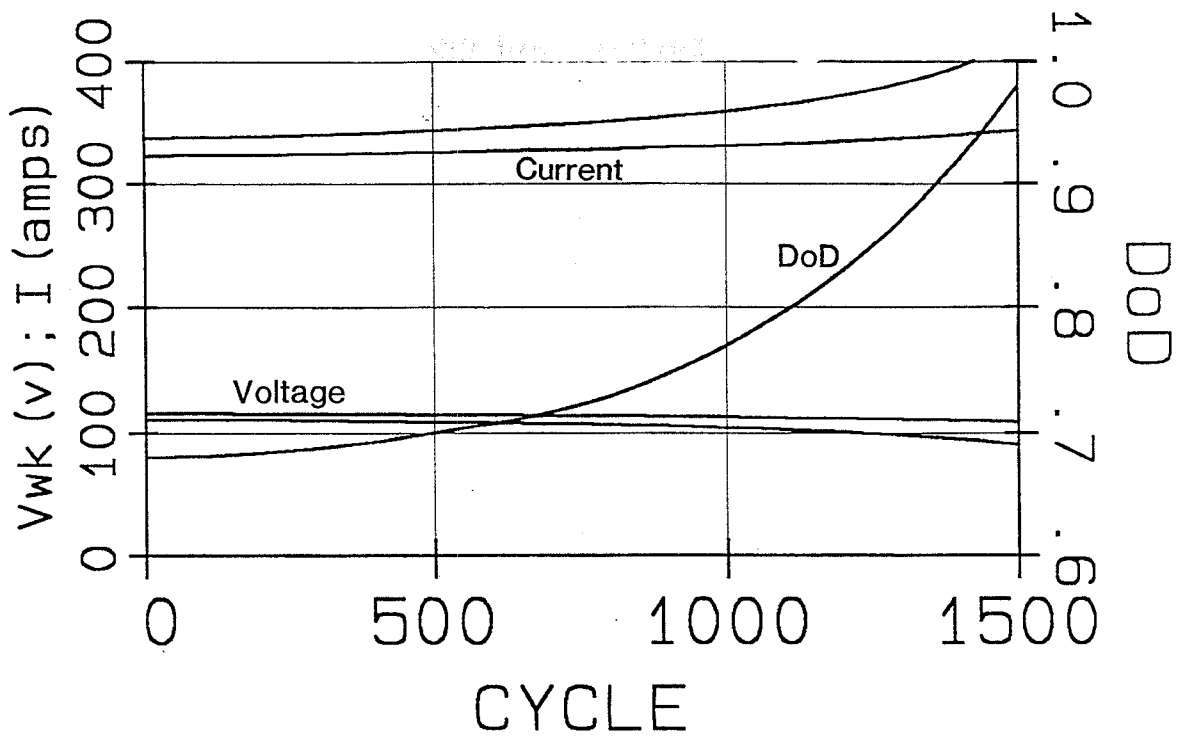


Figure 4-22. 75 kWh Battery Performance at Constant Power for 2 Hours

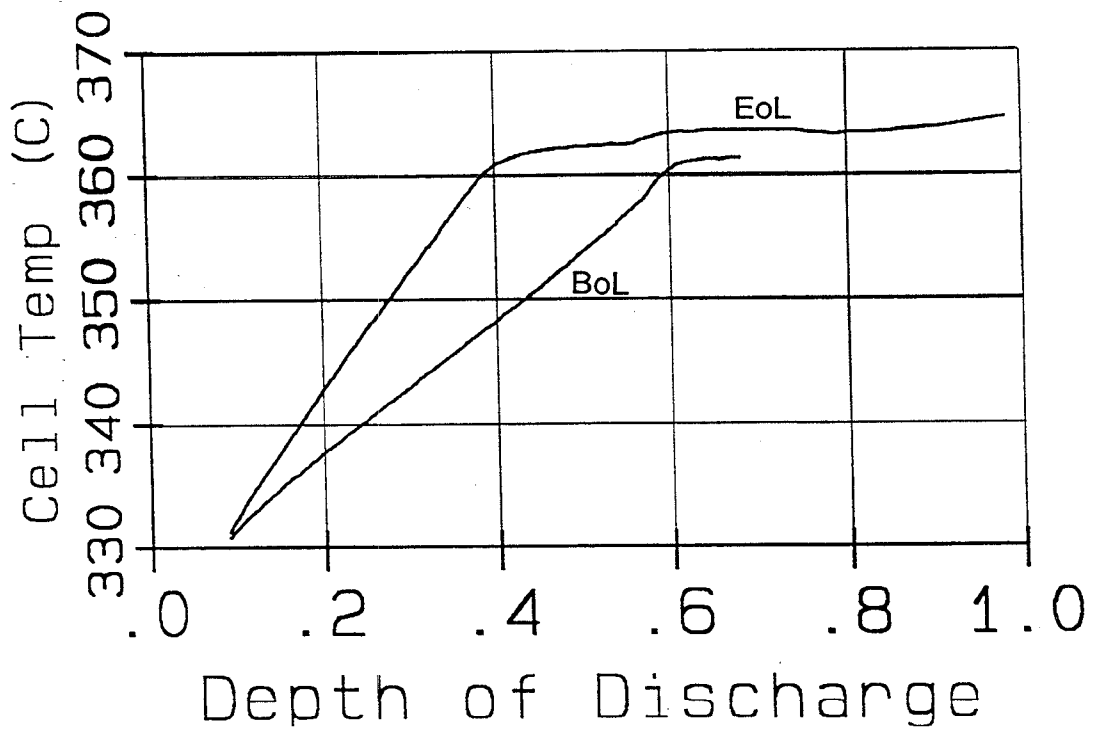


Figure 4-23. Cell Matrix Temperature Rise During 2 hour Sustained Discharge

no cell failures, only 67% of the electrical energy stored is utilized by the end of discharge. Meanwhile, the average cell temperature is expected to rise at a rate limited by the thermal mass of the matrix. The temperature at the end of discharge is just sufficient to initiate the melting of the salt. Later in life as cells fail, the discharge is driven more deeply until the depth-of-discharge of the battery is nearly 100% at the end-of-life (EoL). While the battery voltage remains flat during this time period, the current increases in order to meet the constant power condition. It is at this stage that the complete melting of the salt is utilized to limit the cell temperature rise.

V. COMPONENT DEVELOPMENT

To meet the requirements for a low cost, long life, reliable battery for unattended utility applications, a number of components had to be developed. These included: safe, long lived cells capable of sustaining a reasonable number of thermal cycles; simplified, low cost thermal management systems; reliable, low cost cell-to-cell electrical isolation materials; high temperature fuses to disconnect failed cell strings from the rest of the battery; and a battery management system.

5.1 Cell Design and Component Development

The objective of this task was to develop a cell design which would meet the specific requirements of UES applications. The primary design requirements for the cells are long life (greater than five years), moderate power (one to two hour discharge rate), moderate capacity (greater than 10 Ah but less than 100 Ah), and a low manufacturing cost. In addition to electrical performance and cost requirements, any cell design must exhibit the following characteristics in order to be considered feasible: thermal cycling durability, safety in the event of an electrolyte fracture, and reliable electrical performance.

5.1.1 Preliminary Cell Design

The cell type selected for development under this program was a central sulfur (c/S) cell designed around the dimensions of SPL's XPB electrolyte. The more conventional sodium sulfur cell configuration is a central sodium cell design. However, the c/S design was chosen on the basis of the very long service life such cell configurations have exhibited at SPL. A build of 15 "Technology Demonstration" (TD) cells (Figure 5-1) demonstrated life spans in excess of 8,000 cycles over a period of eight years with continuous cycling. For example, the resistance of TD cell 5601 through 8000 cycles is shown in Figure 5-2. Corrosion of the metal container limits the service life of a typical central sodium cell. This limitation is not observed in the c/S cell configuration because the sulfur/polysulfide electrode is contained within the ceramic electrolyte, which is not corroded by polysulfides.

The physical size and capacity of the preliminary cell (Figure 5-3) were dictated by the size of the XPB electrolyte (33mm OD x 120mm long). This electrolyte size was selected because it was the largest one routinely manufactured by SPL at the time. Larger electrolytes could have been developed for the c/S UES cell, however, doing so would have added unnecessary cost and technical risk to the program. While larger cells may ultimately be desired from the point of view of minimizing battery cost, maintaining cell and battery safety performance becomes more difficult as electrolyte and cell size are increased. Because reasonable safety performance had been demonstrated in the central sodium XPB cells at SPL after several design iterations, it was expected that safe c/S cells of similar size could be made.

The radial, tapered thermocompression bonded (TCB) electrode seals on SPL's TD cell proved to be very effective and durable. However, they required tight tolerances of the

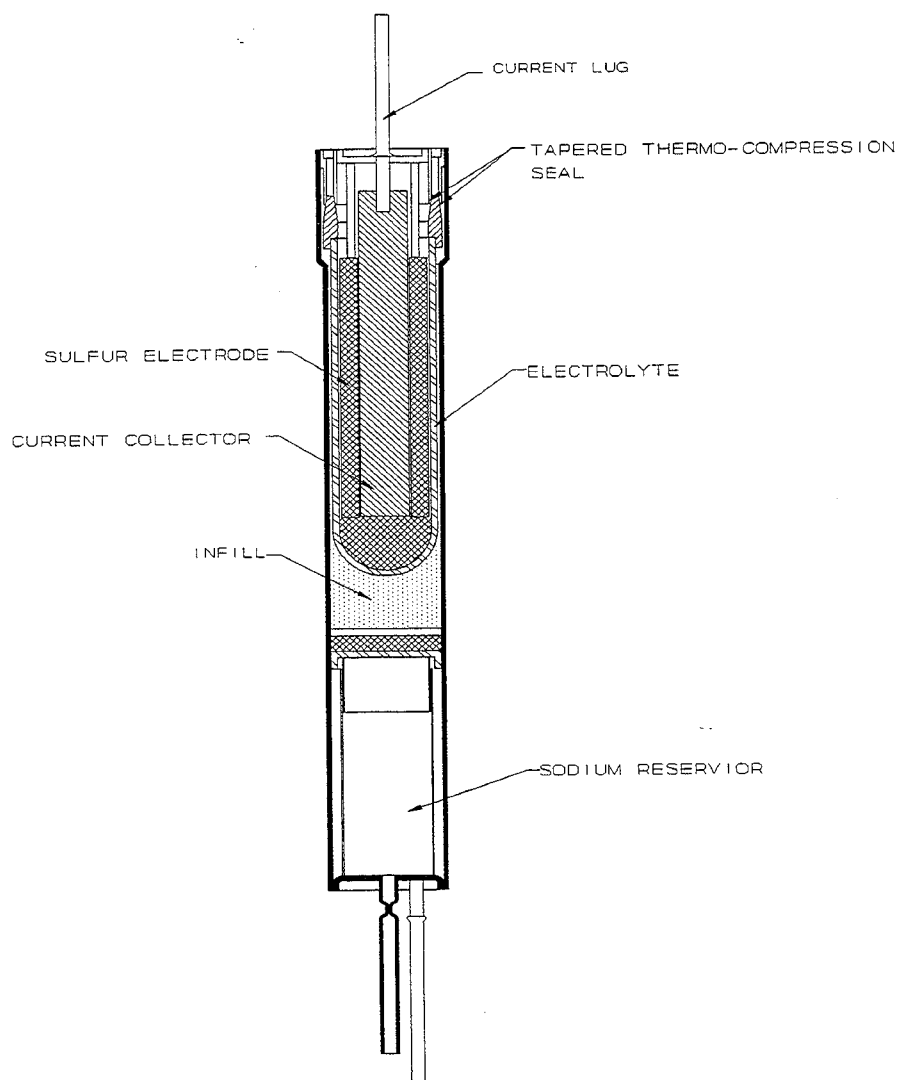


Figure 5-1. SPL's Technology Demonstration Cell Design

machined metal components and of the ceramic seal collar with ground tapers, making it a costly seal. A low cost alternative was chosen using planar TCB seals similar to those which had been developed and successfully used in thousands of PB and XPB cells, as shown in Figure 5-4, fabricated and tested at SPL. Though the electrode seals in the PB and XPB cells were much smaller in diameter (maximum of 18mm) than those which would be required for the c/S cells (37mm), previous success at SPI with TCB seals on flat plate sodium sulfur cells having diameters of 53mm suggested that the larger seals were feasible.

Another major departure of the preliminary c/S cell design from the TD design was replacement of the sodium reservoir at the bottom of the cell by an annular reservoir surrounding the cell. This resulted in a more volumetrically efficient cell design. The

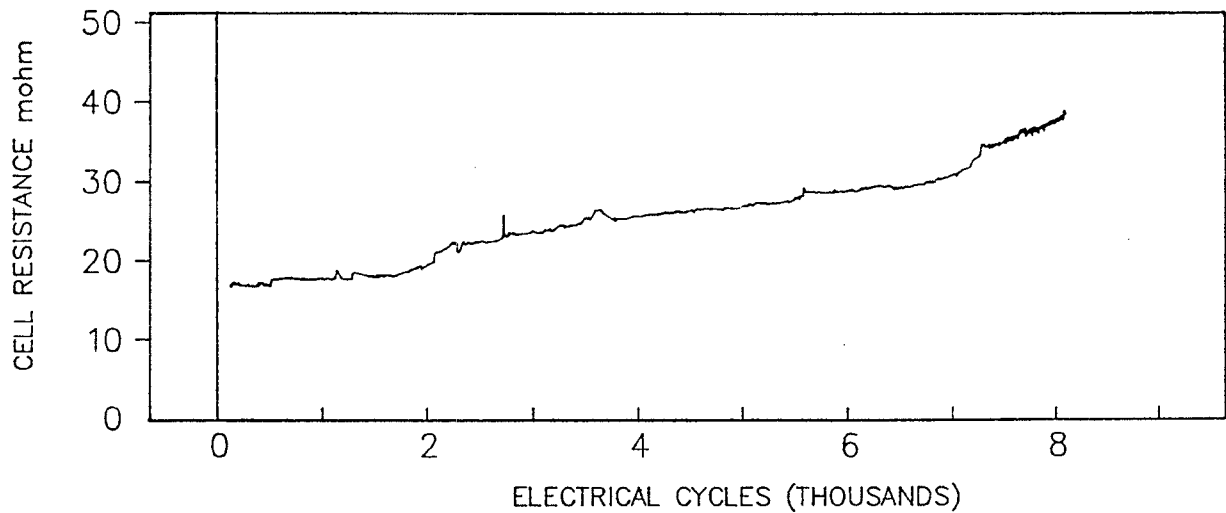


Figure 5-2. Resistance of TD Cell 5601

specifications for the preliminary c/S cell design are shown in Table 5-1. The projected electrical performance is shown in Table 5-2.

Because sodium sulfur batteries operate at elevated temperatures, they must be able to sustain some reasonable number of excursions between operating temperature and ambient temperature throughout their lifetime without damaging the cells or altering their electrical performance characteristics. At the outset of the program, there was no firm specification of the number of thermal cycles which a UES battery must be able to sustain. However, to accommodate cell and battery acceptance testing, battery commissioning, and additional freeze/thaw cycles for battery maintenance and control malfunctions, ten thermal cycles was set as a minimum freeze/thaw cycle goal.

In addition to freeze/thaw durability, safe performance of central sulfur cells during normal and expected abuse conditions must be ensured. Typically, inducing catastrophic electrolyte failure is an excellent technique to assess the intrinsic safety of a cell design. This type of testing had not been conducted for the TD cell. While there was no a priori reason to expect that safe c/S cells could not be fabricated, there were some factors which had to be considered and evaluated. In general, as cell capacity increases, the mass of reactants must increase and, hence, more energy is available for release in the event of an electrolyte fracture. More specifically, cell safety is largely dependent upon the mass of sodium contained within the electrolyte/safety tube annulus – i.e., the wider the annulus, the less safe the cell is. Since the sodium electrode is on the outside of the electrolyte, it is the variations in the outer surface dimensions which become important with regard to safety. The standard methods of fabricating beta"-alumina tend to give relatively good

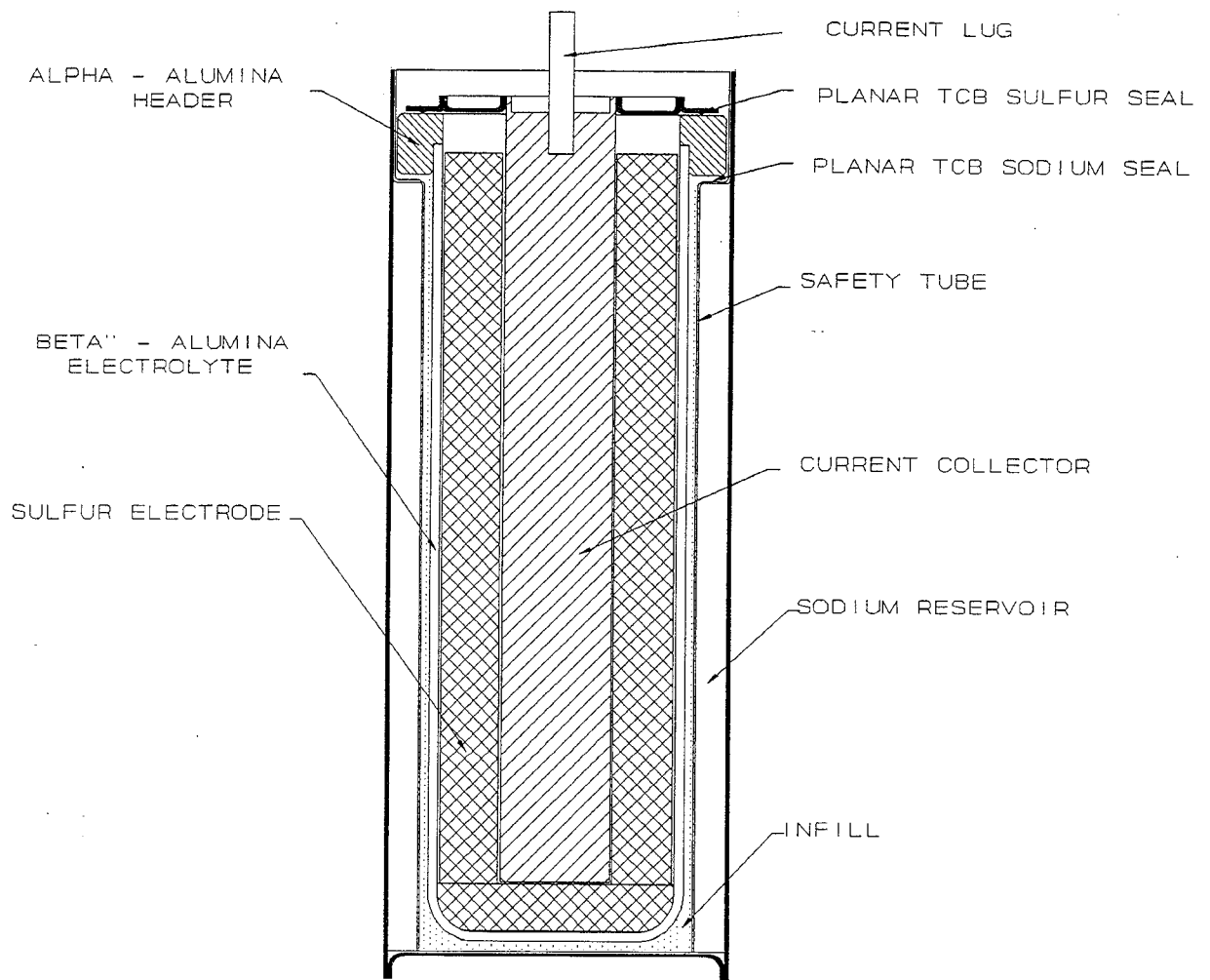


Figure 5-3. Preliminary Central Sulfur Cell Design

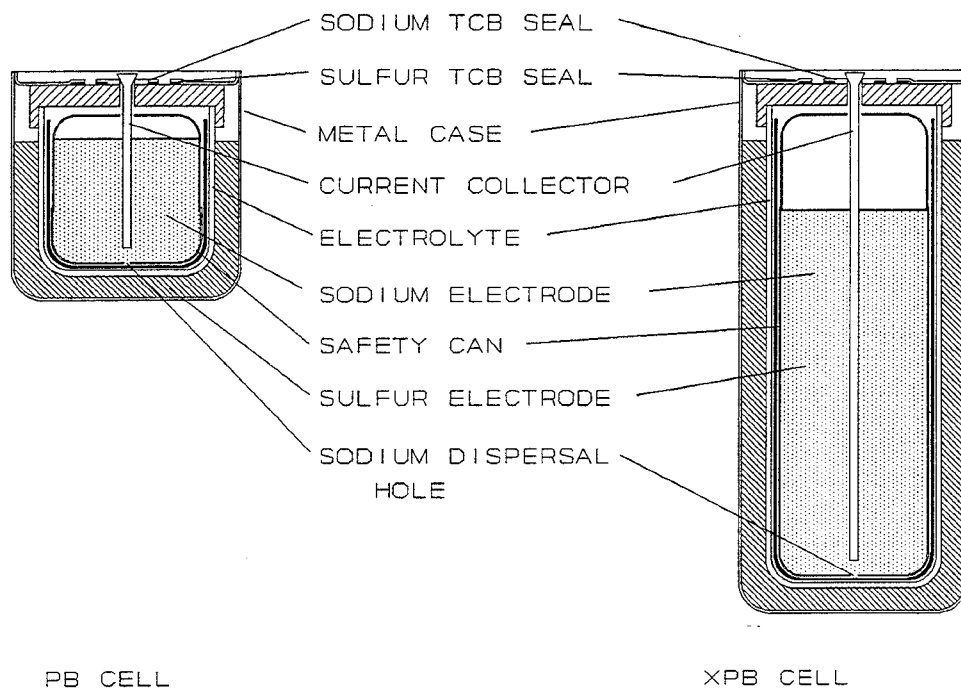


Figure 5-4. PB and XPB Cell Designs

control over internal electrolyte dimensions, but the stack-up of inside diameter and wall thickness tolerances makes the outer dimensions subject to greater variability. The goal established for demonstrating cell safety was that there was to be no breaches in the containment or leaking of reactants in ten cells failed by overcharging with subsequent fracturing of their electrolyte.

Prior to finalizing the details of the design and committing them to hardware, some out-of-cell component experiments were conducted. The purpose of these experiments was to examine electrolyte freeze/thaw durability with an internal sulfur electrode and to further examine the feasibility of the larger ceramic to metal TCB seals.

5.1.1.1 Preliminary Freeze/Thaw Durability Assessment

Freeze thaw durability of c/S cells has long been a concern, but systematic cell trials had not been conducted to either confirm or refute the concern. Further, recent studies at SNL had suggested that electrolyte fracture was likely during thermal cycling of c/S cells due to the thermal expansion coefficient mismatch between the sulfur electrode and the electrolyte tube. In order to address this issue early in the program, several freeze/thaw experiments were planned and executed. These initial experiments examined the behavior of a c/S cathode during thermal cycling.

Table 5-1. Preliminary Cell Design Specifications

DIMENSIONS	44.1 X 114.4mm
MASS	342 gms
PART COUNT	21
ELECTROLYTE	1.4 x 33 x 101.5mm, flat end
SODIUM ELECTRODE	
Sodium mass	36 ± 3 gms
Safety tube thickness	0.25mm
Annulus thickness	1.12mm
Infill/liner	100 grit alumina/0.13mm graphite foil
SULFUR ELECTRODE	
Construction	graphite felt with radially oriented fibers and carbon fiber mat; active base
Sulfur mass	61 - 65 gms
Length	94mm
Thickness	8.33mm
Active electrolyte area	96 cm ²
CURRENT COLLECTOR	
Material	6061-T6 aluminum alloy
Diameter	13.35mm
Coating	0.13mm flame sprayed 80/20 Ni/Cr with 0.25mm isopressed graphite foil

Table 5-2. Preliminary Central Sulfur Cell Performance Projections

Cell Resistance	14.0 mΩ
Theoretical Capacity (to Na ₂ S ₃)	35.5 Ah
Working Capacity	27.0 Ah
Power at C Rate	46.0 W
Specific Energy at C/2 Rate	155.0 Wh/kg
Energy Density at C/2 Rate	296.0 Wh/l

A number of half-cell mock-ups were assembled and tested as follows. An aluminum rod acted as the current collector. Several graphite felt disks were placed over the 6.4mm diameter aluminum rod to act as the graphite felt matrix of an actual cell. Sulfur was cast into the disks and the assembly was allowed to cool. This "precast" was then inserted into an XPB electrolyte which was placed in a beaker of diffusion pump oil. The oil was used to ensure that the assembly would be isothermal. Temperatures were recorded on an X-Y plotter with the Y-axis recording the difference between the oil temperature and the sulfur temperature and the X-axis recording the oil temperature. All samples were heated to 180°C at several different heating rates in an attempt to find an optimum heating rate which would ensure cell survival.

At heating rates of 15°C/hr and 30°C/hr, the half cells survived the first thermal cycle but failed during the heat-up on the second cycle. All failures occurred at approximately 95°C, which corresponds to an expansive phase transformation of sulfur from the alpha phase to the beta phase. All failures occurred at the base of the electrolyte where the sulfur density in the felt was the highest. The forces generated on the electrolyte during the phase transformation caused the failures. The next experiment was an attempt to "outrun" the phase transformation. Since the transformation is somewhat sluggish, the solid state expansion can be avoided by heating the cells rapidly. To test this hypothesis, a sample was assembled as previously described but the heating rate was increased to 60°C/hr. The sample was cycled several times with no failures occurring. While rapid heating eliminated electrolyte fracture, it was obviously not an acceptable solution for a practical battery comprised of many cells.

By the time that these initial experiments had been completed, the preliminary cell design had been completed, and the aluminum rod diameter was changed to match the size of the current collector anticipated for use in an actual cell. The diameter was increased from 6.4mm to 13.5mm. At heating rates of 25°C/hr, 13°C/hr, and 6°C/hr, no electrolyte failures occurred after numerous thermal cycles, indicating that there is a critical current collector diameter above which the probability of electrolyte failure is low enough for satisfactory cell durability.

5.1.1.2 Preliminary Sodium Electrode Seal Trials

The metal-to-ceramic seals which were proposed for use in the c/S cell design were thermocompression bonded using an aluminum alloy interlayer. These are similar in design to the PB cell seals with the following exceptions. First, the PB cell had both the sodium and the sulfur seal in the same plane; in the c/S cell design, the seals opposed each other – one seal formed on the top header surface and one on the bottom. Second, both seals were twice the diameter of the largest PB seal. Third, the cathode sealing ring was made entirely from aluminum eliminating the steel member.

In order to get early data on sealing, chromized PB cathode caps were modified to make large diameter seals to headers using aluminum gaskets. Seals made from these components formed helium leak tight bonds, making them very promising. After several thermal cycles between room temperature and 330°C, the seals remained hermetic.

Concurrent with early seal trials, efforts were made to find a suitable coating for the safety tubes, especially in the seal area. A protective coating was needed to inhibit the growth of a brittle intermetallic layer between the aluminum and mild steel. While the duplex chromized coating applied to the PB components was effective, it was costly and required thicker substrate material to minimize deformation during coating. During the initial design stages, it was believed that thinner seal elements would be better from a thermal stress point of view. Standard bright chrome plating seemed to be a likely candidate and was initially chosen as the coating material for its lower cost compared to crack-free chrome. Seal samples assembled using chrome plated safety cans were characterized by low strength and brittleness. Micrographic examination of these seals showed that an intermetallic layer had formed between the chrome plate and the aluminum. An in-house process for nitriding the chrome plate was then developed and tested. The seal integrity of the nitrided chrome plate increased dramatically, although they were not helium leak tight. Metallography confirmed that the intermetallic compound growth was minimized. In the end, duplex chromizing of the safety tubes was chosen as it was the only coating effective for fabricating strong, leak tight sodium electrode seals.

5.1.1.3 Preliminary Cell Trials

With the preliminary cell design finalized and components acquired, cell building and testing began. These preliminary builds were successful, with cell fabrication being relatively problem free. The early electrical testing of cells without obvious fabrication defects produced performance data which were in good agreement with capacity and resistance projections. Internal resistance values were in the range of 12 - 14 m Ω and f_1 values was approximately 10%, making the working capacity of the cells 28 Ah.

The early electrical and freeze/thaw testing brought to light some additional defects in the cell design. A number of the cells placed on test failed during the initial heat-up or during heat-up on subsequent thermal cycles. Further, a number of cells failed during recharge near the top of charge. All of the first eight cells which failed during testing breached their containers regardless of the cause of failure. Post test analyses (PTA) of the breached cells suggested that the sulfur electrode compartment volume was insufficient to contain all of the reaction products when the sodium electrode was completely discharged. Complete discharge can be due either to electrolyte failure or external short circuiting of the cell. Assuming this was case, the mass of sulfur was reduced from 63 grams to 53 grams. This significantly reduced the severity of subsequent cell breaches; however, it also caused a reduction in the theoretical capacity from 35.5 Ah to 29.5 Ah.

In cells which had failed during charge, the electrolyte had fractured along the junction between the sealing glass and the electrolyte. This suggested that the cause of failure was current focussing due to the geometry of the seal and the electrode. By shortening the sulfur electrodes by 6mm so that the top of the sulfur electrode was below the glass/electrolyte junction, the recharge failures were eliminated.

* f_1 is the fraction of theoretical capacity which is not recoverable on recharge.

After the severity of the cell breaches was reduced by decreasing the sulfur mass, it was possible to determine that the cause of heat-up failures in subsequent cell builds was a result of failure of the sodium electrode seals. The failures occurred at the interface between the aluminum interlayer and the alumina header. When the bonding between the aluminum and alumina was lost, sodium leaked out of the cell and pooled on the top of it, causing a short circuit. The number of cells which failed during the initial heat-up was between 10% and 20% of the cells placed on test. Furthermore, surviving initial heating to operating temperature did not assure that seal failure would not occur during a subsequent thermal cycle. In fact, none of the cells with the original sodium seal design survived more than four thermal cycles. This finding drove the sodium seal development effort which became a significant portion of the overall cell development program.

5.1.2 Seal Development

Developing low cost electrode seals with good freeze/thaw durability was expected to require a significant amount of effort at the outset of the program. As noted previously, out-of-cell thermal cycling trials of large diameter TCB seals were very successful and showed that they could be thermally cycled without failure. However, initial thermal cycling trials of complete cells resulted in a sodium electrode seal failure rate of nearly 20% per cycle. Clearly this was unacceptable, and a seal development effort was undertaken to find a solution.

During testing of the preliminary cell design, no failures of the sulfur seals occurred. However, problems were encountered with melt-through of the aluminum components when making the final closure weld, and leakage of polysulfides through cracks in the final closure welds occurred in several instances. These problems necessitated that further development of the sulfur seal also be pursued.

5.1.2.1 Sodium Seal Development

The failures of the preliminary design cells during heat-up were manifested by sodium leaking through the sodium seal, pooling in the well created by the safety tube and outer container, and eventually shorting the cell. The short circuits usually became evident at temperatures between 280° and 310°C. It was likely that the bond failures occurred at some lower temperature, but until the cell temperature rose, there was insufficient pressure to force sodium past the seal. In some cases, the sodium ignited and melted or burned through the cathode cap, causing additional damage to the cell such as fracture of the electrolyte. Thermal compression bonded seal assemblies which were thermally cycled between room temperature and 350°C for ten cycles without sodium showed no loss of hermeticity in helium leak tests. Therefore, sodium electrode seal failure appeared to be more than a problem of thermal stress induced failure.

5.1.2.1.1 Liquid Metal Embrittlement

An initial investigation into possible cause(s) of the sodium seal failures suggested that liquid metal embrittlement (LME) of aluminum by liquid sodium could have been

responsible for the seal failures. Certainly the three elements required for LME were present – stress, an embrittling liquid metal, and a metal which can be embrittled.

In order to further investigate and quantify the magnitude of the LME problem, a series of mechanical tests of seal assemblies were conducted. TCB seal samples were made by bonding seal rings made from Kovar^R, chromized mild steel, and 410 stainless steel to alpha-alumina headers with 6061 aluminum alloy gaskets. The standard bonding jigs and thermal cycles used for forming cell seals were used. The seals were tested by axially loading the joints on an Instron^R machine until failure occurred. Five samples of each type were tested under three sets of conditions — room temperature in air, at 120°C in sodium, and at 330°C in sodium. The samples tested in sodium were placed, one at a time, into the fixture shown in Figure 5-5 along with enough sodium to completely submerge the seal in sodium when it melted. Installation of the sample and sodium into the fixture was done in a controlled atmosphere glove box to minimize contamination of the sodium by air. Standard vacuum hardware seals were used on the fixture to minimize the possibility of oxygen contamination of the sodium during the test. The data for the seals with chromized mild steel show a clear minimum in strength at a temperature just above the melting point of sodium. This is consistent with an LME mechanism. The results of the strength tests are shown in Table 5-3.

Given that LME was the probable cause of the sodium side seal failures, solving the problem should have been a matter of removing one of the three conditions required for LME to occur — i.e., keeping sodium away from the seal, removing the stress on the seal, or using a metal as the interlayer in the seal which is not subject to LME.

Table 5-3. TCB Seal Strength

SEAL TYPE	23°C, in air (MPa)	330°C, in sodium (MPa)	120°C, in sodium (MPa)
Chromized Mild Steel	14.0±2.8	13.9±2.5	8.2±0.7
Nitrided 410 SS	12.4±1.3	13.5±2.7	NC*
Kovar ^R	9.3±2.4	16.6±3.3	11.3±5.0

*Test was not completed.

5.1.2.1.2 Seal Modification Trials

A number of approaches were taken to resolve the sodium seal freeze/thaw failure problem. The alternatives which were pursued addressed the three elements that are necessary for LME to occur.

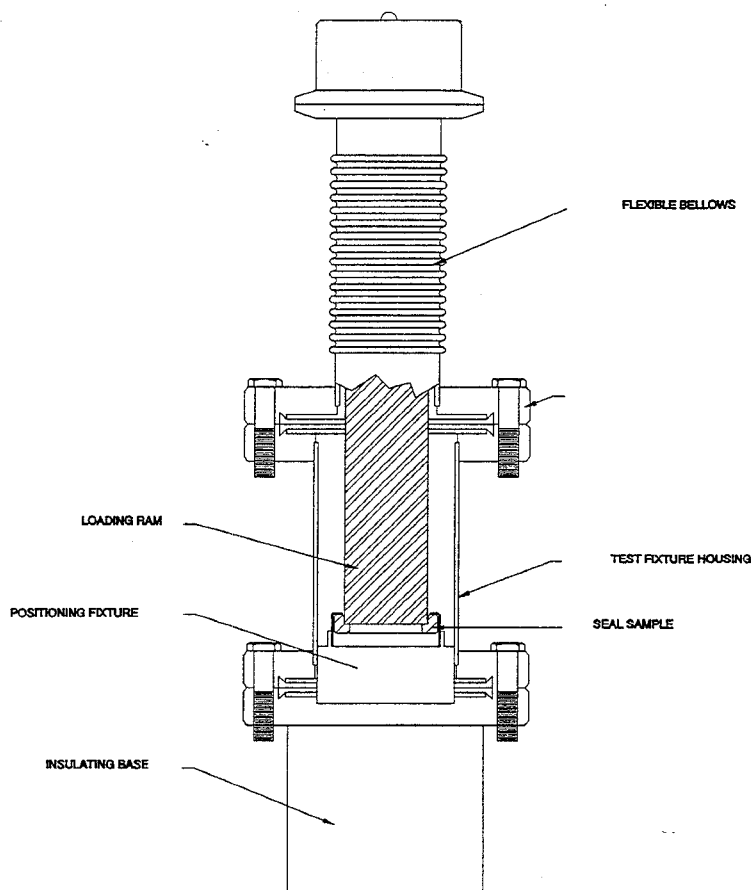


Figure 5-5. Seal Strength Test Fixture

Seal Stress Reduction or Reconfiguration - Modifications to the baseline design to reduce the thermal stresses on the seal included changing the alloy of the metal seal member from chromized mild steel to Kovar^R or nitrided 410 stainless steel; increasing the thickness of the aluminum interlayer; reducing the thickness of the metal seal member; and detaching the safety tube from the seal element. The third modification could also assist in keeping sodium away from the aluminum interlayer. Of these, changing to Kovar^R or 410 stainless steel in combination with detaching the safety tube from the seal member appeared to have resulted in marginal improvement of the seal's durability during thermal cycling:

Another approach was to modify the entire sodium seal configuration to a tapered circumferential seal as was used in the original TD cell. In this configuration, shown in Figure 5-6, the outside diameter of the alumina header was ground with a slight taper. A sealing ring made from Inconel^R 600 with a mating taper and an aluminum alloy interlayer ring were pressed onto the alumina header at an elevated temperature which bonded the ring to the circumference of the header. As the assembly cooled, the aluminum interlayer became compressed between the seal ring and the header due to the higher thermal expansion coefficient of the Inconel^R. With this configuration, the stresses in the aluminum interlayer were always compressive, and shearing of the aluminum interlayer during thermal cycling was eliminated. Five cells with this seal configuration were assembled and tested. The results are shown in Table 5-4.

Reduction of the Susceptibility of the Bonding Alloy to LME - The first approach in this category was to make brazed metal to alumina seals. Though it was recognized that brazed seals could never be cost effective in a commercial cell, it was expected that cells could be produced in which safety and electrolyte freeze/thaw durability could be assessed. The most readily used brazing fillers, copper/silver alloys, were tried, and hermetic seals were produced. However, the silver phase of the filler was rapidly dissolved by liquid sodium resulting in seal lives insufficient to enable freeze/thaw or safety testing. Several non-silver bearing alloys were also tried, but their effective use required facilities and expertise beyond those immediately available at Silent Power. The effort was abandoned in favor of other approaches which would more likely be applicable in commercial cells.

Table 5-4. Sodium Seal Freeze/Thaw Durability

Cell Number	Electrical Cycles	F/T Cycles	Status
-105 Planar	310	13	Off-test. Al weld leakage.
-115 Planar	460+	12	On-test.
-116 Planar	48	9	Off-test. Discharged while frozen.
-121 Planar	267	10	Off-test.
-123 Planar	410	21 10 while discharged	Off-test. Removed for seal evaluation.
-124 Tapered	165	18 8 while discharged	Off-test. Electrolyte failed on 19th thaw.
-125 Tapered	154	10	Off-test. Failed during charge.
-126 Tapered	25	8	Off-test. Discharged while frozen.
-127 Tapered	9	1	Off-test. Failed during second thaw.
-128 Tapered	148	10	Off-test. Degraded performance during cycling.

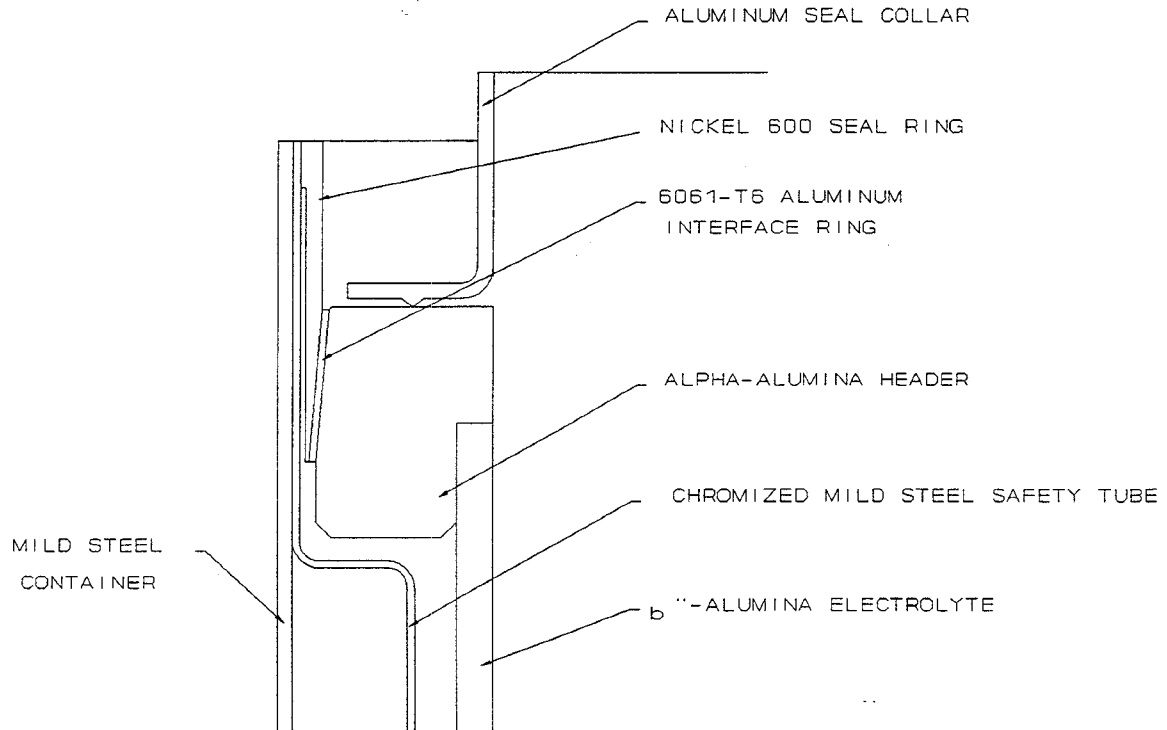


Figure 5-6. Tapered Seal Configuration

The second approach in this category was to change the aluminum alloy used for bonding from the 6061 baseline, while maintaining the baseline geometry shown in Figure 5-7. Alloy 5086 was selected initially for trial, as it is a non-heat treatable alloy and has an eutectic temperature similar to that of 6061. Hermetic seals were produced under bonding conditions which were the same as those in use for 6061 alloy. However, there was no improvement in the freeze/thaw durability of the seals.

The third approach in this category was to use an aluminum-silicon eutectic alloy and a bonding process employing a higher pressure and a lower temperature than specified for the SPI TCB seals. It was believed that this process, taught in German Patent No. DE 43 01 927 A1, would produce seals with greater resistance to general sodium attack. Gaskets $\frac{1}{2}$ mm thick were made from 4032 alloy which contains 12.1% Si and 1.0% Mg and has a eutectic at 432°C. One example in the patent mentions a pressure of 39.2 MPa (5680 psi), but no duration for applying this pressure are indicated. The patent also taught that the eutectic temperature should never be exceeded during the bonding process. The bonding conditions developed were — gasket area 307mm² load 15,700 N, (3530 lbs), a load time of up to five minutes, and a temperature between 450°C and 500°C. Five cells with this seal configuration were assembled and tested with the results shown in Table 5-4. Based on this work, the planar seal with 4032 aluminum interlayers was chosen for the final production cell design.

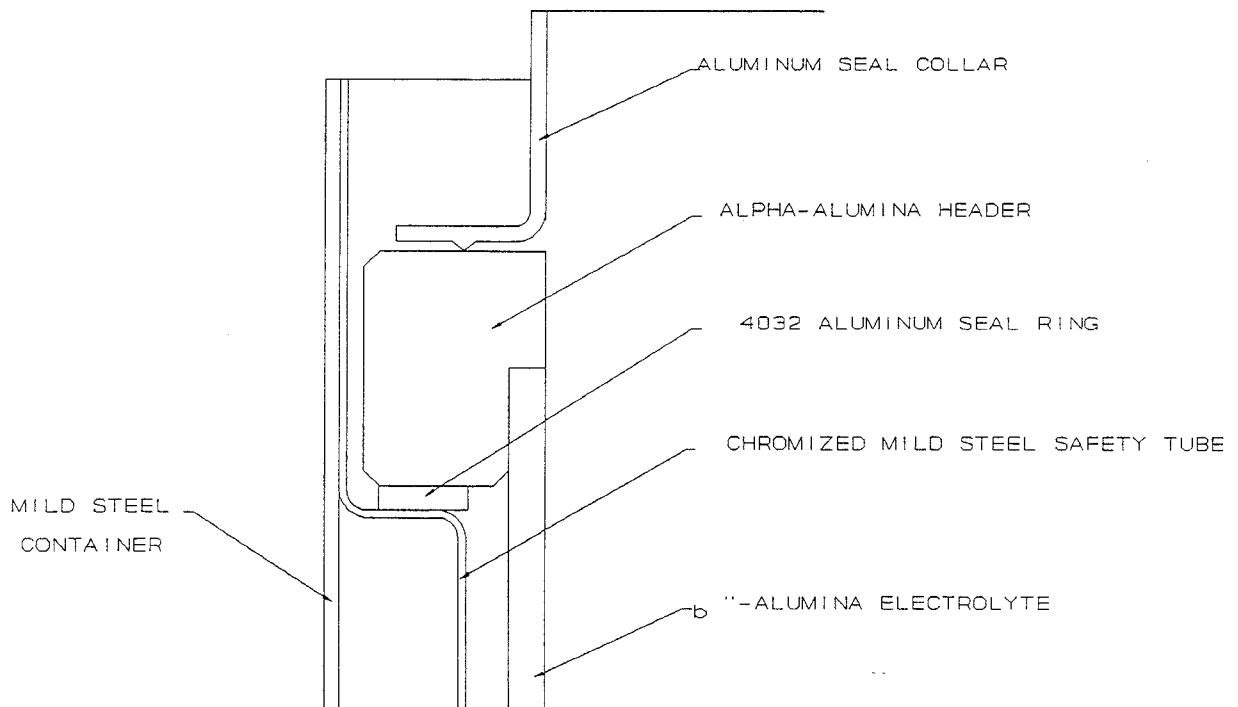


Figure 5-7. Planar Seal Configuration

Elimination of Sodium Contact with the Bonding Alloy - The final solution to eliminating the LME of the sodium seal was to completely eliminate contact between liquid sodium and the seal. To prevent contact between liquid sodium and the seal, a coating of commercial boron nitride paint was applied to the surfaces of the seal after bonding. In order to access these surfaces, it was necessary to detach the safety tube from the sealing flange. This had the concomitant effect of equalizing the pressure at the top and bottom of the safety tube during cell operation. Hence, capillary action was the only force driving sodium into the seal region.

Three cells were fabricated and tested with these modifications. After completing several break-in cycles, the cells were cooled to room temperature and reheated at a rate of 15°C/hr. While at room temperature, each cell was visually inspected for evidence of sodium leakage. Between thermal cycles, the cells were electrically cycled twice to verify capacity and resistance. Two cells survived five thermal cycles with no leakage evident. The third cell began to leak sodium after the fifth freeze. Further testing was discontinued at this point.

While this approach yielded better freeze/thaw durability than the preliminary design, the results were far from sufficient to meet the goal of surviving ten thermal cycles without failure. The boron nitride coating appears to have offered some initial protection, but because it was somewhat porous, sodium apparently worked its way through to the seal.

5.1.2.2 Sulfur Electrode Seal Development

There were few problems with the TCB sulfur electrode seal itself during the program. However, several changes were made to overcome difficulties encountered in making the final closure weld of the sulfur compartment. In the preliminary design, the weldment was 1.8mm; this was sufficient when the alignment of parts was perfect, but this was rarely the case. In many instances, melt-through occurred during welding. The problem was resolved by increasing the length of the weldment by 5mm.

Hot cracking of the sulfur side final closure weld was observed in a number of cells wherein two components made from 6061 aluminum alloy were joined with an autogenous fusion weld. Substituting 5086 aluminum alloy for 6061 alloy in the cathode cap eliminated the hot cracking problem.

During the early sodium electrode sealing trials with low temperature hot pressing, formation of the sulfur seals continued to be done in the original manner with the spring loaded jigs at higher temperatures. In order to minimize the number of fabrication steps, it was desirable to go back to a single bonding operation in which both seals could be formed at the same time. The first attempts at forming the sulfur electrode seals at lower temperatures and higher pressures were completely successful with both 6061 and 5086 aluminum alloys.

5.1.3 Current Collector Coatings

The SPL TD cell current collector consisted of a solid aluminum alloy rod which had been flame sprayed with a layer of 80/20 Nichrome and which was topped by an isostatically pressed layer of graphite foil. While this combination provided a current collector with reasonable performance, additional improvement was desired. For example, after approximately 2000 cycles, the resistance of the cells began to rise and the useable capacity began to decline. Furthermore, it was desirable from an environmental standpoint to minimize the usage of chromium in the cells. For these reasons, an activity was initiated to evaluate a number of alternative materials as coatings for the aluminum current collector.

5.1.3.1 Half Cell Testing

Half cell corrosion testing was performed to provide relative life data of various cathode materials in an electrochemically active melt without incorporating the influence of other cell components. Several electrode types were tested.

All samples tested were immersed in Na_2S_4 , except as noted, and heated to 330°C. The active electrode samples were tested with a control electrode in the melt. The control electrodes were electrically active for only one cycle per week. This was done to provide a means of distinction between degradation due to exposure and degradation due to electrochemical mechanisms. Figure 5-8 shows a schematic drawing of a typical test

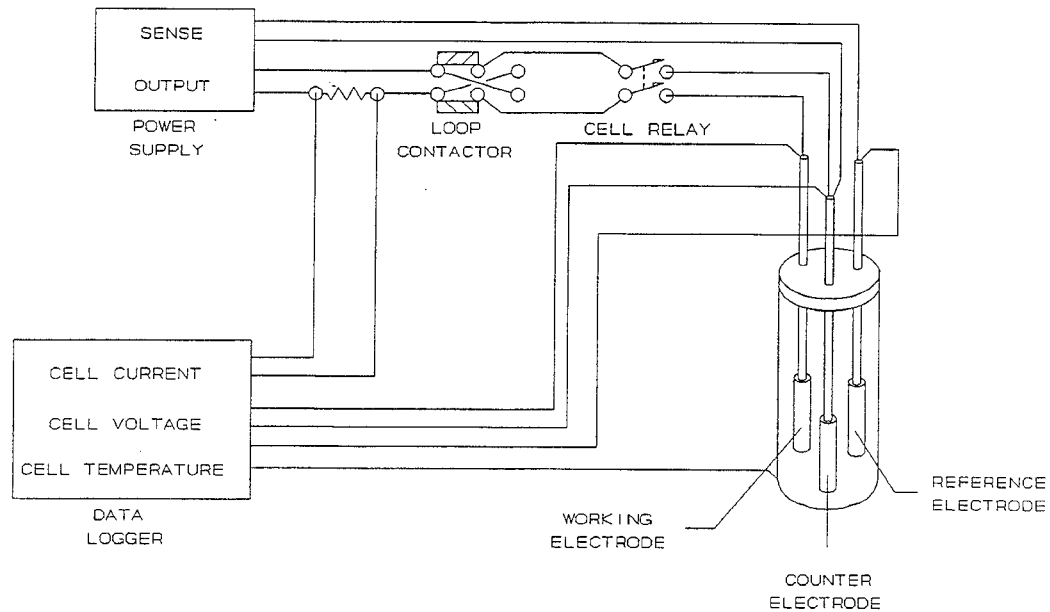


Figure 5-8. Half Cell Corrosion Test Set-Up

set-up used for these experiments. Typical cycles consisted of a 30 minute anodic segment and a 30 minute cathodic segment, with each being separated by a 15 to 30 second open circuit period. During each half cycle segment, the potential between the reference and sample electrodes was maintained at a constant level, and the current between the working sample electrode was recorded.

Though distinctions in performance among different electrodes were observed, it was questionable whether the half cell test results bore a correlation to the performance of the same current collectors in complete cells. Hence, a decision was made to test several coatings in complete cells.

5.1.3.2 Full Cell Testing

Coatings of flame sprayed nichrome and molybdenum, as well as sputtered and ion plated TiN on 6061 aluminum alloy current collectors, were tested in complete cells.

5.1.3.2.1 Molybdenum Coated Current Collectors

Molybdenum was selected as a cathode current collector primarily because it has good stability in the polysulfide melt. Cells were assembled using a thin (0.13mm - 0.15mm) coating of molybdenum, applied by flame spraying to an aluminum pole piece. No additives to aid recharging were included in the sulfur electrode.

Initial testing showed good performance for cell 017, but its resistance and f_1 steadily increased as testing progressed. The rate of change for the resistance rise at the beginning of discharge (BoD) was nearly linear at about 62 m Ω /cycle, which was 25 times

higher than expected. Figure 5-9 shows results from five different cycles for cell 017. While the degradation in relative performance was clearly evident between each cycle, the position and slope of the single-phase region of each charge curve remained nearly constant. This observation strongly suggested that the cause of the increase in cell resistance and f_1 was not due to a loss of sulfur but due to some other mechanism. One explanation for the loss of charge acceptance was that the "catalyzing agent" in the cathode, which is introduced into the sulfur electrode by contamination during fabrication and is needed to allow charge in the two-phase region, was becoming depleted. Alternatively, corrosion products may have been accumulating on the surface of the electrolyte and decreasing the active area.

The sulfur electrodes of three additional cells with molybdenum coated current collectors contained an additive; this was nichrome wire coated with glass except on their ends. The intent was that the nichrome would catalyze the recharge reaction in the cells. The three cells were discharged at a current of 13 A until 18 Ah were removed (75% DOD). Charge was accomplished at a current level of 4 A until a voltage of 2.3 V was reached. This cycling regime continued through 550 electrical cycles, where the charge current was reduced to 2 A with a slight improvement in f_1 .

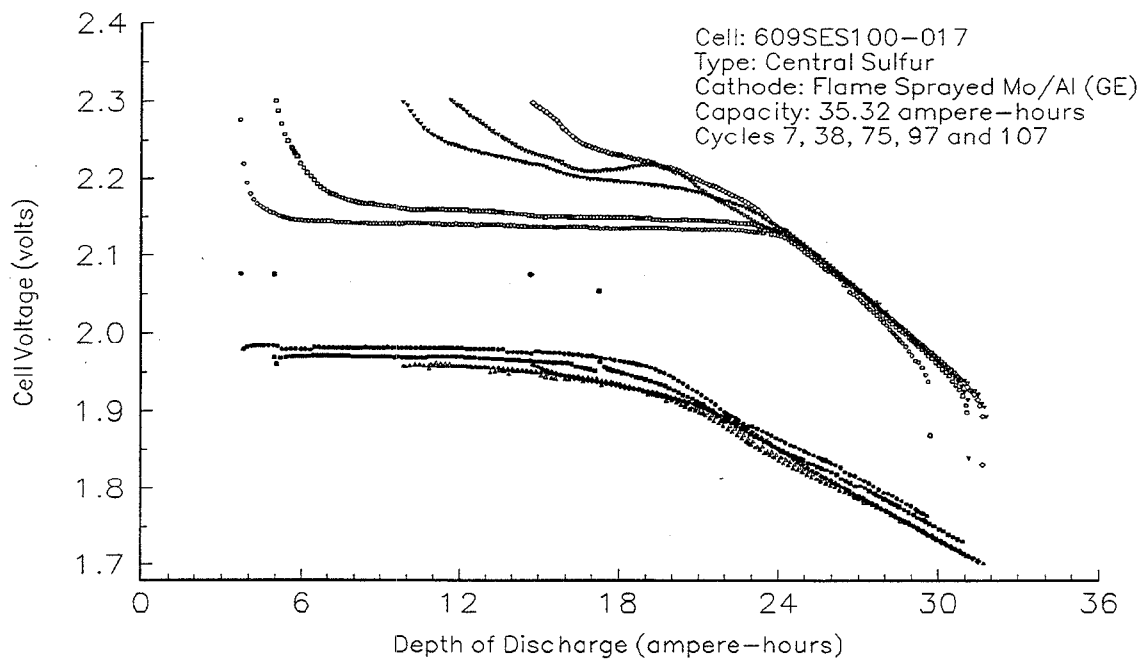


Figure 5-9. Cell Voltages for Cycles 7, 38, 75, 87, and 107 for Cell 017

All three cells showed good initial performance, but the resistance change for cell 035 was higher than that of the other two and roughly took the form of two linear segments. The first segment lasted from cycle 1 through cycle 330 and had a slope of about $30 \mu\Omega/\text{cycle}$. Following cycle 330, the slope increased to $48 \mu\Omega/\text{cycle}$ through the end of testing where the resistance was over $40 \text{ m}\Omega$.

The resistance over the duration of testing for cells 033 and 036 was reasonably consistent. A plot of the resistance vs. cycle number for cell 036, shown in Figure 5-10, is typical for both cells. The resistance for cells 033 and 036 remained relatively flat following a short rise and fall observed in the first 50 cycles. After cycle 330, an upturn in the slope of the resistance at the BoD occurred. The cause in the slope change was unknown but may have been related to an inadvertent discharge to 80% DoD near cycle 330. Cell resistance continued to rise smoothly through cycle 600 where an unscheduled discharge to 92% DoD occurred. Cycling conditions recovered to normal within the next eight cycles, but a step change in cell resistance at the beginning of charge and at the BoD was clearly visible at cycle 600 as shown in Figure 5-10. A decrease in the energy delivered during discharge of 0.5 - 1.0 Wh was observed following cycle 600. Other characteristics of the cell, like the usable capacity and f_1 , did not appear to be affected by the high state of discharge at cycle 600; this is shown in a plot of the DoD discharge and f_1 for cell 036 in Figure 5-11. The cause of the resistance change is likely attributable to an increase in the production of corrosion products in the polysulfide melt at high states of discharge.

5.1.3.2.2 TiN Coated Current Collectors

Six cells were fabricated with TiN coated current collectors and tested. The first group of three cells had their current collectors coated by sputtering at Advanced Modular Power Systems, Inc. The current collectors in the second group of cells were coated by ion plating at Blazers, Inc.

The first group of cells with sputter coated current collectors exhibited relatively poor performance and short lives. After break-in, internal resistances were on the order of $36 \text{ m}\Omega$ and f_1 values were approximately 17%. After 115 cycles, the resistances of two cells began to rise rapidly and were removed from test when they could no longer be cycled. A PTA showed that the TiN coating was corroded over 75% of the surface area of the current collector. The third cell failed as a result of electrolyte fracture after 52 cycles.

The second group of cells, with ion plated current collectors, performed much better. After break-in, the resistances ranged between 11 - 12 $\text{m}\Omega$, and the f_1 's were below 10%. The resistance as a function of cycle number for cell 137 is shown in Figure 5-12. DoD and f_1 as functions of cycle number are shown in Figure 5-13. The step changes in f_1 and DoD shown in Figure 5-12 are artifacts of the test system operation and are not related to cell behavior.

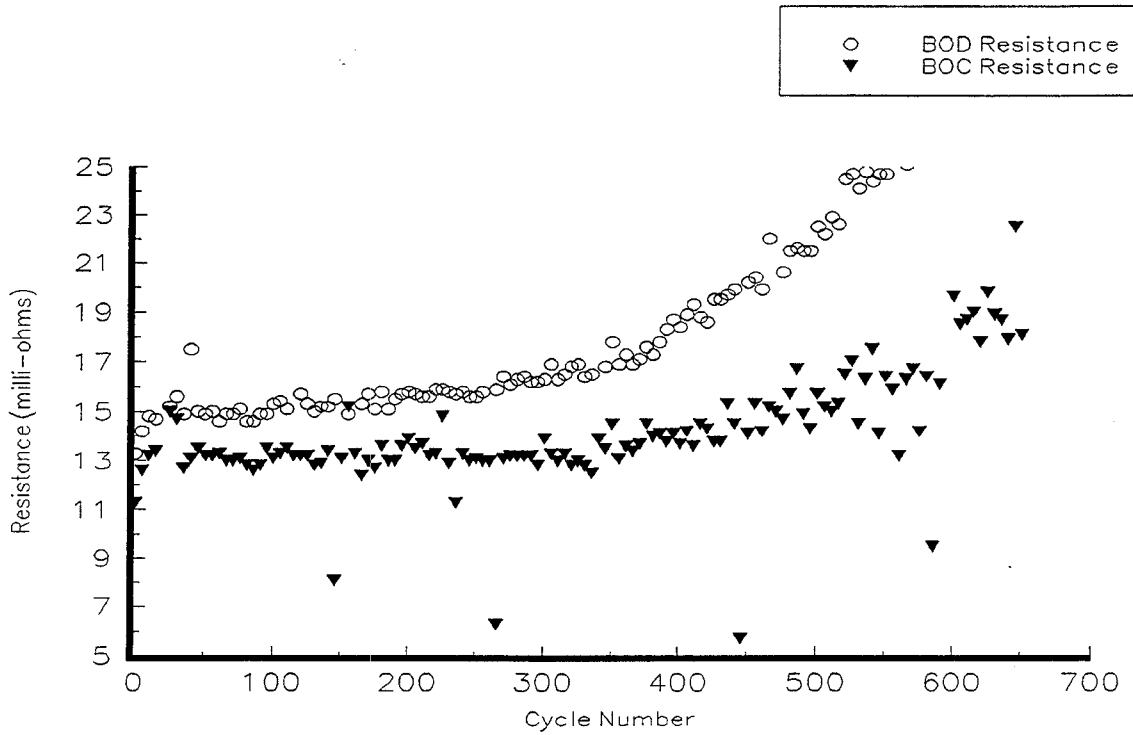


Figure 5-10. Typical Resistance of a Cell with a Molybdenum Coated Current Collector

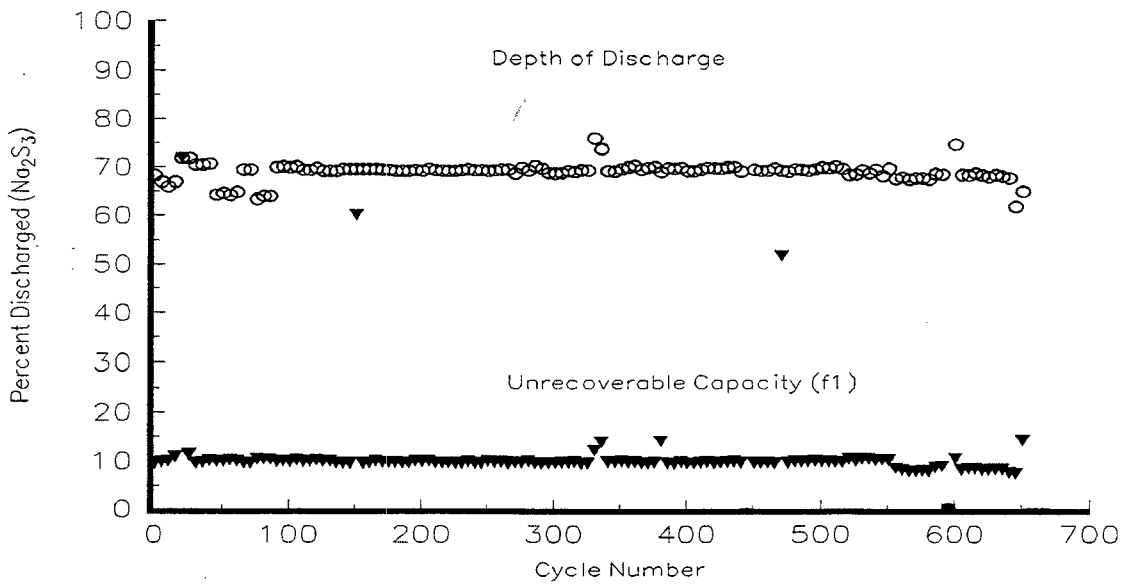


Figure 5-11. Effect of Changing Cycling Conditions on Molybdenum Cell Capacity

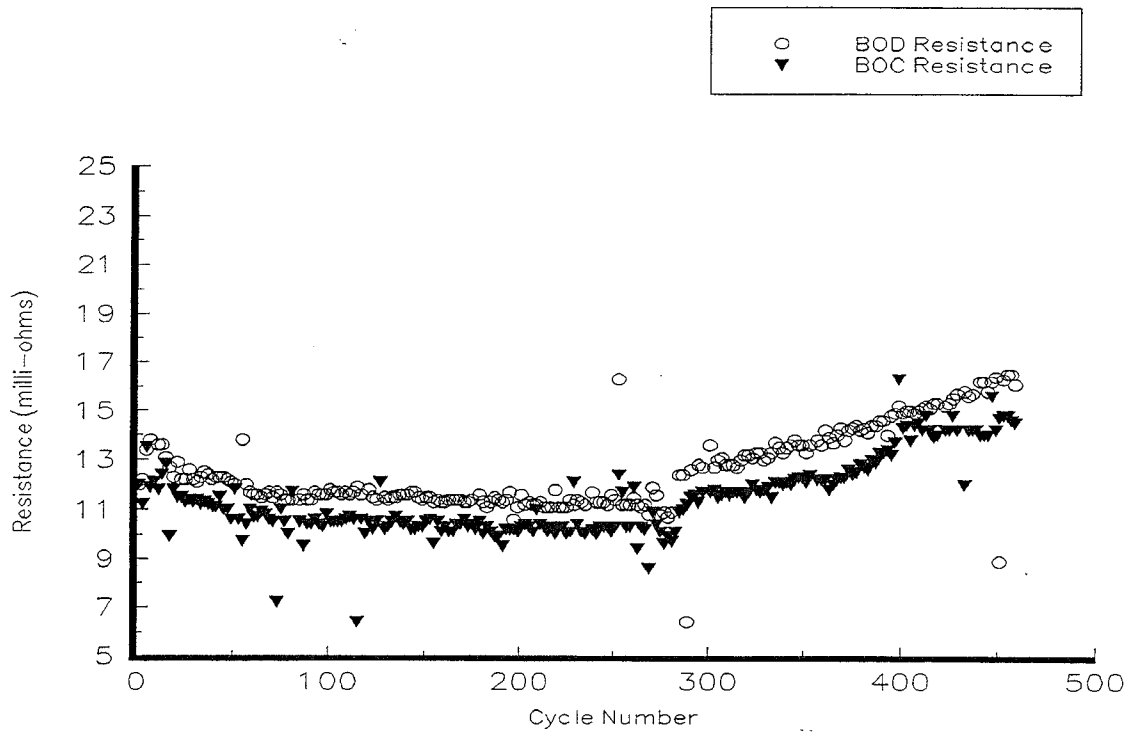


Figure 5-12. Resistance for Cell with an Ion Plated TiN Current Collector

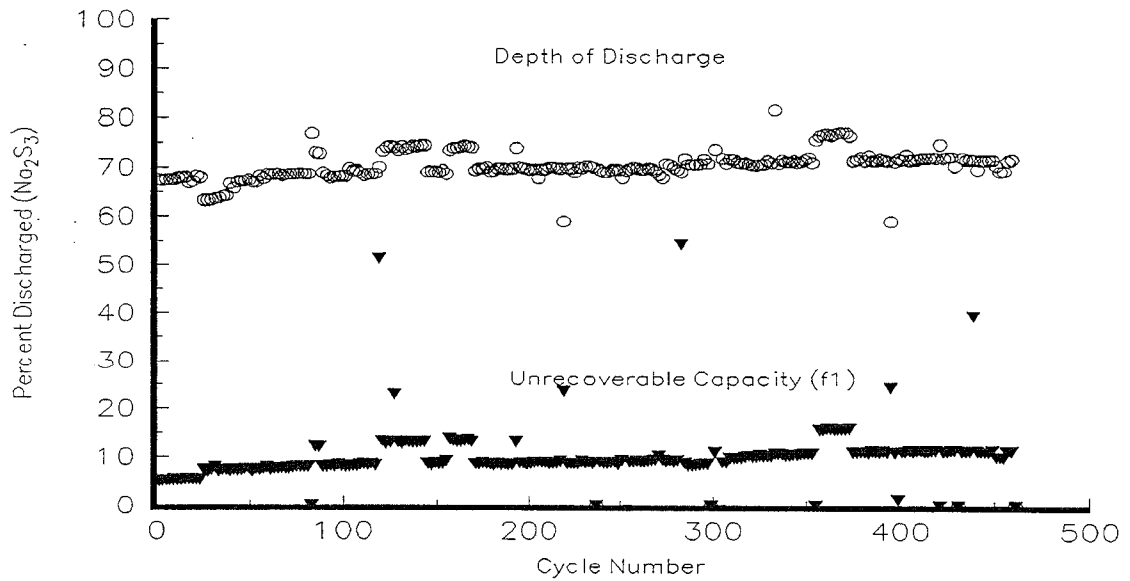


Figure 5-13. DoD and f_1 for Cell with an Ion Plated TiN Current Collector

Two cells remained on test for more than 310 cycles with very good performance, though the resistance of cell 137 was beginning to turn up after 300 cycles. They were removed from test to make room for other cells. The third cell showed an upturn in resistance after 90 cycles and was removed from test after 180 cycles. A PTA showed that more than 50% of the TiN had been corroded away.

While the current collectors coated with ion plated TiN showed very good electrical performance, it appeared that the coating is attacked by polysulfides and therefore is unlikely to provide a long lived solution.

5.1.3.2.3 Nichrome Coated Current Collectors

The remainder of the cells fabricated and tested on the program were fabricated with a flame sprayed coating (0.18mm - 0.30mm thick) of 80/20 Nichrome applied to the aluminum current collector. Nichrome coated current collectors with an isopressed layer of graphite foil were used in the SPL TD cells. The application of the isopressed graphite foil was eliminated from cells built under this program because of difficulties encountered with the application and knowing that it could be incorporated at a later date if required.

In general, the electrical performance of cells with Nichrome coated current collectors was quite satisfactory during early life. The charge acceptance of cells was initially very good as shown in Figure 5-14 for cell 019. Cells with Nichrome coated current collectors tend to have very good rechargeability early in life. With cycling, the f_1 values tend to increase monotonically. A typical example is shown in Figure 5-15 which shows a plot of DoD and f_1 vs cycle number for cell 199. The cell resistance, after the cell has broken-in and the resistance stabilized, tends to follow a similar increasing trend as shown in Figure 5-16.

As the cells aged, the resistance and f_1 continued to increase at a relatively low rate, compared to those noted previously for cells with TiN and molybdenum coated current collectors. Though the performance was not spectacular, it was predictable and consistent. For this reason, Nichrome was selected as the current collector coating for the final production cell design.

Cell 023 remains on test at the end of the program after nearly 38 months and has accumulated over 1800 cycles. Its resistance is shown in Figure 5-17, and its DoD and f_1 are shown in Figure 5-18 as functions of cycle number.

5.1.4 Safety Feature Development

Developing a cell with good safety characteristics was one of the major goals of the program. The safety features incorporated into the preliminary design included a safety tube surrounding the electrolyte, a 0.13mm thick graphite foil lining the inside of the safety tube, and filling the annular gap between the safety tube and the electrolyte with 100 grit fused alumina sand. The width of the safety tube/electrolyte annulus was 1.12mm. The function of the safety tube is to limit the volume of sodium which may react with sulfur in

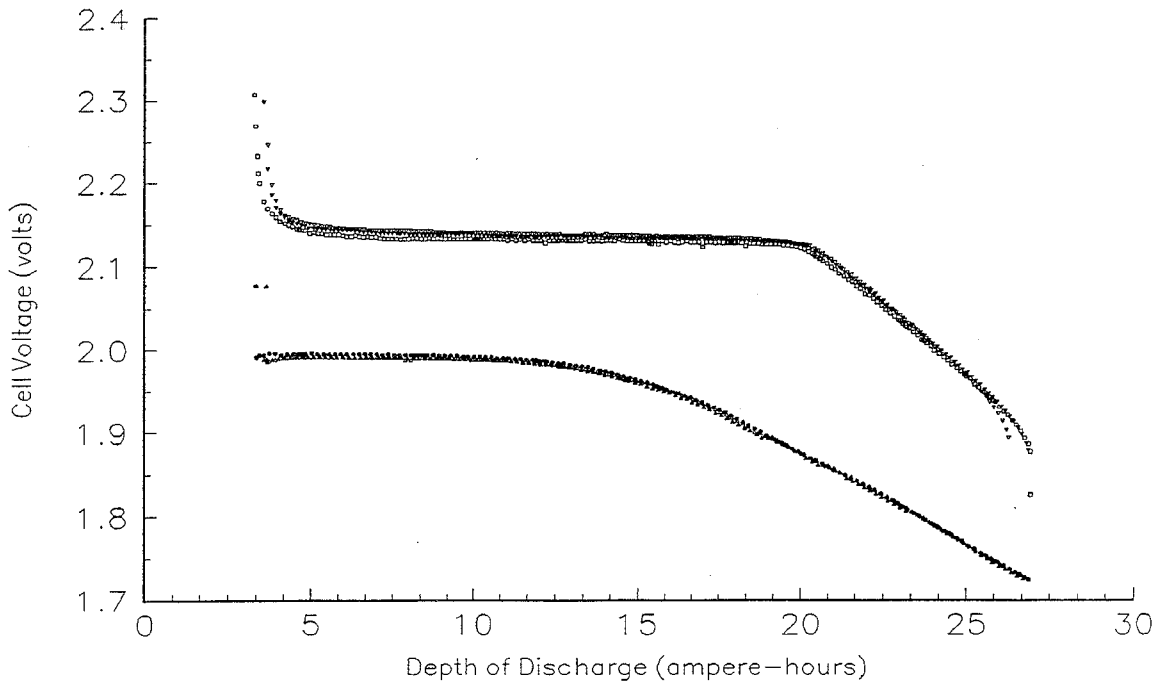


Figure 5-14. Cell Voltages for Cycles 12, 31, and 84 for Cell 019

the event of an electrolyte fracture. The graphite foil liner provides a thermal and corrosion barrier which protects the steel safety tube from melt-through or burn-through in the event of an electrolyte fracture. In addition, it displaces some sodium from the annulus. The alumina sand serves as a wick to transport sodium up along the length of the cell and displaces additional sodium from the annular gap. The bottom end of the safety can is covered with an expanded nickel mesh to keep the alumina sand in place while still allowing passage of sodium between the sodium reservoir and the annular gap.

During early tests of preliminary design cells, a number of cells breached during electrolyte failure. This was attributed to excessive sodium and sulfur loadings of the cell. The volume of the sulfur electrode compartment for the cell containing 63 grams of sulfur was not large enough to accommodate all of the reaction products during failure. During failure of the electrolyte, the sulfur electrode compartment of the cell became overfilled and ruptured the top of the cell. Because of this, the masses of sodium and sulfur were reduced in subsequent cells.

To assess the effectiveness of the preliminary design safety features, five cells were intentionally failed. The procedure for safety testing the cells was as follows. The cells were heated to the operating temperature of 330°C and electrically cycled several times to break-in the cells and to verify electrical performance. Once acceptable electrical performance was verified, each cell was charged at 3.6 amps to 2.3 volts and then trickle charged to a cutoff voltage of 2.8 volts. Electrolyte failure was then induced by raising the

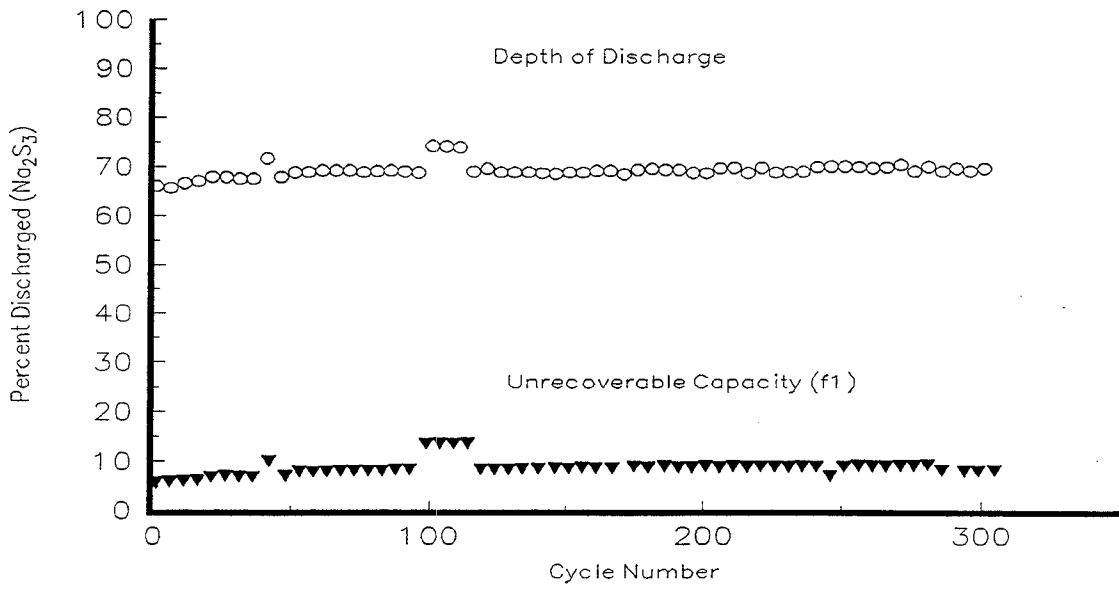


Figure 5-15. Typical f_1 and DoD for a Cell with a Nichrome Coated Current Collector

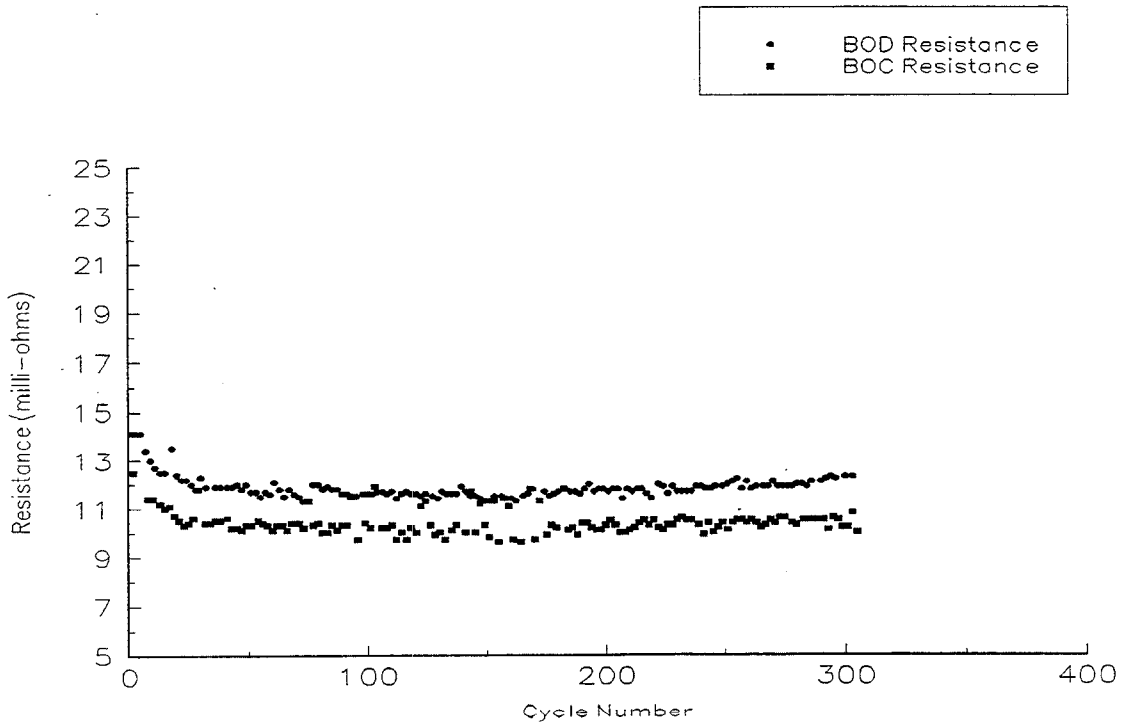


Figure 5-16. Typical Resistance for a Cell with a Nichrome Coated Current Collector

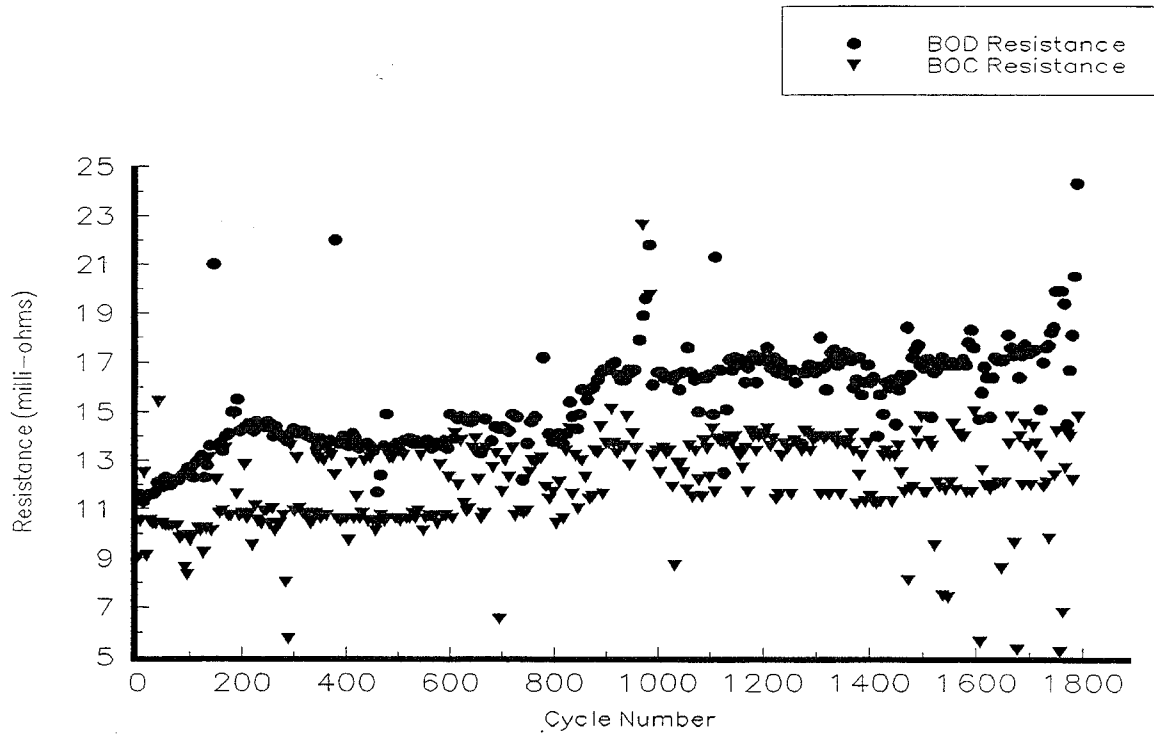


Figure 5-17. Resistance of Longest Lived Cell

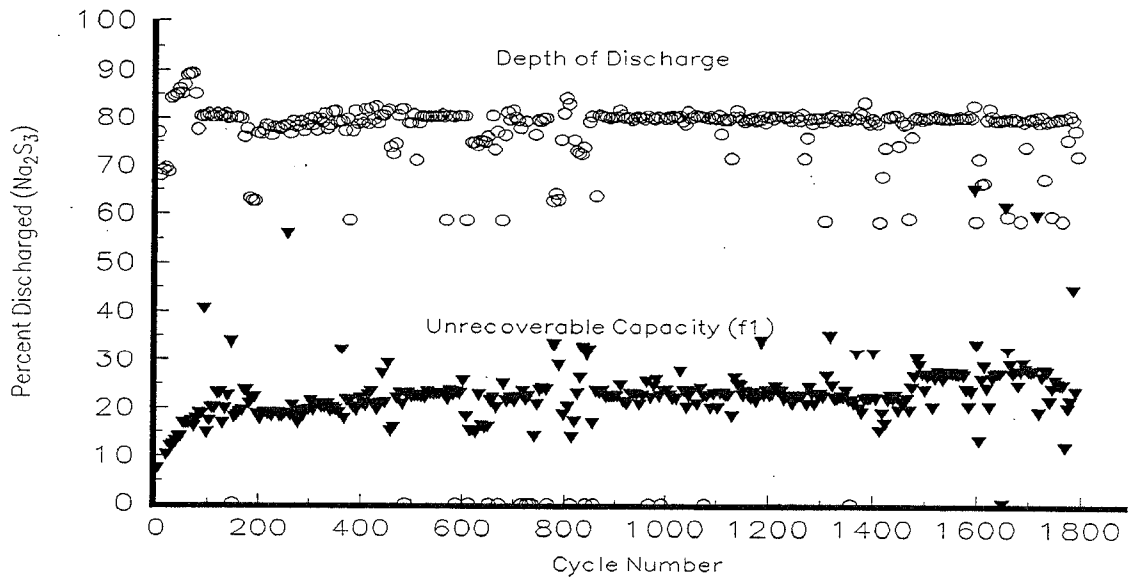


Figure 5-18. DoD and f_1 for Longest Lived Cell

charging voltage in five volt increments every minute until failure occurred. After fracture of the electrolyte occurred, which is denoted by a drop in voltage and an increase in current to the 10 amp limit, current was allowed to pass for 10 seconds. The cell was then open circuited and allowed to stand for 10 minutes. Afterward, a current of 10 amps was passed for two minutes and then reversed for two minutes. This was then repeated. The object of passing current following fracture of the electrolyte was to ensure that maximum mixing of reactants occurred.

The desired outcome of the safety tests was that there be no temperature excursions above 500°C and that no cells breach. The results, summarized in Table 5-5, fell short of this safety goal.

Table 5-5. Preliminary Safety Test Summary

Cell Number	111	112	129	131	133
Voltage @ Failure	50	55	15	25	25
Max Temperature	525	400	630	507	456
Breach/Location	Bottom	No	Top	No	Top
Na Seal Type	BN Coated	BN Coated	Planar	Planar	Tapered
Safety Features	Floating Safety Tube	Floating Safety Tube	15 mil graphite foil in safety tube/electrolyte annulus; graphite foil insulators at top of sulfur electrodes		

Based on these results, several changes were made to the cell design for incorporation into the prototype design. These included: 1) a reduction of the safety tube diameter by 0.5mm in order to reduce the amount of sodium immediately available to react in the event of an electrolyte failure, and 2) the use of a finer sand in the electrolyte/safety tube annulus in order to reduce the rate at which sodium can flow from the reservoir to the electrolyte fracture. Though a further reduction in the safety tube diameter would have been desirable, the variations in the outside diameter of the electrolyte allowed by the current specifications precluded it, as all of the electrolytes for the remainder of the present program had been manufactured by that time. The use of the graphite foil insulators at the top of the sulfur electrode may not have been fully effective due to the fact that they were hand cut and didn't fit tightly around their perimeters, thus allowing hot sodium polysulfides to bypass the insulators. In order to obtain a tighter fit, a die was fabricated for cutting the graphite washers to insure a more uniform fit in the prototype cells.

5.1.5 Sodium Filling Process

In the preliminary cell design, the outer case of the cell consisted of an open ended tube into which a formed end-cap was welded after loading the sodium into the pre-heated cell. Sodium filling was essentially a two step process conducted in a vacuum glove box. First, sodium was impregnated into the infill material occupying the annular gap between the

safety tube and the electrolyte, and then the remainder of the sodium load was added to the reservoir. In order for a cell to function properly, the interstices between the infill particles contained within the electrolyte/safety tube annulus must be completely filled with sodium such that there are no voids or pockets of trapped gas. The effect of any such residual gas pockets is a reduction in the surface area of the electrolyte contacted by sodium which results in an increase in the cell's internal resistance.

Impregnation of the infill with sodium in the preliminary cell design was accomplished by sealing a temporary reservoir with O-rings over the open end of the safety tube, adding liquid sodium to the temporary reservoir, evacuating the glove box containing the assembly to remove the gases from the infill, and then back-filling the glove box with argon to drive sodium into the infill. This method proved to be quite time consuming and unreliable due to the occasional lack of an adequate seal between the temporary reservoir and the safety tube which prevented complete evacuation of gas from the infill. In addition, the cell had to be moved from one vacuum glove box into another to weld the end cap. This transfer had considerable potential for contamination of the sodium by air, which could also have an undesirable effect on the cell's electrical performance.

The outer container was redesigned as a deep drawn, closed end can with a small hole in the closed end through which sodium was admitted. After filling the cell with sodium, a tapered plug was resistance welded into the hole to effect final closure of the sodium reservoir. Impregnation of the infill was accomplished as follows: 1) half of the sodium mass was injected with a syringe into the reservoir of the inverted cell, 2) the evacuation tube was inserted into the hole and sealed with an O-ring to the container as shown in Figure 5-19, 3) the cell was turned upright, 4) the cell interior was evacuated through the tube, and 5) the interior of the cell was back-filled with argon, forcing sodium into the infill.

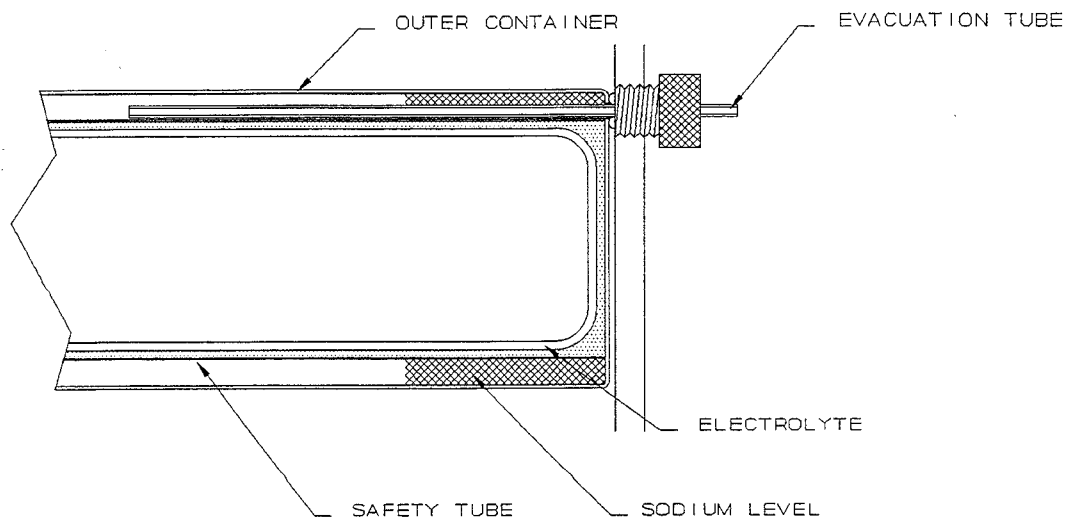


Figure 5-19. Sodium Filling Schematic

Following impregnation, the evacuation tube was removed, the remaining sodium was injected, and the tapered plug was resistance welded into the hole.

With this change in sodium filling, the variation in the sodium mass in the cells was reduced significantly; the standard deviation in the sodium mass was reduced from 8.1% of the average mass to 1.2%. Additionally, the time required for filling a lot of cells was reduced by several hours. Because of problems with the sodium seals, the effect of the sodium filling process change on the consistency of cell performance was not quantitatively determined.

5.1.6 Prototype Cell Design

The objective of the prototype cell design was to incorporate all of the developments throughout the program into a final design of which a significant number of cells would be built and tested. The geometry and size of the prototype cell, shown in Figure 5-20, varied little from that of the preliminary design; most of the design modifications that were incorporated were in the materials and processes used to fabricate the cells and minor

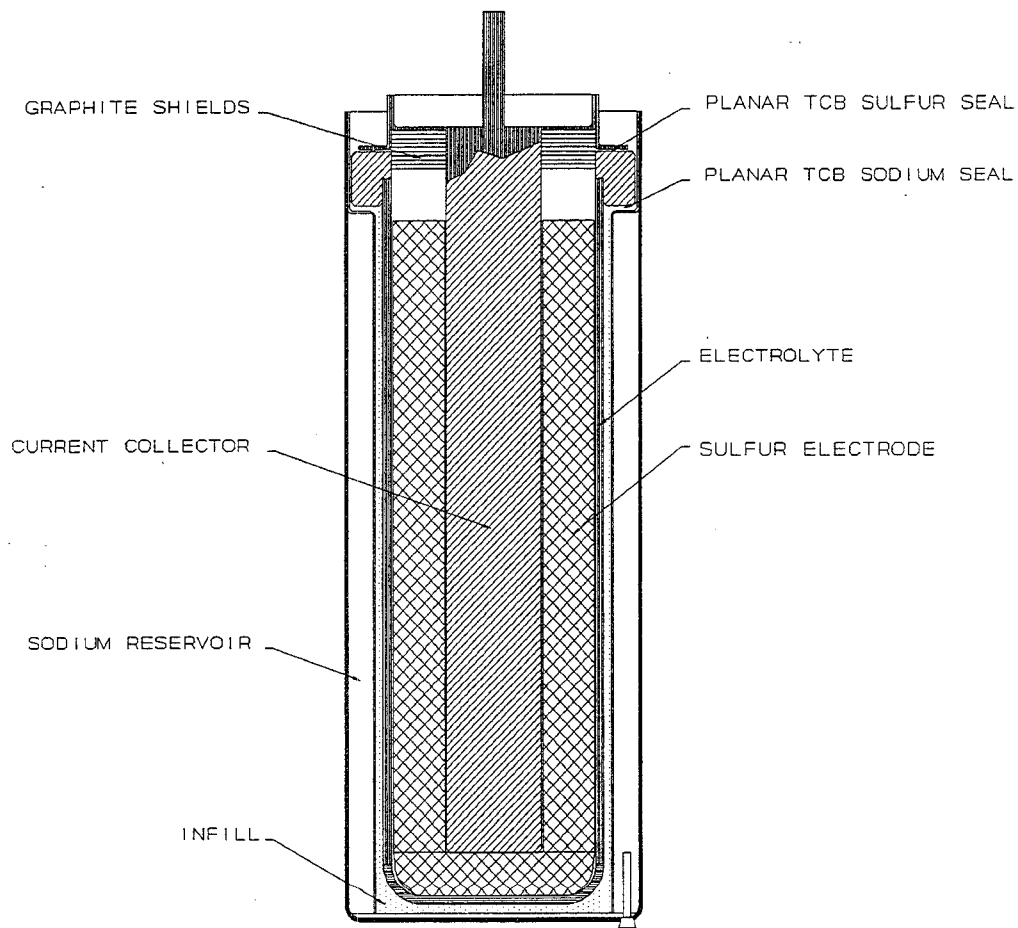


Figure 5-20. Prototype Central Sulfur Cell Design

dimensional alterations. The dimensional changes are summarized in Table 5-6 which compares details of the prototype cell design with those of the preliminary design. All of the modifications incorporated into the prototype design were intended to improve the cell's freeze/thaw, safety, and performance repeatability characteristics.

The safety features in the prototype cell design included a safety tube with a smaller diameter than that in the preliminary design to reduce the volume of sodium contained within the electrolyte/safety tube annulus. The annulus was filled with 180 grit alumina

Table 5-6. Cell Design Specification Comparison

	Preliminary Cell Design	Prototype Cell Design
DIMENSIONS	44.1 x 114.4 mm	44.5 x 111.7 mm
MASS	342 gms	364 gms
PART COUNT	21	26
ELECTROLYTE	1.4 x 33 x 101.5 mm, flat end	1.4 x 33 x 101.5 mm, flat end
SODIUM ELECTRODE		
sodium mass	36 ± 3 gms	34 ± 1 gms
safety tube thickness	0.25 mm	0.5 mm
annulus width	1.12 mm	0.83 mm
infill/liner	100 grit alumina/0.13 mm graphite foil	180 grit alumina/0.13 mm graphite foil
SULFUR ELECTRODE		
construction	graphite felt with radially oriented fibers and carbon fiber mat; active base	graphite felt with radially oriented fibers and carbon fiber mat; active base
sulfur mass	61 - 65 gms	51 - 55 gms
length	94 mm	86 mm
thickness	8.33 mm	8.33 mm
active electrolyte area	96 cm ²	89 cm ²
CURRENT COLLECTOR		
material	6061-T6 aluminum alloy	6061-T6 aluminum alloy
diameter	13.35 mm	13.35 mm
coating	0.13 mm flame sprayed 80/20 Ni/Cr with 0.25 mm isopressed graphite foil	0.13 mm flame sprayed 80/20 Ni/Cr

sand rather than coarser 100 grit sand to reduce the permeability of the infill and thus reduce the rate of sodium flow to the site of an electrolyte fracture. The other modification made to improve cell safety was the incorporation of a number of graphite foil washers in the top of the sulfur electrode compartment. The purpose of these was to thermally insulate the aluminum top cap from hot sodium polysulfides and thereby prevent melting of the aluminum. In order to ensure a tight fit between the washers and the alumina header, a die to precisely cut the washers was designed and fabricated. The reduced sulfur mass was retained in the prototype design. While some sulfur undoubtedly could have been re-introduced back into the cells, the decision was made to err on the side of caution and retain the lower sulfur mass and resulting lower capacity.

As a result of the electrode seal development effort to produce sodium seals which would withstand freeze/thaw, both the sulfur and sodium electrode seals in the prototype cells were different from those in the preliminary design. The materials and processes used to form the seals are summarized and compared with those in the preliminary design in Table 5-7. While the preliminary design sulfur electrode seal had proven to have adequate freeze/thaw durability, the process for forming the seal was changed in order to form it during the same operation as for the forming of the sodium electrode seal. The aluminum alloy type used in the sulfur seal was changed in order to minimize the incidence of hot cracking which occurred in the final sulfur compartment closure weld. The freeze/thaw durability of sulfur electrode seals made with 5086 aluminum had not been fully evaluated, and components were fabricated from both 6061 and 5086 alloys in order to provide a timely fall-back position in the event that freeze/thaw durability proved to be inadequate. The first two cells fabricated with 5086 aluminum alloy sulfur seals were

Table 5-7. Seal Design Comparison

	PRELIMINARY CELL	PROTOTYPE CELL
SULFUR SEAL	planar TCB	planar TCB
material	6061-T6 aluminum alloy	5086 aluminum alloy
interlayer material	none	none
loading method	spring loaded fixture	hot press
bonding temperature	590°C	540°C
SODIUM SEAL	planar TCB	planar TCB
material	nitrided mild steel	chromized mild steel
interlayer material	6061-T6 aluminum	4032 aluminum
loading method	spring loaded fixture	hot press
bonding temperature	590°C	540°C

placed on freeze/thaw testing as soon as they had been fabricated. The sulfur seal on both cells failed during test after seven freeze/thaw cycles. Hence, the prototype design was finalized with 6061 aluminum as the alloy of choice for the sulfur seal.

The sodium seal chosen for use in the prototype design was a planar TCB seal formed by hot pressing. This seal proved to be far superior to the preliminary seal design in terms of its freeze/thaw durability, and initial testing showed it to be marginally better than the tapered TCB seal as was used in SPL's TD cells. Further, it had the potential for eventually being manufacturable at low cost.

The beta"-alumina to alpha-alumina seal configuration and materials were the same in both the preliminary and prototype designs. A sodium borosilicate glass which had been used for a number of years in the Ford sodium sulfur program was used to seal the open end of the electrolyte into a countersink ground into the alpha-alumina header.

The sodium filling process adopted for the prototype cells was that discussed in Section 5.1.5. This process offered greatly reduced variability in the mass of sodium introduced into the cell, and eliminated the need to transfer cells from the controlled atmosphere glove box in which they were filled into a vacuum welding chamber for final closure welding. This minimized the possibility of contaminating the sodium electrode with air.

The projected performance characteristics of the prototype cells are shown in Table 5-8. The most significant changes in projected performance compared to that for the preliminary cell design are related to the cell capacity. Because of the reduction in sulfur mass, the theoretical cell capacity declined from 35.5 Ah to 29.5 Ah, which reduced the specific energy and energy density. Some of the decline in the specific energy was due to the increase in the total mass of the cell.

Table 5-8. Prototype Central Sulfur Cell Performance Projections

Cell Resistance	12 -13 mΩ
Theoretical Capacity (to Na ₂ S ₃)	29.6 Ah
Unrecoverable Capacity (f ₁)	2.95 Ah
Working Capacity	>21 Ah
Power at 1 hr Rate	41 W
Specific Energy at C/2 Rate	116 Wh/kg
Energy Density at C/2 Rate	241 Wh/l
Freeze/Thaw Durability	10 Thermal Cycles at Top of Charge Alternated with an Electrical Cycle
Safety	500°C Peak Temperature and no Breaches during Electrolyte Failure

5.2 Prototype Cell Design Verification and Testing

Following finalization of the prototype cell design, fabrication of 125 cells was initiated. The cells which completed fabrication were placed on test to verify the design. The tests performed consisted of safety, freeze/thaw, and performance testing. Six prototype cells were also shipped to Sandia National Laboratories for testing.

5.2.1 Prototype Cell Fabrication

Out of 125 sets of cell hardware which started fabrication, 100 completed cells were placed on test. The other 25 cells failed at some point during fabrication. Of the 100 cells which were placed on test, 55 had latent fabrication defects — i.e., manufacturing defects which manifested themselves during early testing, causing the cells to fail. The distribution of both fabrication and latent defect failures is summarized in Table 5-9.

The largest number of losses resulted from failure of the final sulfur compartment closure weld. In 32 of these 37 closure welds, the origin of the problem was contamination of the faying surfaces of the weldments by graphite. The contamination occurred when the graphite foil washers, whose purpose was to insulate the aluminum top cap during an electrolyte fracture, were being inserted. The washers and the alumina header were designed to have a slight interference fit to assure a good seal. Since the inside diameters of the header and the aluminum seal ring were the same diameter, contamination of the aluminum was inevitable. Because of delays in getting cells on test and a thermal runaway of the furnace in which the first group of ten cells were being tested, the effect of this contamination wasn't discovered until after 44 cells had been fabricated. After all ten cells

Table 5-9. Fabrication Failure Distribution

FABRICATION FAILURES	25
Thermocompression Bonding	15
Outer Container Installation	4
Sodium Closure Weld	4
Sulfur Closure Weld	2
LATENT DEFECT FAILURES	55
Improper Sodium Fill	1
Sodium Seal Failure during Heat-up	15
Sodium Seal Leakage	4
Sulfur Closure Weld Leakage	35

in the second test group exhibited leakage through the sulfur closure weld, the welds of the remaining 24 cells were carefully inspected under 50X magnification. This revealed microscopic cracks in the welds of all 24 cells. Because all 24 untested cells exhibited cracks in the sulfur closure weld, the 10 cells which were destroyed by overheating were also classified as having latent defects. An attempt was made to rework the remaining 24 cells. Reworking appeared to have been successful in 22 cells in which no cracking was observable in the welds at 50X. However, leakage through the welds did occur in seven cells after they were heated and testing was initiated.

After the cause of the problem was identified, a decision was made to eliminate the graphite washers from the remainder of the cells to be fabricated during the program. Since the graphite washers were part of the safety features of the prototype design, the fifteen cells which were reworked and didn't show signs of leakage after several break-in cycles were intentionally failed in safety tests. By redesigning the sulfur seal components so that the inside diameter of the seal ring is larger than the graphite washers, the full complement of safety features can be incorporated into any future cells without compromising the overall integrity of the cell.

The other aspect of the sulfur electrode closure weld which remains to be fully addressed is the hot cracking of welds made between two 6061 aluminum alloy components. By changing one of the components to 5086, for example, hot cracking can be eliminated. As noted previously, the seal ring can't be made of 5086, for such seals have insufficient freeze/thaw durability. In the prototype design, the separate top cap was eliminated in favor of a single component wherein the current collector and top cap were an integral unit. However, in a production cell, the top cap could be a separate component made of 5086 alloy rather than 6061 alloy.

The next largest number of failures occurred as a result of thermocompression bond failures. Fifteen failures were identified in a leak test following bonding. Of these, 11 resulted from cracking or fracture of the alpha-alumina header, the beta"-alumina electrolyte, or both; three leaked through the sodium seal; and one leaked through the sulfur seal. Passing the leak test after thermocompression bonding, however, provided no assurance that defective seals wouldn't manifest themselves later during fabrication or during initial heating to test temperature. Two cells which failed during installation of the outer container were a result of sodium seal failures, and 20 of the latent defect failures were directly or indirectly a result of sodium seal failures.

The sodium seals in seven of the 15 heat-up failures were examined carefully, and all were found to have failed as a result of fracture of the alpha-alumina under the aluminum interlayer in the seal. A typical example is shown in the photomicrograph in Figure 5-21. In this case, the crack, which is denoted by the arrow in the photomicrograph, extends across the entire width of the aluminum-to-alumina bond. Similar cracking was observed in several assemblies immediately after bonding. The fractures were the result of thermal stresses generated in the joint due to the mismatch in thermal expansion coefficients of the mild steel and the ceramic and the existence of microcracks in the surface of the ceramic that are introduced by grinding the surface of the ceramic.

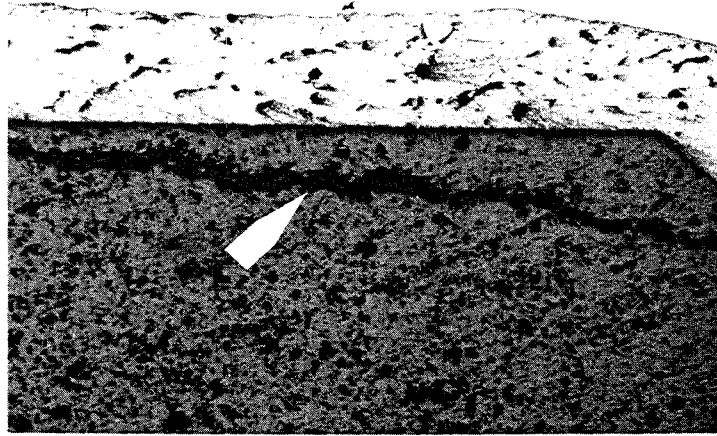


Figure 5-21. Typical Ceramic Fracture in a Failed TCB Sodium Electrode Seal

Eliminating the ceramic fracture is a matter of reducing the thermal stresses on the joint and/or eliminating the surface damage in the ceramic components. The stresses may be reduced by using materials whose thermal expansion coefficients are closer together, increasing the ductility or thickness of the interlayer, or by altering the geometry of the joint. Alternatively, the strength of the ceramic may be improved by lapping and polishing the bonding surfaces of the ceramic to remove the grinding damage; annealing the ceramic after grinding at a temperature near the sintering temperature to blunt the crack tips; or utilizing as-sintered ceramics whose bonding surfaces have not been ground. During the course of the prototype build, the only one of these which could have been considered was increasing the thickness of the interlayer. A number of trials were conducted in which two stacked gaskets were used instead of one, which offered some improvement in seal durability. However, using two gaskets produced more distortion of the safety tube cuff than usual. This distortion resulted from the extra aluminum extruding into the space between the cuff and the header. This caused fit-up problems when installing the outer container and resulted in the loss of two cells during fabrication. In subsequent cells, this distortion was minimized by wrapping several turns of steel foil around the safety tube cuff before pressing. The foil was spot welded to itself to hold it in place during pressing. After pressing, the foil was removed. By redesigning the bonding fixture to include a rigid support for the cuff, it should be possible to eliminate the cuff distortion problem.

It is obvious that the sealing problem has not been completely resolved; however, significant progress has been made. In the long term, additional work is indicated in order to eliminate seal failures. One aspect which should certainly be considered is the use of as-sintered alpha-alumina headers. Not only would these likely improve the seal strength,

the cost of as-sintered ceramics would, in large quantities, be considerably less than similar quantities of ground parts. Further, additional trials are required to optimize the thickness and width of the seal gaskets and to optimize the bonding process parameters.

The final group of fabrication failures occurred during the sodium closure weld operation. In this operation, a tapered, mild steel plug was resistance welded into the sodium fill hole. Two failures resulted from misalignment of the welding fixture and the welding head and the other two resulted from the fill holes being too close to the corner of the container. The first of these can be eliminated by modifying the jig to produce better alignment, and the second can be eliminated through better quality control of the containers.

The overall fabrication yield for the prototype cell build was 36%, which is reasonable for a cell design at this stage of development. Obviously, one could not realistically consider the design to be near a final production design. While many problems remain unresolved, engineering solutions exist for those which have been identified during the prototype build which will raise the manufacturing yield to sufficient levels for the basic design to be viable.

5.2.2 Cell Testing

The initial test plan called for testing 44 nominally identical cells to verify the cell design. Ten cells were to be failed for safety tests, 10 were to be thermally cycled in freeze/thaw tests, and the remaining 24 cells were to be tested to determine performance repeatability. In addition, six cells were to be shipped to the Sandia National Laboratories for testing. The problems encountered during the prototype build necessitated some changes in the test plan.

5.2.2.1 Safety Testing

A total of 15 prototype cells were failed by overcharging, as described in Section 5.1.4, to characterize the safety performance of the cell design. Only one of the 15 cells breached on failure, which is an order of magnitude improvement over the preliminary cell safety tests wherein three of five cells breached. Figure 5-22 shows a plot of the probability that the maximum temperature, T_{max} , attained following electrolyte failure will exceed a given temperature, T , for both the prototype cells and the five preliminary cells. The plot shows a distinct bimodality which indicates a lack of control over some aspect of the manufacturing process or a design flaw. Post test analyses were performed on the breached prototype cell and several of the others. In all cases, the safety tube and the electrolyte were not concentric. In the case of the breached cell, the location of the breach through the side of the safety tube and outer container coincided with the wide side of the annular gap. Hence, when the electrolyte fractured, there was an excessive volume of sodium available to react.

It is expected that by improving the alignment during the bonding process, further improvements in the safety of the c/S cell can be obtained. It is worth noting that, even though the electrolyte failure occurred just below the header, the graphite foil washers installed in the top of the sulfur electrode compartment protected the aluminum top cap

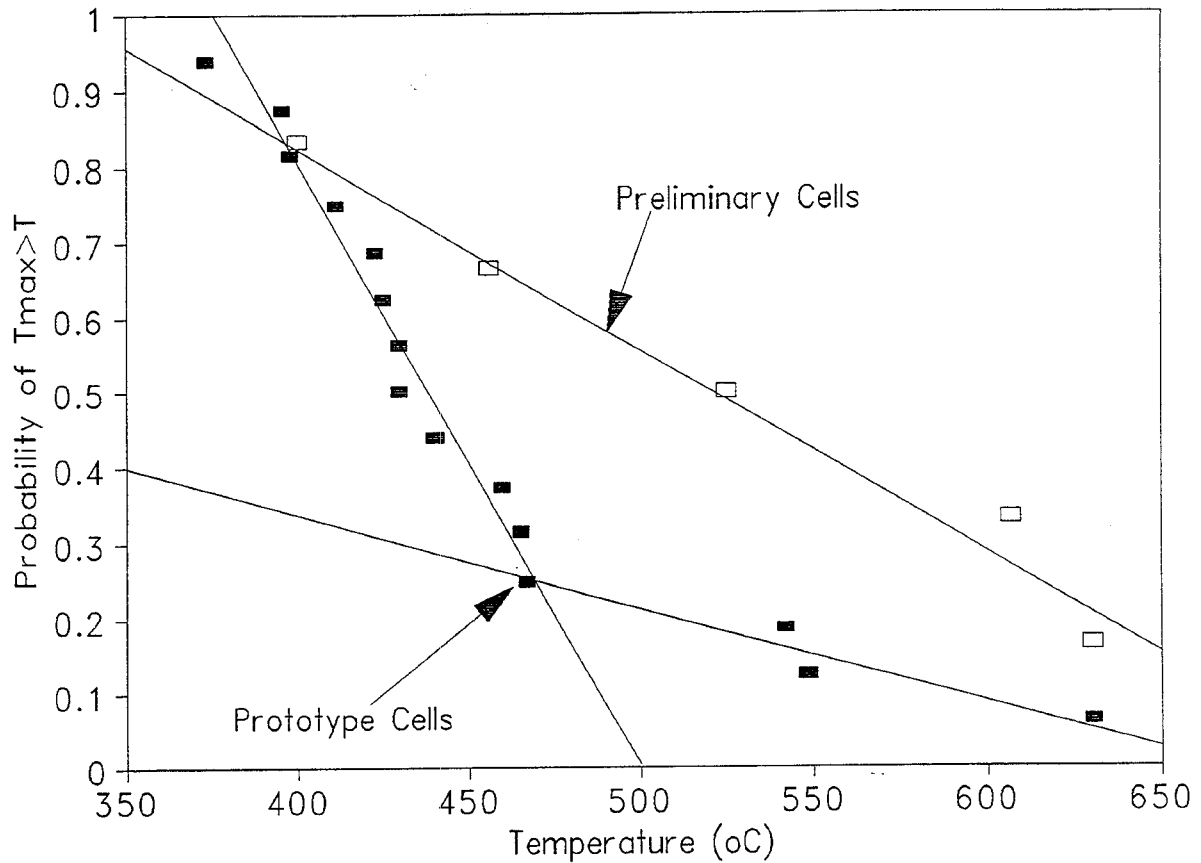


Figure 5-22. Probability of Peak Temperature during Failure Exceeding Specified Temperature

from burning or corroding. In earlier cells without the graphite, this was not the case. The results of these recent safety tests represent a significant accomplishment in the c/S cell development effort.

Additional improvement in safety performance can be attained by reducing the tolerances of the outside diameter and straightness of the electrolytes. The electrophoretic deposition process used to form green electrolyte shapes has been improved significantly since the time when electrolytes were made for this project. The use of electrolyte incorporating these improved manufacturing methods would have provided further improvement in cell safety.

The inside diameter of the electrolytes is governed by the diameter of the mandrel on which the green body is deposited and the shrinkage of the body during firing. By taking steps to ensure that moisture uptake by the suspension during deposition is minimized and by introducing bead milling of the suspension, much greater control over firing shrinkage has been attained. This has resulted in a much narrower range of electrolyte inside diameters. Improved control over electrolyte wall thickness has been accomplished by replacing operator control of the deposition time with a load cell which continuously weighs the deposit and stops deposition when the correct weight has been reached. With these

measures, it is anticipated that the range in basic outside diameter of the electrolytes can be reduced from ± 0.71 mm, which is representative of the electrolytes used on this project, to ± 0.41 mm with no increase in reject rates.

Somewhat more problematic are the variations in outside diameter near the base of the electrolyte and straightness of the electrolyte. These result mainly from viscous creep of the ceramics under their own weight during firing and are more difficult to control. An obvious solution to reduce part-to-part variability would be to tighten the dimensional specifications and increase the component reject rate. By doing so would increase the cost. Alternatively, changing the manner in which the electrolyte tubes are set during firing may reduce the dimensional variability from part-to-part without reducing the manufacturing yield.

5.2.2.2 Freeze/Thaw

Following the finalization of the prototype cell design, thermal cycling of two preliminary cells with planar 4032 alloy sodium seals was continued. At that time, five cells had survived a total of 54 freeze/thaw cycles with one seal failure; the sodium seal on that cell began leaking on its eleventh heat-up.

Cell 123 remained on test for a total of 21 freeze/thaw cycles before being removed from test. Ten of the 21 cycles were performed while the cell was discharged to greater than 70% of theoretical capacity. Following the freeze/thaw cycling (244 days on test) the cell was removed from test (without having failed) to examine the sodium side seal for any evidence of degradation or corrosion. No evidence of either was found.

Cell 115 has completed 25 freeze/thaw cycles at top-of-charge and remains on test. The cell's resistance appears to have increased as a result of the thermal cycling but only during the last several cycles.

Ten prototype cells were tested for freeze/thaw durability. All cells were initialized and subjected to a number of electrical cycles sufficient for their electrical performance to stabilize before thermal cycling was initiated. Heating and cooling was at a rate of 15°C/hr with two electrical cycles performed following each thaw.

Collectively, the ten cells have accumulated a total of 235 freeze/thaw cycles. The number of thermal cycles on each cell ranges between ten and 30 cycles as shown in Table 5-10 along with current test status. Cell 217 had a sodium seal failure after completing 14 freeze/thaw cycles. All cells except cell 168 showed stable electrical performance with thermal cycling. Typical cell resistance and useable capacity are shown in Figures 5-23 and 5-24, respectively. The vertical lines in the graphs indicate where each freeze/thaw

cycle was performed. Cell 168 showed an increase in resistance after its second thermal cycle, as shown in Figure 5-25. Prior to the second freeze/thaw, the resistance had been increasing at a rate of 3.2 $\mu\Omega$ per electrical cycle, which is more than three times the normal rate for the prototype cells. After the second freeze/thaw cycle, the rate of rise in

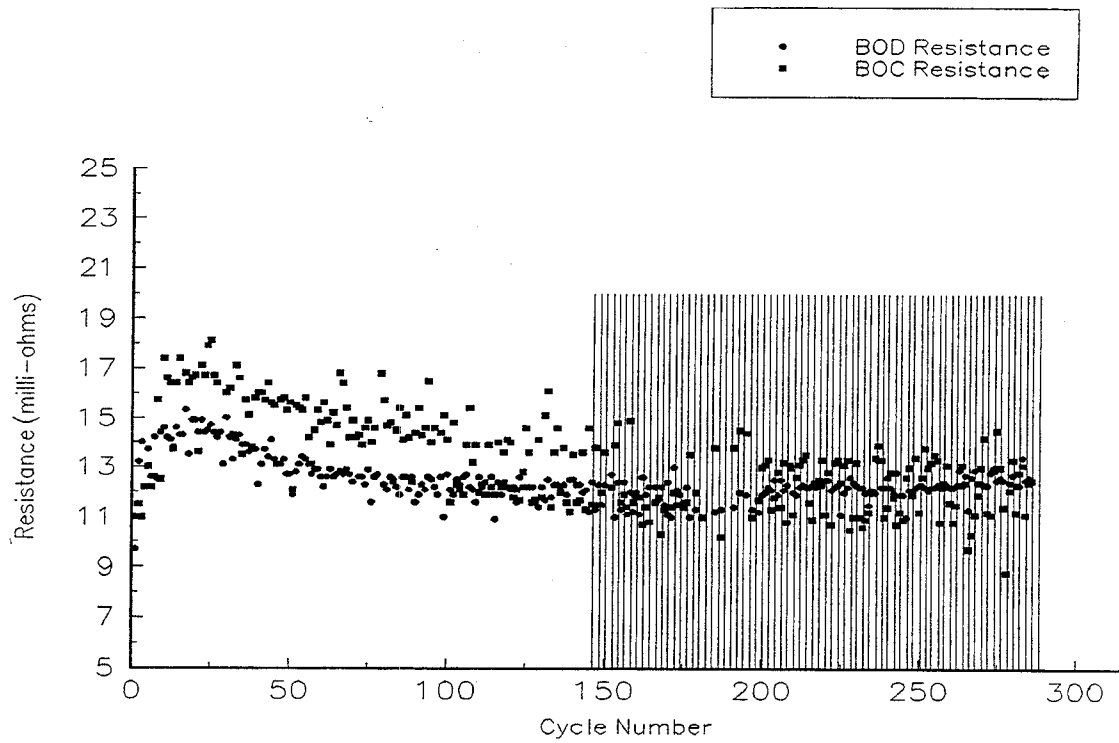


Figure 5-23. Prototype Cell Resistance during Freeze/Thaw Cycling

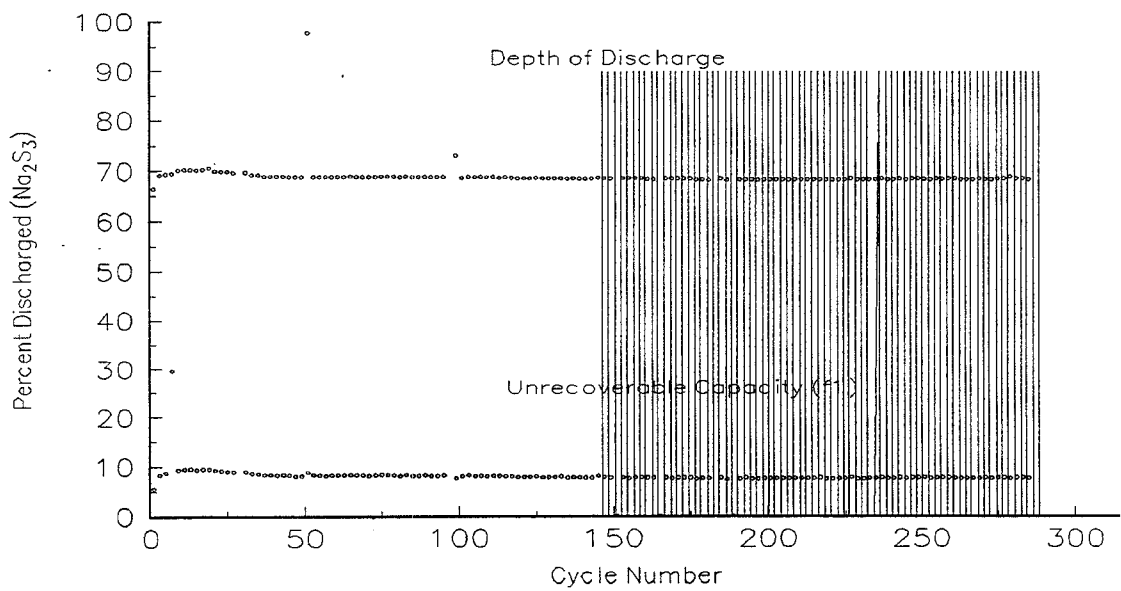


Figure 5-24. Prototype Cell Capacity and f_1 during Freeze/Thaw Cycling

Table 5-10. Freeze/Thaw Test Status

CELL NUMBER	FREEZE/THAW CYCLES	TEST STATUS
168	25	on - resistance increase
217	14	off - Na Seal leakage
218	30	on - stable
220	30	on - stable
221	30	on - stable
226	30	on - stable
246	22	on - stable
253	22	on - stable
254	22	on - stable
258	10	on - stable

resistance increased to 38 $\mu\Omega$ per cycle. After regular freeze/thaw thermal cycling was initiated at cycle 295, the cell's rate of resistance rise appeared to stabilize at around 0.7 $\mu\Omega$ per cycle. The cause of the resistance behavior in this cell was not determined, though it appeared to be an isolated case and not characteristic of this c/S cell design.

The results of the prototype cell freeze/thaw testing far exceeded expectations. The freeze/thaw durability of the sodium seals proved to be very good once the cells having latent manufacturing defects were eliminated from the population. Throughout the program, none of the c/S cells failed during freeze/thaw as a result of electrolyte fracture. This was not the anticipated result based on freeze/thaw experience with SPL's NaS7* cells which showed electrolyte failure to be a problem. During the time period when the NaS7 and TD cells were being fabricated, freeze/thaw cycling tests were not routinely or systematically conducted. The only freeze/thaw cycles occurring were accidental, but the results were not encouraging. The general result of any freeze/thaw cycles which did occur was that cell failure was primarily due to fracture of the ceramic electrolyte. Further, extrapolation of freeze/thaw studies conducted by the Sandia National Laboratories on central sodium cells also suggested that electrolyte fracture in c/S cells would likely occur.

* The NaS7 cell was the predecessor of the TD cell which had an electrolyte length of 580mm – 5 times that of the TD cell.

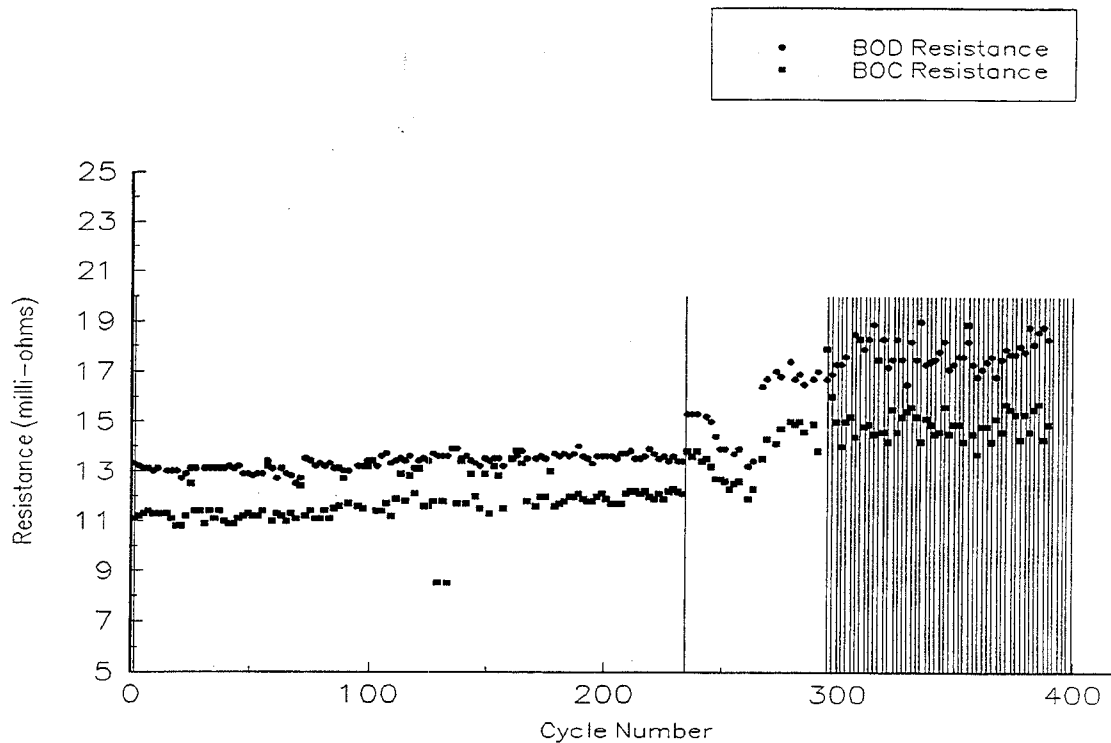


Figure 5-25. Resistance for Cell 168 during Freeze/Thaw Cycling

One hypothesis is that the freeze/durability is related to the manner in which the sulfur electrode freezes and the distribution of residual porosity within the frozen electrode. During cell cool-down, heat is removed from the sulfur electrode through the beta"-alumina electrolyte and the central current collector. If the thermal conductance of the current collector is much lower than that of the electrolyte, solidification of the sulfur electrode begins on the wall of the electrolyte at the bottom of the cell and progresses inward and upward. The material which freezes first, at the bottom of the cell, will be relatively dense, while that freezing last, at the top of the cell, will be more porous. Upon reheating, the expanding and dense sulfur mass with a thermal coefficient of expansion nearly five times that of beta"-alumina exerts considerable force on the electrolyte at the bottom of the cell, causing it to fracture.

If the thermal conductance of the central current collector is sufficiently high relative to that of the electrolyte and if it extends close enough to the bottom of the electrode, solidification of the sulfur will progress outward from the current collector and downward, as well as inward, from the surface of the electrolyte. The net result is that the porosity at the bottom of the sulfur electrode is higher than in the previously described case, making the elastic modulus of the electrode lower which, in turn, reduces the force applied to the electrolyte during subsequent heat-up.

In addition to having an electrolyte five times as long as the prototype cell, the NaS7 cell had an aluminum cored, Inconel current collector with a copper mesh providing a conducting interface between the aluminum and Inconel. Because of the length and lower thermal conductance of the composite current collector, the central sulfur electrodes in

NaS7 cells would have frozen with little porosity at the lower end, and, hence, electrolyte fracture on reheating would have been highly probable.

Given the above hypothesis, there is likely to be an envelope of design parameters – current collector dimensions and thermal conductivity being the most important – within which freeze/thaw survival is probable. Cells outside of the envelope would probably not sustain freeze/thaw. In a future effort, it would be essential to perform detailed thermal analyses and additional experiments to fully validate the hypothesis and to determine the range of design and operational parameters within which freeze/thaw is assured.

5.2.2.3 Cell Performance and Repeatability

Of 29 prototype cells placed on test, 11 had completed over 200 electrical cycles by the time of this report. Stability of cell resistance and useable capacity was generally achieved after a cell had completed between 50 and 100 electrical cycles. The average resistance of these eleven cells is plotted every ten cycles in Figure 5-26. The data spread bar denotes the standard deviation of the resistance. The average resistance for the prototype cells after break-in and stabilization was 13.2 ± 2.3 m Ω . This resistance value was higher than the projected value of 12 m Ω , and the variation between cells was high.

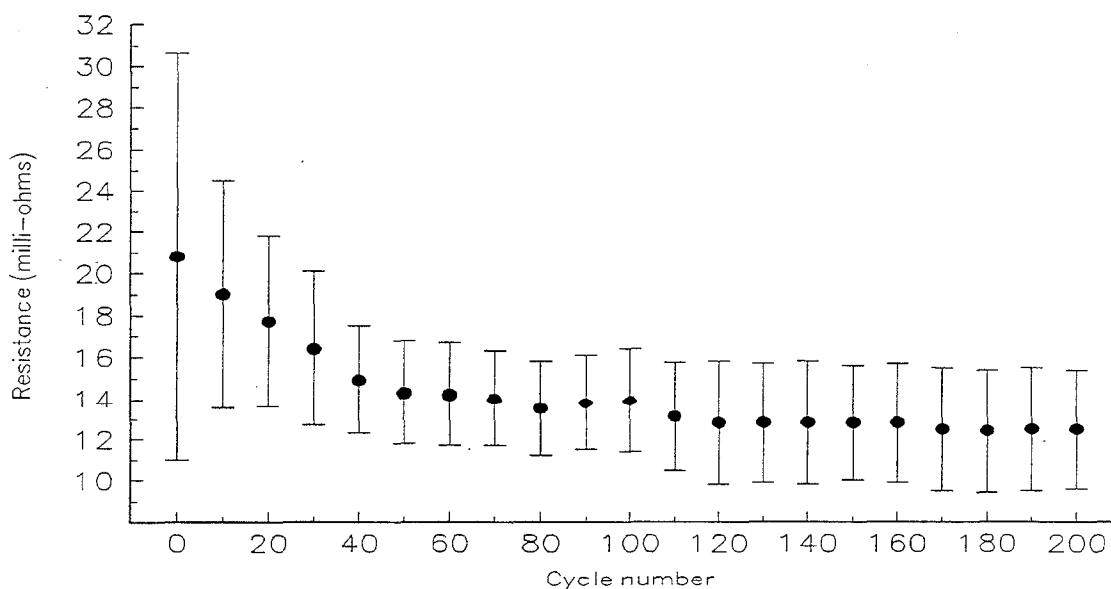


Figure 5-26. Eleven Cell Average Resistance during Break-in

In several cells, stable resistance was observed during the initial few cycles, while others started relatively high and gradually declined to near expected resistance levels. Some cells showed a "hump" in the resistance which typically subsided within about 50 cycles. A typical example of this behavior is shown in Figure 5-23. This resistance rise was observed in a number of the preliminary cells as well and is believed to be due to variability in the beta"-alumina electrolyte used in each cell as a result of moisture degradation during storage.

Even when stored under the best practical conditions and baked out according to prescribed schedules immediately before cell assembly, as all electrolytes used on this program have been, degradation of the ceramic by atmospheric moisture can still occur during long term storage with a deleterious effect on cell performance. Much of the ceramic used for the prototype cells had been in storage for nearly three years. Variability in the resistance of the electrolyte due to moisture degradation was also thought to be responsible for a larger than expected variance in cell resistance after stable performance was achieved.

The average unrecoverable capacity for the same eleven prototype cells is plotted in Figure 5-27. After the cells' performance stabilized, the average f_1 was $8.7 \pm 2.2\%$ of theoretical capacity. This was consistent with the projected value of less than 10% of the cell's theoretical capacity for f_1 .

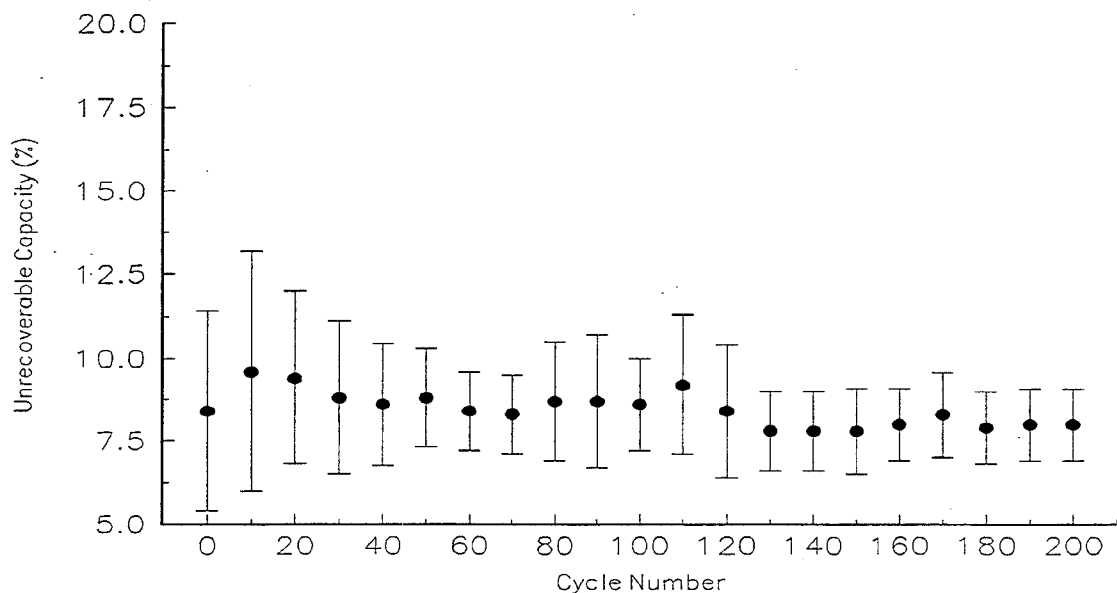


Figure 5-27. Eleven Cell Average f_1 during Break-In

5.3 Battery Component Development

In addition to the development of the c/S cell, other battery components were developed, including: simplified, low cost thermal management systems; reliable, low cost cell-to-cell electrical isolation materials; high temperature fuses to disconnect failed cell strings from the rest of the battery; and a battery management system.

5.3.1 Thermal Management

To sustain complete battery discharge over a two hour duration without overheating, it was necessary to provide a means for removing excess heat from the battery or absorbing it internally. The current sodium sulfur EV batteries are cooled by pumping a high temperature oil through a plenum within the interior of the hot battery and rejecting this heat to the ambient atmosphere through an oil-to-air heat exchanger. For utility applications, a simpler and possibly lower maintenance approach was desired. To address this need for cooling during discharge, two thermal management systems were examined. The first was a passive system utilizing encapsulated molten salts with a melting point near 340°C. The salt would absorb excess thermal energy as it fused, thereby clamping the temperature of the battery during discharge. The second system examined was a thermosyphon design using a perfluorinated hydrocarbon as the working fluid.

5.3.1.1 Molten Salt Thermal Energy Storage

The benefits offered by a passive thermal management system are no parasitic losses for blowers or pumps, improved reliability due to no moving components, and inherent energy conservation. In a stationary battery application wherein unattended operation for long periods of time is required, these benefits of passive thermal management far outweigh the deficiencies and penalties imparted by the increase in weight and volume.

5.3.1.1.1 Molten Salt Thermal Energy Storage Capsule Development

Through a literature search and discussions with Sandia National Laboratories, a eutectic composition of 45% (by weight) LiCl and 55% KCl was selected. The eutectic temperature for this binary system is 355°C, which is well below the maximum desired cell temperature of 385°C. In the previous work, mild steel, stainless steel and Inconel had been evaluated as container materials for the fused salt thermal energy storage (TES) capsules. In order to maximize the thermal communication throughout the battery and thereby minimize thermal gradients, it was desirable to use a material with a higher thermal conductivity. For this reason, an aluminum alloy (3003) was selected.

In order to minimize corrosion of the capsules by the salts due to moisture contamination, precautions were taken to ensure that the salts and capsules themselves were as dry as practically possible. The TES capsules were degreased in an ultrasonic bath of hot, deionized water/detergent solution. This was followed by rinsing in deionized water with additional rinses in acetone and methanol. All parts were dried completely and stored in a drying oven at 110°C until use.

The individual salt components were dried separately in alumina crucibles under vacuum at 100°C for 40 hours. After drying and while still warm, the salts were weighed and mixed thoroughly. The dry salt mixture was then melted in a Vycor^R crucible and heated to a temperature of approximately 500°C to homogenize the melt. The molten salt mixture was poured into the aluminum capsules and allowed to freeze and cool to room temperature.

After the salts had cooled, the casting was removed from the aluminum capsule, trimmed to the specified weight, and reinserted into the capsule. This method proved to be more consistent in obtaining the correct weight of salt than trying to pour a specified weight. Finally, an aluminum end cap was inserted and welded into the capsule.

To verify the integrity of the closure weld, the capsules were thermally cycled once from room temperature to 450°C. While very few capsules leaked, indicating good weld integrity, most of the capsules bulged. Lowering the pressure under which the final closure weld was made from 1 atmosphere to ½ atmosphere produced no significant reduction in the frequency or degree of container bulging. This necessitated that the mass of salts in the capsule be decreased by one gram; this solution eliminated the bulging but had the accompanying effect of reducing the amount of heat which could be absorbed.

To verify the passive thermal management design, a small battery comprised of ten, three-cell series strings was assembled using PB cells. This module contained 11 TES capsules in a tightly bundled array as shown in Figure 5-28. Two experiments were performed consecutively to determine a preferred cell-to-cell isolation material. The first module used 0.2mm thick mica sheets to isolate the cells and TES capsules. Tight packing was maintained throughout testing by constraining the assembly from the outside, mimicking the assembly plan for the large 75 kWh NAS-P_{AC} sub-battery packs. The second battery was assembled by cementing cells and TES capsules together using an MgO based ceramic cement; all components were first coated with the MgO to assure electrical isolation. While the thermal performance of the first assembly proved to be acceptable, the cemented array offered better thermal conductance between cells and TES capsules and, even more importantly, provided protection against potential corrosion by the hot salt in the event that a leak developed in a TES container.

Figures 5-29, 5-30, and 5-31 show constant power discharges of 240 W, 300 W, and 400 W, respectively, followed in each case by a 150 W charge. These conditions correspond to operation of the NAS-P_{AC} battery system at the beginning-of-life (no string failures), mid-life (20% of strings failed), and end-of-life (38% of strings failed) conditions. The maximum rated temperature rise is from 330°C to 375°C during normal operation of the UES battery. This testing was intended to follow the procedures and practices established for the large NAS-P_{AC} battery pack as closely as possible. At the lower power level, however, the starting temperature was raised by approximately 10°C to achieve a sufficient amount of salt melting to verify performance. The utilization of latent-heat energy storage was intended primarily to handle the end-of-life conditions. The data presented in the figures were from a thermocouple attached to the bottom cell adjacent to the TES capsule in the center of the array shown in Figure 5-28. At all power loadings, it was observed by the change in thermal response that the salt began to melt around 354°C and

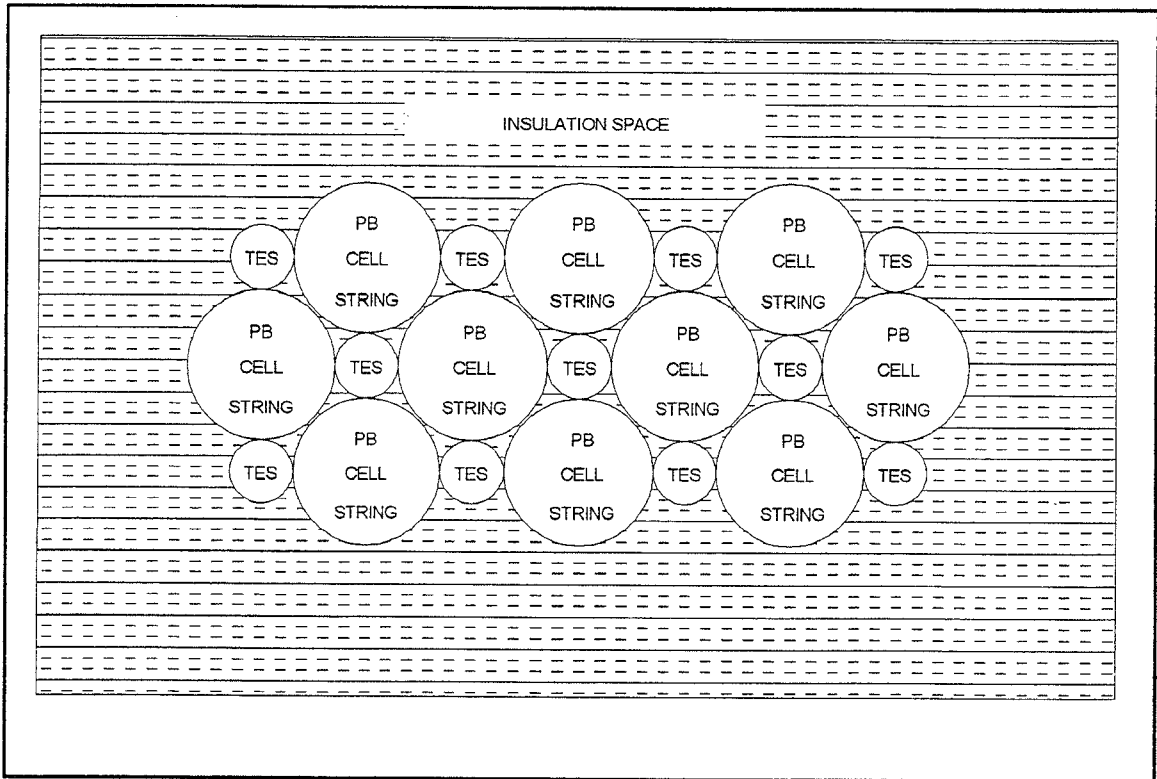


Figure 5-28. 30 Cell Test Module Showing Relative Positions of PB Cell Strings and TES Capsules

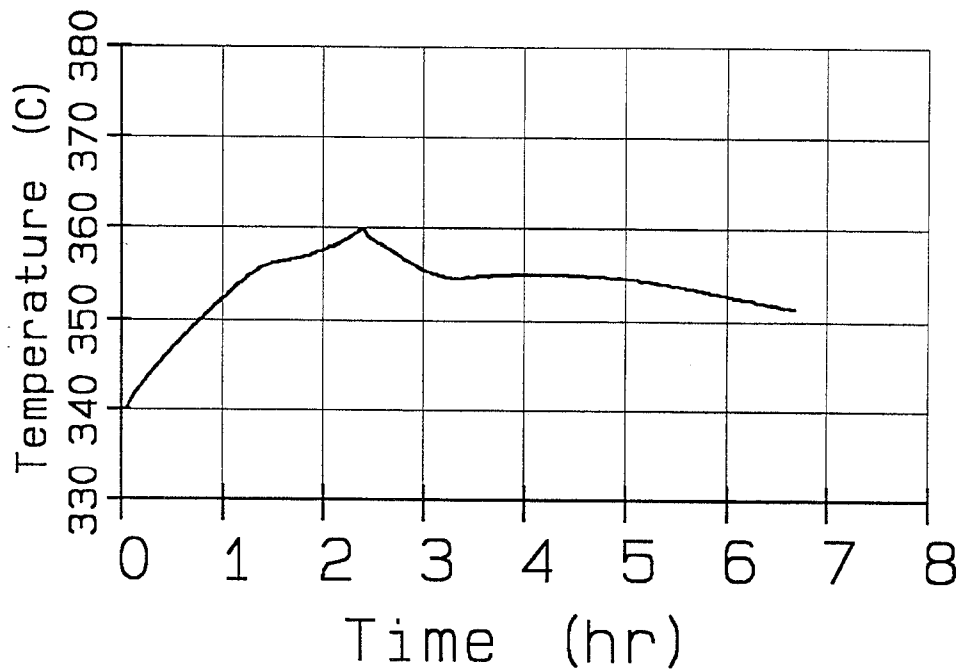


Figure 5-29. Temperature Response of the 30 Cell TES Experiment for the 240 W Discharge Test Condition

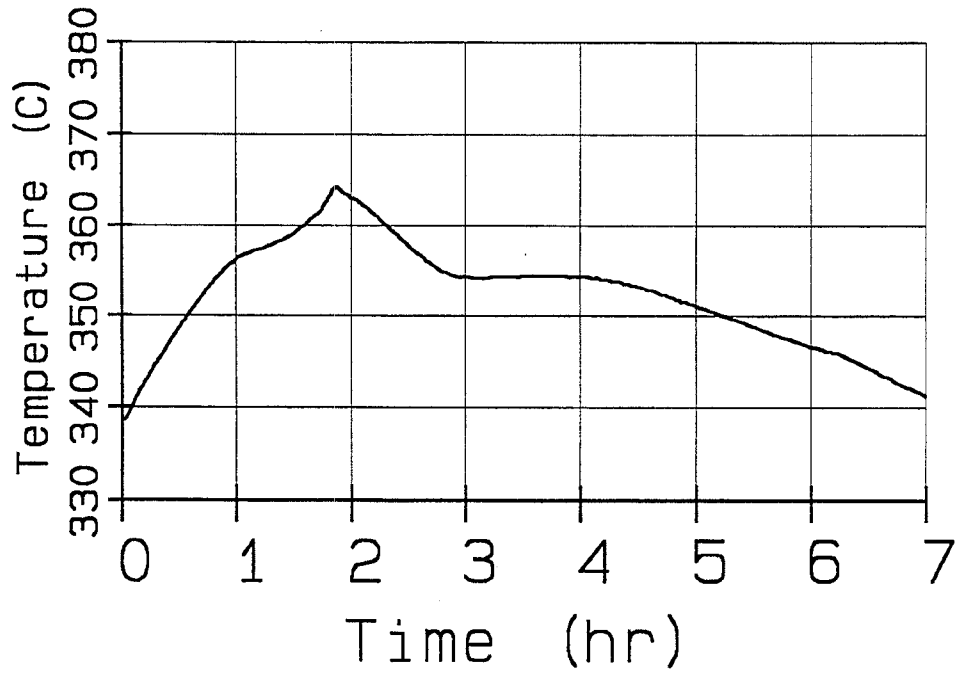


Figure 5-30. Temperature Response of the 30 Cell TES Experiment for the 300 W Discharge Test Condition

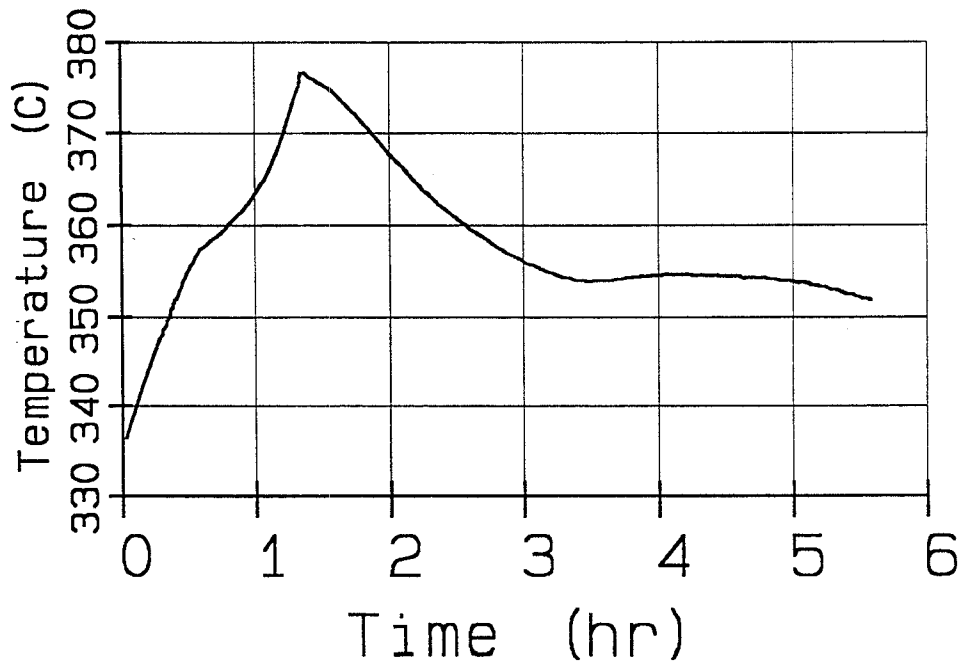


Figure 5-31. Temperature Response of the 30 Cell TES Experiment for the 400 W Discharge Test Condition

absorbed heat from the cell during the remainder of the discharge portion of the cycle. The cell temperature continued to increase through the melting transition at a rate dependent upon the power loading. As shown in Figure 5-32, analysis of the cycle data showed that the maximum cell temperature attained was reduced by approximately 15°C in the module employing latent heat storage versus the computed temperature rise for a module having no latent heat storage. During the charge period, the heat flow is reversed from the salt into the cell matrix effectively extending operating time at temperature. Because the enclosure design utilizes a conventional insulation system to reduce cost and to enable component recycling, the extended time at temperature is useful in offsetting heat loss that would otherwise have to be made up by internal heaters connected to the utility grid.

Careful analysis of the data accounted for 85% of the expected 2610 Joules of latent heat stored by the salt associated with a given cell. The salt capsules used in this test were approximately 20% shorter than the 3-cell string length, and they were elevated from the bottom bank plate by an electrical stand-off. This provides a partial explanation for the lost 15% since the subject thermocouple monitored the bottom cell of the string.

In a separate series of tests, TES capsules were subjected to a temperature excursion sufficient to melt the salt's aluminum containment. The purpose of the test was to assess a worst possible case scenario in which, in the event of an accident, a number of cells are shorted resulting in a thermal excursion above the melting point of the aluminum. The requirement for the test was that the thin steel jacket surrounding the capsule would contain the molten aluminum as well as the salts known to aggressively corrode ferrous

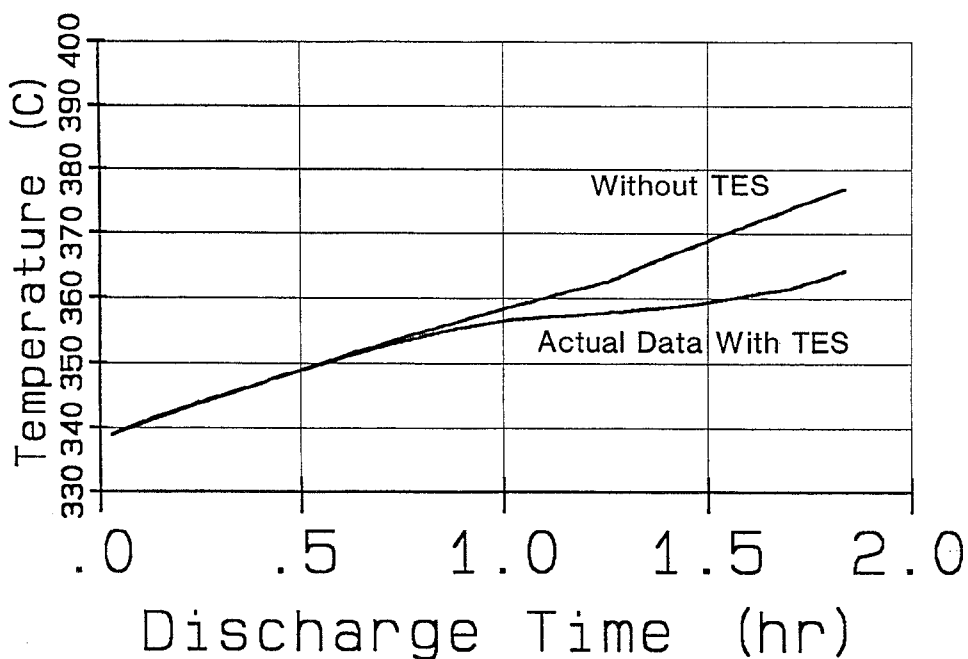


Figure 5-32. Actual Temperature Rise in 30 Cell TES Experiment Compared to Calculated Temperature Rise without TES Capsules

alloys at elevated temperatures. With the ceramic cement applied to the exterior of the mild steel jacket, the jacket remained intact and retained all of the molten aluminum. This was not the case in trials with bare steel jackets. In those tests, the jacket was essentially corroded away. This testing clearly demonstrated the benefit of the cemented array in providing an extra margin of safety in battery design.

The 30 cell assembly was tested to verify the ability of the cemented array to withstand freeze/thaw cycling. In addition to freeze/thaw, one of the 10 strings was purposely shorted to determine what effect, if any, the cemented assembly would have on the observed temperature excursion. A string in the center of the module, having separate terminations, was shorted over a sufficient period of time to cause cell reversal and loss of voltage in that string. The maximum temperature rise was 70°C in the failed string. During the ten minutes subsequent to having shorted the string, surrounding cells experienced a 25°C temperature rise, indicating good thermal communication with the failed string. The conclusion from the test was that nothing serious happened as a result of having completely shorted the string and that the improved thermal contact of the cemented assembly appears to limit the temperature rise in the event of a string of cells shorting.

After carefully reviewing the performance data, the salt leak trials, abuse tests, and the assembly plan for each of these design approaches, a recommendation was made to proceed with the cemented MgO assembly rather than use the mica separators in the 13 kWh battery module to be delivered to SNL.

5.3.1.2 Thermosyphon Cooling System

A thermosyphon based cooling system was explored as a possible alternative to a pumped system. The thermosyphon uses the fluid pressure head instead of that developed by a mechanical pump to circulate the fluid around the coolant loop, thereby reducing system complexity. An experimental apparatus was assembled which simulated a single flow path of a proposed battery cooling system; five such flow paths would be required for an actual 33 kWh UES battery module. Several experiments were then performed with the apparatus to verify the system concept and to evaluate two perfluorinated liquid coolants; these were Fluorinert^R FC-5312 with a boiling point of 215° C and Fluorinert^R FC-71 which boils at 250°C. Additionally, two pressure head levels of 0.30m and 0.45m were investigated.

The experimental apparatus, shown in Figure 5-33, consisted of a 0.69m long boiler section located 0.30m below the condenser/reservoir. During operation, the working fluid was fed into the boiler section through an electrically operated valve. The boiling vapor was returned to the condenser/reservoir where it was cooled and condensed by means of a water cooled copper coil wrapped around the reservoir. The water jacket inlet and outlet water temperatures and flow rate were measured, and, using this data, the amount of heat removed from the condenser was computed. Thermocouples were located at various points along the boiler section as shown in Figure 5-33. The thermocouples were spaced more closely toward the outlet end of the boiler section in an attempt to determine the point at which the last fluid vaporized and began to superheat – i.e., the burn-out point.

Thermocouples were also located in the condenser to monitor the temperature of the liquid and at points along the vapor return and fluid feed lines. These thermocouples were used as controls to ensure that the fluid remained near the boiling point at all times. The entire assembly was wrapped in insulation three inches thick, around which an aluminum foil skin was added. A 16 gauge sheet steel skin was located around the boiler on which thermocouples were permanently mounted. The skin temperatures were used to calculate the losses in the system. A sight glass was initially installed in the base of the return line at the boiler outlet to allow observation of the quality of the returning fluid. However, because the seals deteriorated rapidly, the sight glass was removed to minimize problems associated with loss of vacuum and working fluid.

Filling the system was accomplished by evacuating the system with a roughing pump, adding the working fluid, re-evacuating the system, and valving it off.

After filling, the vapor return line, the fluid feed line, and the valve were heated with the guard heaters to the boiling temperature of the fluid, and water flow through the condenser/reservoir was initiated. Once the temperatures of these sections stabilized, the boiler heaters were energized and the boiler was allowed to heat to 300°C. When the boiler temperature stabilized, the fluid control valve was opened and adjusted until steady state operation was achieved. Temperatures were recorded with a computerized data acquisition. The cooling water flow rate was measured several times during each run in order to calculate the heat rejection rate.

Parasitic heat losses were calculated using skin temperatures measured at the system operating temperature. The calculated value for all parasitic heat losses, including all heat leaks due to wire bundles exiting the insulation, was 40 W. This heat loss was confirmed by heating the system without fluid to the boiling point of the fluid and measuring the power level required to maintain this temperature. This value was found to be 50 W.

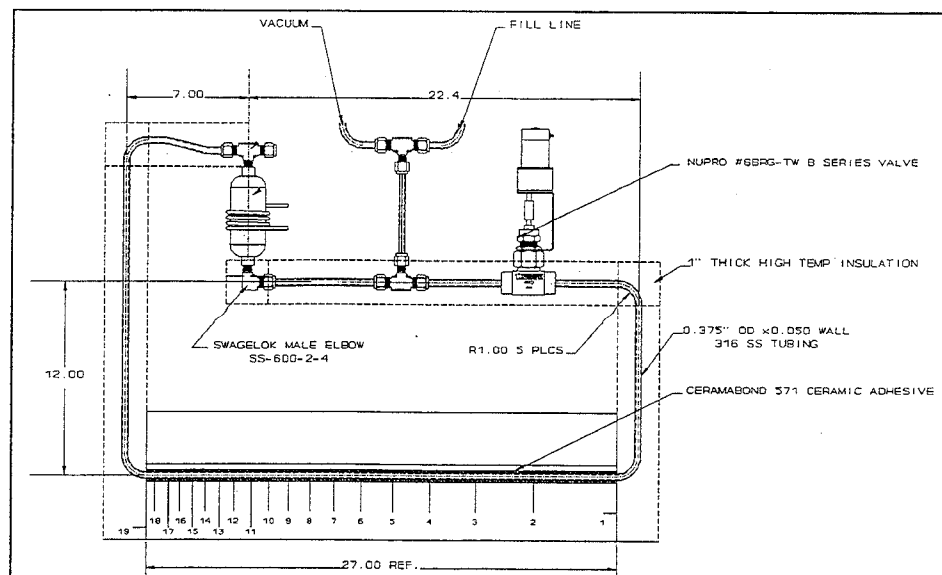


Figure 5-33. Thermosyphon Experimental Apparatus

Figure 5-34 shows a typical response of the thermosyphon system using the FC-71 cooling fluid with a 160 W power input to the boiler. The response time was very short, taking less than five minutes to cool the system from 300°C to 220°C. Other runs were made with boiler input power levels of 200 W, 220 W and 260 W. Each yielded similar results, demonstrating the capability of the system to remove the required amount of heat. A transient heat removal rate as high as 190 W could be achieved, which included removal of sensible heat from the system. However, the limit for steady state heat removal was 170 W. As shown in Figure 5-35, at input power levels above 230 W, the heat removed remained at 170 W, which resulted in superheating of the fluid in the boiler.

Fluorinert FC-5312 was chosen as an alternate fluid because it decomposes at a lower rate at high temperatures than does FC-71. The performance of the thermosyphon filled with this fluid, shown in Figure 5-36, is very similar to that of FC-71. The rate at which steady state was attained after opening the valve was less than five minutes and, as shown in Figure 5-37, the maximum steady state heat removal rate for FC-5312 is also similar to that for FC-71.

It was postulated that the heat removal rate was being limited by the fluid head driving the thermosyphon and that, by lengthening the boiler feed and the vapor return lines, the heat removal rate should be increased due to the elevated pressure head. The thermosyphon head was therefore elevated from its original height of 0.30m to 0.45 m, and additional trials were performed using the FC-5312 fluid only. The results, presented in Figures 5-38 and 5-39, show that the performance of the modified system was similar to the prior series of tests. The maximum heat removal rate, shown in Figure 5-39, was only slightly higher; however, the plateau was more well defined than in the previous trials. These results show that the heat removal rate was not limited by the pressure head for this particular set-up

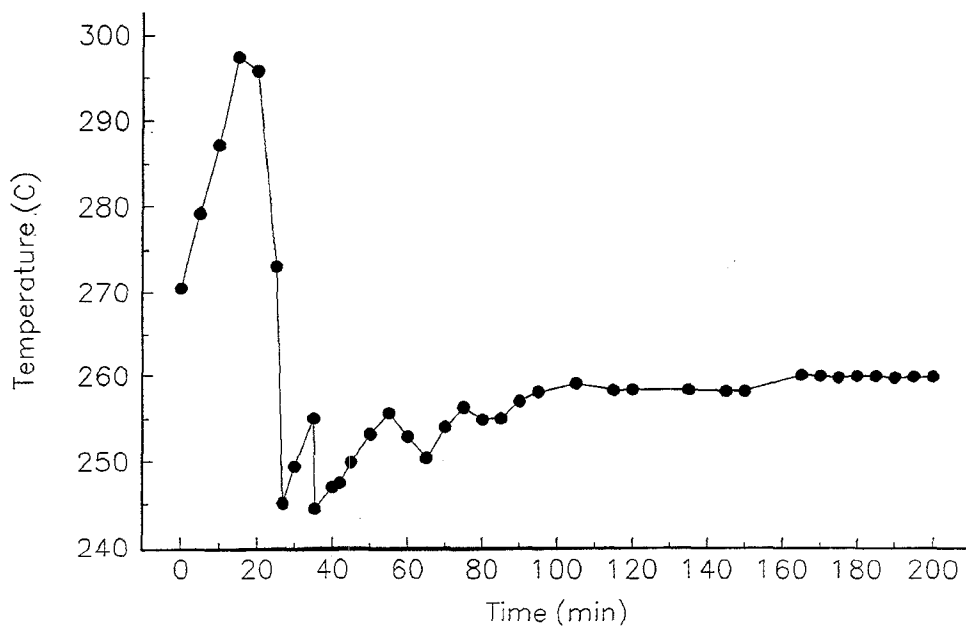


Figure 5-34. Typical Thermosyphon Response for the FC-71 Fluid

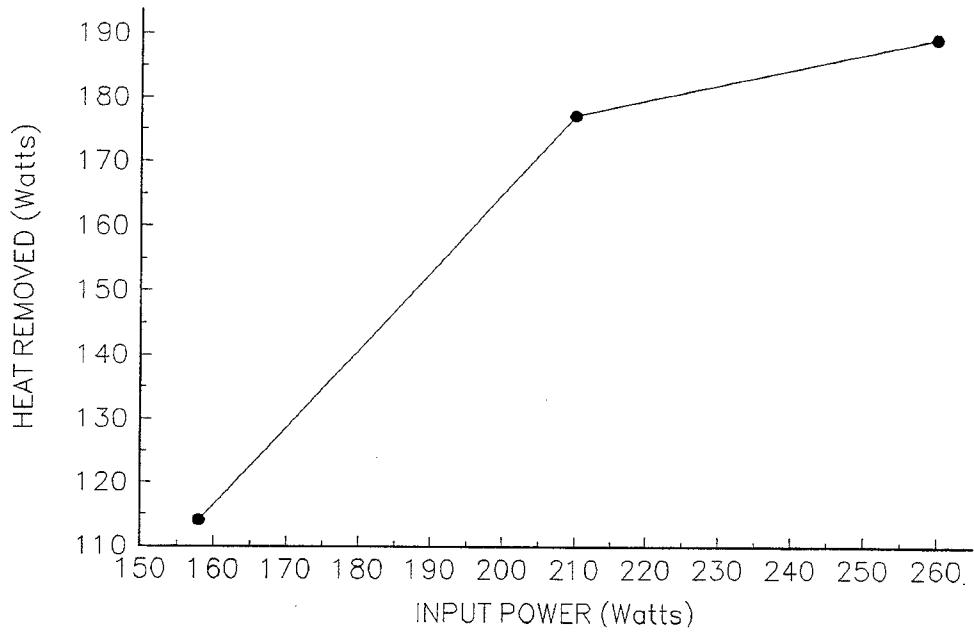


Figure 5-35. Heat Removed as a Function of Boiler Power for the FC-71 Fluid

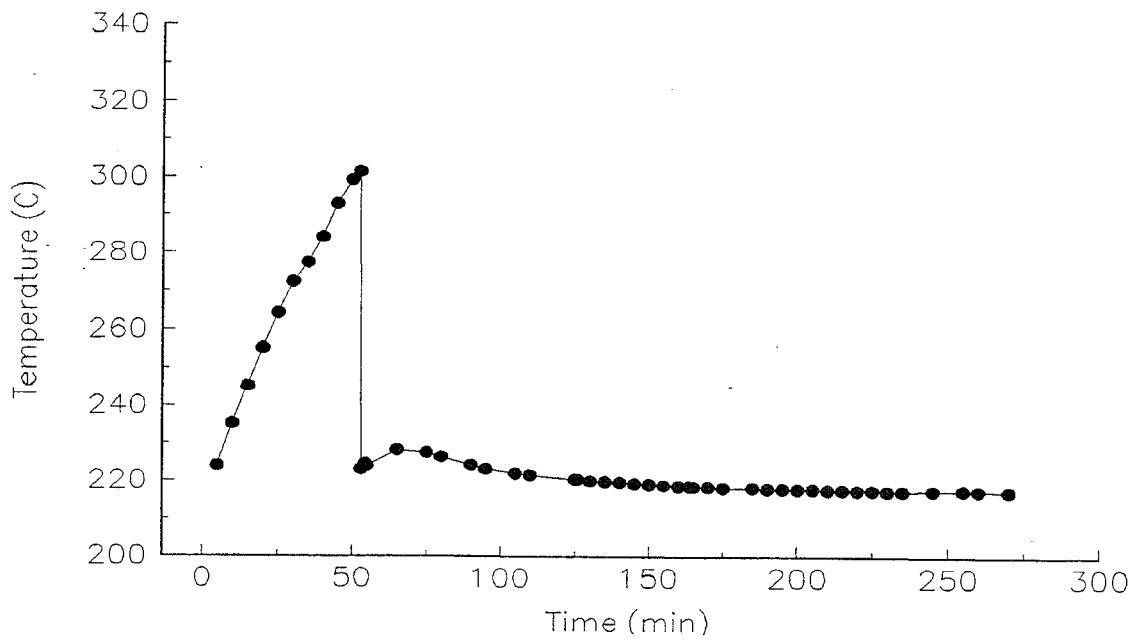


Figure 5-36. Typical Thermosyphon Response for the FC-5312 Fluid

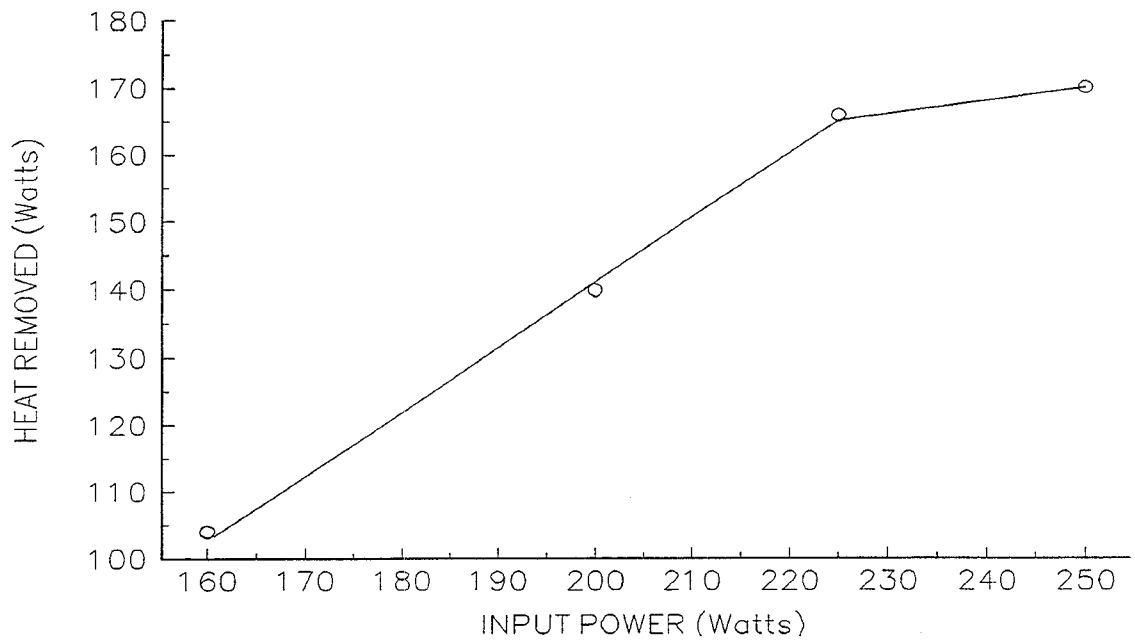


Figure 5-37. Heat Removed as a Function of Boiler Power for the FC-5312 Fluid

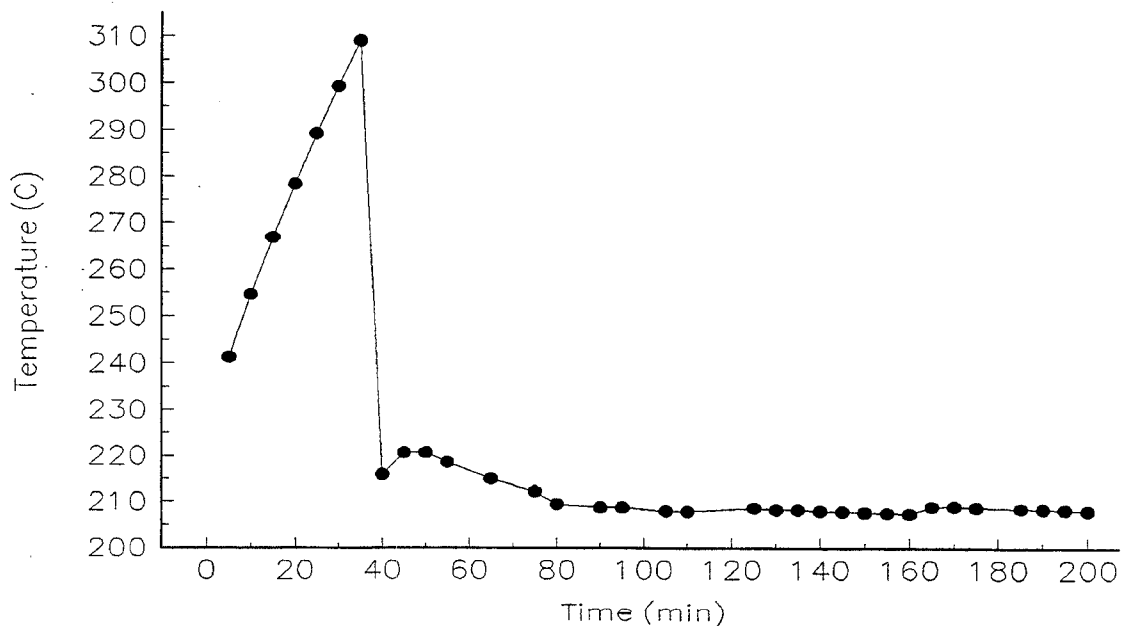


Figure 5-38. Typical Thermosyphon Response for the FC-5312 at an Elevated Head

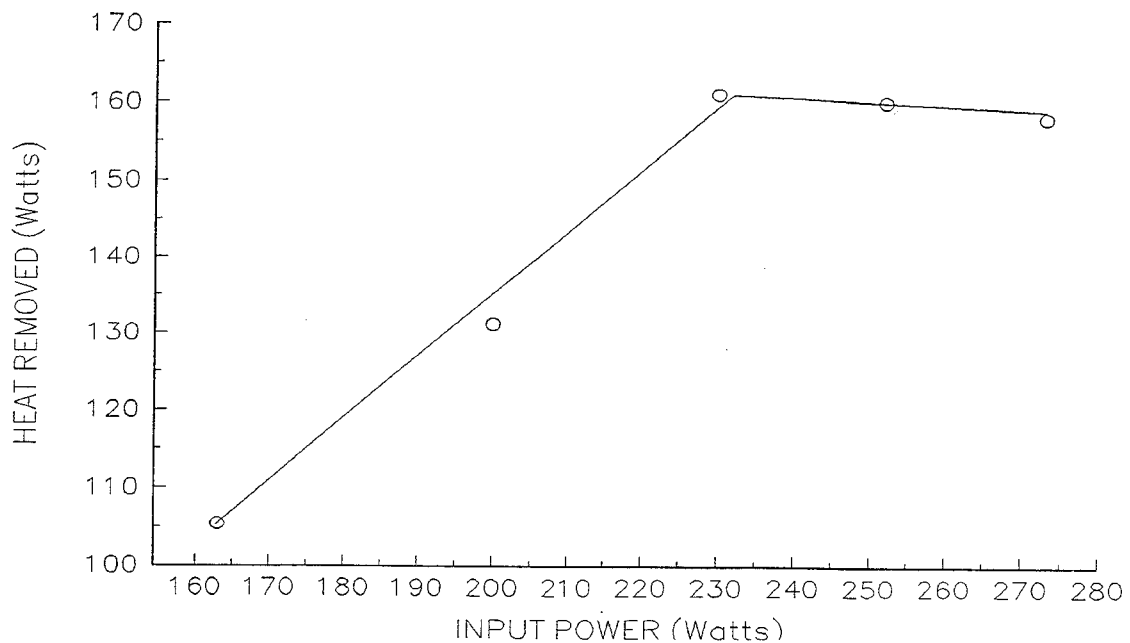


Figure 5-39. Heat Removed as a Function of Boiler Power; FC-5312; 0.45 m Head

but by some other parameter which was not determined. At very high power input levels, the system response time, as shown in Figure 5-40, was very slow, indicating that the fluid was being superheated and that the condenser could not adequately cool the fluid.

Based on the data obtained from these experiments, a thermosyphon cooling system using Fluorinert fluids is feasible. Careful consideration, however, needs to be given to the design of the cooling system to ensure uniform cooling throughout the battery. Further, the manufacturer of Fluorinert^R reports that, when boiled, these fluids decompose in the presence of moisture liberating trace amounts of perfluoroisobutylene (PFIB) and hydrogen fluoride (HF). The rates at which the products are liberated from FC-71 at 300°C have been determined experimentally by the manufacturer to be 2.2 μgrams of PFIB/min/gram of fluid and 3.9 μgrams of HF/min/gram. Data are not available for fluid decomposition rates at the higher temperatures that would be experienced by the fluid at the beginning of each cooling cycle in a battery cooling system. Further studies are therefore warranted to determine the effect that these degradation by-products may have on the materials used to construct the cooling system and to predict the life of the fluid.

5.3.2 Cell-to-Cell Bonding Material Evaluation

The initial UES battery designs specified formed mica sheets to be used as separators between the cell strings and TES capsules. While the mica is a very good electronic insulator, it has poor thermal conductivity and is expensive. Further, the mica separators

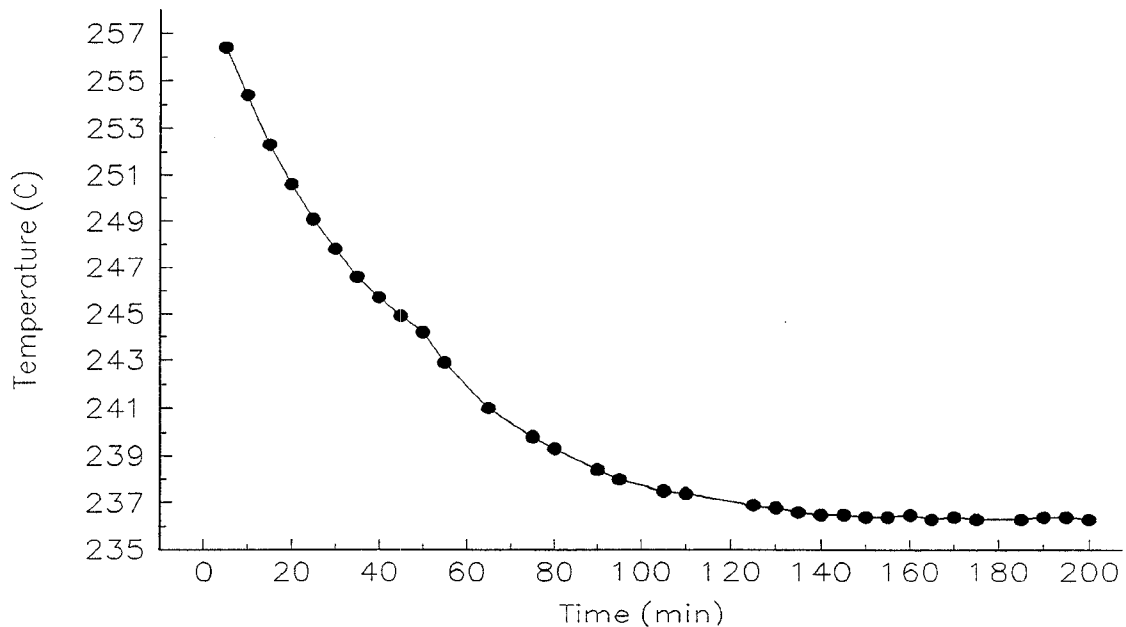


Figure 5-40. Thermosyphon Response at a High Power Input for the FC- 5312

are quite fragile and could be easily damaged during battery assembly, possibly resulting in short circuits in the battery. To circumvent these problems, alternative means were considered for electrically isolating cells and, at the same time, improving cell-to-cell heat transfer characteristics.

The first concept pursued was coating the cells with a material which would increase the emissivity of the cell containers and cementing the cell strings together with thin strips of high temperature adhesive. The materials selected for trials were Stovebright^R high temperature paint and Aremco Ceramabond 571^R ceramic adhesive. Both are relatively low cost, commercially available products. The Ceramabond 571^R had excellent battery use properties – i.e., good adhesion to steel, high temperature stability, good thermal conductivity (11 W/m²K), and high resistivity (>10⁵ Ω-cm @ 500°C).

Mild steel cell cases were painted with Stovebright^R paint and then bonded to each other with strips of Ceramabond 571^R adhesive. The Stovebright^R paint withstood aggressive thermal cycling (25°C to 370°C) but easily pulled away from the surface under the cemented areas when physically disturbed. Additional surface preparation by sand blasting improved the bond; however, there were concerns that the sand blasting process could potentially damage cell strings. Because of these issues, the use of Stovebright^R paint was abandoned.

The next approach taken was to coat the cells with modified Ceramabond^R adhesive and then use additional adhesive to cement cells and strings together. Numerous trials were performed with Ceramabond 571 adhesive on cell containers, cells, and finally cell strings. The objective of these trials was to find a composition with consistent dipping qualities and strong cell-to-cell adhesion. The Ceramabond 571^R is composed of magnesium oxide powder and a proprietary liquid (mostly sodium silicate) mixed together in prescribed proportions. With the additions of deionized water and variations of the solid to liquid ratios, material yielding better coating thickness uniformity and cracking resistance were obtained.

The effectiveness of the Ceramabond^R as a cell coating and cell-to-cell adhesive was assessed by building and testing a ten string module. The cell strings and TES capsules were dipped in the adhesive slurry to coat the surface, air dried, redipped, and air dried again. After all the components were dry, the module was assembled and the cell string tabs were welded to the bank plates. The entire welded assembly was then dipped in the modified Ceramabond 571^R slurry and air dried to bond all the components into a rigid assembly.

Following the testing described in Section 5.3.1.1, a review of all test data and coating trial work indicated that the use of the Aremco Ceramabond^R would be an effective means of electrically isolating cells in the UES modules and would provide sufficient thermal conductance to minimize thermal gradients. Further, the use of the cement provided mechanical rigidity sufficient to allow easy handling of the modules during battery assembly. Based on this work, a decision was made to utilize the Aremco ceramic cement in the deliverable battery module.

5.3.3 Cell String Fuse Development

An important issue in battery design is the ability of the battery to accommodate cell failure without significantly impacting the battery's performance. This is dependent on the electrical network adopted. If cell reliability is very high and there is a low incidence of failure within the target life of the battery, the cell network configuration is of only limited significance. On the other hand, if a limited number of cell failures (1% to 5% of the cell population) has to be accommodated within the battery life, the choice of network configuration becomes critical. If cells failed in a consistent manner, preferably with either zero resistance or infinite resistance, the cell network design would be relatively simple. If all cells failed in a short circuit condition, the preferred battery design would be to have long series strings of cells with parallel connections at the ends only. If cells failed with infinite resistance, the ideal network would be to have parallel connections at every cell. However, sodium sulfur cells generally fail in a manner which is unpredictable, particularly with regard to the resistance of failed cells. The resistance of a failed cell is usually somewhat higher than that of a fully functioning cell, but not high enough to completely block current flow. There are also some rare instances when failed cells have nearly zero resistance. To design a reliable battery, all ranges of failed cell resistance must be accommodated.

Most batteries manufactured to date at SPL have been based on the use of three-, four-, or five-cell series strings networked together to provide the desired battery capacity and voltage. With this arrangement, when a single cell fails, the remaining cells in the string are driven to the top of charge by other parallel strings and current through the string drops to zero, thus eliminating the parasitic loss of a short circuited bank. While this scheme is effective in limiting the impact of a single cell failure on the overall battery performance, there are several drawbacks to this approach. The loss of energy is not that of a single cell but that of the entire string. Further, if all of the cells in a string fail, the bank containing that string becomes shorted, and if the failed string resistance is sufficiently low, thermal runaway could be a concern. Because the non-failed cells in a string with one or more failed cells are held at a higher than normal voltage, there is some concern that they may be more likely to fail, greatly increasing the possibility of having a string in which all cells have failed.

Stimulated by reports of fuse tests initiated at SNL, the behavior of zinc and aluminum fuses at 350°C in air was examined. Zinc, with a melting point of 419.5°C, was chosen to provide overtemperature as well as overcurrent protection.

The governing equation for calculating the maximum temperature in a wire (fuse) passing current is as follows:

$$T_{\max} = T_{\text{ambient}} + \frac{I^2 R^2}{8L_o T}$$

where L_o is the Lorentz number ($= 2.45 \times 10^{-8} \text{ W-}\Omega/\text{K}^2$), I is the current required to blow the fuse, and R is the fuse's resistance. If $T_{\max} = T_{\text{melting}}$, then I and R are not independent. If T_{ambient} is 350°C and T_{\max} is 419.5 °C for zinc and 660.4 °C for alumina, the fuse current/ resistance relationships are shown in Figure 5-41.

A number of experiments with zinc and aluminum fuses were conducted. Rectangular (8 x 30 x 0.62mm) fuse samples of zinc were fabricated with #6 bolt holes at the end and a notched section 1.5mm across in the middle made with a circular punch. The ends were sheathed with copper foil spot welded to the zinc to assure good, low resistance contact with the test fixture. All tests were conducted at 350°C in air. The results of the initial trials with zinc fuses were as expected based on discussion with SNL personnel. When the fuses were heated in air, a shell of oxide formed on the surface of the zinc. When the current through the fuse was raised and the metal melted, the oxide shell held the molten metal in place and the current was not interrupted.

To circumvent this problem, a number of zinc fuse samples were tested with the necked region placed in a strong magnetic field (several kiloGauss) produced by an Alnico^R magnet. The melting occurred only in the necked region with currents of 40 - 50 A to blow the fuse. The resistance of the fuses was $1.4 \pm 0.2 \text{ m}\Omega$. Similar zinc fuse samples placed in the gap of an iron yoke, which is (pinch pump effect, had more extensive areas of melting. Samples placed in the gap of the same iron yoke with five turns of wire in series with the fuse produced results identical to those tested with the permanent magnet.

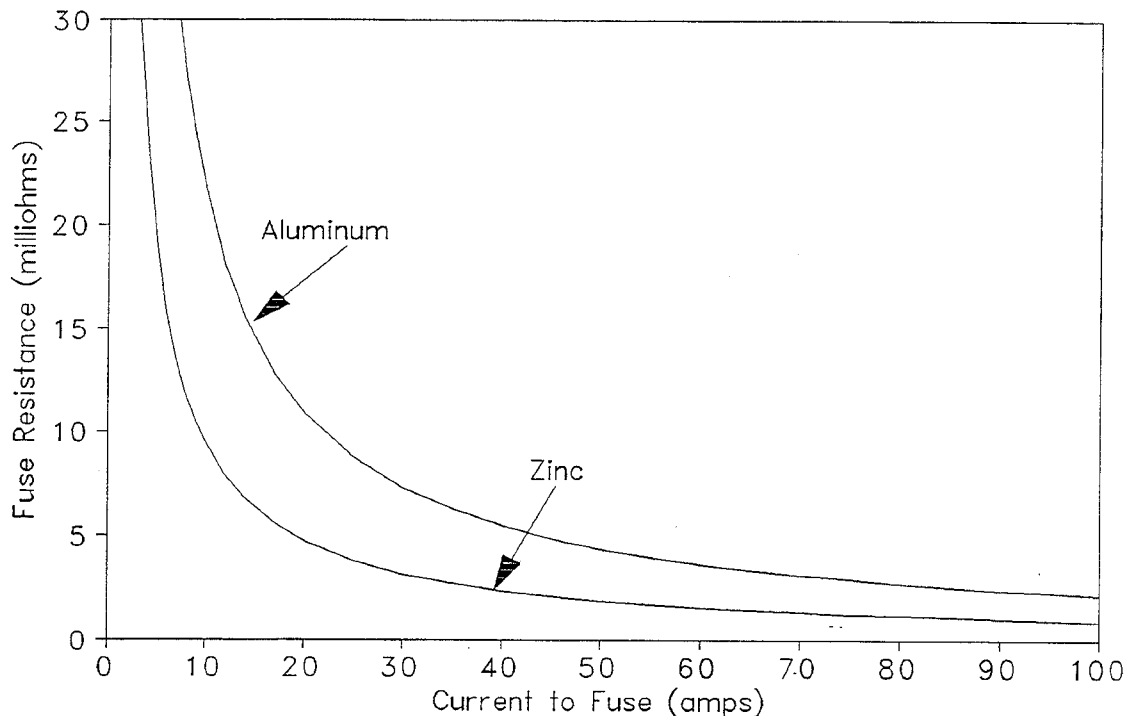


Figure 5-41. Fuse Current/Resistance Relationship

Based upon limited testing, the design requirements identified for the magnetic flux induced fuse are a circular cylindrical iron yoke 25mm O.D. x 13mm I.D. x 6mm thick with a seven turn coil and a gap of 1mm. The field was calculated to be 4π ampere-turns or 3900 Gauss when the fuse blows at 50 A.

Aluminum fuse samples of the same dimensions except 0.13 mm thick were also tested. These samples were clad with 0.005" nickel foil spot welded on the ends where electrical contact was made for improved electrical contact. The resistance of the aluminum samples was 3.9 ± 0.3 m Ω . These all blew cleanly at 45 ± 5 A in the notched section without support or magnetic field. For a plain fuse without the overtemperature feature, these appear to be the best choice. For both zinc and aluminum fuses, the current to blow and the fuse resistance are in qualitative agreement with the simple calculation.

While simple, reliable fuses can be fabricated, their usefulness in batteries is complicated by their relatively high resistance. The resistance of a fuse designed to blow at a given current level can be reduced by using a metal with a lower melting point. However, using a fuse metal whose melting point is too close to the top of the battery operating temperature range could result in a premature failure of the battery in the event of an otherwise non-fatal, temporary thermal excursion.

The use of fuses becomes more viable as the capacity of the cells increases. With larger cells, the current through a string during and after a cell failure will be higher than in the same circumstances with smaller cells. As noted previously, the use of fuses also favors having fewer cells in series per string. However, due to the uncertainty of string current during cell failure, it would be unwise to consider single cell strings. This is due to the fact that a cell could fail with a resistance high enough to limit the current to a level below the fuse current to blow, in which case all cells in parallel with the failed cell would be partially short circuited. With at least two cells in series, the non-failed cell would come to the top of charge and stop current flow through the string.

While the application of an electromagnet driven by the current through the fuse assures that the circuit will be opened upon melting of the fuse link, the weight and volume of the magnet core will significantly impact a battery's mass and volumetric based performance ratings.

5.3.4 Battery Management System Design

The primary functions of the battery management system (BMS) were to monitor battery operation, provide a status signal to the power converter for charge/discharge control, and to record and store system operation data. The UES BMS was connected to the battery in two significant ways. First, the critical voltages, temperatures, and currents were interfaced from the battery to the BMS. Second, a disconnect device, which was a contactor, was connected between the battery and load. In the event that unsafe operating conditions were detected by the BMS, it opened the disconnect device in order to limit the use of the battery by the load.

The BMS was also required to save specific cycle data and to allow retrieval of this information via a remote computer. With the exception of the data retrieval, the BMS was designed to be independent and fault-tolerant. The BMS described here is shown schematically in Figure 5-42 in a typical configuration with the UES battery and load device.

The BMS was designed with the capability to monitor a battery made up of eight sub-batteries or modules arranged in two parallel, four series strings. Each module had up to 16 input channels (voltages, temperatures, and currents) for a total of 128 channels for the entire battery. During use of the battery, if the BMS detected a battery condition that was outside the defined operating limits, it signaled the load device to terminate use of the battery. If, after an appropriate amount of time, this signal was ignored by the load device, the BMS forced the battery "off-line" by opening the contactor. Once the BMS had determined that the battery could be safely operated the battery was then placed back "on-line" by closing the contactor.

Other features of the BMS design included the capability to detect peripheral hardware, thermocouple, and voltage sense lead failures. Additionally, the BMS was designed with the capability to monitor, record, and download battery cycle data to a remote computer for analysis.

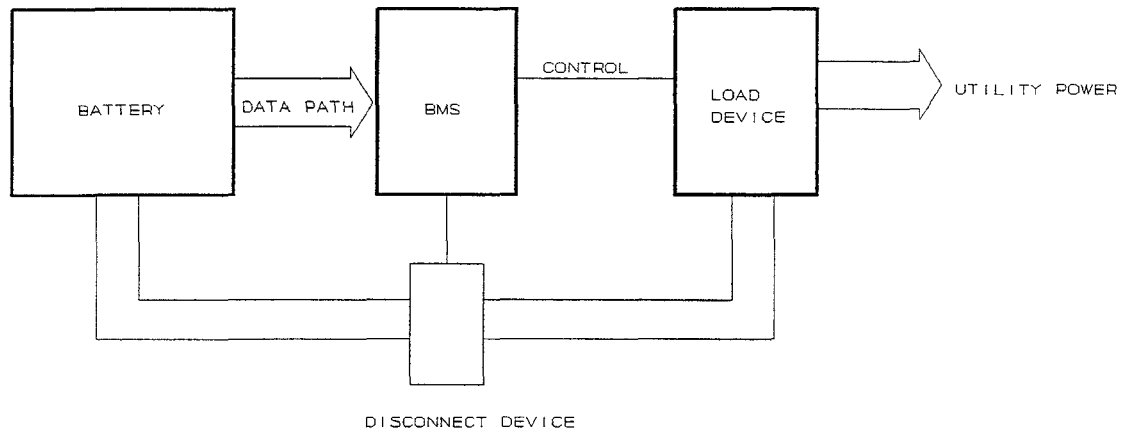


Figure 5-42. Battery Energy Storage System Block Diagram

The control algorithm was based on the rated and theoretical capacity of the battery. Under most conditions, the BMS allowed the load device access to the battery if the remaining available capacity was within the rated capacity.

Specifically, the BMS determined the absolute state of charge of the battery based on its theoretical capacity, open circuit voltages, temperatures, and the amount of charge removed during each previous discharge segment. Then, following a complete charge, the available capacity was recalculated and saved in nonvolatile memory. All of the available capacity was then accessible to the load during the subsequent discharge as long as the temperatures, current, and power levels for each module were maintained within the rated limits. This process was repeated for each cycle until the battery could no longer supply the rated capacity – i.e., it had reached its end of life.

This control algorithm had the advantage of allowing operation of the battery within limits that were easily determined and measured; these included current, power, and temperature. Other battery control algorithms, specifically those that attempt to calculate real time open circuit voltages, required complex battery models that are sensitive to current levels, temperature, state of charge, and the age of the battery.

The BMS hardware consisted of two main sections: the Battery Interface Electronics and a Data Acquisition System. These two main sections are shown in a system block diagram in Figure 5-43. The battery interface electronics were located on the surface of the battery and were powered by the battery itself. The interface electronics converted all bank voltages, temperature, and currents to frequency modulated light pulses. The light pulses were transmitted to the data acquisition system over fiber optic cables for conversion back to a 12-bit digital format. By transmitting data through fiber optics, maximum noise suppression and voltage isolation were achieved.

The data acquisition system consisted of a frequency converter and a single board computer. The frequency converter was made up of sixteen, 12-bit counters connected to a specific battery input (voltage, temperature or a current). A precision 17 ms (5 ppm) one-shot (monostable multivibrator) was common to each of the 16 counters. The one-shot was triggered by the single board computer and enabled counting for the 17 ms time period. Upon completion of the counting period, 12-bit data for each of the 16 channels was latched and can be read by the Single Board Computer.

During normal operation, the BMS functioned without human intervention and supplied a battery trip request (go/no-go) signal to the load device as necessary to prevent damage to the battery. Interaction between the load device and the BMS included no less than two signals: 1) a discharge request signal and 2) a charge request signal. Other input/output signals included analog values that corresponded to the instantaneous power, total energy, and charge supplied by the load device to the end user.

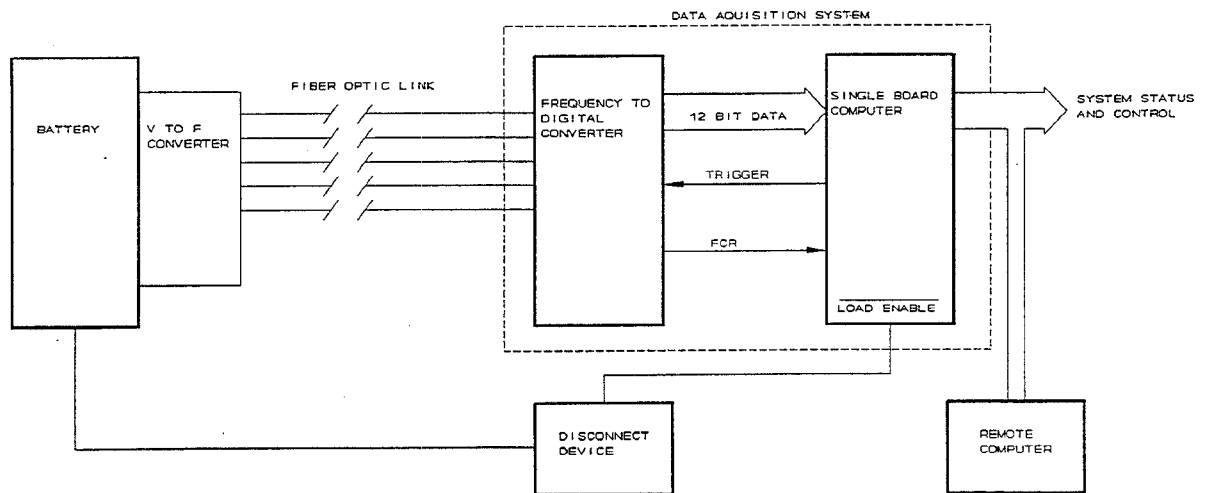


Figure 5-43. Battery Management System Block Diagram

VI. 13 kWh DELIVERABLE MODULE DEVELOPMENT AND TEST

In order to evaluate the battery component concepts developed earlier in the Program, a 13 kWh module was designed, fabricated, and delivered to SNL for testing.

6.1 Deliverable Module Design

A battery module representing one-sixth of a full size NAS-P_{ac} sub-battery (75 kWh) was designed for delivery to SNL. The module was designed to deliver 13 kWh during a two hour discharge at 32 V. The final configuration of the deliverable module combined design elements from SPL electric vehicle batteries as well as new approaches developed specifically for BESS applications.

In its envelope of approximately 700mm x 900mm planform x 400mm height, four banks were connected in series. Figure 6-1 shows the "core" of the deliverable module design. Each bank was comprised of 48, four cell strings. The strings were arranged in a square pack with a TES capsule located in each interstice. Though the string packing was less dense than the hexagonal packing used in SPL's electric vehicle batteries, square packing allowed for the incorporation of a sufficient mass of latent heat storage salts (a LiCl/KCl eutectic) to obtain the required thermal management characteristics without the added expense and fabrication problems a trigonal salt capsule would entail.

The LiCl/KCl eutectic was contained within impact extruded 3003 aluminum alloy tubes with aluminum end caps of the same alloy welded into place. All capsules were thermally cycled between room temperature and 450°C to verify weld integrity and to ensure that the mass of salt was not excessive. The aluminum TES capsules were then placed inside steel tubes to provide secondary containment of the salts in the event of a capsule breach.

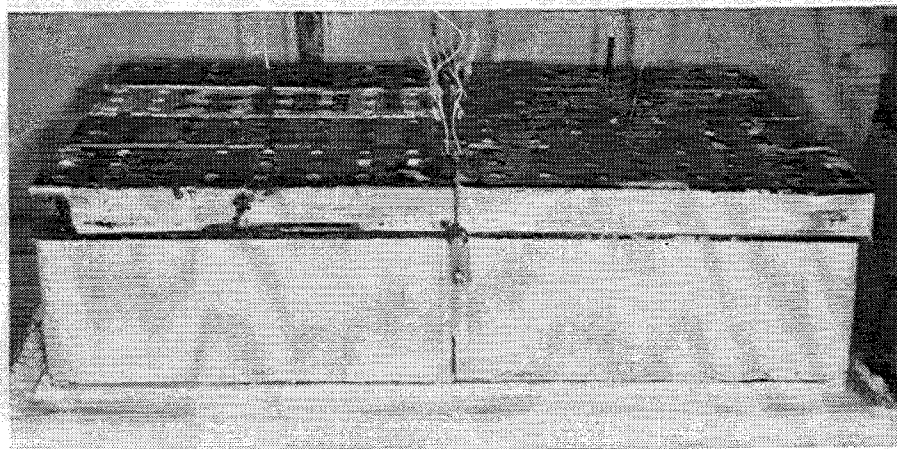


Figure 6-1. Cut-Away View of the "Core" of the Deliverable 13 kWh Sodium Sulfur Module

Machined ceramic spacers were inserted into each end of the steel tubes to prevent the TES capsules from shorting the banks. The steel capsules were also required for containment of the aluminum in the event of a major thermal excursion which could melt the aluminum capsules and short out one or more of the banks. As must now be evident, safety was assigned top priority in the design of the deliverable module. An additional function of the aluminum TES capsule was to maximize thermal conductance through the module core parallel to the cell string axes.

The ceramic cement discussed in Section 5.3.2 was used to electrically isolate the cell strings and to rigidize the banks. Additionally, the cement enhanced the heat transfer between the cell strings and the TES capsules. Furthermore, by encapsulating all components in the cement, additional containment of cell reactants or TES salts would be provided for in the event of breaching.

The enclosure/thermal insulation system utilized multiple layers of ceramic board and blankets in a single walled, sheet metal box. This approach provides for a more cost effective design as compared to the double walled, vacuum insulated thermal enclosure employed on EV batteries. For utility applications, the volume requirement is not as constraining, and, therefore, a "high tech" solution is not warranted. Unless extremely large thicknesses of conventional insulation were used, the disadvantage of employing this design is that the normalized heat loss (W_t/Wh) will be higher than if the EV thermal enclosure were used. Offsetting the impact of increased heat loss during operation, the improved thermal conductance, both horizontally and vertically within the module core, will spread the heat more evenly throughout the core, thereby reducing temperature gradients.

The module was heated using seven mica sheet heaters supplied by Cogebi. Each heater consisted of foil trace heaters laminated between sheets of mica for electrical insulation. Except for the top where two heaters were used, one heater covered each face of the module; there was one for each "half" bank on the top of the module to facilitate wiring. The foil traces were designed to maintain uniform heat input over the surface of the module core. Each heater had two foil traces for redundancy in the event that one trace burned out during module operation or was damaged during assembly or transport. A layer of mica sheet was interposed between the module core and the heaters to minimize the possibility of damage to the heaters during assembly or transport.

Power to the module heaters was controlled by a temperature controller installed in the BMS. A number of thermocouples were installed to monitor the module temperature during testing and to provide a control signal for the heater control.

Charge and discharge current through the module was fed by means of a pair of 9.5mm diameter nickel studs located on opposite sides of the module. These studs were brazed to a current collection bar that was, in turn, spot welded to the sides of the terminal bankplates. The stud diameter was not sized to provide an optimum trade-off between electrical resistance and heat loss but was made larger to insure that the current which could be drawn from the module would never be limited by the size of the studs.

6.2 Module Fabrication

The cells used for fabrication of the 13 kWh deliverable module were manufactured at the SPL pilot plant in Manchester, England, and were assembled into four-cell strings for shipment to SPI in Salt Lake City. Upon arrival, the strings were unpacked and inspected for shipping damage.

6.2.1 Half Bank Assembly

The module was comprised of four, series connected, 480 Ah, 8V banks. To facilitate handling and assembly of the module, the banks were subdivided into halves. Hence, the term "half" bank. The first step in the assembly of these half banks was to dip each of the 24, 4-cell strings making-up the half bank in a Ceramabond 571^R slurry; these were hung and allowed to dry in air overnight. The strings were again dipped and hung to dry; this time, however, they were hung from the opposite string end in order to obtain a more uniform thickness of the coating over the axial length. Before dipping, the tabs used to connect the strings to the bank plates were coated in wax to prevent the cement from sticking to them. After the coating had fully air dried, the wax was removed. Coating of the TES capsules was accomplished in the same manner.

The next step was to assemble the half bank. Twenty-four coated cell strings and 24 TES capsules were stacked into a plastic jig to hold them in proper position while the string tabs were spot welded to the bank plates. Care was taken to make certain that there was no intermixing of cell manufacturing lots within half banks.

After assembly, the half banks were heated to operating temperature and electrically cycled twice to verify capacity. During these tests, several of the half banks experienced string failures. Of ten half banks assembled and tested, four had no string failures, three had one failed string, two had two failed strings, and one (in half Bank 1) had three failed strings. It was a concern that a half bank would have three failed strings. The average failure rate of strings on initial heat-up was reported by SPL to be 5%. It was postulated that the use of the Ceramabond cement was causing or contributing to an excessive rate of string failures. An analysis of the data showed that the distribution of failures was in agreement with the prediction of a binomial distribution. Hence, it was concluded that the use of the cement was not enhancing the rate of failure.

Further, a detailed post test analysis of Bank 1 was conducted, but the analysis revealed nothing unusual which could have caused any string failures. It was conclusively shown that strings with a failed cell could be identified solely on the basis of their room

*

SPL warmed-up cell strings and measured their open circuit voltage prior to assembling them into banks in order to remove those cells having latent defects; on the average, 5% of these strings were rejected.

temperature open circuit voltages. Using a digital voltmeter with an input resistance greater than 10 M Ω , the voltages of all half bank cell strings were measured at room temperature. All strings with four good cells had voltages greater than three volts; strings with one or more failed cells had voltages below 0.5 V. The failures were confirmed by radiography and later by sectioning the cells. This method of cold voltage measurement was subsequently used to identify failed strings in several other half banks so that they could be replaced prior to final module assembly.

After capacity verification testing and cell replacement in two half banks was completed, each half bank was dipped in the Ceramabond cement to bond all of the cell strings and TES capsules together. After the final dipping, the excess cement was allowed to drain away, and the half banks were air dried and heated to 90°C to drive off additional moisture.

The half bank construction formed a "unitized" structure that could accept the internal module structural loads and which could be easily handled for assembly of the module.

6.2.2 Module Assembly

The photographs presented in Figures 6-2 through 6-8 illustrate the module assembly process. Figure 6-2 shows the interior of the module before installation of the banks. The assembly began with the base, one side, and the back surface. There were multiple layers of ceramic blanket insulation, totaling 3 inches of thickness, which limited the module heat loss to less than 400 watts. The base included a ceramic fiberboard to serve as a flat, structurally supporting surface for installing the banks. A low conductivity blanket was then placed on top of the fiberboard. Finally, the base heater and a layer of mica sheet were

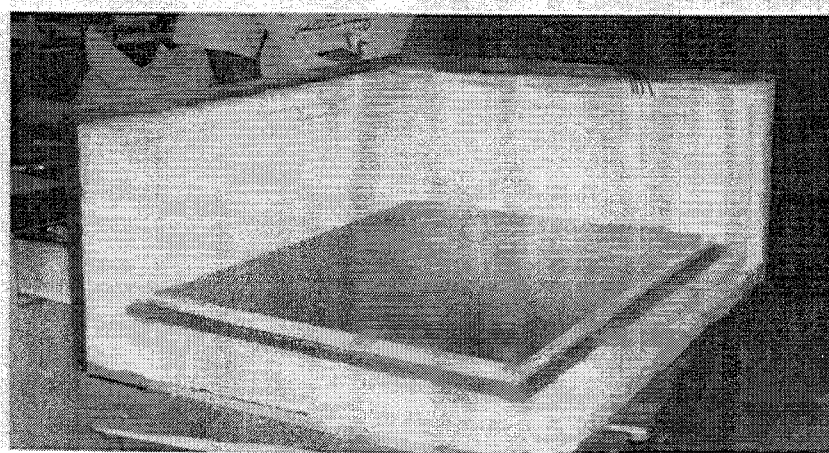


Figure 6-2. Interior of the Deliverable 13 kWh Sodium Sulfur Module Prior to Bank Installation

laid on the top insulating surface. Unitized half banks were slid onto this base utilizing a mica "skid" that was cut to fit the contour of the bank.

Several unanticipated module assembly problems were encountered. The build-up of the ceramic cement on the cells and TES capsules was non-uniform, and, when coupled with the cell strings being slightly bowed, misalignment of the bankplates to the adjoining busplates resulted. This prevented proper welding of the bankplates to the busplates. The resulting mismatch created a slight interference between each of the banks producing an overall growth of the module core. Consequently, the sheet metal box would not fit over the insulated core. To rectify this problem and to allow the banks to be interconnected as planned, 16 TES capsules along the exterior edge of each bank were removed. A sheet of mica was inserted between series-connected banks to provide further electrical insulation. This resulted in proper alignment of the bankplates and busplates for welding and allowed the module to be assembled. The reduction in thermal performance due to elimination of this TES material was calculated to be minimal for the period of time that the module would be tested at Sandia. The full inventory of salt was designed to contribute only near the end-of-life of the module – i.e., after a significant number of cells had failed. The number of cell failures over the 1 to 2 years that the module would be tested at Sandia would not be sufficient to thermally limit its performance.

Figure 6-3 shows a completed 8V, 400 Ah bank with the termination strip being welded to it. The nickel power take-off stud was located in the middle of the termination strip; this served as the negative power lead of the module. When the bank was finally positioned, the power stud fit through an insulation layer and a ceramic bushing located in the back wall of the enclosure.

A close-up of the welding procedure, whereby bankplates were joined to the adjacent busplates, is shown in Figure 6-4. The large spot welder was used to connect half banks in parallel, followed by a series connection between neighboring banks. The latter was accomplished by welding through the six raised castellations shown in the figure.

Figure 6-5 shows the completed bank-to-bank electrical connection with all banks in place. Note that the positive power stud and strip have been welded in place along the exterior edge of the termination plate. The leads in the foreground and those lying on top are thermocouples. The leads on the right are heater leads that were eventually routed to a wiring board lying just under the topmost insulation of the module. All six sides of the interior module have heaters for initial heat-up and for controlling the module temperature against heat loss occurring through each face. Additional heater power was designed into regions around the power studs, where heat leaks during quiescent periods were calculated to be higher.

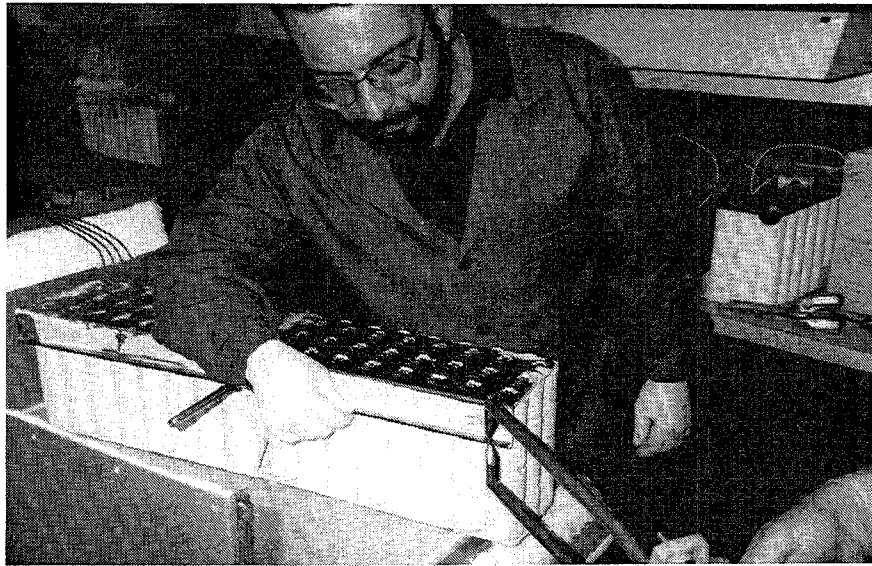


Figure 6-3. An 8V, 400Ah Bank Comprising the 13 kWh Sodium Sulfur Module

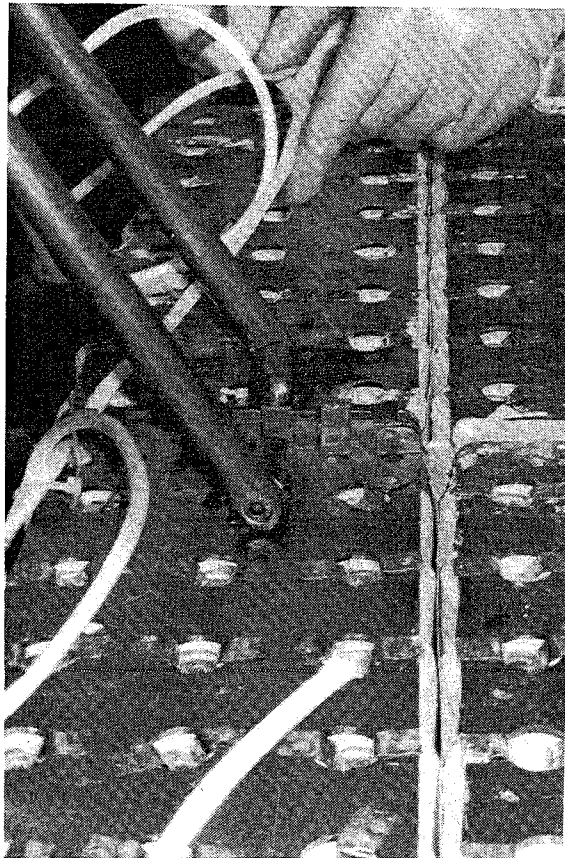


Figure 6-4. The Welding of Adjacent Bank Plates

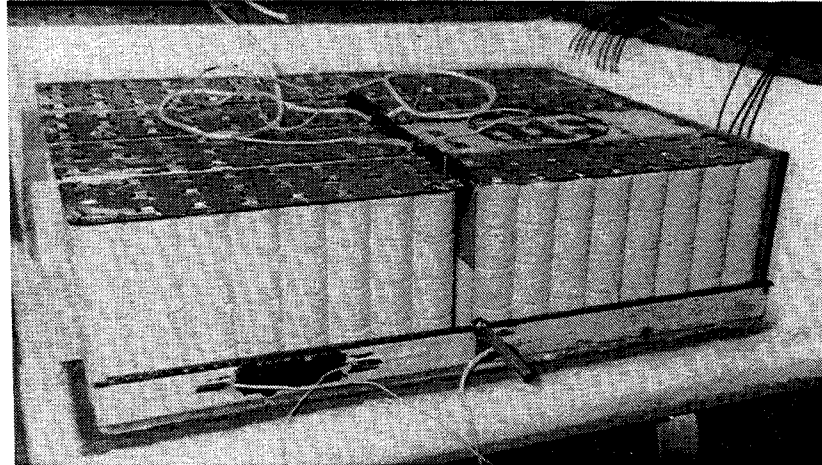


Figure 6-5. Completed Bank Assembly

Figure 6-6 is a top view of the module, showing the top split heaters and the four control thermocouples that have been welded to the middle of each of the interior bankplates. These thermocouples were connected in a box outside the enclosure and were used to calculate the average temperature for module temperature control.

The wiring board at the top of the module is shown in Figure 6-7. The wires bundled on the left are heater wires. The bundle on the right is thermocouple and bank voltage leads. Each bundle went to a separate box on top of the module enclosure. The four bank voltages and nine thermocouple voltages were converted to light pulses and transmitted via an optical fiber link for noise-free communication to the BMS. In addition, the four control thermocouples were connected in parallel and wired directly to the heater controller. This effectively averaged the four signals and provided considerable redundancy to accommodate open circuit thermocouples. An overtemperature thermocouple was wired to control the reserve heaters.

The BMS is shown in Figure 6-8 at a stage before the temperature controller was installed in the center of the front panel. The solid state control relays are mounted on the back wall. The boards on the right translate the arriving optical signals back to voltages for processing by the BMS. The heart of the unit is a single board computer, shown in the forefront. The BMS, with its software adjustable parameters for charge/discharge and overtemperature control, limited and recorded significant event-driven data in nonvolatile RAM. This storage could be dumped periodically to a diagnostic computer through an RS-232 port for subsequent analysis.

Figure 6-9 is a photograph of the finished module before final wiring and the members of the module build team, with the exception of Scott Olsen.

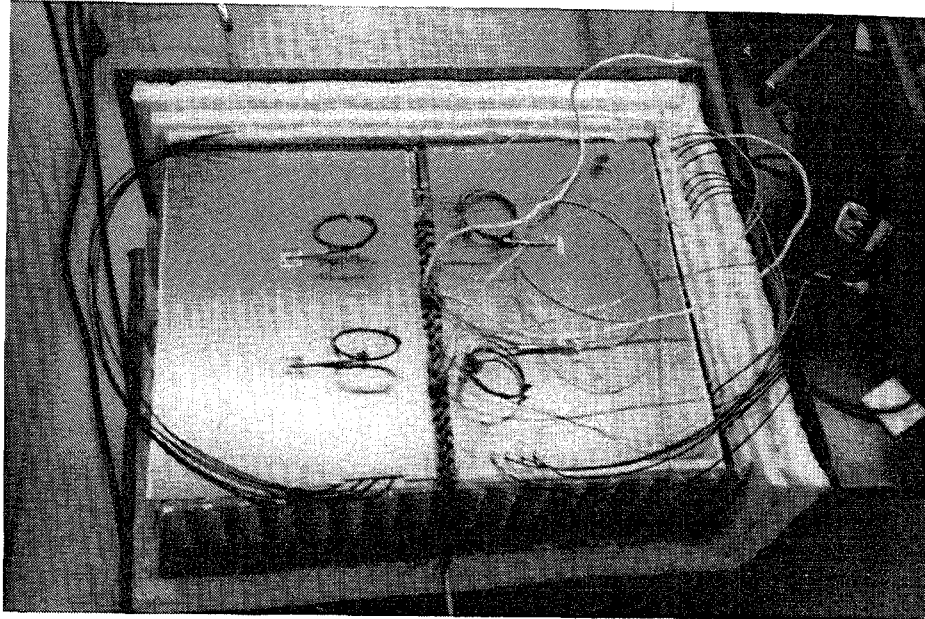


Figure 6-6. The Top View of the Module with Split Heaters and Control Thermocouples In-Place

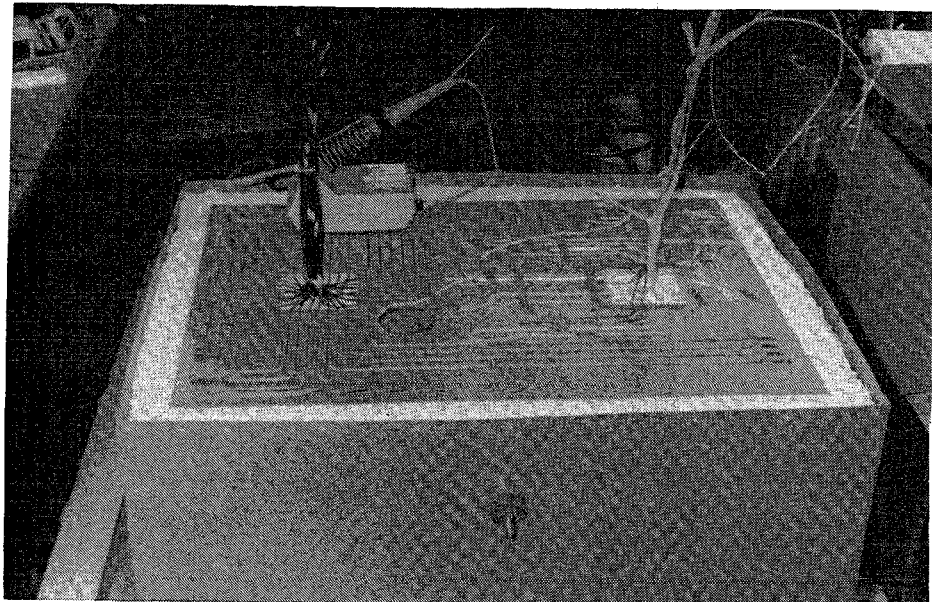


Figure 6-7. Wiring Board Installed on Top of the Module

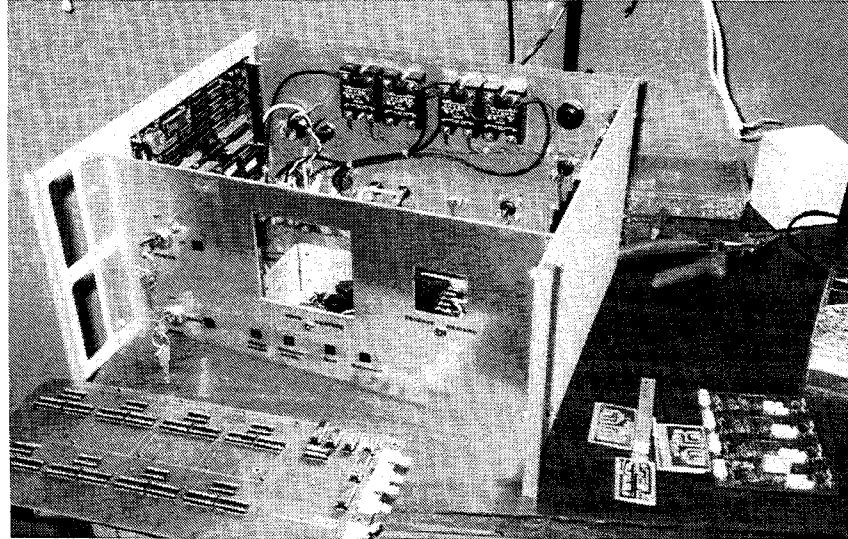


Figure 6-8. Module Management System (BMS) During Assembly



Figure 6-9. Completed 13kWh Module with Assembly Team

Upon completion of the wiring of heaters, thermocouples, and bank voltage sense leads, extensive resistance measurements were made to assure that there were no short circuits in the instrumentation wiring. Measurements were made between each bank voltage lead, the module case, each heater lead, and each thermocouple. No short circuits were detected. After these tests, the open circuit voltages of each bank was measured with the module at room temperature. These measurements are shown in the Column (1) of Table 6-1.

Table 6-1. Bank Voltages of Deliverable Module During Initial Heat-Up

Bank No.	Module Average Core Temperature			
	19°C (1)	100°C (2)	140°C (3)	200°C (4)
1	0.679 v	0.987 v	7.888 v	8.35 v
2	0.530 v	0.814 v	8.032 v	8.36 v
3	0.303 v	0.324 v	7.450 v	8.26 v
4	0.901 v	1.189 v	7.891 v	8.32 v

To verify that the module and heaters were fully functional and to drive off additional moisture from the Ceramabond^R cement, the module was heated at a rate of 4°C/hr to 100°C where the bank voltages were again measured. These measurements are shown in Column (2) of Table 6-1. The unexpectedly low voltages raised a concern that the banks may be partially shorted. Bank 3 was of greatest concern, for its voltage was essentially unchanged from that measured at room temperature. Though the voltages for Banks 1, 2, and 4 were lower than expected, they did increase as the module was heated. Following conversations with SPL personnel, it was concluded that the "wet" cement was electrically loading the banks and that the only course of action was to continue heating the module to drive off as much moisture as possible. Data from Aremco, the manufacturer of Ceramabond^R, stated that complete curing and drying of the cement was not accomplished until temperatures above 350°C were reached.

The module was then heated to 140°C at a rate of 7°C/hr and held there for 60 hours at which time another set of bank voltages were recorded. These are shown in Column (3) of Table 6-1. The module was then heated to 200°C and allowed to stand overnight. The voltages recorded at that time are shown in Column (5) of Table 6-1. These voltages agreed quite well with expected voltages, though that for Bank 3 was still slightly low. It was concluded at this point that the module was functional and could be shipped to SNL.

6.3 Module Testing

The UES module was installed and commissioned at the SNL facility on September 9, 1994. The objectives of the testing were to: 1) confirm the module's electrical performance ratings, 2) identify its capability to meet basic cycling requirements associated with several promising candidate UES applications, 3) gain experience with the integrated BMS, and 4) determine the service life using a preferred customer peak shaving requirement.

During heat-up and early testing, the BMS behaved erratically. This behavior was eventually traced to condensation of moisture in the circuitry mounted on the module enclosure. The origin of the moisture was residual water that was still trapped in the Ceramabond 571^R cement. As the module was heated to its test temperature of 350°C, the final curing and drying of the cement occurred. It was anticipated that some additional water would be driven off during heat-up to operating temperature but not to the levels that were actually experienced. The only openings in the module enclosure through which the moisture could escape were those through which the instrumentation and heater leads passed into the boxes mounted on the surfaces of the module. Since the boxes and their contents were cooler than the enclosure surfaces, moisture did condense causing some shorting of the instrumentation. When the cement was fully cured and dried, the instrumentation box covers were replaced with no further problems occurring.

After completing six cycles, the bank resistances ranged between 3.2 and 3.4 mΩ, and the total module resistance was 13.1 mΩ, which was in good agreement with the predicted value of 12.9 mΩ. Based on the initial cycles, the available module capacity was calculated to be 460 Ah when discharged to 100% depth of discharge (30.40 V_{oc}). Surface temperature measurements at various points on the exterior of the module averaged 44.5°C, which was consistent with a heat loss through the insulation of 230 W.

The module was then subjected to 44 constant current discharge cycles (at a C/3 rate) to a DoD of 408 Ah. During this time, several minor software problems in the BMS were being evaluated and corrected. At cycles 52 and 53, 6 kW constant power discharges were performed. Cycle 53 was terminated early due to an overtemperature condition in the module. Inspection of the data showed that, while the average module temperature was well within the specified operating limits, the busplates in the module had overheated. The problem was traced to a faulty power supply in the load which oscillated when operated at the high current levels needed for the constant power discharge. The high frequency oscillations caused the busplates to heat more rapidly than individual cell strings, thus causing the overtemperature condition.

Throughout the first 55 cycles, the available capacity of the module was declining and was limited by Bank 2. The rate of capacity loss was a little more than 1 Ah/day. However, due to an oversight in not providing the BMS software with the coding to detect and warn of trends in capacity, this gradual loss in capacity was not observed until cycle 65 where the capacity dropped below the 408 Ah design limit. At cycle 85, the module exhibited a very rapid decline in capacity.

By the beginning of January 1995, the module had completed 114 cycles. Its useable capacity had declined to 353 Ah, well below the rated capacity of 400 Ah. Bank voltage measurements showed that Bank 1, which was the most negative bank, had the lowest capacity, raising concern that it may have been internally shorted. To test for an internal short, the module was discharged until Bank 1 was in the single phase region, where voltage is dependent upon state of charge, and was allowed to stand over a weekend; Bank 1 voltage was continuously monitored over this period. A leakage current of 42 mA was detected and traced to leakage through the power supplies in the module test equipment. One BMS interface board powered each of the four banks and drew a current of 17 mA. Once the power supplies were disconnected, the leakage current stopped. These current levels were sufficient to account for more than 1 Ah/day loss in module capacity.

The banks were individually charged at low currents through the bank voltage sense leads, and another series of tests was performed. On cycle 124, the module was again discharged until Bank 1 registered 7.2 V, and the open circuit voltages for all four banks were monitored. Figures 6-10 through 6-13 show the voltages for each bank during discharge and open circuit stand over a weekend. Figure 6-10 shows the occurrence of approximately a 1 A step in Bank 1. This step in the voltage curve corresponded to a 6 W load on the bank and was a strong indication that something was happening within Bank 1. Figures 6-11, 6-12, and 6-13 show the voltage curves for Banks 2, 3, and 4, respectively, over the same time period. It is obvious that whatever happened in Bank 1 during this open circuit stand was isolated to Bank 1 and did not affect the other three banks.

The capacity of the module fluctuated with continued testing but with a less steep rate of decline. The capacity for cycles 124 through 133 is shown in Table 6-2. Testing of the module was finally terminated on February 20, 1995, after 133 electrical cycles when the capacity declined to 296 Ah. The decision to terminate testing was based on concerns that, with as many as 23 strings having had failed in Bank 1, there was a probability that additional cell failures could easily result in one of the strings having four failed cells. Such a condition could result in the bank becoming short circuited. The module was then cooled and returned to Silent Power for post test analysis.

Because of the premature failure of the module, only two of the four test objectives were accomplished; these being the confirmation of the electrical performance ratings and experience having been gained with the integrated BMS.

6.4 Post Test Analysis

In order try to ascertain the cause of the early failure of the deliverable module, it was subjected to a detailed post test analysis. Prior to dismantling the module, the heaters and thermocouples were tested for continuity. No open circuits were discovered. Tests were also performed to determine whether there were any shorts between the bankplates and thermocouples or heaters. None were found.

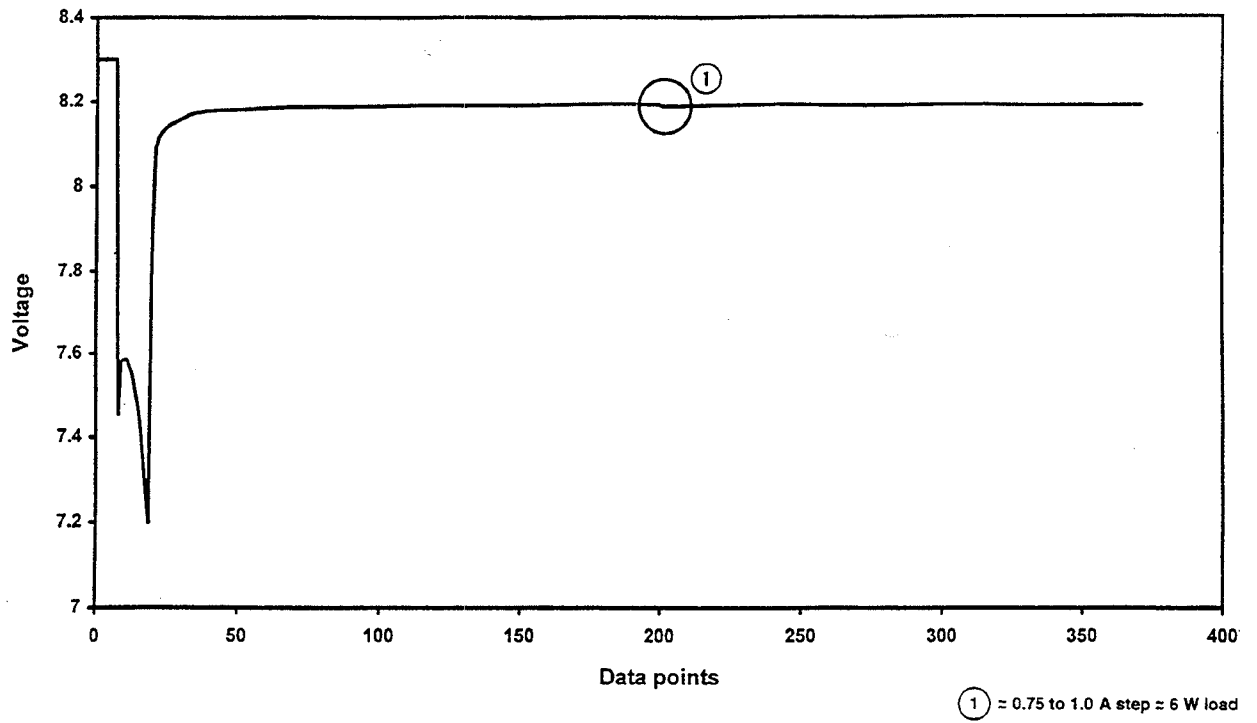


Figure 6-10. Cycle 124 Discharge and Hold, Bank 1 Open Circuit Voltage Monitor

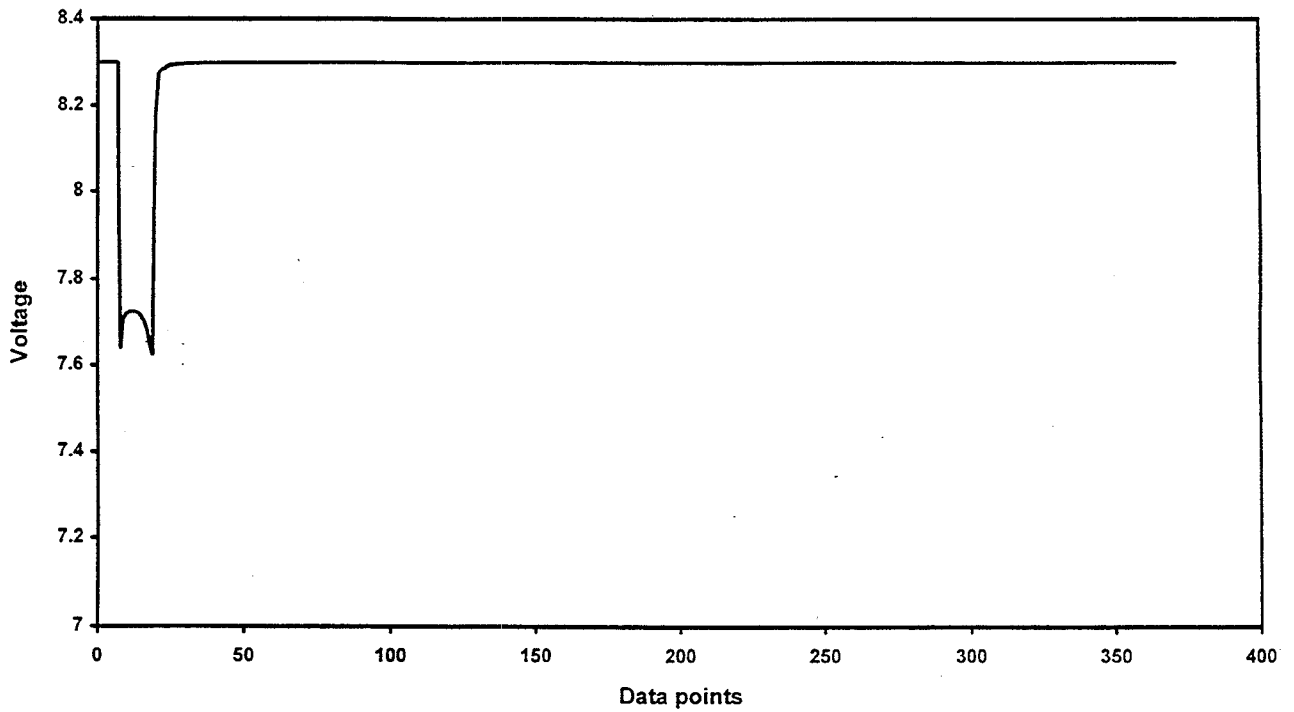


Figure 6-11. Cycle 124, Bank 2 Open Circuit Voltage Monitor

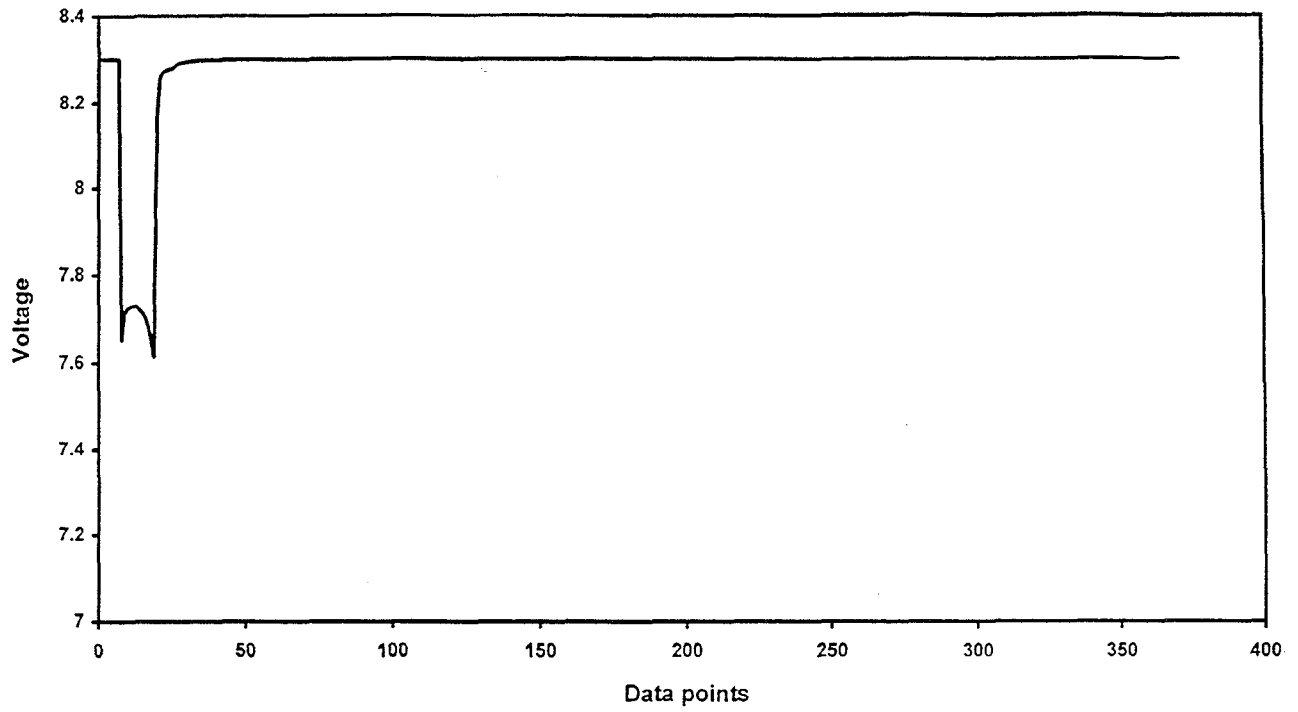


Figure 6-12. Cycle 124, Bank 3 Open Circuit Voltage Monitor

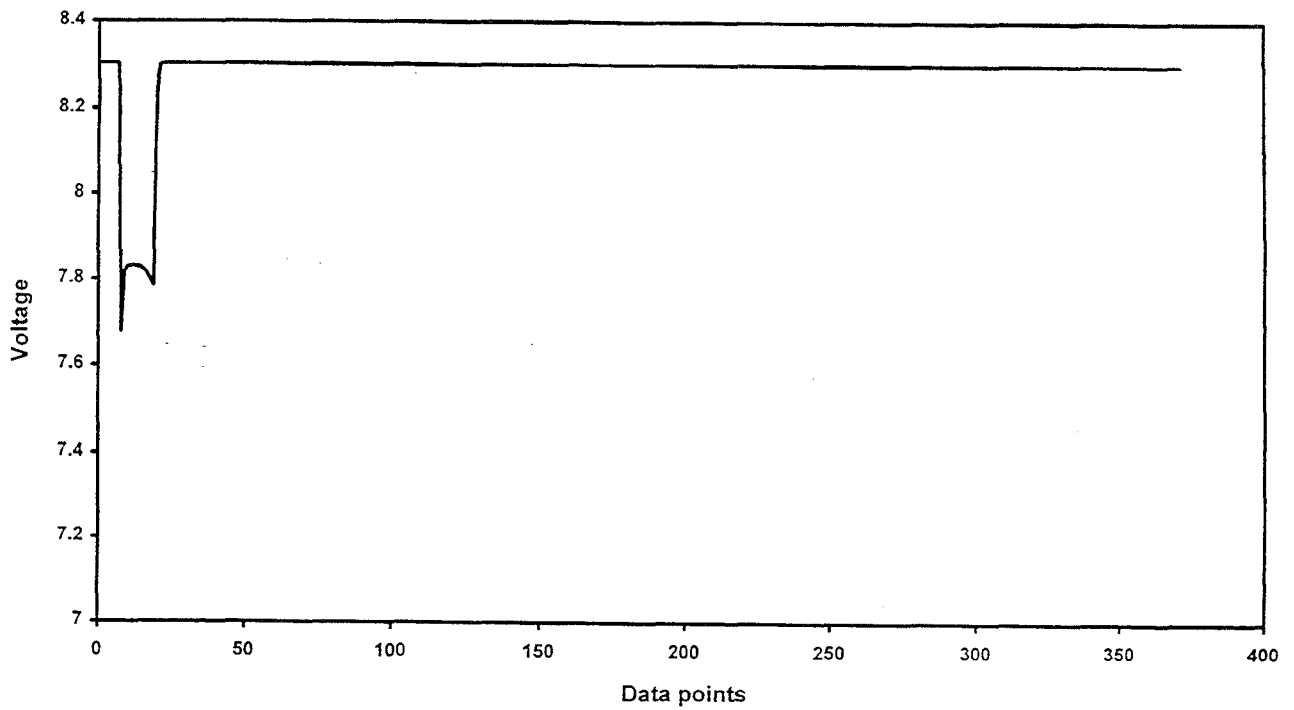


Figure 6-13. Cycle 124, Bank 4 Open Circuit Voltage Monitor

**Table 6-2. Available Module Capacity Toward the EoL
for the Deliverable 13kWh Module**

Cycle Number	Available Capacity (Ah)
124	327
125	298
126	307
127	313
128	292
129	298
130	294
131	299
132	295
133	296

The instrumentation and heater lead wires were then cut, and the outer enclosure was removed. As shown in Figure 6-14, the inside surface of the mild steel enclosure was covered with a superficial layer of rust which had bonded the outer insulating blanket to the enclosure. This was a further indication that a substantial amount of water was driven out of the Aremco cement during heat-up and early testing.

The wiring board and wiring on the top of the banks were examined for any evidence of damage which could have indicated the presence of intermittent short circuits. None were found. The remaining layers of insulation, as well as the side and top heaters, were carefully removed and examined for any evidence of foreign material. There was no evidence that any major cell breaches had occurred based on the appearance of the insulation.

Once all of the overlying layers of insulation were removed, the exposed surfaces of the banks were examined. The appearance of the banks was very good. As shown in Figure 6-15, for example, none of the cement coating on the cell strings had spalled from the strings, and in fact, relatively little cracking of the coating was evident. However, the adhesion of the coating to the cell strings was not particularly good, and, with only moderate effort, large pieces of the coating could be removed.



Figure 6- 14. PTA of Deliverable 13kWh Module Showing a Layer of Rust on the inside Surface of the Enclosure

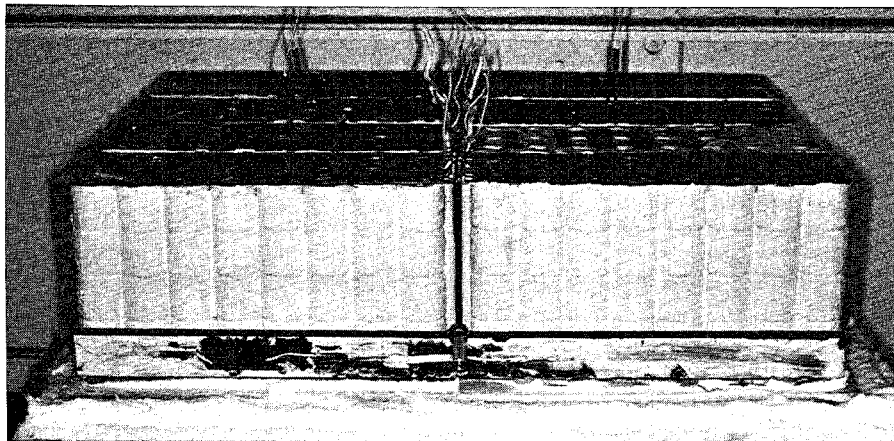


Figure 6-15. PTA of the Deliverable 13kWh Module Showing the Clean Appearance of the Top of the Banks

The spot welds of the busplates to the adjoining bankplates were drilled, and the banks were then removed. The appearance of the cement on the remaining surfaces of the banks was the same as on the outer surfaces. The tabs joining the cell strings to the bankplates were cut, and the cell strings and TES capsules carefully removed. As they were removed, all of the cell strings were labeled with their location in the banks, and they were examined for any evidence of container breach. One cell exhibited a minor amount of leakage of sodium through the TCB seal, but no other container breaches had occurred. Because the module had been at temperature for such a short period of time, the lack of breaches caused by corrosion of containers even in failed cells was not too surprising. Further, as the cell strings and TES capsules were being removed, an examination was made for any evidence of shorting. Again, none was found.

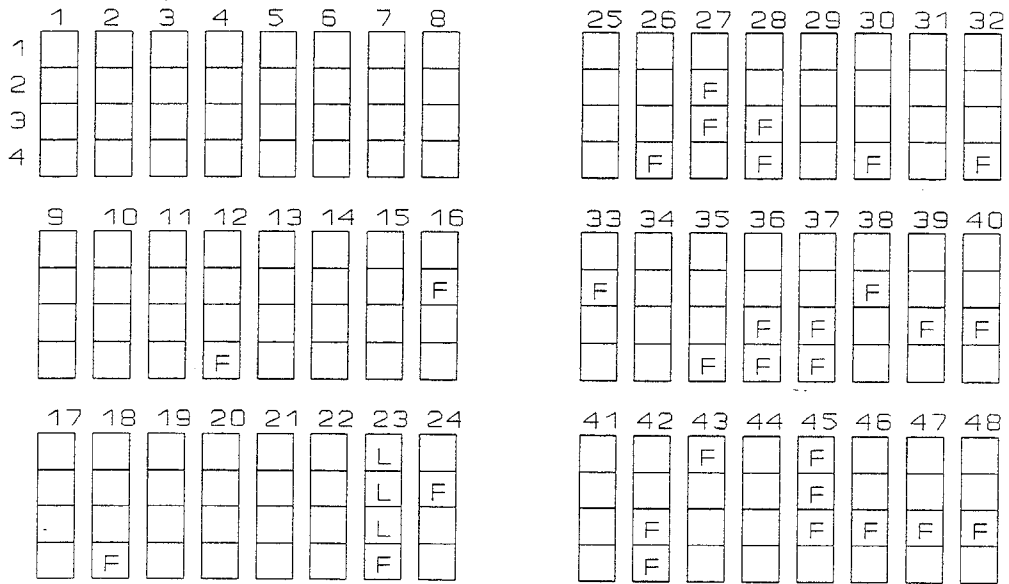
The strings were radiographed and the sodium levels within the safety tubes measured on the radiographs. When cells fail due to fracture of the electrolyte, there is usually no sodium remaining in the safety can. When cells do not fully recharge, the sodium level within the safety can is lower than in surrounding cells. Those cells with low sodium levels or with no sodium visible on the radiographs were considered to have failed. The locations of the failed cells in the four banks are denoted by the letter "F" in Figures 6-16 through 6-19, while those with low sodium are denoted by the letter "L".

The number of failed strings and cells by bank, half bank, and cell manufacturing lot number are tabulated in Table 6-3. From these data, several things are immediately apparent. The variation from one cell manufacturing lot to another is large. The percentage of failed strings from cell lot # 2684 was 60.4% compared to 24.0% in lot # 2691, and 6.25% failed strings in lot # 2707. However, if grouped by bank number, the number of string failures decreases from 23 in Bank 1, which was the most negative bank, to three in Bank 4, which was the most positive; there were 16 and 13 string failures, respectively, in Banks 2 and 3. Whether the rate of string failure within the four banks was influenced by their position in the module cannot be fully determined based on the data from this module alone, and no hypothesis has been advanced to explain this observation. Further, consideration of the distribution of failures among the half banks comprising Banks 1 and 2 would suggest that lot-to-lot variations of cell quality were more likely responsible. Personnel at SPL were contacted to determine if any manufacturing or test data were available which would support the assumption that variations in cell quality was a major factor. The quality control records at SPL showed that all three lots were within specifications. A random sampling of failed cells from each manufacturing lot were sectioned and examined, but no notable trends were observed.

Considering only those cells which failed with ceramic fractures, another observation illustrated in Figures 6-16 through 6-19 is the distribution of locations of failed cells within the strings. The numbers of failed cells by string position were 20 bottom cells, 23 second from the bottom, 10 third from the bottom, and five at the top. It has been suggested that, because the half banks were again dipped in the aqueous based cement after assembly and dried standing upright, the lower cells in the strings may have experienced lower resistance short circuits for a longer period of time due to slumping of the cement slurry. Also, the short circuits could have damaged the cells' electrolytes; this may have caused their failure at a later time. Before the cement is fully cured and dried, it is somewhat conductive. Brief experiments have shown that the resistance of the cement between a cell and a TES capsule is as low as 620 Ω at room temperature. Upon heating to dry and cure the cement, its resistance first rose and then fell to 1000 Ω at 300°C. With additional time at temperature, the resistance increased further as the cement cured and dried. More experiments are required to fully ascertain whether the use of the cement and the resultant temporary, soft short circuits of the cells is detrimental to cell and module/battery life.

There were two cell strings within the module in which the sodium level in all four cells was low relative to those in neighboring strings. A likely explanation for the low sodium level in all strings is that one or more cells in the string had a sulfur electrode which polarized badly during recharge, thus preventing the string from coming to the top of charge.

BANK 1



HALF BANK 3
 CELL LOT 2691
 5 STRING FAILURES
 6 CELL FAILURES

HALF BANK 9
 CELL LOT 2684
 18 STRING FAILURES
 25 CELL FAILURES

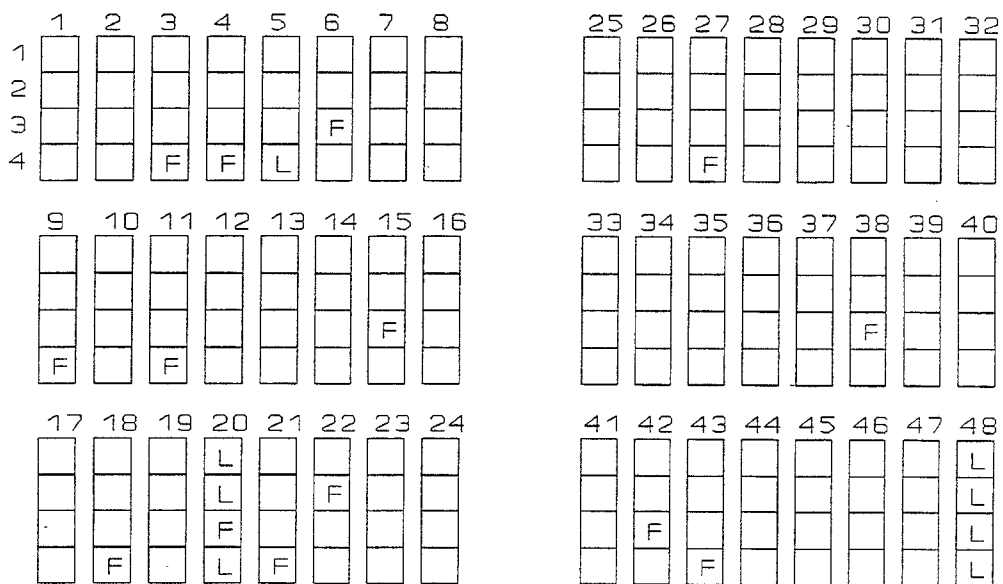
KEY

F - Failed Cell

L - Low Level of Sodium in Safety Can

Figure 6-16. Deliverable 13kWh Module: Distribution of Failed Cells in Bank 1

BANK 2



HALF BANK 10
CELL LOT 2684
11 STRING FAILURES
11 CELL FAILURES

HALF BANK 7
CELL LOT 2691
5 STRING FAILURES
4 CELL FAILURES

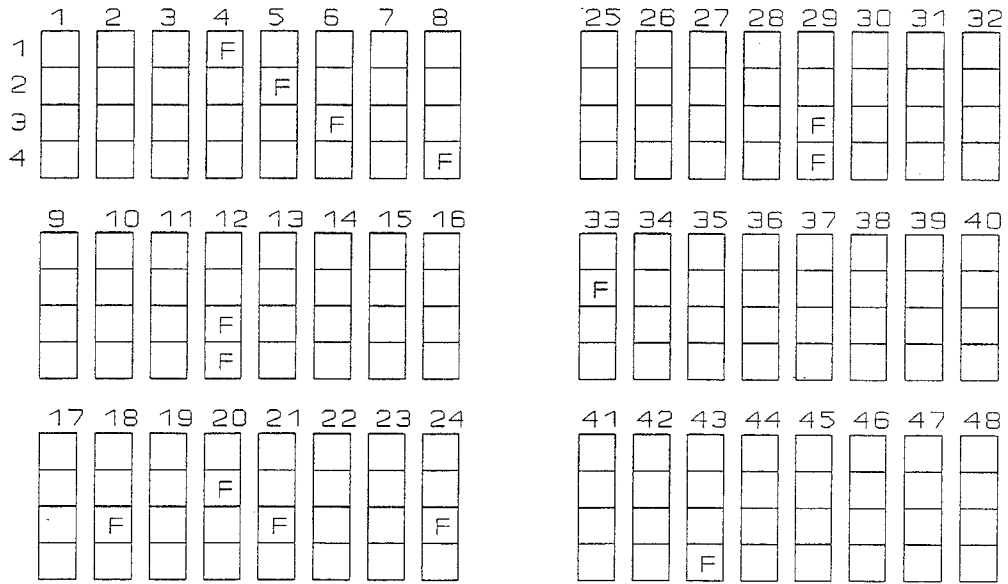
KEY

F - Failed Cell

L - Low Level of Sodium in Safety Can

Figure 6-17. Deliverable 13kWh Module: Distribution of Failed Cells in Bank 2

BANK 3



HALF BANK 2
 CELL LOT 2691
 9 STRING FAILURES
 10 CELL FAILURES

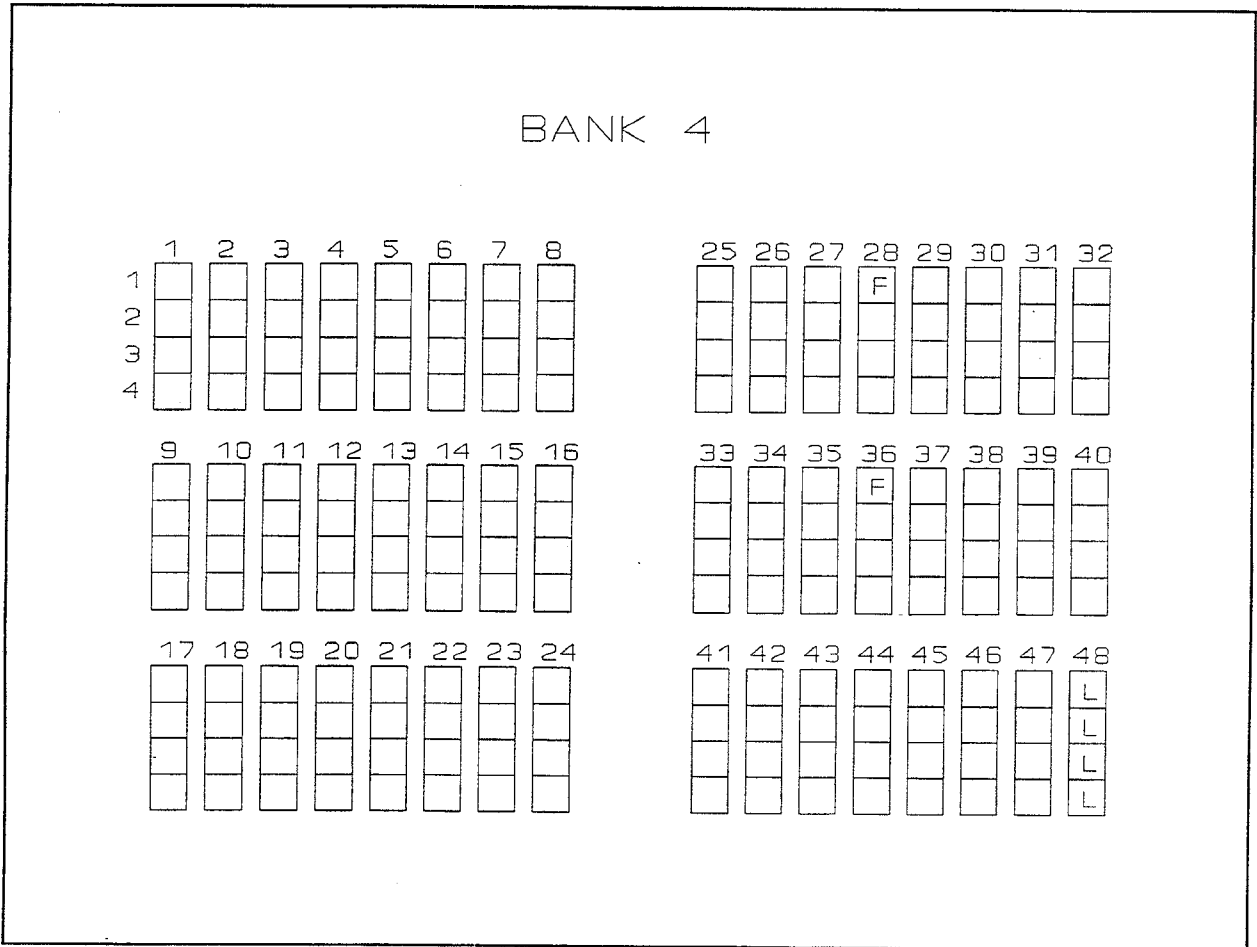
HALF BANK 8
 CELL LOT 2691
 4 STRING FAILURES
 5 CELL FAILURES

KEY

F - Failed Cell

L - Low Level of Sodium in Safety Can

Figure 6-18. Deliverable 13kWh Module: Distribution of Failed Cells in Bank 3



HALF BANK 5
CELL LOT 2707
NO STRING FAILURES
NO CELL FAILURES

HALF BANK 6
CELL LOT 2707
3 STRING FAILURES
2 CELL FAILURES

KEY

F - Failed Cell

L - Low Level of Sodium in Safety Can

Figure 6-19. Deliverable 13kWh Module: Distribution of Failed Cells in Bank 4

Table 6-3. Failed Cell Distribution in the Deliverable 13kWh Module

Bank ID	Half Bank ID	Cell Lot #	# of Failed Strings	# of Failed Cells
1	3	2691	5	6
	9	2684	18	25
2	10	2684	11	11
	7	2691	58	4
3	2	2691	9	10
	8	2691	4	5
4	5	2707	0	0
	6	2707	3	2

It appears that the early failure of the module was a result of a high rate of failures of cells in a single manufacturing lot (lot # 2684). However, the manner in which the module was fabricated may have had a significant influence on the life of the module as well.

VII. HARDWARE DEVELOPMENT SUMMARY AND RECOMMENDATIONS FOR FUTURE WORK

7.1 Cell Development

Overall, the results of the central sulfur (c/S) cell development effort were favorable and represented significant advances in the technology. A c/S cell was chosen for development to meet UES applications requirements of long life, moderate capacity and power, and potential for low manufacturing cost when fully developed. In order to show technical feasibility of c/S cells, freeze/thaw durability, cell safety, and performance reliability had to be demonstrated. These objectives were satisfactorily accomplished, though a number of issues remain to be resolved before the cell is ready for commercial production.

The cell development task started with the preliminary cell design which was loosely based on a c/S cell that had been developed at SPL in the early 1980's. This cell, designated the Technology Demonstration or TD cell, exhibited life times greater than 8 years. The major differences between the preliminary c/S design and the TD design were the configuration of the electrode seals and the sodium reservoir. Both changes were introduced to reduce the eventual manufacturing cost of the cell and its volume. Over the course of the program, a number of component design changes were incorporated into and tested in the preliminary design; more than 145 of these cells were fabricated and tested. A large part of the development effort was devoted to developing a sodium electrode seal which was not susceptible to environment assisted cracking during thermal cycling. Several current collector coating materials were evaluated in an effort to find a non-chromium bearing material which would perform at least as well as nichrome. Other developments were improved safety features and an improved method for filling cells with sodium. At the end of the cell component development effort, the best component designs and materials were incorporated into the prototype design for fabrication and testing of a number of nearly identical cells.

Fabrication of 125 prototype cells was attempted. Of these, 25 failed at various points during the build process, and 55 of the cells that were placed on test failed as a result of latent manufacturing defects. Of the combined build and latent defect failures, 35 were associated with sodium electrode seals and 37 were associated with sulfur compartment final closure welds. Forty-five prototype cells were tested for freeze/thaw durability, safety, and early life performance.

The freeze/thaw durability of the prototype cells far exceeded the goal established at the beginning of the program. This goal was to have no cell failures – either due to fracture of the electrolyte or breaching of the electrode seals – in a population of 10 cells exposed to 10 freeze/thaw cycles; the freeze/thaw cycling was to be performed at top-of-charge. In the group of ten prototype cells tested, all ten survived a minimum of ten thermal cycles without failure. In fact, throughout the program, no cells failed during freeze/thaw cycling as a result of electrolyte fracture. Several cells were also subjected to a number of freeze/thaw cycles when fully discharged without failure. No goal had been set for this test condition.

The prototype c/S cell did not fully meet the goal established for safety. The goal was that no cells in a population of 10 would breach – either its container or electrode seals – when failed by inducing fracture of the electrolyte by overvoltage; furthermore, the maximum temperature of the failed cell had to remain below 500°C. Fifteen prototype cells were safety tested, and, of these, only one breached its container. However, three of the prototype cells exhibited temperature excursions over 500°C following failure.

The 20 remaining prototype cells were electrically cycled to evaluate their early life performance. At the close of the program, eleven cells had completed over 200 cycles and their performance had stabilized. Most of the cells required between 50 and 100 cycles before their resistance and rechargeability stabilized. The resistance of many of the cells was over 30 mΩ at the beginning of test. After break-in, the average resistance of an eleven cell sample was 13.2 ± 2.3 mΩ compared to the design goal of 12 to 13 mΩ. The rechargeability of the cells was generally good during the first few cycles, with average f_1 values of $8.7 \pm 2.2\%$ of theoretical capacity.

Clearly, more work needs to be done to optimize the cell design and fabrication processes in order to attain acceptably low manufacturing costs and to raise the quality of the cells to a point where they can be used with confidence in utility batteries. If at some time in the future the decision is made to commercialize batteries with c/S cells, a number of cell issues need to be resolved. Among the most important of these are: TCB seals, final sulfur compartment closure welds, cell safety, cell life, and freeze/thaw durability.

Though good progress was made with regard to making reliable sodium electrode TCB seals, further work is required to reduce the number of manufacturing and latent defect failures. Most of the seal failures encountered during the prototype build appeared to be due to fracture of the alpha-alumina header which occurred during the bonding operation or as a result of stresses induced during cool-down. One possible area for improvement is elimination of microcracks in the alumina ceramic caused by diamond grinding. If ceramic components could be used in the as-fired condition, the population of microcracks would be much reduced. The elimination of diamond grinding would also result in a substantial cost reduction. By optimizing the bonding process and component design to minimize the stresses induced in the ceramic, further improvement in yields and reliability should be attainable. With regard to the sodium seals, the issue of seal calendar life remains to be addressed. This will require extensive long term testing and, possibly, development of alternate sealing alloys if the present materials prove deficient.

Another area requiring development is the elimination of cracking in the final closure welds. Improvements in yield should be attainable by redesigning the weldments so that the graphite foil shields can be installed without contaminating the weldments. Further attention should also be given to the choice of the aluminum alloys used. Less cracking occurs in welds 5086 and 6061 alloys than in welds of 6061 to itself.

Additional improvement is required in the area of cell safety. This can be accomplished by more tightly controlling the width of the annulus between the electrolyte and safety tube. Better alignment of the safety tube with the electrolyte during seal bonding will reduce the

variability in the annulus's width. Tightening the tolerances on the outside diameter of the electrolyte and better controlling the bulge on the closed end will reduce the annulus width variability as well and will also allow a small diameter safety tube to be used. Tighter electrolyte tolerances can obviously be attained by rejecting more components which will result in higher electrolyte costs. Alternatively, it may be possible to effect some reduction in closed end bulging by altering the manner in which the electrolytes are set during firing.

Cell life was not included as a task under the current program. Since the duration of the program was significantly shorter than the cell life required to achieve a battery life of five years, satisfaction of a cell life goal could not be determined by program's end. Furthermore, cell life was being addressed on other Silent Power programs, and the demonstrated life of the TD cell provided confidence that the necessary cell life could be obtained. Even though container corrosion is not a major concern in c/S cells, resistance rise and capacity loss as cell failure mechanisms remain unresolved and still require attention.

The freeze/thaw performance of the prototype cells far exceeded expectations, but it must be noted that the reasons for the successful freeze/thaw results are not fully understood and may be highly dependant on specific cell design details. Assuming this may be case, a further understanding of the mechanisms governing freeze/thaw durability needs to be established. Further, if freeze/thaw survivability is design dependant, the boundaries of the design envelope within which freeze/thaw survival is assured need to be firmly established.

7.2 Deliverable Module

To demonstrate a number of design features in a battery intended to specifically meet UES requirements, a 13 kWh module was designed, fabricated, and delivered to SNL for testing. Incorporated into the deliverable module were: 1) TES capsules filled with a salt mixture with a melting point near the upper operating temperature limit of the module; 2) conventional insulation combined with a single skin enclosure for low cost, maintenance free, and reliable thermal management; 3) a magnesia/sodium silicate cement applied to cell strings and TES capsules to provide for electrical isolation, improved heat transport, and the mechanical rigidity of the banks; and, 4) an integrated BMS which controlled module temperatures, monitored module performance, and protected the module from abuse by the power converter system.

After several break-in cycles, the module internal resistance stabilized at 13.1 m Ω , which was in good agreement with the 12.9 m Ω predicted. During the first 44 constant current discharge cycles at C/3 to 100% of the module's rated capacity (408 Ah), the available module capacity (rated capacity plus reserve capacity) stabilized at 460 Ah. This was consistent with having no more than two failed strings in any one bank in the module. Following shipment to Sandia, there was no indication that any additional string failures had occurred during heat-up and break-in. After a few minor BMS software problems were

corrected, the module performed as expected. The module was unable to deliver its rated capacity of 408 Ah after 65 cycles. After five months on test and 133 cycles, the module capacity had declined to 296 Ah, so testing was discontinued.

A post test analysis of the module showed that the rapid loss of capacity was mainly due to a high number of failed strings comprised of cells from a single manufacturing lot. The rate at which the module capacity declined was aggravated by the fact that cells from the three manufacturing lots were not uniformly distributed throughout the module. Had this been done, the life of the module, defined as the point at which the module was no longer able to deliver the rated capacity of 400 Ah, would have been somewhat longer. During cycle 53, the failure of one of the power supplies in the load being used to test the module failed, causing high frequency oscillations to be fed back into the module. The only observed result of this was a rise in the temperature of the busplates which caused the BMS to terminate the test. It was speculated that the incident may have damaged cells, thereby initiating the rapid loss of cells and attendant module capacity loss.

The use of a MgO cement to provide electrical isolation between cell strings and TES capsules proved to be effective, though its use did create several minor problems during assembly and initial module operation. The cement was applied to the cell strings by dipping, which resulted in excessive thickness; this, in turn, necessitated removal of $\frac{1}{3}$ of the TES capsules. Through development of suitable spraying techniques for coating the strings, the thickness can be made more uniform and better control over the battery core dimensions maintained. There were also concerns that temporary short circuiting of the banks by the uncured cement may have contributed to the module's early string failures. To ascertain the extent of this problem, a number of well-controlled experiments need to be performed to compare the performance of otherwise identical modules with and without cement. Further, performing an in situ final cure of the cement appeared to be ill advised. While doing so reduced the number of thermal cycles which the cells underwent during assembly, it caused the cement to remain wet and conductive for a longer period of time and may have had a deleterious effect on the module.

Throughout most of the testing, the BMS performed as expected. It exhibited some erratic behavior at the beginning of the testing which was eventually traced to condensation of water within the module/BMS interface boxes mounted on the surface of the module. Eliminating the in situ curing of the cement in future modules and batteries would eliminate the condensation problem. The BMS had not been initially programmed to report any change in module capacity until it dropped below the rated capacity. Incorporating the change was simple and was useful for the diagnostic testing being performed at Sandia, the software modification would probably have limited value in an actual field application.

Because of the shortened availability of the deliverable module, the capability of the proposed battery design to satisfy the UES load profiles identified as being ideally suited for sodium sulfur was not demonstrated. Furthermore, the planned life assessment under a peak shaving regime could not be undertaken.

REFERENCES

1. "Sodium Sulfur Battery Development, Final Report, 1985 - 1990", SNL/DOE Contract No. 48-8837, prepared by Silent Power, Ltd., Runcorn, England.
2. "Sodium/Sulfur Battery Development – Commercialization Planning", Final Report, prepared by Chloride Silent Power, Ltd, Wayne, Pennsylvania, EPRI Report No. GS-7184, Project No. 2123-4, March 1991.
3. Butler, P., "Battery Energy Storage for Utility Applications: Phase 1 – Opportunities Analysis", Sandia Report SAND94 - 2605, October 1994.
4. Akhil, A., et al, "Battery Energy Storage: A Preliminary Assessment of National Benefits (The Gateway Study)", Sandia Report, SAND93 - 3900, December 1993.

ACKNOWLEDGMENTS

Silent Power, Inc. (SPI) would like to thank the DoE/OUT and, in particular, Dr. Russ Eaton, for their friendship, support and confidence in Silent Power through the years. Also, Silent Power would like to acknowledge the technical help and direction provided by Sandia National Laboratories that has even preceded the start of the *Sodium Sulfur Battery Engineering for Stationary Energy Storage* Program; appreciation is extended to Paul Butler, Abbas Akhil, Rudy Jungst, Jim Freese, and Terry Unkelhaeuser. Sandia's support in the area of the Opportunities and Applications Assessment was especially invaluable in the implementation of the Program. Also, Silent Power appreciates the efforts of the Sandia Test Team in living with and working out the bugs in the deliverable module. Silent Power owes a special thanks to Jeffrey Braithwaite, who was the Sandia Project Manager, for the technical direction that he provided as well as his supportive overseeing of the Program.

Also, Silent Power wants to acknowledge the support provided by the Sandia consultants in the area Applications Assessment; this includes Energetics, Rajat Sen and Associates and Switch Technologies.

Finally, the authors would like to thank their respective organizations, people who worked hard to produce the best that was possible:

In Valley Forge (Engineering Design and Program Management):

Bill Auxer (SPI President) for his wisdom and guidance and willingness to provide the interface to England and Germany along with the necessary frequent travel;

Judi Dilworth (Office Manager) for her diligence in handling all of the reporting in addition to all of our business needs;

Gary Smith (Engineering Design) who was responsible for the deliverable battery design and build activity;

George Chambers (Subcontract Design), who succeeded Gary, and handled the design of the NaS-P_{AC} system;

Don Dale (Subcontract EE) who applied his experience to the NaS-P_{AC} system electrical design and thermal mockup.

In Salt Lake City (Cell and Battery Development and Test):

Hal Maughan (Finance Manager) for his expertise in implementing policy and benefits, in addition to establishing good business accounting practices;

Stephanie Collinsworth (Office Manager) for her friendly demeanor while providing a number of functions including reception, secretarial, procurement and health and safety;

Scott Olsen (Test Manager) for his all around electronics expertise which was applied not only to testing, but also to developing the entire battery management system for the deliverable battery;

Dan Lustig (Test Technician) for his responsible test and electrical support;

Dave Carmen (Mechanical Engineer) for his part on the cell assembly team, which included sealing and welding, for his engineering design support and playing a key role in some of the unique battery development activities;

Linda Hatch (Manufacturing) for her major role on the cell manufacturing team, materials receiving and preparation, glazing, sulfur electrode fabrication and sodium filling operations, as well as cell matrix cementing;

Neill Weber (the Father of Sodium Sulfur, alias Shivas Irons) for his important contributions to cell development including sealing and chemical corrosion protection expertise;

Chad Tanner (Technician) for his resourcefulness in helping to assemble the deliverable battery, in addition to his normal maintenance tasks.

THANKS

Albert Koenig - Program Manager

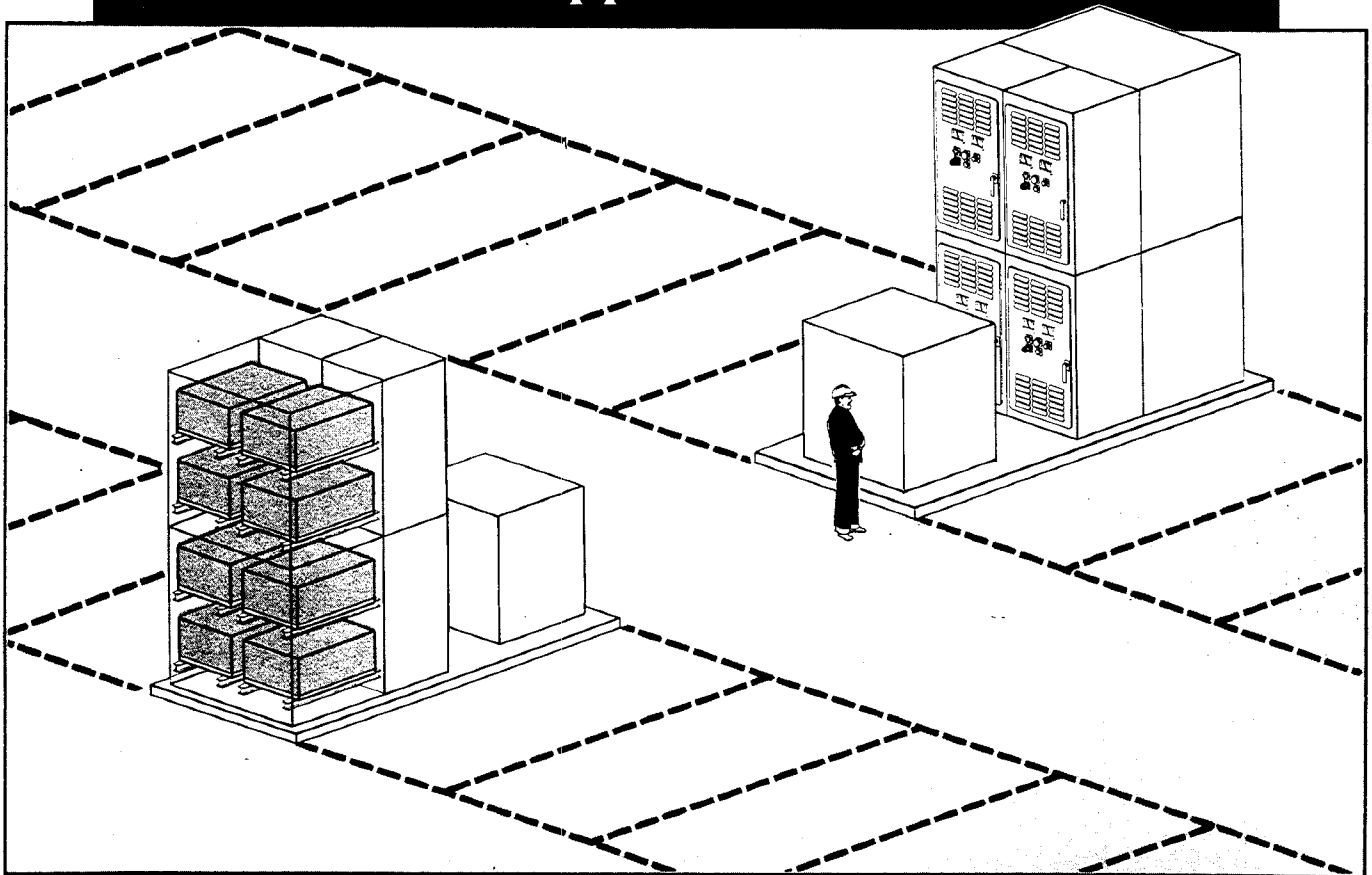
Jim Rasmussen - Component Development Task Leader

APPENDIX A

**Sodium Sulfur AC Unit Battery
for Utility Energy Storage Applications
Brochure**

November 1991

A Sodium Sulfur AC Unit Battery for Utility Energy Storage Applications



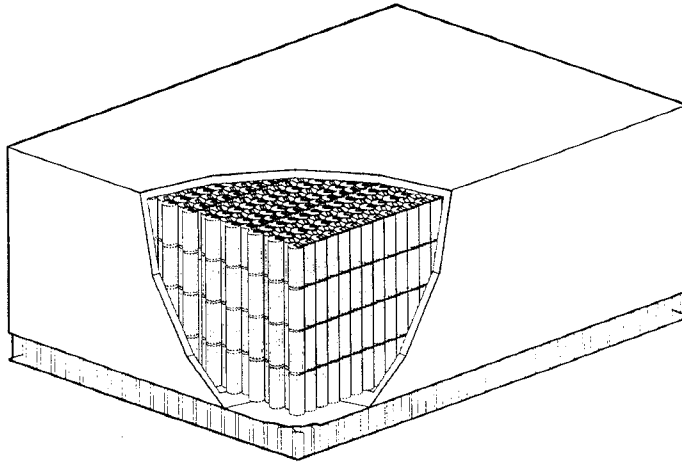
1000 kWh Sodium Sulfur AC Battery Stacked Installation

Why an Advanced Battery . . . like Sodium Sulfur?

- 1000 kWh AC Battery in a Single Truck Haul
(2-500 kWh AC Units)
- Dual Cycle Capability: Shallow and Deep Discharge
to Meet Your Specific Application
- The Potential for a Low Life Cycle Cost:
 - 2-Year Maintenance Free Installation Initially
 - Projected 8-Year Life
- Projected Competitive First Cost of \$500/kWh (AC Unit)
- Lower Footprint: 1/4 that of Lead Acid Battery Plants

**BETA
POWER**

Battery Module Specifications



Battery Module

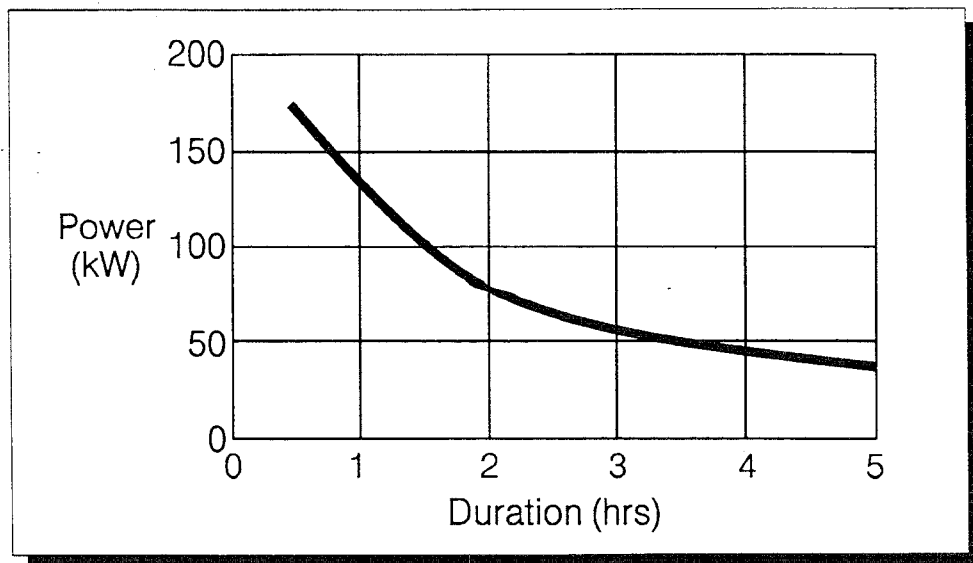
- 150 kWh
- 200 VDC (nom)
- Voltage Range: 240-170 VDC (full charge-discharge @ C/2)
- Dimensions: 3.50' x 5.00' x 2.00'

Weight: 4500 lbs.

Maintenance Free

No Self Discharge

Battery Module Rated Power Response Under Steady Load



CASE 1:

Battery Application Study

Puerto Rico Electric Power Authority Project

- **Type of UES Application:** - Frequency Control
- Voltage Stabilization
- Alternate Spinning Reserve
- **Requirements:** - Battery Rated Energy: 14 MWh
- Total Energy Throughput/Day is 2.5 x Rated Energy

Frequency Regulation: 7500 hours/year (equal charge/discharge)

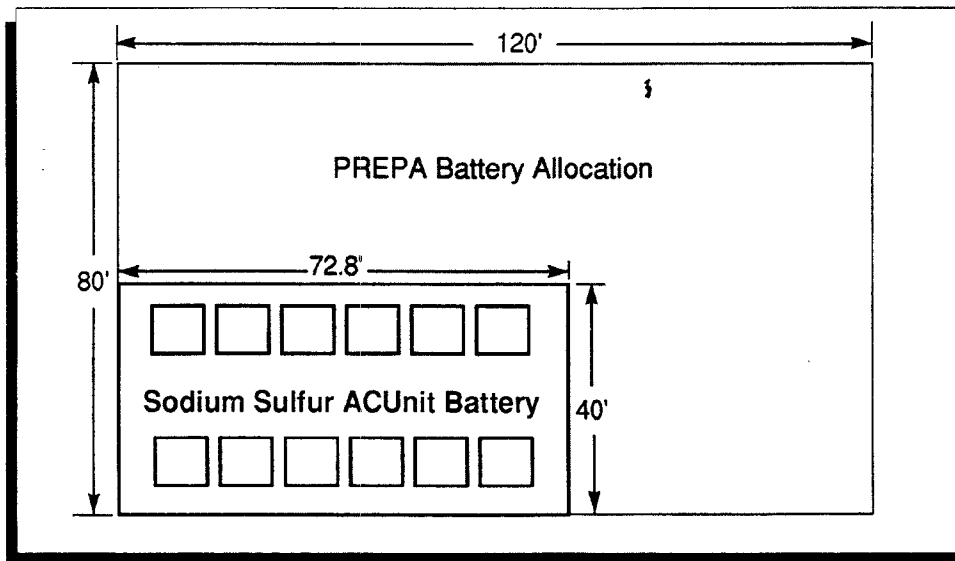
FR Schedule:	Power Level	% of
	2	82
	6	12
	10	6

Spinning Reserve: Average 55 times/year

SR Schedule:	Power Level	Duration
	20	15
	20-0	15

Sodium Sulfur Battery Plant Layout

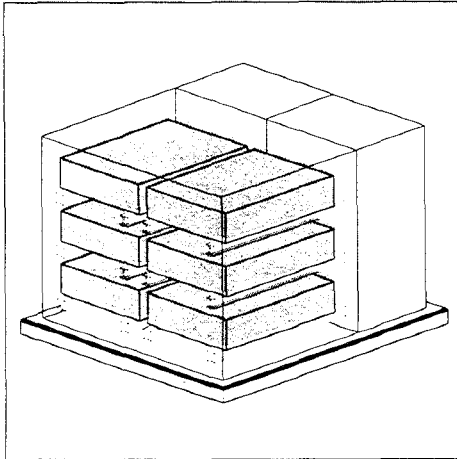
- Employing 12-1000 kWh Stacked ACUnits to provide 14 MWh
- Inverter Rating per ACU: 1700 kW



CASE 2:

Battery Application Study San Diego Trolley Substation

- Type of UES Application: Peaking Demand
- Requirements:
 - 600 VDC (nom)
 - 420 kWh
 - 210 kW (C/2 Rate)
 - 2 high demand periods per day (2 hours @ 7:30 AM and 5:30 PM)



**210 kW Sodium Sulfur AC Unit Battery
for the San Diego Trolley Project**

Sodium Sulfur AC Unit Battery Design

Specifications:

- 1 AC Unit Battery
- 3 Modules (6 half modules)
- 600 VDC (nom)
- Voltage Range: 720-530
- Inverter Rating: 240 kW
- Plan Area: 54 sqft
- Weight: 15,700 lb

Perceived Benefits

- **20% of Lead Acid Battery Weight and Footprint**
- **Initial Cost Projection: 25% of the SDTP Lead Acid Battery System**
- **Maintenance Free Operation over Lifetimes Comparable to the Lead Acid System**

**BETA
POWER**

Beta Power, Inc.
Subsidiary of Chloride Silent Power, Ltd.

489 Devon Park Drive - Suite 315 - Wayne, Pa 19087

APPENDIX B

NaS-P_{AC} Battery Energy Storage
Brochure

November 1994

Silent Power
ENERGY STORAGE TECHNOLOGY



NaS-P_{AC} Battery Energy Storage
the solution to clean, compact, affordable, dedicated power

Silent Power ENERGY STORAGE TECHNOLOGY

NaS-P_{AC} is an acronym for sodium sulfur AC power. It is an advanced battery energy storage (BES) system consisting of three elements: a battery for storing DC energy, a power converter (PCS) for charging the battery from the grid and converting the DC energy in the battery back to AC for use, and a control system which allows power to be dispatched as required depending on battery system status. These elements are integrated into a turnkey product thereby eliminating the expense associated with the "custom" design of most existing BES facilities and minimizing most of the field labor. The system, depending on the needs of the application, is designed around standard 300 kW, line-commutated or self-commutated power converters, which meet IEEE-519 standards for voltage and current harmonic suppression.

The NaS-P_{AC} system is available for continuous duty or pulsed operation. The former includes one and two-hour battery options, while the latter addresses the specific needs of customers demanding power quality superior to what a utility may be able to guarantee. As indicated by the sustained performance curves in Figure 1, the individual batteries are the same in each case, but the number of discrete batteries and the PCS are chosen to meet the needs of the application. The battery is the most unique element of this modular system.

NaS-P_{AC} System Capability
Continuous Duty

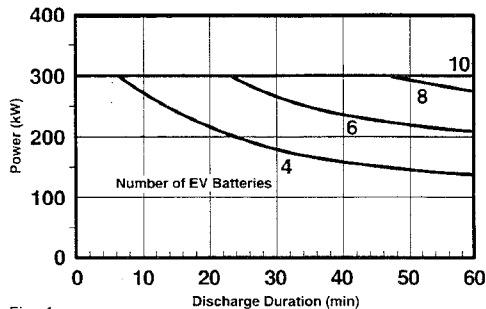


Fig. 1

The NaS-P_{AC} system employs sodium sulfur batteries from Silent Power, Ltd. (See Fig. 2) These batteries are uniquely suited to electric vehicles (EV), in that they pack 3X the energy of lead acid batteries in the same weight or volume. Unlike lead acid, they have excellent deep discharge cycle life. Recent advances in sodium sulfur battery performance have resulted in a battery with twice the power capability to meet the demands of EV acceleration. For BES applications, these characteristics translate to a very compact and efficient (80% at C/1 rate) energy storage system, offering easy transportability and limited portability.

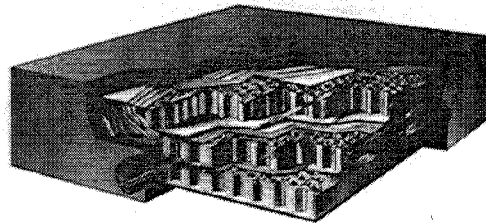


Fig. 2

The sodium sulfur battery operates at high temperatures inside of a thermal enclosure. The temperatures of the outer battery container, however, are only a few degrees above ambient temperature. Unlike lead acid, these batteries operate just as effectively in cold weather as in hot, which allows the system to be deployed conveniently outside. While in use, the battery maintains its own temperature. During long standby periods, typically 1 day, the battery should be plugged-in to automatically maintain temperature through supplemental heat. For BES stationary applications, the user is oblivious to this demand, because the unit is connected to the utility. The heat loss is typically 5W/kWh stored, or the equivalent to 2 light bulbs per EV battery. This is no more of a parasitic than normal self-discharge is to lead acid batteries. There is no self-discharge for sodium sulfur batteries.

NaS-P_{AC} BES Systems Applications

The full range of usefulness for BES systems has yet to be explored. For utilities, BES is intended to off-load some of the centralized peak generation burden on distributed BES systems located close to centers of load growth. In this concept, batteries are charged during off-peak times and are available to be remotely dispatched during peak times. *The major advantages of BES is the ability to be sited anywhere that they are needed to serve. This is power that is environmentally clean and available instantaneously.* The BES system is ideal for renewable generation (wind, photovoltaics, etc.) and as distributed generation stations for opportunity charging of electric vehicles. There is no spin-up time requirement and no maintenance or engineering support is needed to maintain rotating equipment. Instead, batteries are warranted for replacement after five years, as the only scheduled maintenance.

Combined Customer Reliability Peak Shaving

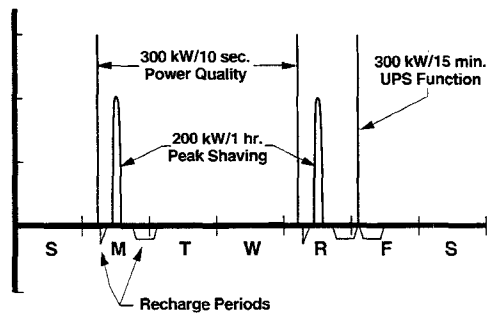
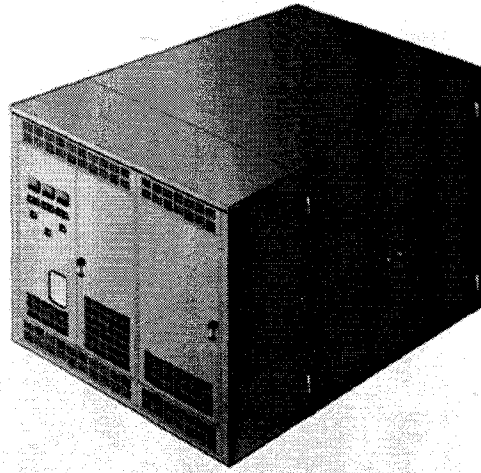


Fig. 3

The most obvious uses for stationary energy storage systems are within utilities and as turnkey packages that utilities might offer to their customers to enhance reliability. Voltage sags, spikes and short outage periods tend to play havoc on sensitive process equipment, such as molding and extrusion lines, causing considerable downtime for industrial customers. The BES system can be designed and connected to insure power quality and, when necessary, provide uninterruptible power



supply (UPS) functions to sustain the line until the fault clears (See Fig. 3). As to whether ownership resides with the utility or the customer, this is left up to the determination of benefits/cost perceived by each party. In addition a BES system provides an opportunity for utility customers to save on demand charges by shaving monthly peaks. In principle, this could return 20-30% on the investment with a 2-3 year pay back, depending on how "peaky" the load is, the serving utility demand charges, and the amount of storage required to insure that the peaks are clipped. The utility could share in the benefit by having the utility dispatch the stored energy at a customer site in anticipation of the utility's peak. This form of demand side management helps the utility to operate more efficiently without necessarily having to shed load. Excellent opportunities exist to reduce demand in diverse applications, from transportation, such as commuter rail services, to the dairy industry's milking schedules. (See Fig. 4)

In some cases, a utility may be able to benefit from the strategic use of BES to defer an upgrade to a transmission line and/or to a distribution substation, mandated by load growth. In this scenario (See Fig. 5), system portability is demonstrated by four NaS-PAC units totalling 1.2 MW contained on two standard trailers at a distribution substation. The power is dispatched during seasonal peaks to prevent load shedding and outages. Afterwards the system

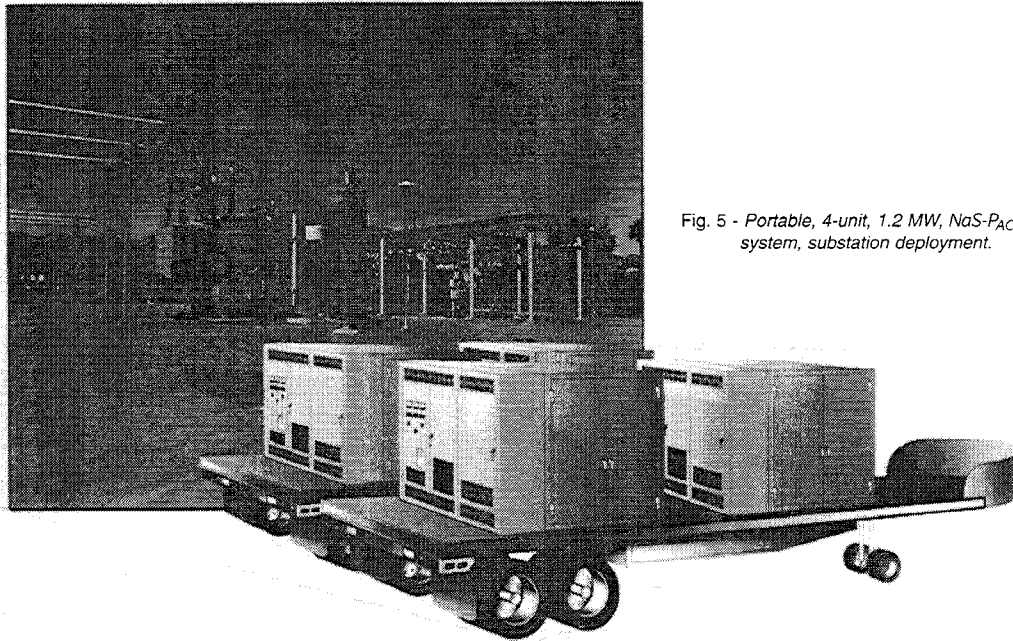


Fig. 5 - Portable, 4-unit, 1.2 MW, NaS-PAC system, substation deployment.

can be transported to other sites to handle specific problems. Certainly the practicality of shipping a NaS-PAC BES system is less burdensome than the transportation of a substation transformer, yet the latter is commonly recognized as a 'band-aid' solution to local utility power problems.

NaS-PAC - Commuter Rail Service Application

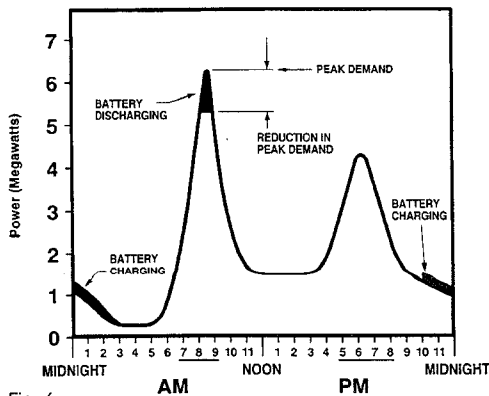
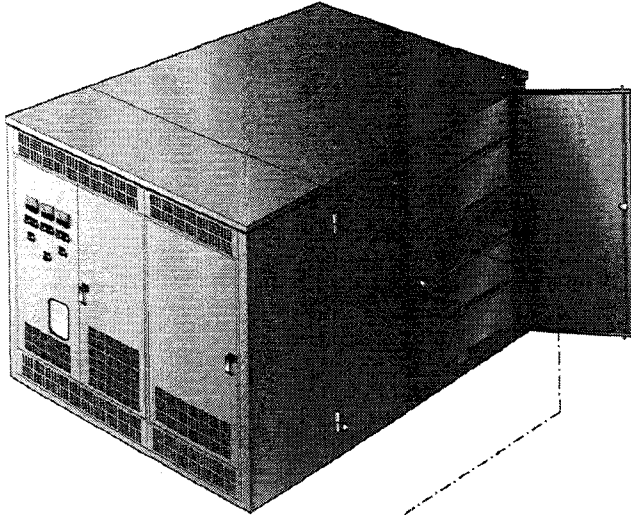


Fig. 4

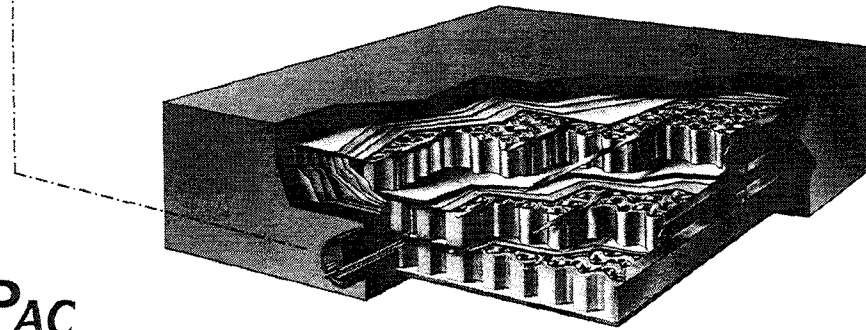
Because of a recent utility outage, a sewage treatment plant was fined heavily by the Environmental Protection Agency for dumping raw sewage into a stream for several hours. This could have been averted by a dedicated BES system without having to resort to the purchase of a diesel generator and its associated service contract. The fine itself would have paid for a NaS-PAC system capable of riding through the outage. Here again is an opportunity for a utility to offer uninterruptible service. With the utilities facing increased competition through deregulation, it seems prudent to improve customer relations through competitive pricing and services. The role that the NaS-PAC BES system can play in providing some of these services is only limited by the knowledge base of utility applications engineers and corporate resource planning personnel. Industry, hospitals, schools, shopping centers and commercial establishments, government offices and military complexes and even residential developments are just some of the practical applications for BES systems serving an extended UPS function.

Silent Power
ENERGY STORAGE TECHNOLOGY

NaS-PAC Modular Battery Energy Storage Unit



- 300 kW, 480 VAC, 3 Phase Power Converter
- Multi-battery Options for Pulsed and Continuous 1-2 Hour Operation
- Pad Mounted and Ready to Use
- Dimensions: 7'W x 7.5'H x 8'D
- Weight: 16,000 lbs.



- 40 kWh, 240-320 VDC
- Sodium Sulfur Technology from Silent Power, Ltd.
- Sealed
- No Maintenance
- Self Contained Electrical and Thermal Management

NaS-PAC Replaceable Battery Pack

For more information, please contact
our Battery Applications Manager.

Silent Power
ENERGY STORAGE TECHNOLOGY

Silent Power, Inc.
Subsidiary of Silent Power GmbH

Wayne, PA (610) 341-9205
(610) 341-9206 FAX

Salt Lake City, UT (801) 486-5071
(801) 486-5075 FAX

Distribution

ABB Power T&D Co., Inc.
Attn: P. Danfors
16250 West Glendale Drive
New Berlin, WI 53151

ABB Power T&D Co., Inc.
Attn: H. Weinrich
1100 Cornwall Road
Monmouth Junction, NJ 08852

Argonne National Laboratories
Attn: G. Henriksen
CTD, Building 205
9700 South Cass Avenue
Argonne, IL 60439

AT&T Energy Systems
Attn: K. Bullock
3000 Skyline Drive
Mesquite, TX 75149

Bechtel
Attn: W. Stolte
P.O. Box 193965
San Francisco, CA 94119-3965

C&D Charter Power Systems, Inc.
Attn: S. Misra
3043 Walton Road
P.O. Box 239
Plymouth Meeting, PA 19462-0239

California State Air Resources Board
Attn: J. Holmes
Research Division
P.O. Box 2815
Sacramento, CA 95812

Corn Belt Electric Cooperative
Attn: R. Stack
P.O. Box 816
Bloomington, IL 61702

Electric Power Research Institute
Attn: S. Eckroad
3412 Hillview Avenue
P. O. Box 10412
Palo Alto, CA 94303

Electrochemical Consultants, Inc.
Attn: P. Symons
1295 Kelly Park Circle
Morgan Hill, CA 95037

Energetics, Inc.
Attn: H. Lowitt
7164 Columbia Gateway Drive
Columbia, MD 21046

Energetics, Inc.
Attn: P. Taylor
7164 Columbia Gateway Drive
Columbia, MD 21046

Exxon Research Company
Attn: P. Grimes
P.O. Box 536
1900 East Linden Avenue
Linden, NJ 07036

GNB Battery Technologies
Industrial Battery Company
Attn: J. Szymborski
Woodlake Corporate Park
829 Parkview Blvd.
Lombard, IL 60148-3249

Innovative Power Sources
Attn: Ken Belfer
1419 Via Jon Jose Road
Alamo, CA 94507

Kenetech/U.S. Power Systems
Attn: Michael Behnke
6952 Preston Avenue
Livermore, CA 94550

Lawrence Berkeley Laboratory
Attn: K. Kinoshita
University of California
One Cyclotron Road
Berkeley, CA 94720

Lucas Controls, Inc.
Attn: Donald J. Lucas
10925 Miller Rd., Ste. A
Dallas, TX 75355-1848

J. Meglen
P.O. Box 3232
Oakton, VA 22124

National Renewable Energy Laboratory
Attn: C. Hammel
1617 Cole Blvd.
Golden, CO 80401-3393

Northern States Power
Attn: M. Rogers
414 Nicollet Mall
Minneapolis, MN 55401

NRECA
Attn: J. Nesh
4301 Wilson Blvd.
Arlington, VA 22203

Pacific Gas & Electric
Attn: R. Winter
2303 Camino Ramon, Suite 200
San Ramon, CA 94583

PECO Energy
Attn: W. Gardner
955 Chesterbrook Blvd.
Wayne, PA 19087

R. K. Sen & Associates
Attn: R. Sen
4733 Bethesda Avenue, Suite 608
Bethesda, MD 20814

Salt River Project
Attn: H. Lundstrom
MS PAB 357, Box 52025
Phoenix, AZ 85072-2025

SEIA
Attn: S. Sklar
122 C Street NW
4th Floor
Washington, DC 20001-2104

Silent Power, Inc.
Attn: J. Rassmussen
163 West 1700 South
Salt Lake City, UT 84115

Silent Power, Inc.
Attn: W. Auxer
390 Anthony Rd.
King of Prussia, PA 19406

Silent Power Systems (3)
Attn: A. Koenig
20 Mineral Springs Rd.
Coatesville, PA 19320

Southern California Edison
Attn: R. Schweinberg
2244 Walnut Grove Avenue
P.O. Box 800
Rosemeade, CA 91770

Southern Company Services
Attn: B. Rauhe
800 Shades Creek Parkway
Birmingham, AL 35209

Switch Technologies
Attn: J. Hurwitch
4733 Bethesda Ave., Ste. 680
Bethesda, MD 20814

U.S. Department of Energy
Attn: K. Klunder
Office of Energy Management
EE-10 FORSTL
Washington, DC 20585

U.S. Department of Energy
Attn: C. Platt
Office of Energy Management
EE-12 FORSTL
Washington, DC 20585

U.S. Department of Energy
Attn: R. Eaton
Golden Field Office
1617 Cole Blvd., Bldg. 17.
Golden, CO 80401

U.S. Department of Energy
Attn: A. Landgrebe
Office of Propulsion Systems
EE-321 FORSTL
Washington, DC 20585

Virginia Power
Attn: Gary Verno
Innsbrook Technical Center
5000 Dominion Boulevard
Glen Ellen, VA 23233

R. Weaver
777 Wildwood Lane
Palo Alto, CA 94303

Westwood Energy Group
Attn: R. Costello
127 Burgess Ave.
Westwood, MA 02090

Windtec Energy, Ltd.
Attn: Fred Noble
PO Box 457
North Palm Springs, CA 92258

Yuasa-Exide Inc.
Attn: N. Magnani
P.O. Box 14145
645 Penn Street
Reading, PA 19601

Zaininger Engineering Co., Inc.
Attn.: H. Zaininger
1590 Oakland Road, Suite B2111
San Jose, CA 95131

ZBB Battery Technologies, Inc.
Attn: P. Eidler
5757 N. Green Bay Avenue
P. O. Box 591
Milwaukee, WI 53201

MS0340 J. Braithwaite (1832)
MS0613 A. Akhil (1525)
MS0613 P. Butler (1525)
MS0613 J. Freese (1525)
MS0613 A. Gray (1525) (10)
MS0613 T. Unkelhaeuser (1525)
MS0953 W. Alzheimer (0953)
MS9018 Central Technical Files (8523-2)
MS0899 Technical Library (4414) (5)
MS0619 Print Media (12615)
MS0100 Document Processing for
DOE/OSTI (7613-2) (2)